DAMPING SUBSYNCHRONOUS RESONANCE OSCILLATIONS USING A VSC HVDC BACK-TO-BACK SYSTEM

A Thesis

Submitted to the College of Graduate Studies and Research

in Partial Fulfillment of the Requirements

For the Degree of Master of Science

in the Department of Electrical Engineering

University of Saskatchewan

Saskatoon, Saskatchewan

By

Guosheng Tang

PERMISSION TO USE

I agree that the Library, University of Saskatchewan, may make this thesis freely available for inspection. I further agree that permission for copying of this thesis for scholarly purpose may be granted to the professor or professors who supervised the thesis work recorded herein or, in their absence, by the Head of the Department or the Dean of the College in which the thesis work was done. It is understood that due recognition will be given to me and to the University of Saskatchewan in any use of the material in this thesis. Copying or publication or any other use of this thesis for financial gain without approval by the University of Saskatchewan and my written permission is prohibited.

Request for permission to copy or to make any other use of the material in this thesis in whole or part should be addressed to:

Head of the Department of Electrical Engineering
57 Campus Drive
University of Saskatchewan
Saskatoon, Saskatchewan
Canada S7N 5A9

ABSTRACT

A problem of interest in the power industry is the mitigation of severe torsional oscillations induced in turbine-generator shaft systems due to Subsynchronous Resonance (SSR). SSR occurs when a natural frequency of a series compensated transmission system coincides with the complement of one of the torsional modes of the turbine-generator shaft system. Under such circumstances, the turbine-generator shaft system oscillates at a frequency corresponding to the torsional mode frequency and unless corrective action is taken, the torsional oscillations can grow and may result in shaft damage in a few seconds.

This thesis reports the use of a supplementary controller along with the Voltage Source Converter (VSC) HVDC back-to-back active power controller to damp all SSR torsional oscillations. In this context, investigations are conducted on a typical HVAC/DC system incorporating a large turbine-generator and a VSC HVDC back-to-back system. The generator speed deviation is used as the stabilizing signal for the supplementary controller.

The results of the investigations conducted in this thesis show that the achieved control design is effective in damping all the shaft torsional torques over a wide range of compensation levels. The results and discussion presented in this thesis should provide valuable information to electric power utilities engaged in planning and operating series capacitor compensated transmission lines and VSC HVDC back-to-back systems.

ACKNOWLEDGEMENTS

I would like to express my sincere gratitude and appreciation to my research supervisor, Dr. Sherif O. Faried, for his valuable guidance, criticisms and consistent encouragement throughout the course of this research work. I would also like to acknowledge Dr. Faried's patience and helpful suggestions in the preparation of this thesis. I also express my appreciation to the Advisory Committee members.

I would also like to express my appreciation to my graduate study teachers, Dr. N.A. Chowdhury, Dr. Rajesh Karki and Dr. Ramakrishna Gokaraju for strengthening my knowledge on electrical engineering. My appreciation also goes to Dr. A. Eldamaty for his assistance in providing some calculations for this thesis.

I wish to express thanks to Dr. Faried, the University of Saskatchewan and the Natural Science and Engineering Research Council of Canada for awarding me a graduate scholarship and other financial assistances that helped me going through the M. Sc. program.

Finally, I would like to thank my parents and parents-in-law, my brothers and sisters, and all my friends, for the support they provided me. Special thanks go out to my wife and daughter, Li Zhang and Mengxi Tang, for your love and encouragement.

TABLE OF CONTENTS

LIST OF FIGURES

LIST OF TABLES

LIST OF SYMBOLS

A	state matrix
B	control or input matrix
C	capacitor in the compensated transmission line
C_V	steam valve position
$\dot{C}_{VOPEN}, \dot{C}_{VCLOSE}$	maximum permitted rate of opening and closing the steam valve respectively
C_{dc}	capacitor in DC link of the VSC HVDC back-to-back system
$D_E, D_g, D_B, D_A, D_I, D_H$	damping coefficient of the corresponding inertia
DW_{sh}	output angular speed of the angular speed regulator amplifier
$D_{a+}, D_{b+}, D_{c+}, D_{a-}, D_{b-}, D_{c-}$	Voltage Source Converter (VSC) diodes
D_i	damping coefficient of the i^{th} rotating mass
E_{fd}	exciter output voltage
E_R	output voltage of the voltage regulator amplifier
E_{ref}	reference voltage of the excitation system
E_{SB}	feedback stabilizing signal of the excitation system
e_a, e_b, e_c	stator three-phase voltages respectively
e_d, e_q	stator voltages in the d-q reference frame
e_{fd}	field voltage
F_B, F_A, F_I, F_H	power fraction of the stages of the turbine
f_s	triangular signal frequency in VSC
$f0, f1, f2, f3, f4, f5$	torsional modes frequencies

f_1	modulating frequency in VSC
I	current flowing from a VSC to an AC system
I_B, I_E	injected currents at buses "*B*" and "*E*" of the VSC HVDC back-to-back link respectively
I_{Bsh}, I_{Esh}	injected currents at voltage sources of the VSC HVDC back-to-back link respectively
i_B, i_E	currents through the inverter and rectifier stations of the VSC HVDC back-to-back link respectively
i_{Ba}, i_{Bb}, i_{Bc}	currents through the inverter station in phase a, b, c
i_{Bd}, i_{Bq}	currents through the inverter station in the d-q reference frame
i_{Ea}, i_{Eb}, i_{Ec}	currents through the rectifier station in phase a, b, c
i_{Ed}, i_{Eq}	currents through the rectifier station in the d-q reference frame
i_{Bdc}	current flowing from the dc side to ac side at the inverter station
i_{Edc}	current flowing from the ac side to dc side at the rectifier station
i_a, i_b, i_c	stator currents in phase a, b, c
i_d, i_q	stator currents in the d-q reference frame
i_{dc}	current through the dc capacitor
i_{fd}, i_{1d}, i_{1q}, i_{2q}	field and damping winding currents in the d-q reference frame respectively
i_o	output current in one-leg of the VSC
K_A	gain of the voltage regulator amplifier
K_{Bd}, K_{Ed}	gains of the active power controller
K_E	exciter constant
K_{Eg}, K_{gB}, K_{BA}, K_{AI}, K_{IH}	stiffness of the connecting shafts
K_F	feedback stabilizing loop gain of the exciter system
K_I, K_P	coefficients of the PI supplementary controller
Kg	speed regulation in governor system

$K_{i,i+1}$	stiffness between i^{th} and $(i+1)^{th}$ mass-spring
K_{ω}	gain of the supplementary controller
L_B, L_E	inductances in the inverter and rectifier stations of the VSC HVDC back-to-back system respectively
L_T	total inductance of the electric system
L_{ad}, L_{aq}	mutual inductances
L_d, L_q	d and q synchronous inductances
L_{ffd}, L_{11d}, L_{11q}, L_{22q}	rotor and damping windings self inductances respectively
Lim_max, Lim_min	maximum and minimum amplitude modulation ratios of the active power controller output control signal respectively
M_E, M_g, M_B, M_A, M_I, M_H	inertia constants of exciter, generator, two low-pressure turbines, intermediate-pressure turbine and high-pressure turbine respectively
M_i	inertia constant of the i^{th} rotating mass
m_B, m_E	amplitude modulation ratios of the control signal (active power controller output control signals)
m_{Br}, m_{Er}	output power in active power regulator amplifier
m_a	amplitude modulation ratio
m_f	frequency modulation ratio
P	real power
P_A, P_B, P_I, P_H	power of the stages of the turbine
P_{Bdc}	active power flowing from the inverter station of the VSC HVDC back-to-back link
P_{Bdcref}	reference active power in the inverter station
P_E	active power at bus "E" of the VSC HVDC back-to-back link
P_{Edc}	active power flowing into the rectifier station of the VSC HVDC back-to-back link
P_{Edcref}	reference active power in the rectifier station

P_{Esh}	active power flowing into the rectifier station of the VSC HVDC back-to-back link
PI	proportional integral
P_a	generator accelerating power
P_{dc}	active power flowing through the VSC HVDC back-to-back link
P_{dcref}	reference active power flowing through the VSC HVDC back-to-back link
P_m	mechanical power
Q	reactive power
Q_E	reactive power at bus "E" of the VSC HVDC back-to-back link
Q_{Esh}	reactive power flowing into the rectifier station of the VSC HVDC back-to-back link
R_B, R_E	resistances in the inverter and rectifier stations of the VSC HVDC back-to-back link respectively
R_L	resistance of the series capacitor compensated transmission line (Line 1)
R_{L2}, R_{L3}	Line2 and Lin3 resistances respectively
R_a	armature resistance
R_{fd}, R_{1d}, R_{1q}, R_{2q}	rotor and damp windings resistances respectively
S	complex power delivered to the infinite bus in the IEEE first benchmark model
s	Laplace transformation operator
S_E	complex power injected at bus "E" of the VSC HVDC back-to-back link
S_{Esh}	complex power flowing into the rectifier station of the VSC HVDC back-to-back link
T_A, T_E, T_F	time constant in excitation system
T_{Bd}, $T_{Ed,}$ T_{mb}, T_{me}	time constant in active power controller

T_{LB}, T_{LA}, T_{IP}, T_{HP}	input torques of two low-pressure turbines, intermediate-pressure turbine and high-pressure turbine respectively
T_{a+}, T_{b+}, T_{c+}, T_{a-}, T_{b-}, T_{c-}	VSC switches
T_e	air-gap torque
T_g, T_{ch}, T_{rh}, T_{co}	time constant in governor and turbine system
T_m	time constant in supplementary controller
T_{mb}, T_{me}	time constant in active power controller
T_{m0}	initial mechanical torque
U	input vector
V_B, V_E	bus voltages of the VSC HVDC back-to-back link respectively
V_{Ba}, V_{Bb}, V_{Bc}	bus "*B*" voltages in phase a, b, c
V_{Bd}, V_{Bq}	bus "*B*" voltages in the d-q reference frame
V_{Bsh}, V_{Esh}	shunt voltages of the VSC HVDC back-to-back link
V_{Bsha}, V_{Bshb}, V_{Bshc}	source voltages of the inverter station in phase a,b,c
V_{Bshd}, V_{Bshq}	shunt voltages of the inverter station in the d-q reference frame
V_C	voltage across the series capacitor of the compensated transmission line
V_{Cd}, V_{Cq}	voltages across the series capacitor in the d-q reference frame
V_{Ea}, V_{Eb}, V_{Ec}	bus "*E*" voltages in phase a, b, c
V_{Ed}, V_{Eq}	bus "*E*" voltages in the d-q reference frame
V_{Esha}, V_{Eshb}, V_{Eshc}	source voltages of the rectifier station in phase a,b,c
V_{Eshd}, V_{Eshq}	shunt voltages of the rectifier station in the d-q reference frame

V_L	voltage across the inductance of the series capacitor compensated transmission line
V_{Ld}, V_{Lq}	voltages across the inductance in the d-q reference frame
V_R	voltage across the resistance of the series capacitor compensated transmission line
V_{Rd}, V_{Rq}	voltages across the resistance in the d-q reference frame
V_{Rmax}, V_{Rmin}	maximum and minimum ceiling voltages of the excitation system respectively
V_a, V_b, V_c	three phase voltages on the AC side
V_{aN}	converter phase "a" output voltage related to neutral point
V_{ao}	converter phase "a" output voltage related to middle point of the dc capacitor
V_b	infinite bus voltage
$V_{control}$	control signal
$\hat{V}_{control}$	control signal peak amplitude
V_{dc}	voltage across the dc capacitor
V_s	AC system voltage
V_{sh}	VSC source voltage
V_{sh1}, V_{sh2}	VSC HVDC back-to-back link source voltages
V_t	generator terminal voltage
V_{td}, V_{tq}	generator terminal voltages in the d-q reference frame
V_{tri}	triangular signal
$\hat{V}_{tri}$	triangular signal peak amplitude
$V1$, $V2$, $V3$, $V4$, $V5$	system bus voltages
V_I, V_{II}	system I and II voltages respectively
X	state vector

X_B, X_E	reactances of the inverter and rectifier stations of the VSC HVDC back-to-back link respectively
X_C	series capacitor reactance
X_{Esh}	shunt reactance of the rectifier station
X_L	reactance of the series capacitor compensated transmission line (Line 1)
$X_{L2,} X_{L3}$	Line 2 and Line3 reactances respectively
X_{L_T}	total inductive reactance of the electric system
X_{ad}, X_{aq}	d and q leakage reactances of the generator
X_d, X_q	d and q synchronous reactances
X_{dc}	reactance of the dc capacitor
X_{ffd}, X_{11d}, X_{11q}, X_{22q}	self reactances of the field and the damping windings respectively
X_l	converter reactance
Z_{sh}	shunt impedance of the VSC
Z_{Bsh}, Z_{Esh}	shunt impedances of the inverter and rectifier stations of the VSC HVDC back-to-back link respectively
Ψ_d, Ψ_q	stator flux linkages in d-q components
Ψ_{fd}, Ψ_{1d}, Ψ_{1q}, Ψ_{2q}	rotor flux linkages in d-q components
δ	generator power angle
δ_E, δ_B, δ_A, δ_I, δ_H	rotor angles of exciter, two low-pressure turbines, intermediate-pressure turbine and high-pressure turbine respectively
δ_{Esh}, δ_{Bsh}	phase angles of shunt voltages of the VSC HVDC back-to-back link respectively
δ_{sh}	phase angle of the VSC source voltage
ϕ	phase angle of the current flowing from a VSC to an AC system
θ	phase angle of the bus voltage

θ_B, θ_E	phase angles of the bus voltages of the VSC HVDC back-to-back link respectively
ω	angular velocity
ω_E, ω_B, ω_A, ω_I, ω_H	angular velocity of exciter, two low-pressure turbines, intermediate-pressure turbine and high-pressure turbine respectively
$\omega_e(f_e)$	subsynchronous natural frequency
ω_{ref}	reference angular velocity
$\omega_0(f_0)$	synchronous frequency
Δ	prefix to denote a small deviation in the initial operating point
0	suffix to denote the initial operating operation

1 INTRODUCTION

Growth of electric power transmission facilities is restricted despite the fact that bulk power transfers and use of transmission systems by third parties are increasing. Transmission bottlenecks, non-uniform utilization of facilities and unwanted parallel-path or loop flows are not uncommon. Transmission system expansion is needed, but not easily accomplished. Factors that contribute to this situation include a variety of environmental, land-use and regulatory requirements. As a result, the utility industry is facing the challenge of the efficient utilization of the existing AC transmission lines.

Flexible AC Transmission Systems (FACTS) technology is an important tool for permitting existing transmission facilities to be loaded, at least under contingency situations, up to their thermal limits without degrading system security [1-4]. The most striking feature is the ability to directly control transmission line flows by structurally changing parameters of the grid and to implement high-gain type controllers, based on fast switching.

FACTS controllers are power electronic based controllers which can influence transmission system voltage, currents, impedances and/or phase angle rapidly. Thus, such controllers can improve the security of a power system by enhancing its steady-state and transient stability or by damping the subsynchronous resonance oscillations. FACTS application studies require an understanding of the individual FACTS controllers as well as openness to the application of novel approaches.

1.1 Flexible AC Transmission Systems

FACTS and FACTS controller are defined by the IEEE as [5]:

> "*Flexible AC Transmission System (FACTS):* Alternating-current transmission systems incorporating power electronic-based and other static controllers to enhance controllability and increase power transfer capability."

> "*FACTS Controller:* A power electronic-based system and other static equipment that provide control of one or more AC transmission system parameters."

The availability of the modern semiconductor devices such as the Gate Turn-Off thyristor (GTO), and the Insulated Gate Bipolar Transistor (IGBT) [6], has led to the development of a new generation of power electric converters. These devices, unlike the conventional thyristors which have no intrinsic turn-off ability, are of the fully controlled type. The most common converters, which employ the self commutating, high voltage, high current, and high switching frequency power electronic devices, are the Voltage Source Converters (VSCs).

A number of FACTS controllers which use VSCs as their basic building block have been already in operation in various parts of the world. The most popular controllers are: the Static Compensator (STATCOM) [7,8], the Static Synchronous Series Compensator (SSSC) [9,10], the Unified Power Flow Controller (UPFC) [11,12], and the Voltage Source Converter High-Voltage Direct-Current (VSC HVDC) [3,13,14].

1.1.1 The Voltage Source Converter

Several VSC topologies are currently used in actual power system operations, such as the single-phase full bridge (H-bridge), the conventional three-phase, two-level converter, and the three-phase, three-level converter based on the neutral-point-clamped converter [2]. There are other VSC topologies that are based on combinations of the neutral-point-clamped and multilevel converters. The common purposes of these topologies are: to minimize the operating frequency of the semiconductors inside the VSC and to produce a high-quality sinusoidal voltage waveform with minimum or no filtering requirements.

The topology of a conventional two-level VSC using IGBT switches is shown in Figure 1.1. It consists of six IGBTs, with two IGBTs placed on each leg. Moreover, each IGBT is provided with a diode connected in an anti-parallel connection to allow bidirectional current flow. Two equally sized capacitors are placed on the DC side to provide a source of reactive power.

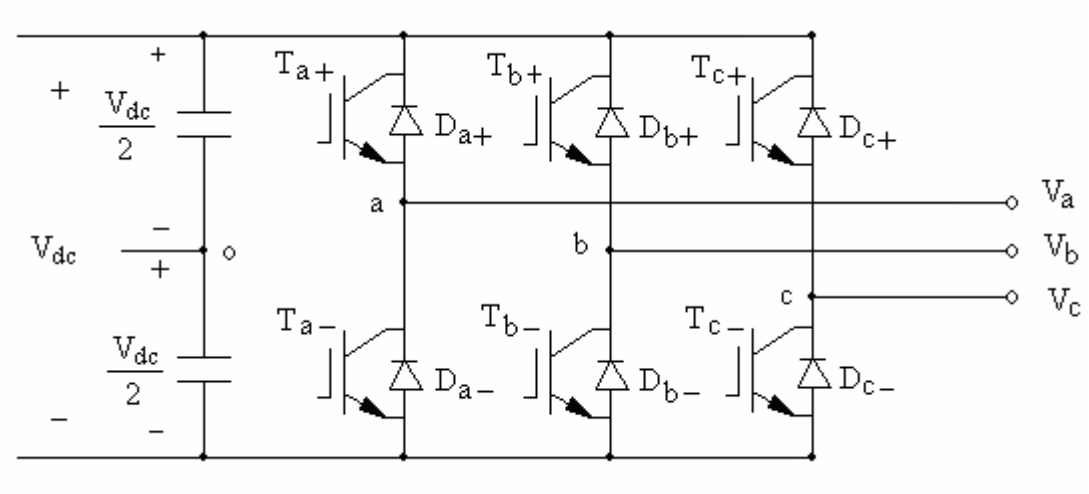

Figure 1.1 Topology of a three-phase, two-level VSC using IGBTs.

The switching control module, not shown in the circuit of Figure 1.1, is an integral component of the VSC. Its duty is to control the switching sequence of the various semiconductor devices in the VSC, aiming at producing an output voltage waveform, which is close to a sinusoidal waveform as near as possible, with high power controllability and minimum switching loss.

The current VSC switching strategies aimed at utility application may be classified into two main categories [15]:

1. Fundamental frequency switching: the switching of each semiconductor device has only one turn-on, turn-off per power cycle. The output waveform is a quasi-square-wave which often has an unacceptable high harmonic content. It is current practice to use several six-pulse VSCs, arranged to form a multiple structure, to achieve better waveform quality and high power ratings [2].

2. Pulse-Width-Modulation (PWM): the switches are forced to be turned on and off at a rate considerably higher than the fundamental frequency. The output wave is chopped and the width of the resulting pulse is modulated. Undesirable harmonics in the output waveform are shifted to the higher frequencies, and filtering requirements are much reduced. The sinusoidal PWM scheme remains one of the most popular because of its simplicity and effectiveness [6].

These switching techniques are, however, far from perfect. The fundamental frequency switching technique requires complex transformer arrangements to achieve an acceptable level of waveform distortion. The PWM technique incurs high switching loss, but it is expected that future semiconductor devices will reduce this by a significant margin, making PWM the perfect switching technique.

1.1.2 Pulse-Width Modulation Control

The basic PWM switching scheme can be explained using the simple one-leg switch-mode inverter shown in Figure 1.2.

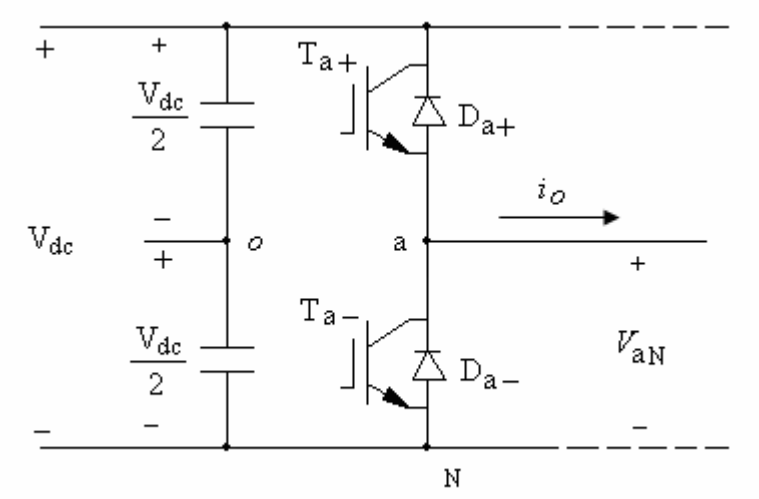

Figure 1.2 One-leg switch-mode inverter.

In order to produce a sinusoidal output voltage waveform at a desired frequency, a sinusoidal control signal at the desired frequency is compared with a triangle waveform, as shown in Figure 1.3 (a). The frequency of the triangular waveform establishes the inverter switching frequency f_s, and is generally kept constant along with its

amplitude $\hat{V}_{tri}$. The frequency f_s is also called the carrier frequency. The control signal $V_{control}$ is used to modulate the switch duty ratio and has a frequency f_1, which is the desired fundamental frequency of the inverter voltage output (f_1 is also called the modulating frequency), recognizing that the inverter output voltage will not be a perfect sine wave and will contain voltage components at harmonic frequencies of f_1. The amplitude modulation ratio m_a is defined as

$$m_a = \frac{\hat{V}_{control}}{\hat{V}_{tri}} \tag{1.1}$$

where $\hat{V}_{control}$ is the peak amplitude of the control signal.

The frequency modulation ratio m_f is defined as

$$m_f = \frac{f_s}{f_1} \tag{1.2}$$

In the inverter of Figure 1.2, the switches T_{a+} and T_{a-} are controlled based on the comparison of $V_{control}$ and V_{tri}, and the following output voltage results, independent of the direction of the current i_o:

$$V_{control} > V_{tri}, \qquad T_{a+} \text{ is on}, \qquad V_{ao} = \frac{V_{dc}}{2}$$

or

$$V_{control} < V_{tri}, \qquad T_{a-} \text{ is on}, \qquad V_{ao} = -\frac{V_{dc}}{2} \tag{1.3}$$

Since the two switches are never off simultaneously, the output voltage V_{ao} fluctuates between two values ($\frac{V_{dc}}{2}$ and $-\frac{V_{dc}}{2}$). The voltage V_{ao} and its fundamental frequency component (dashed curve) are shown in Figure 1.3 (b).

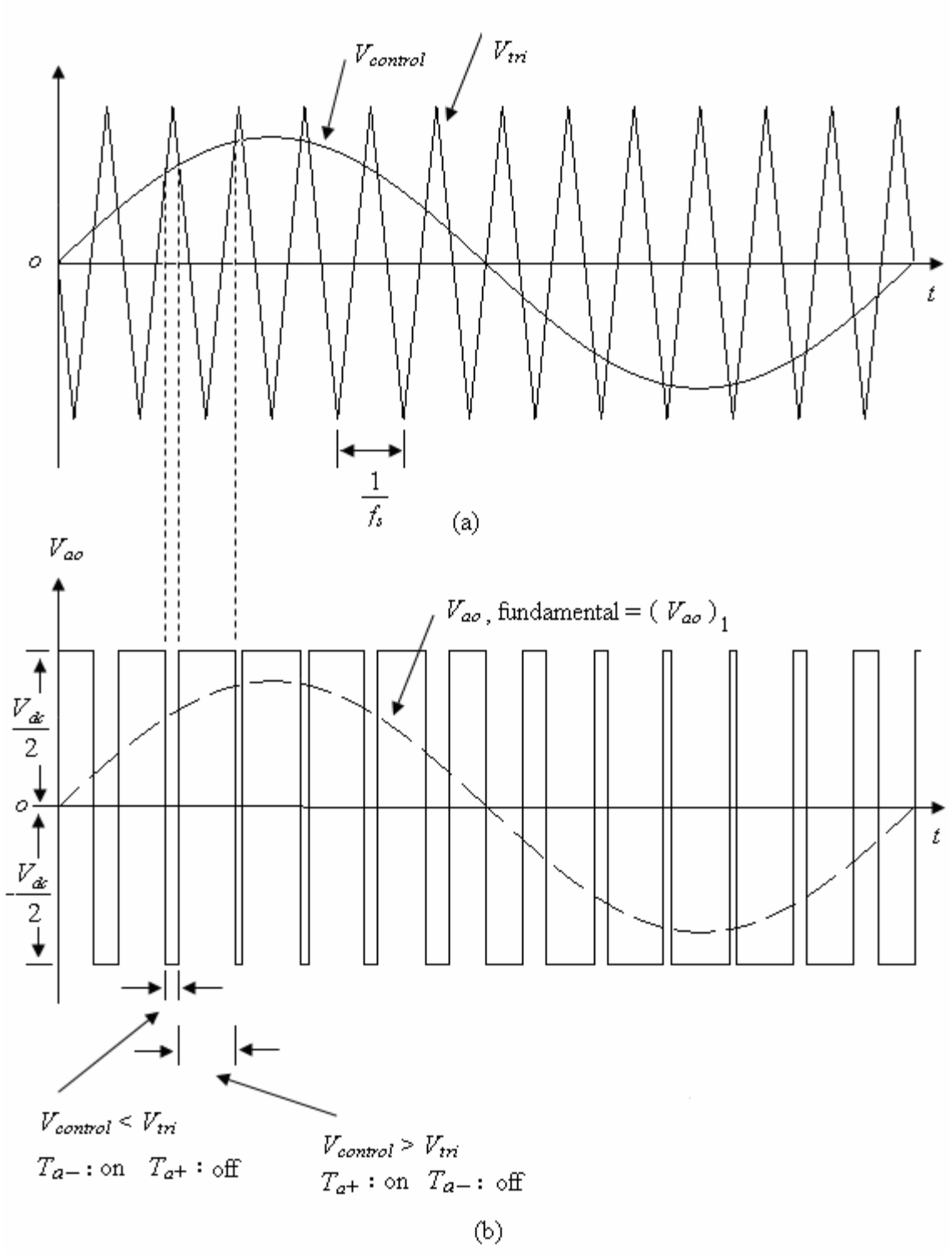

Figure 1.3 Operation of a pulse-width modulator: (a) comparison of a sinusoidal fundamental frequency with a high frequency triangular signal; (b) resulting train of square-waves.

With PWM, it is possible to create any phase angle or amplitude (up to a certain limit) by changing the PWM pattern, which can be done almost instantaneously. Hereby, PWM offers the possibility to control both the active and the reactive power independently.

This makes the PWM VSC close to an ideal component in the transmission network. From a system point of view, it acts as a motor or generator without a mass that can control the active and the reactive power almost instantaneously. Furthermore, it does not contribute to the short circuit power as the ac current can be controlled [16].

1.1.3 Principle of Voltage Source Converter Operation

Consider a VSC connected to an AC system through a lossless reactor as illustrated in Figure 1.4. The converter produces an AC voltage with a fundamental frequency equal to that of the AC reference voltage. The voltage at the supply bus is assumed to be $V_s\angle 0^0$, and the AC voltage produced by the VSC is taken to be $V_{sh}\angle\delta_{sh}$. X_l is the reactance of the converter reactor.

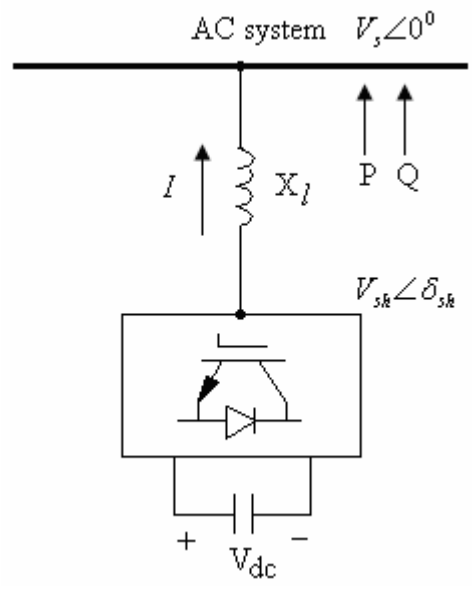

Figure 1.4 A VSC connected to an AC system.

The active and the reactive power can be expressed respectively as

$$P = \frac{V_{sh} V_s}{X_l} \sin \delta_{sh} \tag{1.4}$$

$$Q = \frac{V_{sh} V_s}{X_l} \cos \delta_{sh} - \frac{V_{sh}^2}{X_l} \tag{1.5}$$

A complete derivation of Equations (1.4) and (1.5) is given in Appendix A. With respect to these two Equations, the following observations are noticed:

1. The active power flow between the AC source and the VSC is controlled by the phase angle δ_{sh}. The active power flows into the AC source from the VSC for $\delta_{sh} > 0$, and flows out of the AC source from the VSC for $\delta_{sh} < 0$,

2. The reactive power flow is determined mainly by the amplitude of the AC source voltage, V_s, and the VSC output fundamental voltage, V_{sh}, as the angle δ_{sh} is generally small. For $V_{sh} > V_s$, the VSC generates reactive power and while it consumes reactive power when $V_{sh} < V_s$.

Because of its key steady-state operational characteristics and impact on system voltage and power flow control, the VSC is becoming the basic building block employed in the new generation of FACTS controllers.

1.2 High-Voltage Direct-Current Transmission

High-Voltage Direct-Current (HVDC) transmission has advantages over ac transmission in the following situations [17]:

1. Underwater cables longer than about 30 km; AC transmission is impractical for such distances because of the high capacitance of the cable requiring intermediate compensation stations.

2. Asynchronous link between two ac systems where ac ties would not be feasible because of system stability problems or a difference in nominal frequencies of the two systems.

3. Transmission of large amounts of power over long distance by overhead lines. HVDC transmission is a competitive alternate to ac transmission for distance in excess of about 600 km.

HVDC systems have the ability to rapidly control the transmitted power. Therefore, they have a significant impact on the stability of associated ac power systems.

1.2.1 Voltage Source Converter-Based High-Voltage Direct-Current

The VSC HVDC system is the most recent HVDC technology. It consists of two VSCs, one of which operates as a rectifier and the other as an inverter. The two converters are connected either back-to-back or joined by a DC cable, depending on the application. Its main function is to transmit a constant DC power from the rectifier station to the inverter station, with high controllability. A schematic representation of a VSC HVDC back-to-back system is shown in Figure 1.5 [3]. In this figure, m and δ are, respectively, the amplitude modulation ratio and phase angle of the control signal of the station. These four parameters (two for each station) are the output control signals to the VSC HVDC system.

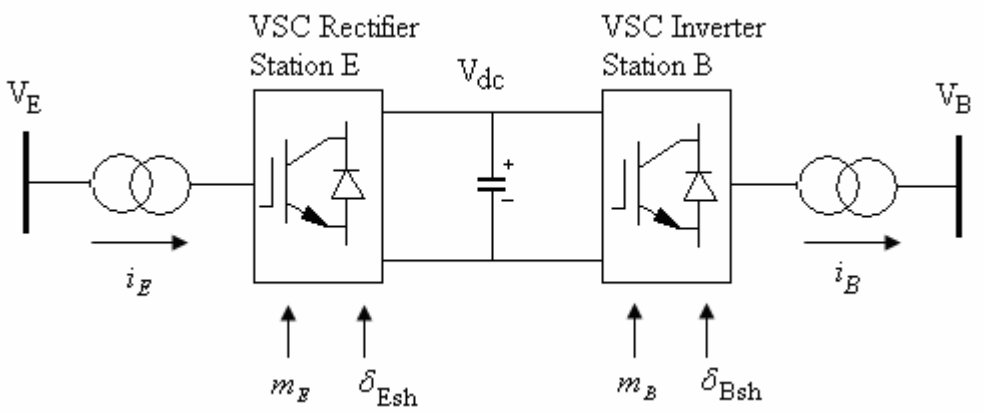

Figure 1.5 A VSC HVDC back-to-back system.

The VSC HVDC has several main advantages against the conventional HVDC based on thyristors [17]. They are [13]:

1. Independent control of the active and reactive power output from each terminal.
2. Reduced requirements for harmonic filters.

3. Improvements of the power quality and system stability.

4. Elimination of the requirement for a local power generation.

These features make the VSC HVDC attractive for connection of weak ac system, island networks, and renewable energy sources, which may be located in remote area, to a main grid. The world's first VSC HVDC installation was the Hällsjön project in central Sweden in March, 1997 [14].

1.3 Subsynchronous Resonance (SSR)

A problem of interest in the power industry in which FACTS controllers could play a major role is the mitigation of Subsynchronous Resonance (SSR) oscillations. SSR is a dynamic phenomenon in the power system which has certain special characteristics. The definitions of subsynchronous oscillation and SSR are given by the IEEE as [18,19]:

> "*Subsynchronous oscillation* is an electric power system condition where the electric network exchanges significant energy with a turbine-generator at one or more of the natural frequencies of the combined system below the synchronous frequency of the system following a disturbance from equilibrium. The above excludes the rigid body modes of the turbine-generator rotors."

> "*Subsynchronous Resonance (SSR)* encompasses the oscillatory attributes of electrical and mechanical variables associated with turbine-generators when coupled to a series capacitor compensated transmission system where the oscillatory energy interchange is lightly damped, undamped, or even negatively damped and growing."

1.3.1 SSR: Basic Phenomenon

Consider the simple power system shown in Figure 1.6. It consists of a large turbine-generator which is connected to an infinite bus system through a series capacitor compensated transmission line. The generator is driven by a multi-stage turbine, where the various stages of the turbine (HP, IP and LP) and the generator rotor (GEN) are coupled by elastic shafts.

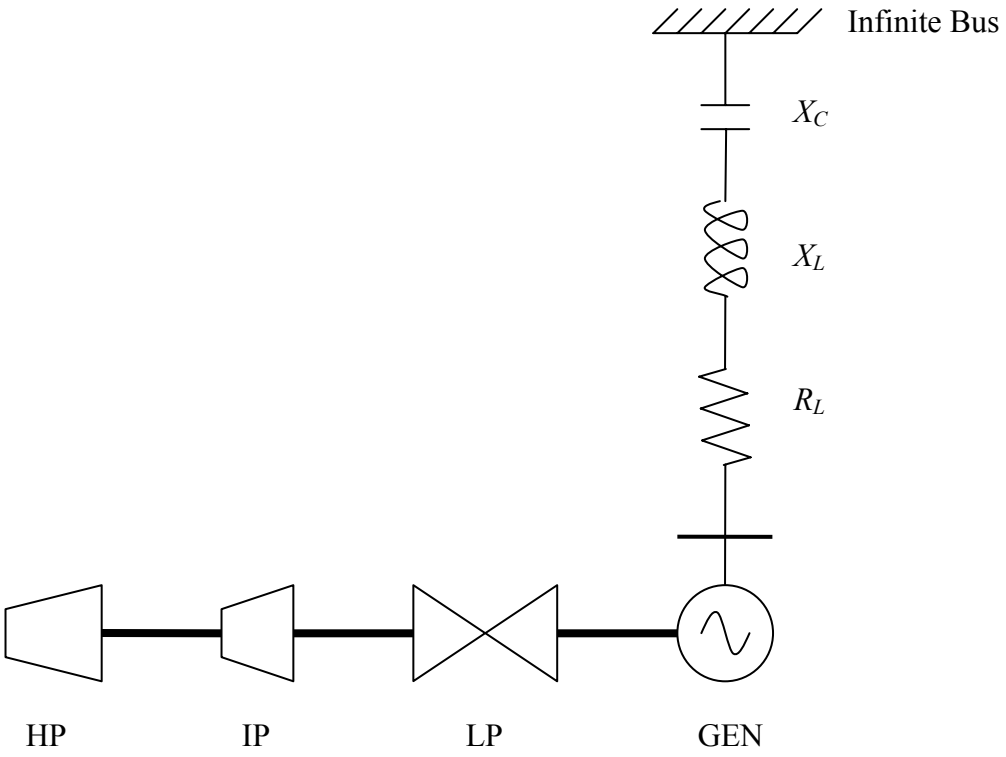

Figure 1.6 A series capacitor compensated power system.

The natural resonance frequency for the electrical system is given by

$$\omega_e = \frac{1}{\sqrt{L_T C}} = \frac{\omega_0}{\sqrt{(\omega_0 L_T)(\omega_0 C)}} = \omega_0 \sqrt{\frac{X_C}{X_{L_T}}} \quad \text{rad/s} \tag{1.3}$$

or

$$f_e = f_0 \sqrt{\frac{X_C}{X_{L_T}}} \quad \text{Hz} \tag{1.4}$$

where ω_0 is the system synchronous frequency ($\omega_0 = 2\pi f_0$, f_0 = 60 Hz), X_C is the capacitive reactance, and X_{L_T} is the total inductive reactance of the electric system, which comprises the generator subtransient reactance and the transmission line inductive reactance.

In practice, f_e is always below the synchronous frequency f_0 since the compensation levels of transmission line are usually less than 100%. For this reason, f_e is called the subsynchronous natural frequency of the electrical system.

The shaft system of the turbine-generator has (N-1) natural torsional frequencies where N is the number of the rotating masses. These torsional frequencies are functions of the inertia of the different masses and the stiffness of the connected shafts. Due to the physical properties of the shaft materials and the mechanical design of the turbine-generator shaft system, the torsional natural frequencies are also subsynchronous. Thus, the basic interaction between the electrical and mechanical systems is due to the closeness of f_e to the natural torsional frequencies of the turbine-generator shaft system. SSR can occur in the following three forms [19, 20]:

1. **Torsional Interaction**: this is due to an interaction and exchange of energy between the series compensated electrical system and the turbine-generator mechanical system. This can lead to growing shaft torque oscillations at one of the natural torsional frequencies of the turbine-generator shaft system. Torsional interaction can occur when the generator is connected to a series compensated electrical system that has one or more natural frequencies, which are the synchronous frequency complements of one or more of the spring-mass natural frequencies. Generally, shaft torques due to torsional interaction can be expected to build up at a relatively slow rate such that damaging torque levels would not be reached in less than a minute or so.

2. **Induction Generator Effect**: this is a pure electrical phenomenon that is due to the fact that, when subsynchronous currents flow in the armature circuit of a synchronous generator, the generator appears as a negative-resistance circuit at the prevailing subsynchronous frequencies. If the apparent resistance is greater than the inherent positive resistance of the circuit at one of the natural frequencies of the electrical circuit, growing subsynchronous voltages and currents will be expected in the system and at the generator. This could result in voltages and currents large enough to be damaging to the generator and power system equipment. In addition, if the subsynchronous currents in the generator armature are at the frequency corresponding to one of the turbine-

generator spring-mass modes, large oscillatory shaft torques may result. As in the case of torsional interaction, a relatively slow oscillation growth rate would be expected.

3. Torque Amplification: this phenomenon occurs when a fault on a series compensated power system, and its subsequent clearing, results in a high-energy storage in the series capacitor banks, which then discharge their energy through a generator in the form of a current having a frequency that corresponds to one of the natural torsional frequencies of the turbine-generator mechanical system. Unlike torsional interaction and induction generator effect, the growth rate for torque amplification is high and oscillating shaft torques might be expected to reach a damaging level within 0.1 second.

The ultimate hazard of SSR is a shaft fraction at full load and rated speed. The damage of such an occurrence cannot be accurately predicted, but extensive equipment damage could occur with a safety hazard to personnel. A more likely most-severe hazard would be crack initiation at the surface of one of the turbine-generator shafts, indicating fatigue and requiring shaft replacement, resulting in a unit outage of 90 days or more.

1.4 Research Objectives and Scope of the Thesis

A wide variety of methods are already employed by utilities for damping SSR oscillations. These include the use of generator excitation control [21,22], power system stabilizer [23,24], static VAR compensator (SVC) [25-27] and static phase shifter [28]. In the recent reported studies on the mitigation of the SSR oscillations using FACTS devices, attention has been focused on the Thyristor Controlled Series Capacitor (TCSC), the STATCOM and the SSSC [29-32]. Relatively few studies, however, have been published on the application of VSC HVDC systems in damping SSR oscillations.

The main objective of this research work is to investigate the possibility of using an existing VSC HVDC back-to-back link in a power system as a supplementary controller to damp SSR oscillations in a nearby turbine-generator. In particular, attention is focused on the problem of the severe torsional torques induced in the turbine-generator shafts during large disturbances (torque amplification). It is expected that this research

will help utilities make decisions in regard to optimum planning and operation of VSC HVDC systems. The objectives of this research include:

1. The use of the VSC HVDC back-to-back link active power controller and the generator speed deviation as a supplementary signal to damp all SSR torsional oscillations over the whole range of practical compensation levels.

2. Investigate the performance of the designed controllers in damping SSR oscillations at the critical compensation levels using time-domain simulations.

3. Study the effects of the compensation level, the controller structure and its parameters, as well as the system loading on the damping of SSR oscillations.

There are five chapters in this thesis. The main topics of each chapter are as follows:

Chapter 1 introduces the fundamental concepts related to VSC FACTS controllers and the SSR phenomenon. The scope and objectives of the research are also presented in this chapter.

Chapter 2 presents the development of a complete small signal model of a single-machine infinite bus system. The eigenvalue technique is used to investigate the effect of the level of compensation of the transmission line on SSR oscillations. The system used for such an investigation is described and the detailed dynamic models of its individual components are also presented in this chapter.

Chapter 3 introduces a dynamic model of a power system incorporating a VSC HVDC back-to-back link. A comprehensive approach for designing the time-domain simulation analysis program is established and a sample case study is presented.

Chapter 4 demonstrates the effectiveness of the proposed VSC HVDC back-to-back link controllers in damping SSR oscillations through several cases of time-domain simulation studies.

Chapter 5 summarizes the research described in this thesis and presents some conclusions.

2 SMALL-SIGNAL ANALYSIS OF SUBSYNCHRONOUS RESONANCE PHENOMENON

2.1 Introduction

The differential and algebraic equations which describe the dynamic performance of the synchronous machine and the transmission network are, in general, nonlinear. For the purpose of stability analysis, these equations may be linearized by assuming that a disturbance is considered to be small. Small-signal analysis using linear techniques provides valuable information about the inherent dynamic characteristics of the power system and assists in its design.

This chapter presents an analytical method useful in the study of small-signal analysis of subsynchronous resonance (SSR), establishes a linearized model for the power system, and performs the analysis of the SSR using the eigenvalue technique. It is believed that by studying the small-signal stability of the power system, the engineer will be able to find countermeasures to damp all subsynchronous torsional oscillations.

2.2 Eigenvalue Analysis

Torsional interaction involves energy interchange between the turbine-generator and the electric network. Therefore, the analysis of SSR requires the representation of both the electromechanical dynamics of the generating unit and the electromagnetic dynamics of the transmission network. As a result, the dynamic system model used for SSR studies is of a higher order and greater stiffness than the models used for stability studies.

There are two main analytical methods for small-signal analysis, they are: frequency scanning technique [20,33] and eigenvalue analysis [34]. The former computes the equivalent impedance as seen from the internal buses of generators looking into the network, for the different values of frequency. This method is particularly suited for preliminary analysis of SSR. The latter is performed with the network and the generator modeled by a system of linear simultaneous differential equations. The results provide both the natural frequencies of oscillation as well as the damping of each frequency. This technique, thus, will be used for conducting the small-signal analysis to provide a comprehensive understanding of the various aspects of the SSR phenomenon.

The performance of a dynamic system, such as the power system, may be described by a set of *n* first-order nonlinear ordinary differential equations, which may be linearized in the following standard expression:

$$\Delta \dot{X} = A\Delta X + B\Delta U \tag{2.1}$$

where

Δ --- prefix to denote a small deviation about the initial operating point

ΔX --- the state vector

ΔU --- the input vector

A --- the state matrix

B --- the control or input matrix

The stability of the system is given by the eigenvalues of matrix A as follows:

1. A real eigenvalue is associated with a non-oscillatory mode. A negative real eigenvalue represents a decaying mode. The larger its absolute value, the fast is the decay. A positive real eigenvalue represents aperiodic instability.

2. Complex eigenvalues always occur as conjugate pairs, and each pair corresponds to an oscillatory mode. The real part of the eigenvalues represents the damping, and the imaginary part represents the frequency of oscillation. A negative real

component represents a damped oscillation; on the other hand, a positive real component represents an oscillation with an increasing amplitude.

Therefore, the negativeness of the real part of all eigenvalues assures the system stability. The more negative the real part, the sooner the response of the associated mode dies.

2.3 Small-Signal Analysis Study System

The system used in the small-signal analysis of SSR in this thesis is the IEEE first benchmark model for computer simulation of subsynchronous resonance [35]. This system, shown in Figure 2.1, consists of a single series-capacitor compensated transmission line connecting a large turbine-generator to a large system. The shaft system of the turbine-generator unit consists of a high-pressure turbine (HP), an intermediate-pressure turbine (IP), two low pressure turbines (LPA & LPB), the generator rotor (GEN), and its rotating exciter (EXC). The system data and the initial operating conditions of the system are given in Appendix B.

2.4 Power System Modeling

The nonlinear differential equations of the system under study are derived by developing individually the mathematical models which represent the various components of the system, namely the synchronous machine, the turbine-generator mechanical system, the governor system, the excitation system, and the transmission line. Knowing the mutual interaction among these models, the whole system differential equations can be formed.

2.4.1 Modeling of the Synchronous Machine

Figure 2.2 shows a schematic diagram of a conventional synchronous machine [34,36]. The stator circuit consists of a three-phase winding produces a sinusoidally space distributed magnetomotive force. The rotor of the machine carries the field (excitation) winding which is excited by a dc voltage. The electrical damping due to the eddy currents in the solid rotor and, if present, the damper winding is represented by three equivalent damper circuits; one on the direct axis (d-axis) and the other two on the

quadrature axis (q-axis). The performance of the synchronous machine can be described by the equations given below in the d-q reference frame [34]. In these equations, the convention adopted for the signs of the voltages and currents are that v is the impressed voltage at the terminals and that the direction of positive current i corresponds to generation. The sign of the currents in the equivalent damper windings is taken positive when they flow in a direction similar to that of the positive field current.

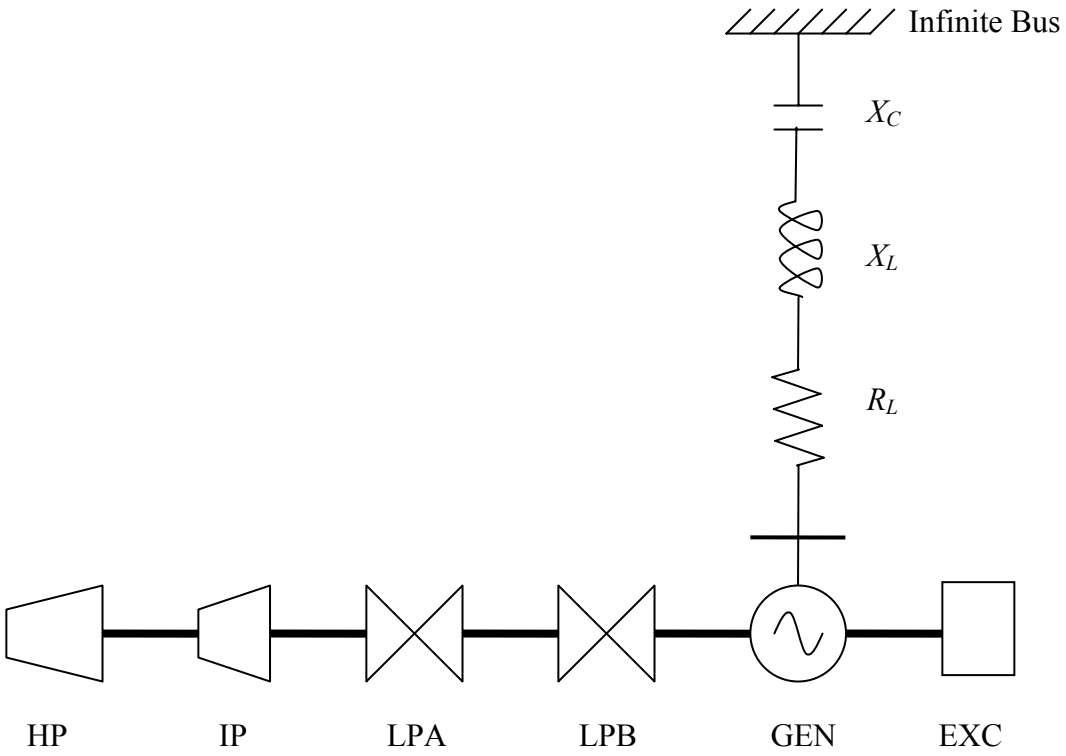

Figure 2.1 The IEEE first benchmark model for computer simulation of subsynchronous resonance.

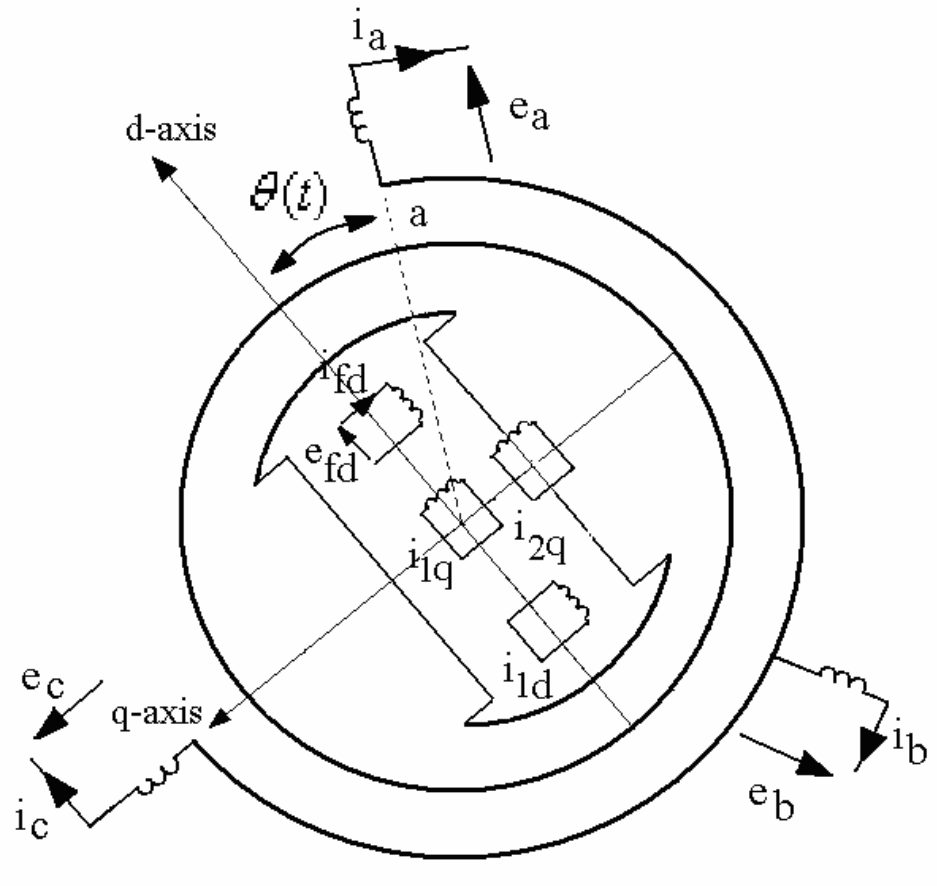

a, b, c: Stator three-phase winding

fd: Field (excitation) winding

e_{fd}: Field voltage

1d: d-axis damper winding

1q: The first q-axis damper winding

2q: The second q-axis damper winding

$\theta(t)$: Angle by which the d-axis leads the magnetic axis of phase a winding, electrical rad.

Figure 2.2 Schematic diagram of a conventional synchronous machine.

With time t expressed in seconds, the angular velocity ω expressed in rad/s ($\omega_0 = 377 rad/\sec$) and the other quantities expressed in per unit, the stator equations become:

$$e_d = \frac{1}{\omega_0}\frac{d\Psi_d}{dt} - \frac{\omega}{\omega_0}\Psi_q - R_a i_d \tag{2.2}$$

$$e_q = \frac{1}{\omega_0}\frac{d\Psi_q}{dt} + \frac{\omega}{\omega_0}\Psi_d - R_a i_q \tag{2.3}$$

The rotor equations:

$$e_{fd} = \frac{1}{\omega_0}\frac{d\Psi_{fd}}{dt} + R_{fd} i_{fd} \tag{2.4}$$

$$0 = \frac{1}{\omega_0}\frac{d\Psi_{1d}}{dt} + R_{1d} i_{1d} \tag{2.5}$$

$$0 = \frac{1}{\omega_0}\frac{d\Psi_{1q}}{dt} + R_{1q} i_{1q} \tag{2.6}$$

$$0 = \frac{1}{\omega_0}\frac{d\Psi_{2q}}{dt} + R_{2q} i_{2q} \tag{2.7}$$

The stator flux linkage equations:

$$\Psi_d = -L_d i_d + L_{ad} i_{fd} + L_{ad} i_{1d} \tag{2.8}$$

$$\Psi_q = -L_q i_q + L_{aq} i_{1q} + L_{aq} i_{2q} \tag{2.9}$$

The rotor flux linkage equations:

$$\Psi_{fd} = L_{ffd} i_{fd} + L_{ad} i_{1d} - L_{ad} i_d \tag{2.10}$$

$$\Psi_{1d} = L_{ad} i_{fd} + L_{11d} i_{fd} - L_{ad} i_d \tag{2.11}$$

$$\Psi_{1q} = L_{11q} i_{1q} + L_{aq} i_{2q} - L_{aq} i_q \tag{2.12}$$

$$\Psi_{2q} = L_{aq} i_{1q} + L_{22q} i_{2q} - L_{aq} i_q \tag{2.13}$$

The air-gap torque equation:

$$T_e = \Psi_d i_q - \Psi_q i_d \tag{2.14}$$

The overall differential equations which describe the transient performance of the synchronous machine are given by the following matrix equation:

$$\left[\frac{dX_{syn}}{dt}\right] = \left[At_{syn}\right]\left[X_{syn}\right] + \left[Bt_{syn}\right]\begin{bmatrix} V_{td} \\ V_{tq} \\ e_{fd} \end{bmatrix} \tag{2.15}$$

where

$$\left[X_{syn}\right] = \begin{bmatrix} i_d & i_q & i_{fd} & i_{1q} & i_{1d} & i_{2q} \end{bmatrix}^T$$

$$\left[At_{syn}\right] = \left[L\right]^{-1}\left[Qt\right]$$

$$\left[Bt_{syn}\right] = \left[L\right]^{-1}\left[Rt\right]$$

$$\left[L\right] = \begin{bmatrix} -L_d & 0 & L_{ad} & 0 & L_{ad} & 0 \\ 0 & -L_q & 0 & L_{aq} & 0 & L_{aq} \\ -L_{ad} & 0 & L_{ffd} & 0 & L_{ad} & 0 \\ 0 & -L_{aq} & 0 & L_{11q} & 0 & L_{aq} \\ -L_{aq} & 0 & L_{ad} & 0 & L_{11d} & 0 \\ 0 & -L_{aq} & 0 & L_{aq} & 0 & L_{22q} \end{bmatrix} \tag{2.16}$$

$$\left[Qt\right] = \begin{bmatrix} \omega_0 R_a & -\omega L_q & 0 & \omega L_{aq} & 0 & \omega L_{aq} \\ \omega L_d & \omega_0 R_a & -\omega L_{ad} & 0 & -\omega L_{ad} & 0 \\ 0 & 0 & -\omega_0 R_{fd} & 0 & 0 & 0 \\ 0 & 0 & 0 & -\omega_0 R_{1q} & 0 & 0 \\ 0 & 0 & 0 & 0 & -\omega_0 R_{1d} & 0 \\ 0 & 0 & 0 & 0 & 0 & -\omega_0 R_{2q} \end{bmatrix}$$

$$\left[Rt\right] = \begin{bmatrix} \omega_0 & 0 & 0 \\ 0 & \omega_0 & 0 \\ 0 & 0 & \omega_0 \\ 0 & 0 & 0 \\ 0 & 0 & 0 \\ 0 & 0 & 0 \end{bmatrix}$$

here, the superscript ^{T} means matrix transpose.

Linearized and rearranged Equation (2.15) is written as

$$\left[\frac{d\Delta X_{syn}}{dt}\right] = \left[A_{syn}\right]\left[\Delta X_{syn}\right] + \left[B_{syn}\right]\left[\Delta U_{syn}\right] \tag{2.17}$$

where

$$\left[\Delta X_{syn}\right] = \left[\Delta i_d \quad \Delta i_q \quad \Delta i_{fd} \quad \Delta i_{1q} \quad \Delta i_{1d} \quad \Delta i_{2q}\right]^T$$

$$\left[\Delta U_{syn}\right] = \left[\Delta V_{td} \quad \Delta V_{tq} \quad \Delta e_{fd} \quad \Delta\omega\right]^T$$

$$\left[A_{syn}\right] = \left[L\right]^{-1}\left[Q\right]$$

$$\left[B_{syn}\right] = \left[L\right]^{-1}\left[R\right]$$

$[L]$: same as in Equation (2.16) (2.18)

$$\left[Q\right] = \omega_0 \begin{bmatrix} R_a & -L_q & 0 & L_{aq} & 0 & L_{aq} \\ L_d & R_a & -L_{ad} & 0 & -L_{ad} & 0 \\ 0 & 0 & -R_{fd} & 0 & 0 & 0 \\ 0 & 0 & 0 & -R_{1q} & 0 & 0 \\ 0 & 0 & 0 & 0 & -R_{1d} & 0 \\ 0 & 0 & 0 & 0 & 0 & -R_{2q} \end{bmatrix}$$

$$\left[R\right] = \begin{bmatrix} \omega_0 & 0 & 0 & \Psi_{q0} \\ 0 & \omega_0 & 0 & -\Psi_{d0} \\ 0 & 0 & \omega_0 & 0 \\ 0 & 0 & 0 & 0 \\ 0 & 0 & 0 & 0 \\ 0 & 0 & 0 & 0 \end{bmatrix}$$

2.4.2 Modeling of the Transmission Line

A series capacitor-compensated transmission line [22,37] may be represented by the *RLC* circuit shown in Figure 2.3. In the voltage phasor diagram shown in Figure 2.4, the rotor angle δ is the angle (in elec. Rad) by which the q-axis leads the reference voltage V_b. The differential equations for the circuit elements, after applying Park's

transformation [34], can be expressed in the d-q reference frame by the following matrix expressions.

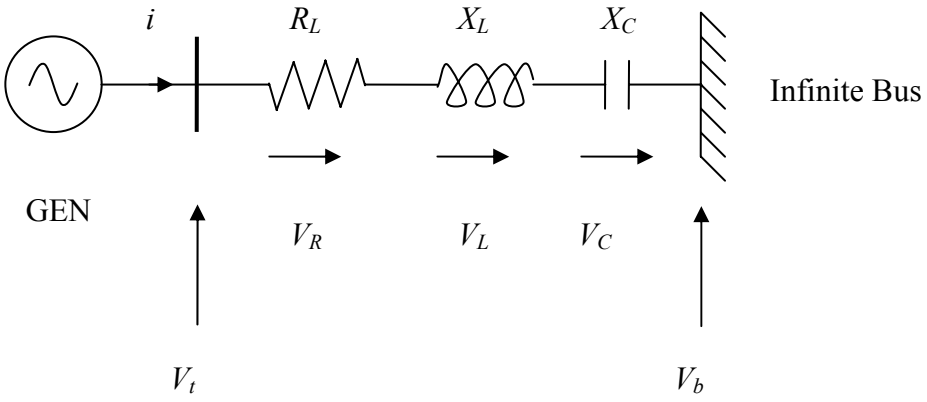

Figure 2.3 A series capacitor-compensated transmission line.

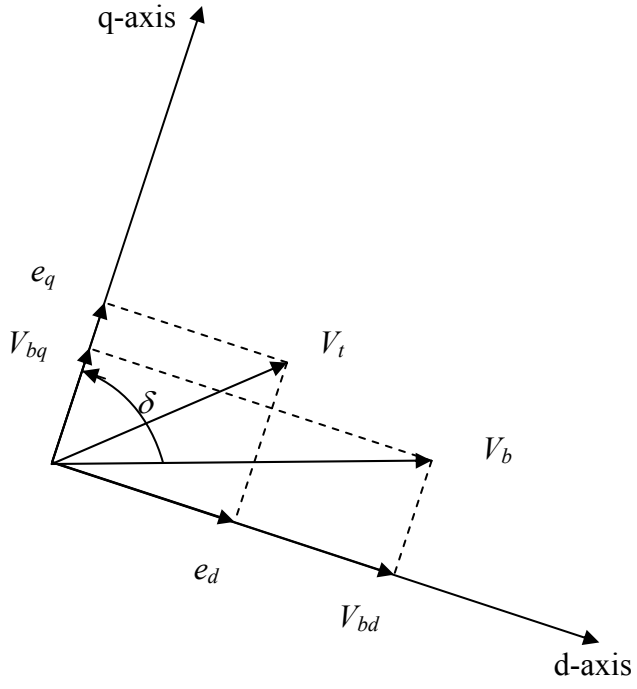

Figure 2.4 Voltage phasor diagram.

The voltage across the resistance:

$$\begin{bmatrix} V_{Rd} \\ V_{Rq} \end{bmatrix} = \begin{bmatrix} R_L & 0 \\ 0 & R_L \end{bmatrix} \begin{bmatrix} i_d \\ i_q \end{bmatrix} \tag{2.19}$$

The voltage across the inductance:

$$\begin{bmatrix} V_{Ld} \\ V_{Lq} \end{bmatrix} = \begin{bmatrix} 0 & -\frac{\omega}{\omega_0} X_L \\ \frac{\omega}{\omega_0} X_L & 0 \end{bmatrix} \begin{bmatrix} i_d \\ i_q \end{bmatrix} + \begin{bmatrix} \frac{X_L}{\omega_0} & 0 \\ 0 & \frac{X_L}{\omega_0} \end{bmatrix} \begin{bmatrix} \frac{di_d}{dt} \\ \frac{di_q}{dt} \end{bmatrix} \tag{2.20}$$

The voltage across the capacitor:

$$\begin{bmatrix} \frac{dV_{Cd}}{dt} \\ \frac{dV_{Cq}}{dt} \end{bmatrix} = \begin{bmatrix} \omega_0 X_C & 0 \\ 0 & \omega_0 X_C \end{bmatrix} \begin{bmatrix} i_d \\ i_q \end{bmatrix} + \begin{bmatrix} 0 & \omega \\ -\omega & 0 \end{bmatrix} \begin{bmatrix} V_{Cd} \\ V_{Cq} \end{bmatrix} \tag{2.21}$$

The overall equations of the transmission line can be written as

$$\begin{bmatrix} \frac{dV_{Cd}}{dt} \\ \frac{dV_{Cq}}{dt} \\ V_{td} \\ V_{tq} \end{bmatrix} = [Att] \begin{bmatrix} V_{Cd} \\ V_{Cq} \end{bmatrix} + [Rt1] \begin{bmatrix} \frac{di_d}{dt} \\ \frac{di_q}{dt} \end{bmatrix} + [Rt2] \begin{bmatrix} i_d \\ i_q \end{bmatrix} + [Btt][V_b] \tag{2.22}$$

where

$$[Att] = \begin{bmatrix} 0 & \omega \\ -\omega & 0 \\ 1 & 0 \\ 0 & 1 \end{bmatrix}$$

$$[Rt1] = \begin{bmatrix} 0 & 0 \\ 0 & 0 \\ \frac{X_L}{\omega_0} & 0 \\ 0 & \frac{X_L}{\omega_0} \end{bmatrix}$$

$$[Rt2]=\begin{bmatrix} \omega_0 X_C & 0 \\ 0 & \omega_0 X_C \\ R_L & -\dfrac{\omega}{\omega_0} X_L \\ \dfrac{\omega}{\omega_0} X_L & R_L \end{bmatrix} \tag{2.23}$$

$$[Btt]=\begin{bmatrix} 0 \\ 0 \\ \sin\delta \\ \cos\delta \end{bmatrix}$$

The linearized form of Equation (2.22) is given by

$$\begin{bmatrix} \dfrac{d\Delta V_{Cd}}{dt} \\ \dfrac{d\Delta V_{Cq}}{dt} \\ \Delta V_{td} \\ \Delta V_{tq} \end{bmatrix} = [At]\begin{bmatrix} \Delta V_{Cd} \\ \Delta V_{Cq} \end{bmatrix} + [R1]\begin{bmatrix} \dfrac{d\Delta i_d}{dt} \\ \dfrac{d\Delta i_q}{dt} \end{bmatrix} + [R2]\begin{bmatrix} \Delta i_d \\ \Delta i_q \end{bmatrix} + [Bt]\begin{bmatrix} \Delta\omega \\ \Delta\delta \end{bmatrix} \tag{2.24}$$

where

$$[At]=\begin{bmatrix} 0 & \omega_0 \\ -\omega_0 & 0 \\ 1 & 0 \\ 0 & 1 \end{bmatrix}$$

$$[R1]=\begin{bmatrix} 0 & 0 \\ 0 & 0 \\ \dfrac{X_L}{\omega_0} & 0 \\ 0 & \dfrac{X_L}{\omega_0} \end{bmatrix}$$

$$[R2]=\begin{bmatrix} \omega_0 X_C & 0 \\ 0 & \omega_0 X_C \\ R_L & -X_L \\ X_L & R_L \end{bmatrix} \tag{2.25}$$

$$[Bt] = \begin{bmatrix} V_{Cq0} & 0 \\ -V_{Cd0} & 0 \\ -\dfrac{X_L}{\omega_0} i_{q0} & V_{bq0} \\ \dfrac{X_L}{\omega_0} i_{d0} & V_{bd0} \end{bmatrix}$$

2.4.3 Modeling of the Turbine-Generator Mechanical System

The turbine-generator mechanical system [22,34], shown in Figure 2.5, consists of a high-pressure turbine (HP), an intermediate-pressure turbine (IP), two low-pressure turbines (LPA & LPB), the generator rotor (GEN) and the exciter (EXC). They together constitute a linear six-mass-spring system.

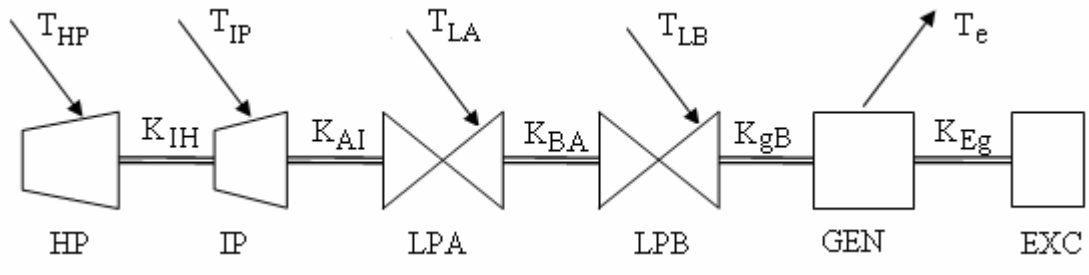

Figure 2.5 Structure of a typical six-mass shaft system model.

Assuming that M is the inertia constant in seconds, D is the damping coefficient in p.u. torque/p.u. speed for each rotating mass and K is a stiffness in p.u. torque/rad for each shaft section, the equations of the i^{th} mass of an N-mass spring system shown in Figure 2.6 are given by

$$\frac{M_i}{\omega_0}\frac{d\omega_i}{dt} = T_i + K_{i-1,i}(\delta_{i-1} - \delta_i) - K_{i,i+1}(\delta_i - \delta_{i+1}) - \frac{D_i}{\omega_0}(\omega_i - \omega_0) \tag{2.26}$$

$$\frac{d\delta_i}{dt} = \omega_i - \omega_0 \tag{2.27}$$

where

$$K_{i-1,i}\Big|_{i=1} = 0, \qquad K_{i,i+1}\Big|_{i=N} = 0, \qquad i = 1, 2, ..., N \tag{2.28}$$

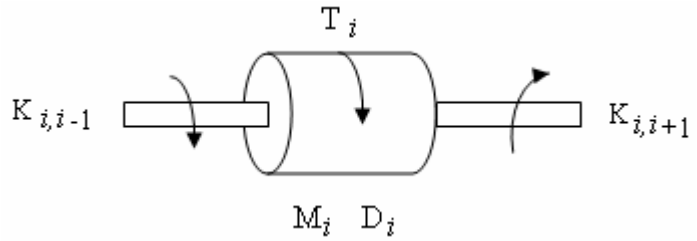

Figure 2.6 The i[th] mass of an N-mass spring system.

When Equations (2.26) to (2.28) are applied to the linear six-mass-spring system of Figure 2.5, the shaft system equations are written as:

$$\frac{M_E}{\omega_0}\frac{d\omega_E}{dt} = K_{Eg}(\delta - \delta_E) - \frac{D_E}{\omega_0}(\omega_E - \omega_0)$$

$$\frac{d\delta_E}{dt} = \omega_E - \omega_0$$

$$\frac{M_g}{\omega_0}\frac{d\omega}{dt} = -T_e + K_{gB}(\delta_B - \delta) - K_{Eg}(\delta - \delta_E) - \frac{D_g}{\omega_0}(\omega - \omega_0)$$

$$\frac{d\delta}{dt} = \omega - \omega_0$$

$$\frac{M_B}{\omega_0}\frac{d\omega_B}{dt} = \frac{\omega_0}{\omega_B}P_A + K_{BA}(\delta_A - \delta_B) - K_{gB}(\delta_B - \delta) - \frac{D_B}{\omega_0}(\omega_B - \omega_0)$$

$$\frac{d\delta_B}{dt} = \omega_B - \omega_0 \tag{2.29}$$

$$\frac{M_A}{\omega_0}\frac{d\omega_A}{dt} = \frac{\omega_0}{\omega_A}P_A + K_{AI}(\delta_I - \delta_A) - K_{BA}(\delta_A - \delta_B) - \frac{D_A}{\omega_0}(\omega_A - \omega_0)$$

$$\frac{d\delta_A}{dt} = \omega_A - \omega_0$$

$$\frac{M_I}{\omega_0}\frac{d\omega_I}{dt} = \frac{\omega_0}{\omega_I}P_I + K_{IH}(\delta_H - \delta_I) - K_{AI}(\delta_I - \delta_A) - \frac{D_I}{\omega_0}(\omega_I - \omega_0)$$

$$\frac{d\delta_I}{dt} = \omega_I - \omega_0$$

$$\frac{M_H}{\omega_0}\frac{d\omega_H}{dt} = \frac{\omega_0}{\omega_H}P_H - K_{IH}(\delta_H - \delta_I) - \frac{D_H}{\omega_0}(\omega_H - \omega_0)$$

$$\frac{d\delta_H}{dt} = \omega_H - \omega_0$$

The overall shaft equations are given by the following matrix equation

$$\left[\frac{dX_{ms}}{dt}\right] = [At_{ms}][X_{ms}] + [Bt_{ms}][U_{tms}] \tag{2.30}$$

where

$$[X_{ms}] = [\delta_E \quad \delta \quad \delta_B \quad \delta_A \quad \delta_I \quad \delta_H \quad \omega_E \quad \omega \quad \omega_B \quad \omega_A \quad \omega_I \quad \omega_H]^T$$

$$[U_{tms}] = [\omega_0 \quad P_H \quad P_I \quad P_A \quad T_e]^T$$

$$[At_{ms}] = \begin{bmatrix} 0_{6x6} & I_{6x6} \\ As1 & As2 \end{bmatrix}$$

$$[As1] = \omega_0 \begin{bmatrix} -\frac{K_{Eg}}{M_E} & \frac{K_{Eg}}{M_E} & 0 & 0 & 0 & 0 \\ \frac{K_{Eg}}{M_g} & -\frac{K_{gB}+K_{Eg}}{M_g} & \frac{K_{gB}}{M_g} & 0 & 0 & 0 \\ 0 & \frac{K_{gB}}{M_B} & -\frac{K_{BA}+K_{gB}}{M_B} & \frac{K_{gB}}{M_B} & 0 & 0 \\ 0 & 0 & \frac{K_{BA}}{M_A} & -\frac{K_{AI}+K_{BA}}{M_A} & \frac{K_{AI}}{M_A} & 0 \\ 0 & 0 & 0 & \frac{K_{AI}}{M_I} & -\frac{K_{HI}+K_{AI}}{M_I} & \frac{K_{HI}}{M_I} \\ 0 & 0 & 0 & 0 & \frac{K_{HI}}{M_H} & -\frac{K_{HI}}{M_H} \end{bmatrix}$$

$$[As2]=\begin{bmatrix} -\frac{D_E}{M_E} & 0 & 0 & 0 & 0 & 0 \\ 0 & -\frac{D_g}{M_g} & 0 & 0 & 0 & 0 \\ 0 & 0 & -\frac{D_B}{M_B} & 0 & 0 & 0 \\ 0 & 0 & 0 & -\frac{D_A}{M_A} & 0 & 0 \\ 0 & 0 & 0 & 0 & -\frac{D_I}{M_I} & 0 \\ 0 & 0 & 0 & 0 & 0 & -\frac{D_H}{M_H} \end{bmatrix} \tag{2.31}$$

$$[Bt_{ms}]=\begin{bmatrix} -1_{6x1} & 0_{6x1} & 0_{6x1} & 0_{6x1} & 0_{6x1} \\ \frac{D_E}{M_E} & 0 & 0 & 0 & 0 \\ \frac{D_g}{M_g} & 0 & 0 & 0 & -\frac{\omega_0}{M_g} \\ \frac{D_B}{M_B} & 0 & 0 & \frac{\omega_0^{\,2}}{\omega_B M_B} & 0 \\ \frac{D_A}{M_A} & 0 & 0 & \frac{\omega_0^{\,2}}{\omega_A M_A} & 0 \\ \frac{D_I}{M_I} & 0 & \frac{\omega_0^{\,2}}{\omega_I M_I} & 0 & 0 \\ \frac{D_H}{M_H} & \frac{\omega_0^{\,2}}{\omega_H M_H} & 0 & 0 & 0 \end{bmatrix}$$

Here, the $[\boldsymbol{I}_{nxn}]$ is an *n* by *n* identity matrix, 0_{mxn} is an *m* by *n* matrix with all elements zero, and -1_{6x1} is a 6 by 1 matrix with all elements -1.

Linearzing and rearranging Equation (2.30) yields to

$$\left[\frac{d\Delta X_{ms}}{dt}\right]=[A_{ms}][\Delta X_{ms}]+[B_{ms}][\Delta U_{ms}] \tag{2.32}$$

where

$$[\Delta X_{ms}]=[\Delta\delta_E \quad \Delta\delta \quad \Delta\delta_B \quad \Delta\delta_A \quad \Delta\delta_I \quad \Delta\delta_H \quad \Delta\omega_E \quad \Delta\omega \quad \Delta\omega_B \quad \Delta\omega_A \quad \Delta\omega_I \quad \Delta\omega_H]^T$$
$$[\Delta U_{ms}]=[\Delta T_e \quad \Delta P_H \quad \Delta P_I \quad \Delta P_A]^T$$

$$[A_{ms}] = \begin{bmatrix} 0_{6x6} & I_{6x6} \\ As21 & As22 \end{bmatrix}$$

[$As21$] is the same with [$As1$] in Equation (2.31) (2.33)

$$[As22] = \begin{bmatrix} -\frac{D_E}{M_E} & 0 & 0 & 0 & 0 & 0 \\ 0 & -\frac{D_g}{M_g} & 0 & 0 & 0 & 0 \\ 0 & 0 & -\frac{T_{m0}F_B + D_B}{M_B} & 0 & 0 & 0 \\ 0 & 0 & 0 & -\frac{T_{m0}F_A + D_A}{M_A} & 0 & 0 \\ 0 & 0 & 0 & 0 & -\frac{T_{m0}F_I + D_I}{M_I} & 0 \\ 0 & 0 & 0 & 0 & 0 & -\frac{T_{m0}F_H + D_H}{M_H} \end{bmatrix}$$

$$[B_{ms}] = \omega_0 \begin{bmatrix} 0_{7x1} & 0_{7x1} & 0_{7x1} & 0_{7x1} \\ -\frac{1}{M_g} & 0 & 0 & 0 \\ 0 & 0 & 0 & \frac{1}{M_B} \\ 0 & 0 & 0 & \frac{1}{M_A} \\ 0 & 0 & \frac{1}{M_I} & 0 \\ 0 & \frac{1}{M_H} & 0 & 0 \end{bmatrix}$$

2.4.4 Governor and Turbine System

The block diagram of the four-stage turbine and the associated electro-hydraulic governor [38] is shown in Figure 2.7. The corresponding data are given in Appendix B.

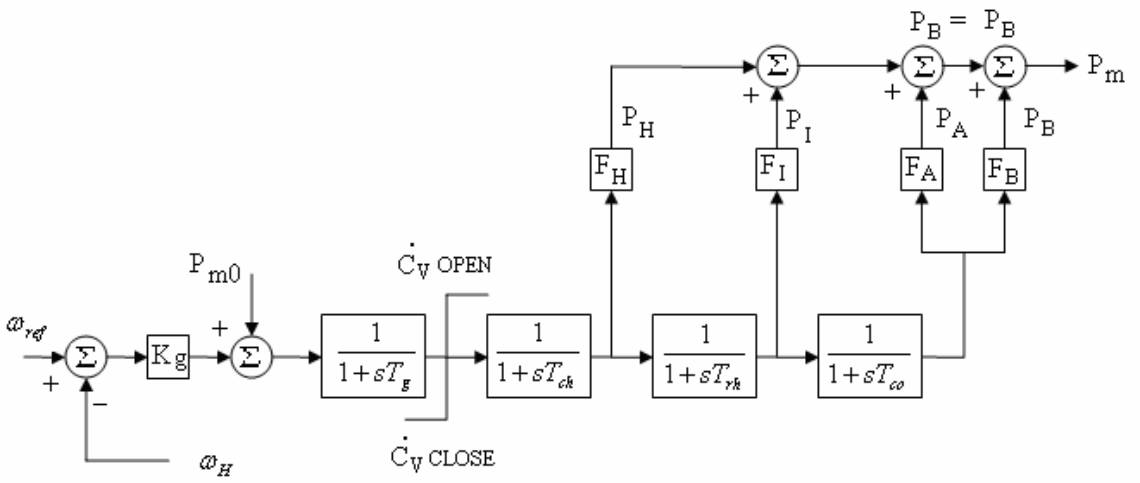

Figure 2.7 Block diagram of the governor and the turbine.

The corresponding state-space equation can be derived from the block diagram and is given by

$$\left[\frac{dX_g}{dt}\right] = \left[At_g\right]\left[X_g\right] + \left[Bt_g\right]\begin{bmatrix}\omega_0 \\ P_{m0} \\ \omega_H\end{bmatrix} \tag{2.34}$$

where

$$\left[X_g\right] = \begin{bmatrix}C_V & P_H & P_I & P_A\end{bmatrix}^T$$

$$\left[At_g\right] = \begin{bmatrix} -\frac{1}{T_g} & 0 & 0 & 0 \\ \frac{F_H}{T_{ch}} & -\frac{1}{T_{ch}} & 0 & 0 \\ 0 & \frac{F_I}{F_H T_{rh}} & -\frac{1}{T_{rh}} & 0 \\ 0 & 0 & \frac{F_A}{F_I T_{co}} & -\frac{1}{T_{co}} \end{bmatrix} \tag{2.35}$$

$$\left[Bt_g\right] = \begin{bmatrix} \frac{K_g}{T_g\omega_0} & \frac{1}{T_g} & -\frac{K_g}{T_g\omega_0} \\ 0 & 0 & 0 \\ 0 & 0 & 0 \\ 0 & 0 & 0 \end{bmatrix}$$

The linearized form of Equation (2.34) is given by

$$\left[\frac{d\Delta X_g}{dt}\right] = [A_g][\Delta X_g] + [B_g]\begin{bmatrix}\Delta P_{m0}\\ \Delta\omega_H\end{bmatrix} \tag{2.36}$$

where

$$[\Delta X_g] = [\Delta C_V \quad \Delta P_H \quad \Delta P_I \quad \Delta P_A]^T$$

$$[A_g] = \begin{bmatrix} -\frac{1}{T_g} & 0 & 0 & 0 \\ \frac{F_H}{T_{ch}} & -\frac{1}{T_{ch}} & 0 & 0 \\ 0 & \frac{F_I}{F_H T_{rh}} & -\frac{1}{T_{rh}} & 0 \\ 0 & 0 & \frac{F_A}{F_I T_{co}} & -\frac{1}{T_{co}} \end{bmatrix} \tag{2.37}$$

$$[B_g] = \begin{bmatrix} \frac{1}{T_g} & -\frac{K_g}{T_g\omega_0} \\ 0 & 0 \\ 0 & 0 \\ 0 & 0 \end{bmatrix}$$

2.4.5 Excitation System

The block diagram representation of the excitation system used in this study [22,34] is shown in Figure 2.8, and the corresponding data are given in Appendix B.

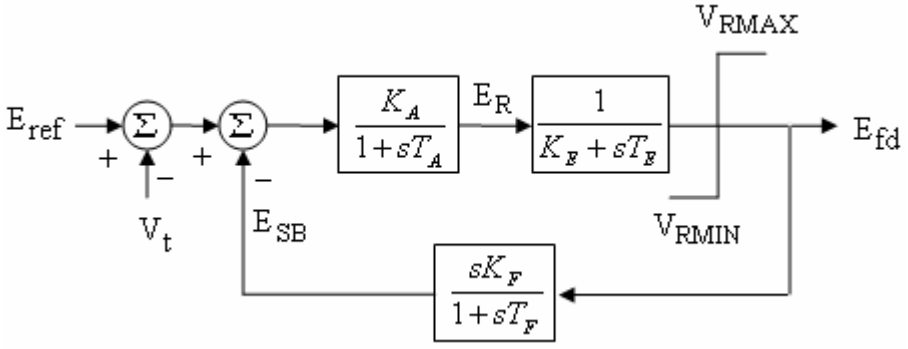

Figure 2.8 Block diagram of the excitation system.

Utilizing the relationship between the excitation system output voltage and the field voltage given by $E_{fd} = \frac{L_{ad}}{R_{fd}} e_{fd}$, the state-space equation of the excitation system can be derived from its block diagram and is given by

$$\left[\frac{dX_v}{dt}\right] = [At_v][X_v] + [Bt_v]\begin{bmatrix} V_t \\ E_{ref} \end{bmatrix} \tag{2.38}$$

where

$$[X_v] = \begin{bmatrix} e_{fd} & E_R & E_{SB} \end{bmatrix}^T$$

$$[At_v] = \begin{bmatrix} -\frac{K_E}{T_E} & \frac{1}{T_E}\frac{R_{fd}}{L_{ad}} & 0 \\ 0 & -\frac{1}{T_A} & -\frac{K_A}{T_A} \\ -\frac{K_E K_F}{T_E T_F}\frac{L_{ad}}{R_{fd}} & \frac{K_F}{T_F T_E} & -\frac{1}{T_F} \end{bmatrix} \tag{2.39}$$

$$[Bt_v] = \begin{bmatrix} 0 & 0 \\ -\frac{K_A}{T_A} & \frac{K_A}{T_A} \\ 0 & 0 \end{bmatrix}$$

Linearized Equation (2.38) is written as

$$\left[\frac{d\Delta X_v}{dt}\right] = [A_v][\Delta X_v] + [B_v]\begin{bmatrix} \Delta V_t \\ \Delta E_{ref} \end{bmatrix} \tag{2.40}$$

where

$$[\Delta X_v] = \begin{bmatrix} \Delta e_{fd} & \Delta E_R & \Delta E_{SB} \end{bmatrix}^T$$

$$[A_v] = \begin{bmatrix} -\frac{K_E}{T_E} & \frac{1}{T_E}\frac{R_{fd}}{L_{ad}} & 0 \\ 0 & -\frac{1}{T_A} & -\frac{K_A}{T_A} \\ -\frac{K_E K_F}{T_E T_F}\frac{L_{ad}}{R_{fd}} & \frac{K_F}{T_F T_E} & -\frac{1}{T_F} \end{bmatrix} \tag{2.41}$$

$$[Bt_v] = \begin{bmatrix} 0 & 0 \\ -\frac{K_A}{T_A} & \frac{K_A}{T_A} \\ 0 & 0 \end{bmatrix}$$

2.5 Small Signal Model of A Single Machine Infinite Bus System

The overall model of the system under study can be derived by performing the following mathematical manipulations for the interactions among the various components of the system [37].

The electrical parts of the system: combining Equations (2.17) and (2.24) to form the following equations

$$\begin{bmatrix} \frac{d\Delta X_{syn}}{dt} \\ \frac{d\Delta V_{Cd}}{dt} \\ \frac{d\Delta V_{Cq}}{dt} \end{bmatrix} = [Amt] \begin{bmatrix} \Delta X_{syn} \\ \Delta V_{Cd} \\ \Delta V_{Cq} \end{bmatrix} + [Bmt] \begin{bmatrix} \Delta e_{fd} \\ \Delta\omega \\ \Delta\delta \end{bmatrix} \tag{2.42}$$

$$\begin{bmatrix} \Delta V_{td} \\ \Delta V_{tq} \end{bmatrix} = [Ci] \begin{bmatrix} \Delta X_{syn} \\ \Delta V_{Cd} \\ \Delta V_{Cq} \end{bmatrix} + [Di] \begin{bmatrix} \Delta e_{fd} \\ \Delta\omega \\ \Delta\delta \end{bmatrix} \tag{2.43}$$

The mechanical parts of the system: combining Equations (2.32), (2.36), and (2.40) to form the following equations

$$\begin{bmatrix} \frac{d\Delta X_{ms}}{dt} \\ \frac{d\Delta X_{g}}{dt} \\ \frac{d\Delta X_{v}}{dt} \end{bmatrix} = [Ap1] \begin{bmatrix} \Delta X_{ms} \\ \Delta X_{g} \\ \Delta X_{v} \end{bmatrix} + [Ap2] \begin{bmatrix} \Delta T_e \\ \Delta V_t \end{bmatrix} + [Bp] \begin{bmatrix} \Delta P_{m0} \\ \Delta E_{ref} \end{bmatrix} \tag{2.44}$$

There are, however, two non-state variables ΔT_e and ΔV_t that must be eliminated.

The linearized form of the air-gap torque Equation (2.14) is given by

$$\Delta T_e = [Tedq0][\Delta X_{syn}] \tag{2.45}$$

where

$$[Tedq0] = \begin{bmatrix} i_{q0}(L_q - L_d) & i_{d0}(L_q - L_d) + i_{fd0}L_{ad} & i_{q0}L_{ad} & -i_{d0}L_{aq} & i_{q0}L_{ad} & -i_{d0}L_{aq} \end{bmatrix} \tag{2.46}$$

The linearized terminal voltage equation $V_t^{\,2} = V_{td}^{\,2} + V_{tq}^{\,2}$ is given by

$$\Delta V_t = \begin{bmatrix} \frac{V_{td0}}{V_{t0}} & \frac{V_{tq0}}{V_{t0}} \end{bmatrix} \begin{bmatrix} \Delta V_{td} \\ \Delta V_{tq} \end{bmatrix} \tag{2.47}$$

Combining Equations (2.43), (2.45), and (2.47) to form the following equation

$$\begin{bmatrix} \Delta T_e \\ \Delta V_t \end{bmatrix} = [Cmt] \begin{bmatrix} \Delta X_{syn} \\ \Delta V_{Cd} \\ \Delta V_{Cq} \end{bmatrix} + [Dmt] \begin{bmatrix} \Delta e_{fd} \\ \Delta \omega \\ \Delta \delta \end{bmatrix} \tag{2.48}$$

The overall system equations derived by combining Equation (2.42), (2.44), and (2.48) are written by

$$\left[\frac{d\Delta X}{dt}\right] = [A][\Delta X] + [B][\Delta U] \tag{2.49}$$

where

$$\begin{aligned} [\Delta X] = [&\Delta\delta_E \quad \Delta\delta \quad \Delta\delta_B \quad \Delta\delta_A \quad \Delta\delta_I \quad \Delta\delta_H \quad \Delta\omega_E \quad \Delta\omega \quad \Delta\omega_B \ldots \\ &\Delta\omega_A \quad \Delta\omega_I \quad \Delta\omega_H \quad \Delta C_v \quad \Delta P_H \quad \Delta P_I \quad \Delta P_A \quad \Delta e_{fd} \quad \Delta E_R \quad \Delta E_{SB} \ldots \\ &\Delta i_d \quad \Delta i_q \quad \Delta i_{fd} \quad \Delta i_{1q} \quad \Delta i_{1d} \quad \Delta i_{2q} \quad \Delta V_{Cd} \quad \Delta V_{Cq}]^T \end{aligned}$$

$$[\Delta U] = \begin{bmatrix} \Delta P_{m0} & \Delta E_{ref} \end{bmatrix}^T \tag{2.50}$$

The complete electrical and mechanical model of a one-machine, infinite-bus system for SSR study is a 27th order system.

The detail manipulations for forming the overall system equations are shown in Appendix C.

2.6 Effect of Series Capacitor Compensation on SSR

The six-mass model of the turbine-generator shaft system shown in Figure 2.5 has five torsional modes in addition to the rigid body mode (mode 0). Figure 2.9 shows the natural frequencies and mode shapes of such a system. In this figure, the torsional modes are numbered sequentially according to mode frequency and number of phase reversals in the mode shape. Mode 0, thus, signifies that the six masses oscillate in unison without a shaft twist and Mode N has the N^{th} lowest frequency and a mode shape with N phase reversals. The total number of modes including Mode 0 is equal to the number of inertial elements in the spring-mass model.

The negative damping (undamping) due to the torsional interaction for the turbine-generator is evaluated using eigenvalue analysis by varying the degree of series compensation from to 0 to 100%. The results of this variation in compensation are shown in Figure 2.10. These results are obtained by calculating the eigenvalues for the coupled electrical and mechanical system (overall system model). The electrical system is varied by "sweeping" the series compensation from 0 to 100% in 1% steps. It is worth noting here that the percentage compensation is defined as

$$\%\ compensation = \frac{X_C}{X_L} \times 100 \tag{2.51}$$

The system eigenvalues for the critical compensation levels are given in Table 2.1.

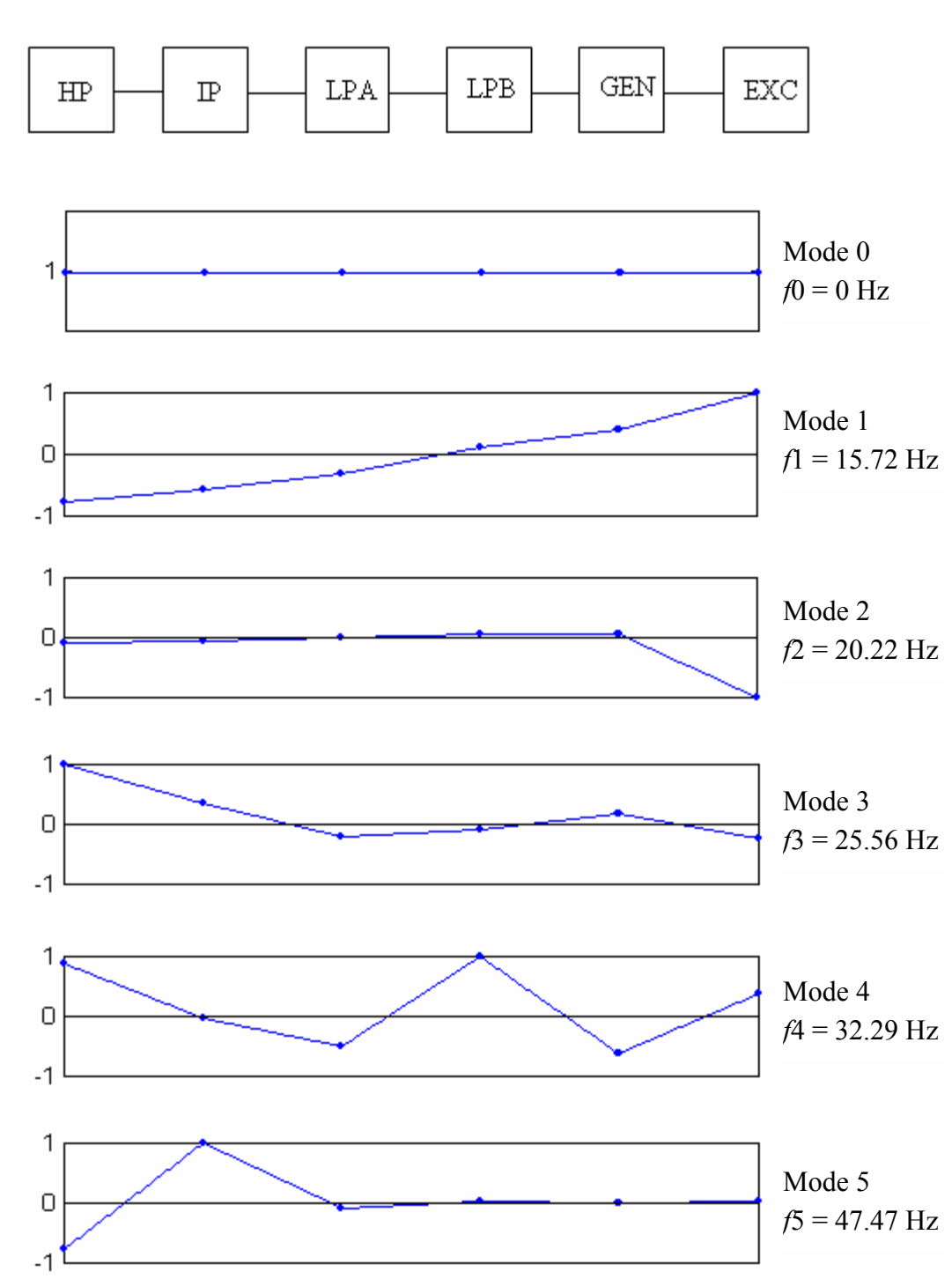

Figure 2.9 Natural frequencies and mode shapes of the turbine-generator shaft system.

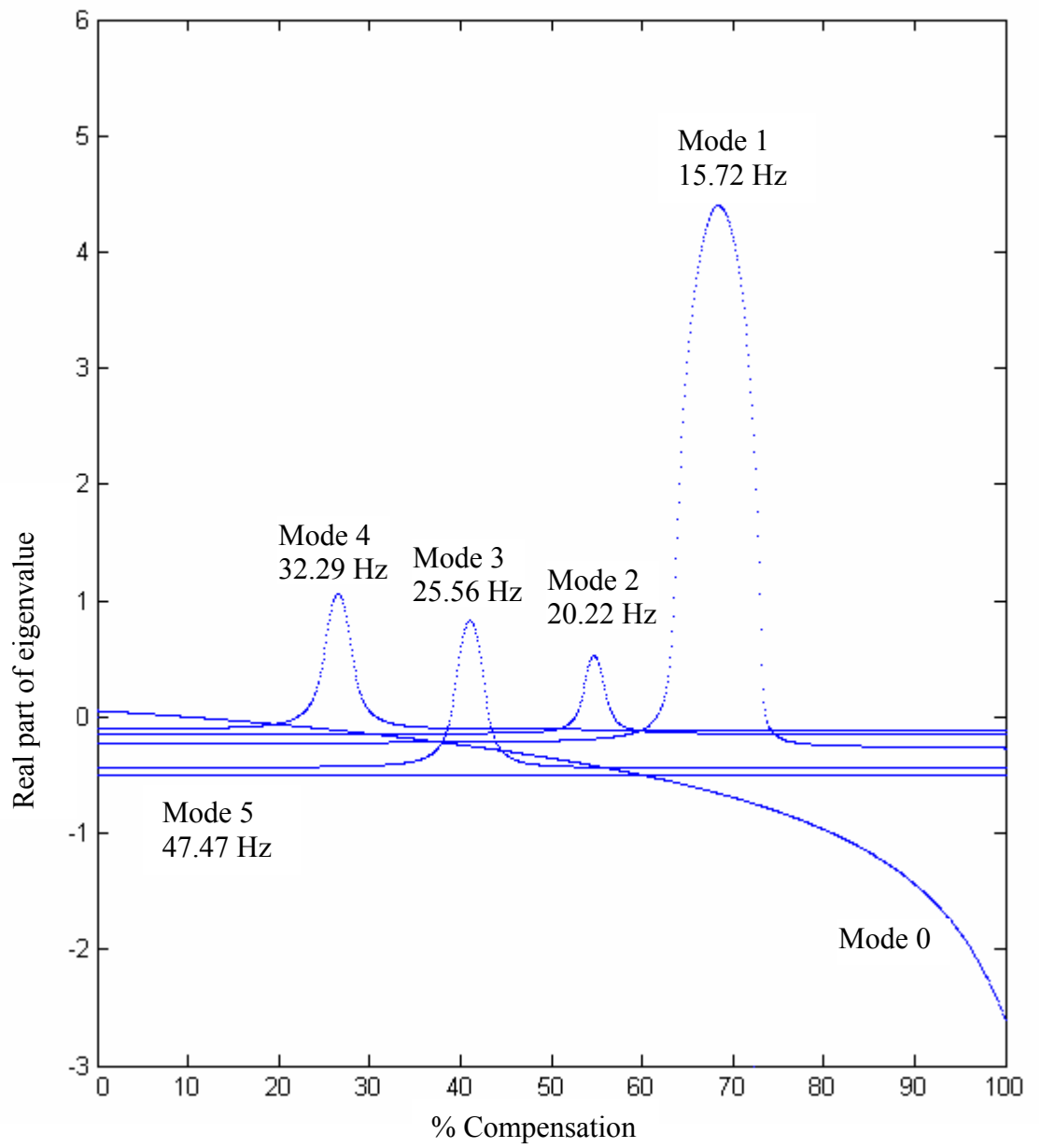

Figure 2.10 The real part of SSR mode eigenvalues as a function of the percentage compensation ($S = 0.90 - j0.392$ p.u.).

Table 2.1 Eigenvalues of SSR modes (Mode 1-5), rigid body mode (Mode 0), electrical mode and the other modes ($S = 0.90 - j0.392$ p.u.).

Modes	% Compensation Level			
	26.5%	41.1%	54.7%	68.4%
Mode 5	-0.4955 ± j298.28	-0.4955 ± j298.28	-0.4955 ± j298.28	-0.4955 ± j298.28
Mode 4	**1.0640 ± j202.95**	-0.1012 ± j202.83	-0.1074 ± j202.90	-0.1090 ± j202.94
Mode 3	-0.4262 ± j160.75	**0.8283 ± j160.58**	-0.4323 ± j160.5	-0.4385 ± j160.58
Mode 2	-0.1430 ± j127.06	-0.1405 ± j127.09	**0.5257 ± j127.05**	-0.1411 ± j126.99
Mode 1	-0.2205 ± j99.20	-0.2163 ± j99.39	-0.1887 ± j99.91	**4.3989 ± j98.93**
Mode 0	-0.1146 ± j8.31	-0.2508 ± j9.18	-0.4189 ± j10.21	-0.6569 ± j11.55
Elec.	**-5.0370 ± j203.06**	**-4.3126 ± j160.53**	**-2.8155 ± j127.02**	**-5.5446 ± j98.78**
Other modes	-9970.3	-9970.3	-9970.2	-9970.2
	-6.0479 ±j550.85	-6.1458 ±j593.71	-6.2129 ±j627.11	-6.2668 ±j656.75
	-95.494	-95.841	-96.155	-96.372
	-32.669	-32.68	-32.677 ± j0.59	-33.203 ± j1.0
	-31.074	-31.833		
	-10.316	-10.295	-10.273	-10.247
	-5.4194	-6.0133	-6.7453	-7.7667
	-2.4406	-2.4433	-2.4508	-2.4604
	-1.3792 ± j0.86	-1.1202 ± j0.92	-0.87615 ± j0.91	-0.63387 ± j0.83
	-1.6613	-1.665	-1.6659	-1.6657
	-0.14205	-0.14216	-0.14225	-0.14232

Examining Figure 2.10 and Table 2.1 yields to the following observations:

- There are four unstable torsional modes (Modes 1, 2, 3, and 4). Each of these modes has its largest SSR interaction when the real part of its eigenvalue is a maximum.
- Mode 1 exhibits the most severe undamping with a peak at 68.5% series compensation.
- Mode 5 damping is seen to have a small constant negative value over the whole range of series compensation.
- The frequency of the electrical mode (capacitor) decreases with the increase of the compensation level, which is below the synchronous frequency and, therefore, may excite the torsional oscillation modes.
- The other eigenvalue modes listed in Table 2.1 are stable, like the generator windings, the excitation system, and the governor system and the turbine.

2.7 Summary

This chapter presented the investigations of the subsynchronous resonance phenomenon under small disturbances. These investigations are conducted on the IEEE first benchmark model which consists of a large turbine-generator connecting to an infinite bus system through a series capacitor compensated transmission line.

In order to develop the linear system model, the nonlinear differential equations of each component of the system are derived and then linearized. These set of linearized equations were grouped and mathematically manipulated in order to obtain the overall system model in a state-space form. The effect of the series capacitor compensation on SSR was investigated using eigenvalue analysis. The results of these investigations have provided the critical compensation levels in the system under investigations.

3 DAMPING SUBSYNCHRONOUS RESONANCE OSCILLATIONS UNDER LARGE DISTURBANCES USING A VSC HVDC BACK-TO-BACK SYSTEM

3.1 Introduction

As it has been mentioned in Chapter 1, the new generation of FACTS controllers based on VSCs can play a major role in the mitigation of the subsynchronous resonance torsional oscillations induced in the turbine-generator shaft system. SSR oscillations may be excited by small or large disturbances in the power system. SSR oscillations resulting from small (minute) disturbances are usually small. However, they can build up with time to large values causing shaft failure. On the other hand, large power system disturbances, such as short circuits, induce large growing SSR torsional oscillations in the turbine-generator shaft system. These oscillations may exceed the endurance limit of the turbine-generator shaft and, hence, cause a shaft fatigue in a period of a few seconds.

The VSC HVDC back-to-back system is a several million dollars FACTS controller. Therefore, it is uneconomical to install such a controller in the power system primarily for the purpose of damping SSR. An already existing VSC HVDC back-to-back system can be utilized, however, to damp SSR oscillations induced in a nearby turbine-generator.

This chapter presents the application of the VSC HVDC back-to-back system for damping subsynchronous resonance oscillations. In this context, the active power controller of such a system is used along with the generator speed deviation, as a supplementary signal, to design an integrated controller capable of damping SSR

oscillations. A digital time-domain simulation study case of the power system with the designed controllers during a three-phase fault is presented at the end of the chapter.

3.2 System under Study

The single line diagram of the HVAC/DC system under investigation in this thesis is shown in Figure 3.1. It consists of a turbine-generator which is connected via a transformer to a large AC system (System I) through a series capacitor compensated transmission line (Line 1). The VSC HVDC back-to-back system is located between the turbine-generator and another large AC system (System II). The rectifier station of the VSC HVDC system is connected to the generator bus through a transmission line (Line 2) while its inverter station is connected to System II through another transmission line (Line 3). The data of the system of Figure 3.1, excluding the VSC HVDC system, are the same as those of the IEEE first benchmark model given in Appendix B.

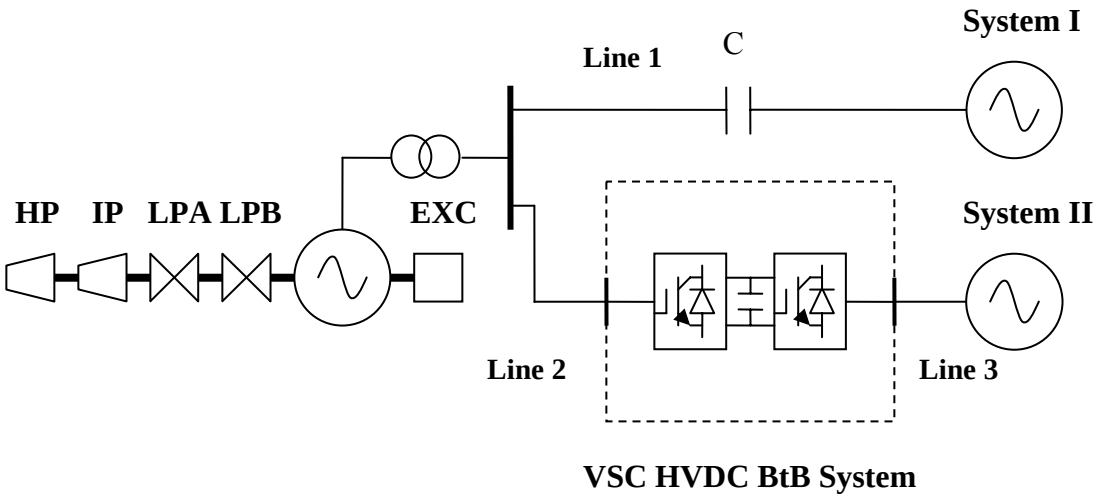

Figure 3.1 The HVAC/DC system under study.

In order to develop the mathematical model for the HVAC/DC system, the differential equations of the turbine-generator, the turbine-generator mechanical system and the series capacitor compensated transmission line given in Chapter 2 are used here again. The two large AC systems are represented simply as constant amplitude sinusoidal

voltage at synchronous frequency. The VSC HVDC back-to-back system and its controllers are modeled as described in the next two sections.

3.3 Modeling of VSC HVDC

There are three types of modeling of VSC HVDC. The first model is the electromagnetic model for detailed equipment investigations [39]. The second model is the steady-state model for system steady-state operation evaluations [3,40]. The third model is the dynamic model which is used in power system stability and transient torque studies [12,41]. The first model is more suitable for studying electromagnetic transients in the range of milliseconds where the VSCs are represented using switches. This type of modeling is not appropriate for power oscillation studies. The steady-state model is developed to study the steady-state performance of the power system as well as for the calculation of the initial operating conditions of dynamic studies. The dynamic model is developed by combining the dynamic equations of the power system with the VSC HVDC dynamic equations.

3.3.1 VSC HVDC Back-to-Back System Steady-State Model

From the principles of VSC operation outlined in Chapter 1, it may be argued that, for the purpose of fundamental frequency analysis, each converter station of the VSC HVDC back-to-back system may be adequately represented by a complex voltage source $\boldsymbol{V}_{sh}$ behind its transformer impedance Z_{sh}. These two synchronous voltage sources represent the fundamental Fourier-series component of the switched voltage waveforms at the AC converter terminals of the VSC HVDC back-to-back system. A VSC HVDC back-to-back system installed between buses "*E*" and "*B*" can, therefore, be modeled at steady-state as shown in Figure 3.2. The two shunt impedances are assumed to be purely inductive. The total real power injected to the power system by two voltage sources is equal to zero at steady-state. However, there is a real power exchange between the two sources.

For power flow studies, the two-voltage source model of the VSC HVDC back-to-back system is converted into two power injections as shown in Figure 3.3.

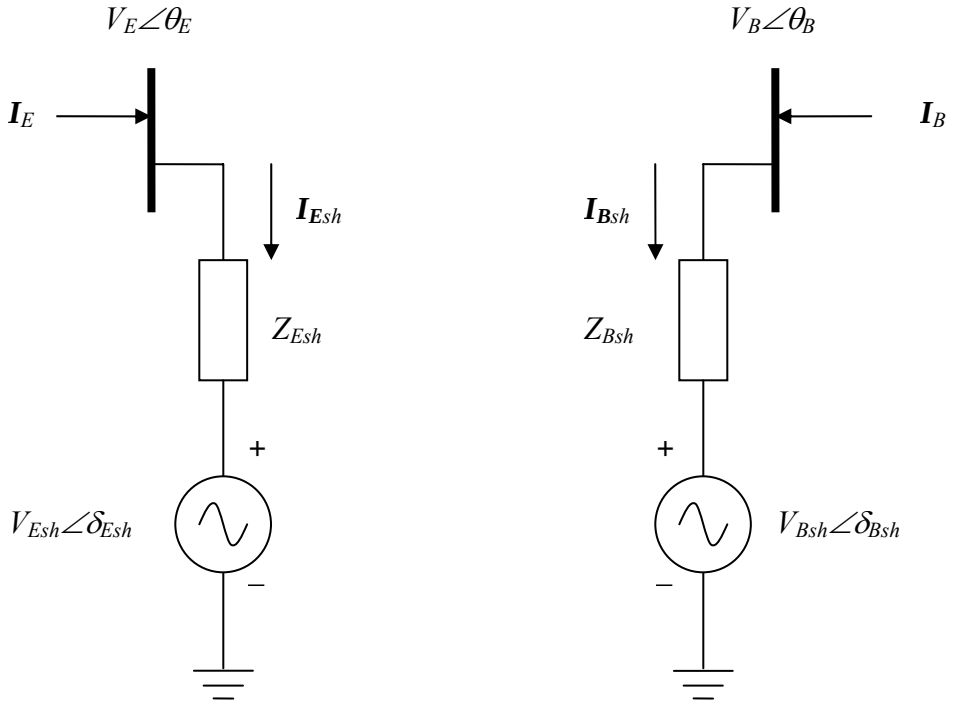

Figure 3.2 A VSC HVDC equivalent circuit for power flow studies and steady-state analysis.

Figure 3.3 The VSC HVDC back-to-back injected power model.

The active and reactive components of the complex power injected at bus "*E*" can be expressed as:

$$S_E = P_E + jQ_E = V_E\left(\frac{V_E - V_{Esh}}{Z_{Esh}}\right)^* \tag{3.1}$$

$$P_E = V_E V_{Esh} B_{Esh} \sin\left(\theta_E - \delta_{Esh}\right) \tag{3.2}$$

$$Q_E = -V_E{}^2 B_{Esh} - V_E V_{Esh} B_{Esh} \cos(\theta_E - \delta_{Esh}) \tag{3.3}$$

where

$$Z_{Esh} = jX_{Esh}$$

$$B_{Esh} = -\frac{1}{X_{Esh}} \tag{3.4}$$

and the superscript * denotes the complex conjugate.

The complex power flowing into the rectifier and its components are described by the following equations:

$$S_{Esh} = P_{Esh} + jQ_{Esh} = V_{Esh}\left(\frac{V_{Esh} - V_E}{Z_{Esh}}\right)^* \tag{3.5}$$

$$P_{Esh} = V_{Esh} V_E B_{Esh} \sin(\delta_{Esh} - \theta_E) \tag{3.6}$$

$$Q_{Esh} = -V_{Esh}{}^2 B_{Esh} - V_{Esh} V_E B_{Esh} \cos(\delta_{Esh} - \theta_E) \tag{3.7}$$

The power equations for bus "*B"* and the inverter are obtained simply by replacing the subscripts "*E"* and "*Esh"* by "*B"* and "*Bsh"*, respectively.

The losses associated with the VSC HVDC back-to-back system operation are typically neglected and, therefore, it neither absorbs nor injects real power with respect to the system during steady-state operation. Physical interpretation of this statement is that the voltage of the dc link capacitor remains constant at the pre-specified value V_{dc}. This constraint that must be satisfied by the VSC HVDC back-to-back system at steady-state is expressed mathematically as:

$$\mathrm{Re}\left\{V_{Esh} I_{Esh}{}^* + V_{Bsh} I_{Bsh}{}^*\right\} = 0 \tag{3.8}$$

With the help of Equations (3.1) to (3.7), the power constraint in Equation (3.8) can be represented as:

$$\delta_{Esh} = \theta_E - \sin^{-1}\left\{\frac{V_{Bsh}V_B B_{Bsh}}{V_{Esh}V_E B_{Esh}}\sin(\delta_{Bsh} - \theta_B)\right\} \tag{3.9}$$

The Gauss-Seidel or Newton-Raphson techniques are used to solve the power system load flow. Equation (3.9) is used to modify the power flow program to update the value of δ_{Esh} during consecutive iterations in order to satisfy the power constraint of Equation (3.8).

3.3.2 VSC HVDC Back-to-Back System Dynamic Model

Figure 3.4 shows a schematic diagram of a VSC HVDC back-to-back system connected to buses "*E*" and "*B*" through two shunt transformers. The equivalent circuit per phase of this system is shown in Figure 3.5.

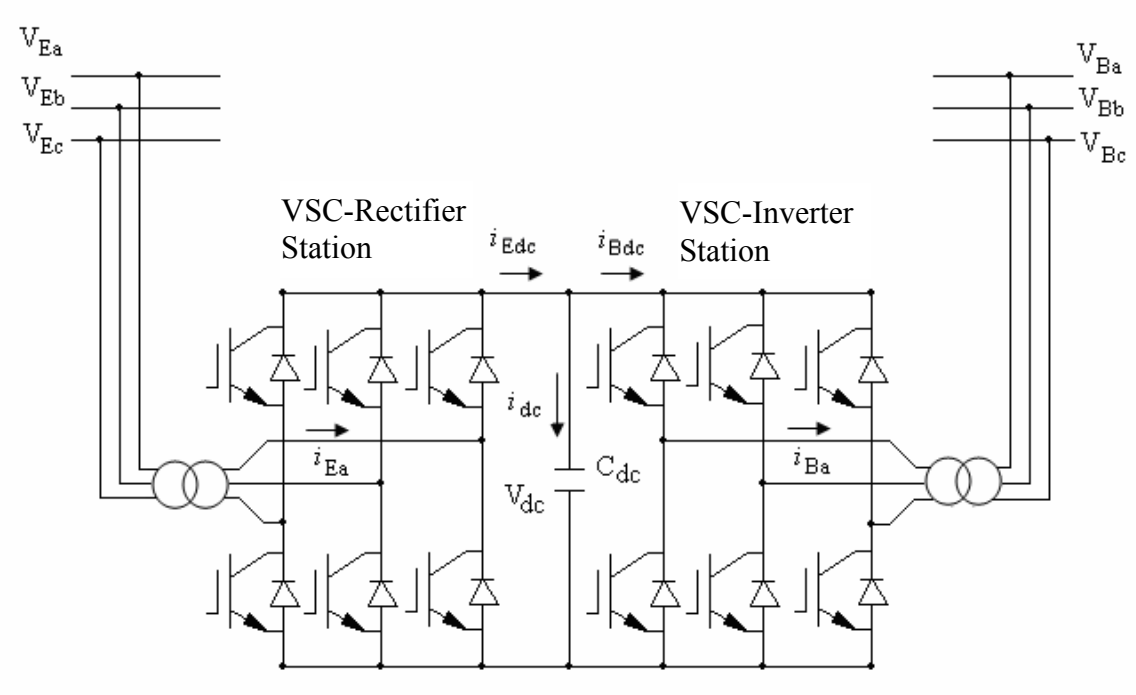

Figure 3.4 A three-phase schematic diagram of a VSC HVDC back-to-back system.

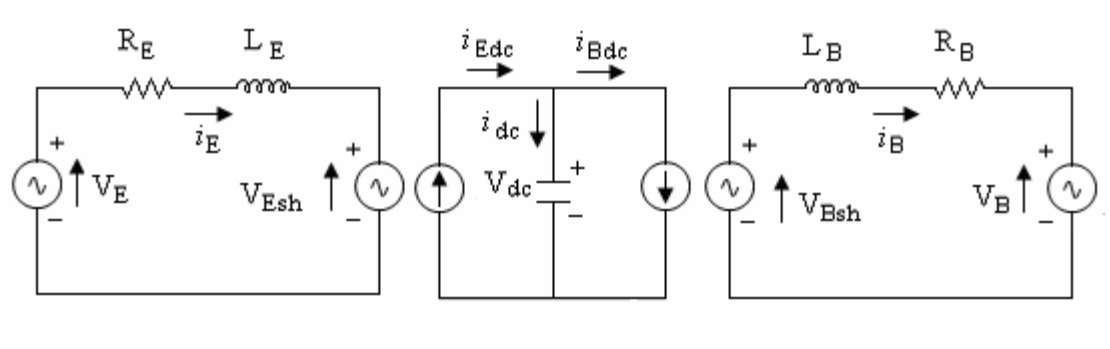

Figure 3.5 A VSC HVDC back-to-back system equivalent circuit for dynamic analysis.

Based on the principle of the VSC operation, regardless of the adopted sinusoidal PWM scheme, the voltage sources, V_{Esh} and V_{Bsh} are defined as follows:

$$V_{Esh} = \frac{m_E V_{dc}}{2} \angle \delta_{Esh} \tag{3.10}$$

$$V_{Bsh} = \frac{m_B V_{dc}}{2} \angle \delta_{Bsh} \tag{3.11}$$

where the constant $\frac{1}{2}$ relates the ac and dc voltages.

3.3.3 Differential Equations for the VSC HVDC Back-to-Back System

Adopting the time t in seconds, the angular ω and ω_0 in rad/s and the other quantities in per unit, the dynamic equations for the rectifier station are expressed as:

$$\frac{L_E}{\omega_0}\begin{bmatrix} \frac{di_{Ea}}{dt} \\ \frac{di_{Eb}}{dt} \\ \frac{di_{Ec}}{dt} \end{bmatrix} = -\begin{bmatrix} R_E & 0 & 0 \\ 0 & R_E & 0 \\ 0 & 0 & R_E \end{bmatrix}\begin{bmatrix} i_{Ea} \\ i_{Eb} \\ i_{Ec} \end{bmatrix} + \begin{bmatrix} V_{Ea} \\ V_{Eb} \\ V_{Ec} \end{bmatrix} - \begin{bmatrix} V_{Esha} \\ V_{Eshb} \\ V_{Eshc} \end{bmatrix} \tag{3.12}$$

Similarly, the dynamic equations for inverter station are given by:

$$\frac{L_B}{\omega_0}\begin{bmatrix}\frac{di_{Ba}}{dt}\\ \frac{di_{Bb}}{dt}\\ \frac{di_{Bc}}{dt}\end{bmatrix}=-\begin{bmatrix}R_B & 0 & 0\\ 0 & R_B & 0\\ 0 & 0 & R_B\end{bmatrix}\begin{bmatrix}i_{Ba}\\ i_{Bb}\\ i_{Bc}\end{bmatrix}-\begin{bmatrix}V_{Ba}\\ V_{Bb}\\ V_{Bc}\end{bmatrix}+\begin{bmatrix}V_{Bsha}\\ V_{Bshb}\\ V_{Bshc}\end{bmatrix} \tag{3.13}$$

After applying Park's transformation to Equations (3.12) and (3.13), and performing some matrix operations, the differential equations for the two converters in the d-q reference frame can be written as:

$$\frac{L_E}{\omega_0}\begin{bmatrix}\frac{di_{Ed}}{dt}\\ \frac{di_{Eq}}{dt}\end{bmatrix}=\begin{bmatrix}-R_E & \omega\frac{L_E}{\omega_0}\\ -\omega\frac{L_E}{\omega_0} & -R_E\end{bmatrix}\begin{bmatrix}i_{Ed}\\ i_{Eq}\end{bmatrix}+\begin{bmatrix}V_{Ed}\\ V_{Eq}\end{bmatrix}-\begin{bmatrix}V_{Eshd}\\ V_{Eshq}\end{bmatrix} \tag{3.14}$$

$$\frac{L_B}{\omega_0}\begin{bmatrix}\frac{di_{Bd}}{dt}\\ \frac{di_{Bq}}{dt}\end{bmatrix}=\begin{bmatrix}-R_B & \omega\frac{L_B}{\omega_0}\\ -\omega\frac{L_B}{\omega_0} & -R_B\end{bmatrix}\begin{bmatrix}i_{Bd}\\ i_{Bq}\end{bmatrix}-\begin{bmatrix}V_{Bd}\\ V_{Bq}\end{bmatrix}+\begin{bmatrix}V_{Bshd}\\ V_{Bshq}\end{bmatrix} \tag{3.15}$$

The equation for DC link capacitor is given by

$$\frac{1}{\omega_0}C_{dc}\frac{dV_{dc}}{dt}=i_{Edc}-i_{Bdc} \tag{3.16}$$

Multiplying both sides of Equation (3.16) by V_{dc} gives:

$$V_{dc}\frac{1}{\omega_0}C_{dc}\frac{dV_{dc}}{dt}=V_{dc}i_{Edc}-V_{dc}i_{Bdc} \tag{3.17}$$

The instantaneous powers at the ac and dc terminals of each converter are equal, giving power balance equation:

$$V_{dc}i_{Edc}=V_{Eshd}i_{Ed}+V_{Eshq}i_{Eq} \tag{3.18}$$

$$V_{dc}i_{Bdc}=V_{Bshd}i_{Bd}+V_{Bshq}i_{Bq} \tag{3.19}$$

Equation (3.17) can, therefore, be rewritten as:

$$\frac{1}{\omega_0} C_{dc} \frac{dV_{dc}}{dt} = \frac{1}{V_{dc}} \begin{bmatrix} V_{Eshd} & V_{Eshq} \end{bmatrix} \begin{bmatrix} i_{Ed} \\ i_{Eq} \end{bmatrix} - \frac{1}{V_{dc}} \begin{bmatrix} V_{Bshd} & V_{Bshq} \end{bmatrix} \begin{bmatrix} i_{Bd} \\ i_{Bq} \end{bmatrix} \tag{3.20}$$

The differential equations representing the dynamics of the VSC HVDC back-to-back system are given by Equations (3.14), (3.15), and (3.20).

The VSC HVDC source voltages phasor diagram is shown in Figure 3.6. With reference to this figure, the voltage sources in the d-q reference frame are given by

$$V_{Eshd} = \frac{m_E V_{dc}}{2} \sin(\delta - \delta_{Esh}) \tag{3.21}$$

$$V_{Eshq} = \frac{m_E V_{dc}}{2} \cos(\delta - \delta_{Esh}) \tag{3.22}$$

$$V_{Bshd} = \frac{m_B V_{dc}}{2} \sin(\delta - \delta_{Bsh}) \tag{3.23}$$

$$V_{Bshq} = \frac{m_B V_{dc}}{2} \cos(\delta - \delta_{Bsh}) \tag{3.24}$$

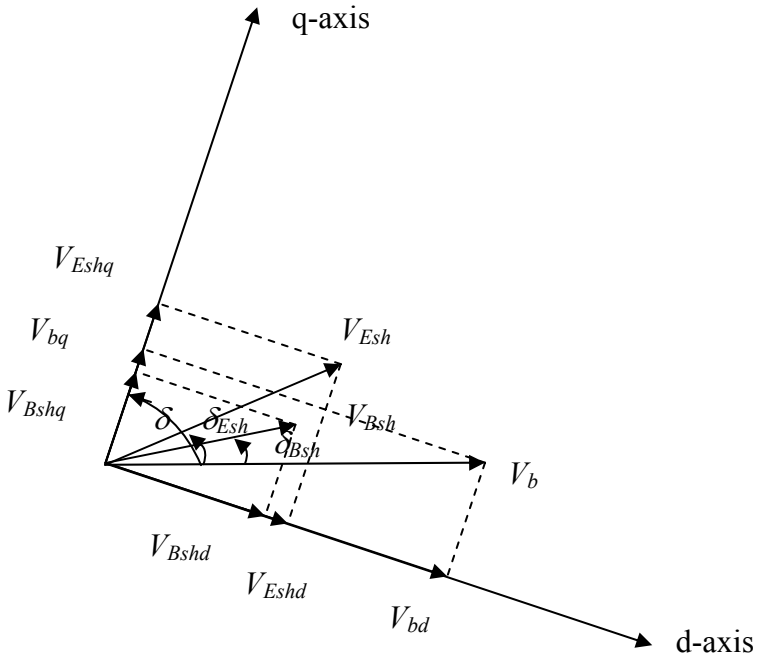

Figure 3.6 The VSC HVDC source voltages phasor diagram.

Substituting Equations (3.21) to (3.18) into Equations (3.14), (3.15) and (3.20), gives

$$\frac{L_E}{\omega_0}\begin{bmatrix}\frac{di_{Ed}}{dt}\\ \frac{di_{Eq}}{dt}\end{bmatrix}=\begin{bmatrix}-R_E & \omega\frac{L_E}{\omega_0}\\ -\omega\frac{L_E}{\omega_0} & -R_E\end{bmatrix}\begin{bmatrix}i_{Ed}\\ i_{Eq}\end{bmatrix}-\frac{m_E V_{dc}}{2}\begin{bmatrix}\sin(\delta-\delta_{Esh})\\ \cos(\delta-\delta_{Esh})\end{bmatrix}+\begin{bmatrix}V_{Ed}\\ V_{Eq}\end{bmatrix} \tag{3.25}$$

$$\frac{L_B}{\omega_0}\begin{bmatrix}\frac{di_{Bd}}{dt}\\ \frac{di_{Bq}}{dt}\end{bmatrix}=\begin{bmatrix}-R_B & \omega\frac{L_B}{\omega_0}\\ -\omega\frac{L_B}{\omega_0} & -R_B\end{bmatrix}\begin{bmatrix}i_{Bd}\\ i_{Bq}\end{bmatrix}+\frac{m_B V_{dc}}{2}\begin{bmatrix}\sin(\delta-\delta_{Bsh})\\ \cos(\delta-\delta_{Bsh})\end{bmatrix}-\begin{bmatrix}V_{Bd}\\ V_{Bq}\end{bmatrix} \tag{3.26}$$

$$\begin{aligned}\frac{dV_{dc}}{dt}=&\omega_0\frac{m_E}{2C_{dc}}\begin{bmatrix}\sin(\delta-\delta_{Esh}) & \cos(\delta-\delta_{Esh})\end{bmatrix}\begin{bmatrix}i_{Ed}\\ i_{Eq}\end{bmatrix}\\ &-\omega_0\frac{m_B}{2C_{dc}}\begin{bmatrix}\sin(\delta-\delta_{Bsh}) & \cos(\delta-\delta_{Bsh})\end{bmatrix}\begin{bmatrix}i_{Bd}\\ i_{Bq}\end{bmatrix}\end{aligned} \tag{3.27}$$

Since in per unit system, $X_E = L_E$ and $X_{dc} = \frac{1}{C_{dc}}$, Equations (3.25), (3.26) and (3.27) can be written as

$$\begin{bmatrix}\frac{di_{Ed}}{dt}\\ \frac{di_{Eq}}{dt}\end{bmatrix}=\begin{bmatrix}-\omega_0\frac{R_E}{X_E} & \omega\\ -\omega & -\omega_0\frac{R_E}{X_E}\end{bmatrix}\begin{bmatrix}i_{Ed}\\ i_{Eq}\end{bmatrix}-\begin{bmatrix}\frac{\omega_0}{X_E}\frac{m_E}{2}\sin(\delta-\delta_{Esh})\\ \frac{\omega_0}{X_E}\frac{m_E}{2}\cos(\delta-\delta_{Esh})\end{bmatrix}\begin{bmatrix}V_{dc}\end{bmatrix}+\begin{bmatrix}\frac{\omega_0}{X_E} & 0\\ 0 & \frac{\omega_0}{X_E}\end{bmatrix}\begin{bmatrix}V_{Ed}\\ V_{Eq}\end{bmatrix} \tag{3.28}$$

$$\begin{bmatrix}\frac{di_{Bd}}{dt}\\ \frac{di_{Bq}}{dt}\end{bmatrix}=\begin{bmatrix}-\omega_0\frac{R_B}{X_B} & \omega\\ -\omega & -\omega_0\frac{R_B}{X_B}\end{bmatrix}\begin{bmatrix}i_{Bd}\\ i_{Bq}\end{bmatrix}+\begin{bmatrix}\frac{\omega_0}{X_B}\frac{m_B}{2}\sin(\delta-\delta_{Bsh})\\ \frac{\omega_0}{X_B}\frac{m_B}{2}\cos(\delta-\delta_{Bsh})\end{bmatrix}\begin{bmatrix}V_{dc}\end{bmatrix}-\begin{bmatrix}\frac{\omega_0}{X_B} & 0\\ 0 & \frac{\omega_0}{X_B}\end{bmatrix}\begin{bmatrix}V_{Bd}\\ V_{Bq}\end{bmatrix} \tag{3.29}$$

$$\begin{aligned}\frac{dV_{dc}}{dt}=&\frac{1}{2}\omega_0 m_E X_{dc}\begin{bmatrix}\sin(\delta-\delta_{Esh}) & \cos(\delta-\delta_{Esh})\end{bmatrix}\begin{bmatrix}i_{Ed}\\ i_{Eq}\end{bmatrix}\\ &-\frac{1}{2}\omega_0 m_B X_{dc}\begin{bmatrix}\sin(\delta-\delta_{Bsh}) & \cos(\delta-\delta_{Bsh})\end{bmatrix}\begin{bmatrix}i_{Bd}\\ i_{Bq}\end{bmatrix}\end{aligned} \tag{3.30}$$

The state-space equations of the VSC HVDC back-to-back system are then given by:

$$\left[\frac{dX_{DC}}{dt}\right] = [At_{DC}][X_{DC}] + [Bt1_{DC}]\begin{bmatrix} V_{Ed} \\ V_{Eq} \end{bmatrix} + [Bt2_{DC}]\begin{bmatrix} V_{Bd} \\ V_{Bq} \end{bmatrix} \tag{3.31}$$

where

$$[X_{DC}] = \begin{bmatrix} i_{Ed} & i_{Eq} & i_{Bd} & i_{Bq} & V_{dc} \end{bmatrix}^T$$

$$[At_{DC}] = \begin{bmatrix} -R_E\frac{\omega_0}{X_E} & \omega & 0 & 0 & -\frac{\omega_0}{X_E}\frac{m_E}{2}\sin\delta_{Es} \\ -\omega & -R_E\frac{\omega_0}{X_E} & 0 & 0 & -\frac{\omega_0}{X_E}\frac{m_E}{2}\cos\delta_{Es} \\ 0 & 0 & -R_B\frac{\omega_0}{X_B} & \omega & \frac{\omega_0}{X_B}\frac{m_B}{2}\sin\delta_{Bs} \\ 0 & 0 & -\omega & -R_B\frac{\omega_0}{X_B} & \frac{\omega_0}{X_B}\frac{m_B}{2}\cos\delta_{Bs} \\ k_E\sin\delta_{Es} & k_E\cos\delta_{Es} & k_B\sin\delta_{Bs} & k_B\cos\delta_{Bs} & 0 \end{bmatrix}$$

$$\delta_{Es} = \delta - \delta_{Esh} \qquad \delta_{Bs} = \delta - \delta_{Bsh}$$

$$k_E = \frac{1}{2}\omega_0 m_E X_{dc} \qquad k_B = -\frac{1}{2}\omega_0 m_B X_{dc}$$

$$[Bt1_{DC}] = \begin{bmatrix} \frac{\omega_0}{X_E} & 0 \\ 0 & \frac{\omega_0}{X_E} \\ 0 & 0 \\ 0 & 0 \\ 0 & 0 \end{bmatrix} \tag{3.32}$$

$$[Bt2_{DC}] = \begin{bmatrix} 0 & 0 \\ 0 & 0 \\ -\frac{\omega_0}{X_B} & 0 \\ 0 & -\frac{\omega_0}{X_B} \\ 0 & 0 \end{bmatrix}$$

3.4 The VSC HVDC Back-to-Back Controllers

Figure 3.7 shows a schematic diagram of the VSC HVDC back-to-back controllers that comprise two main controllers, namely the active power and the supplementary controllers.

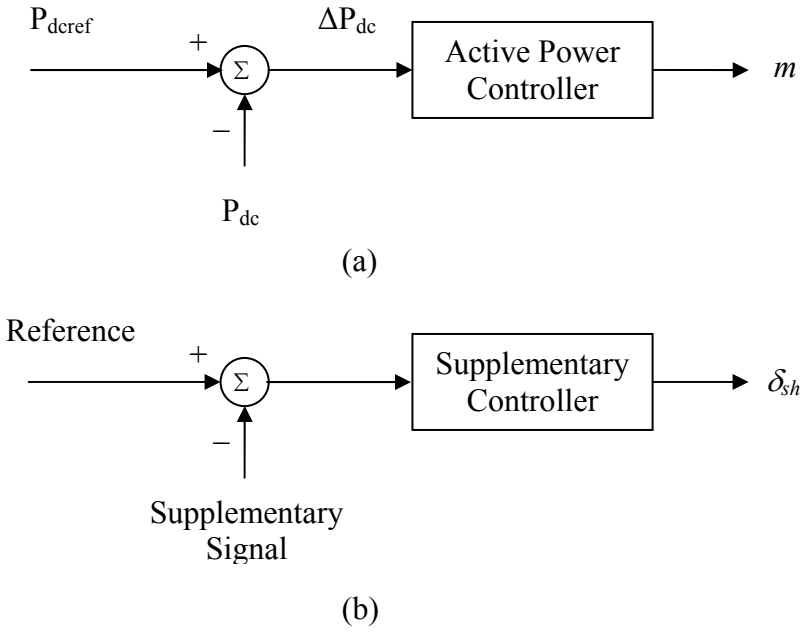

Figure 3.7 The VSC HVDC Back-to-Back controllers: (a) active power controller, (b) supplementary controller.

3.4.1 The Active Power Controller

The main function of this controller is to regulate the active power flow on both sides of the VSC HVDC back-to-back system. This is done through the two proportional type controllers shown in Figure 3.8. Each of these controllers has one gain and two time constants.

The state-space equations of the active power controller are derived from the transfer functions of Figure 3.8 and are given by the following equations:

$$\left[\frac{dX_{cm}}{dt}\right] = [At_{cm}][X_{cm}] + [Bt_{cm}]\begin{bmatrix} P_{Edcref} \\ P_{Edc} \\ P_{Bdcref} \\ P_{Bdc} \end{bmatrix} \tag{3.33}$$

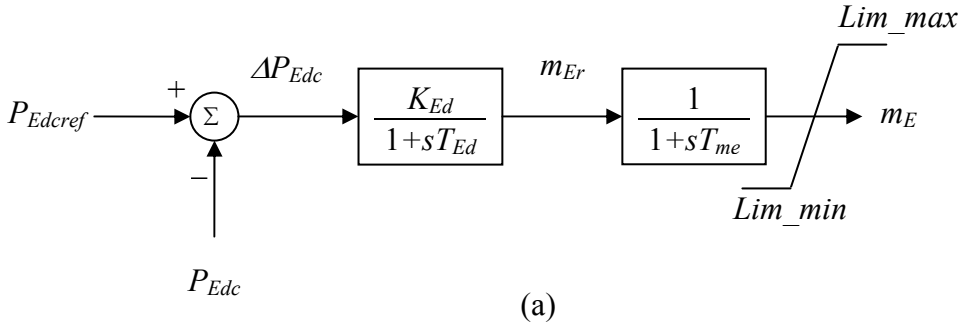

(a)

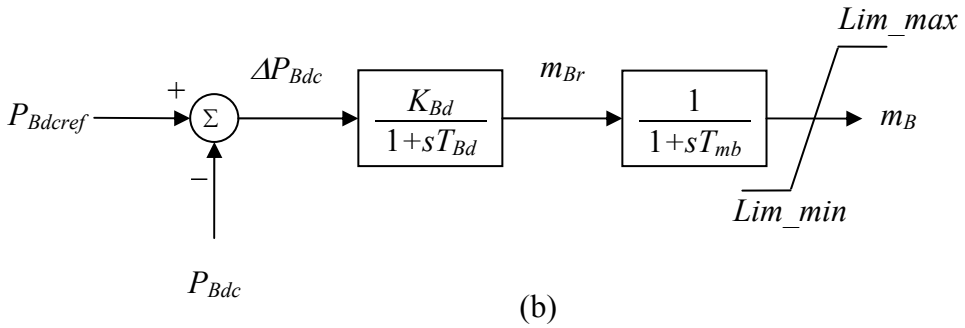

(b)

Figure 3.8 The VSC HVDC back-to-back active power controller: (a) rectifier, (b) inverter.

where

$$[X_{cm}] = [m_E \quad m_{Er} \quad m_B \quad m_{Br}]^T$$

$$[At_{cm}] = \begin{bmatrix} -\frac{1}{T_{me}} & \frac{1}{T_{me}} & 0 & 0 \\ 0 & -\frac{1}{T_{Ed}} & 0 & 0 \\ 0 & 0 & -\frac{1}{T_{mb}} & \frac{1}{T_{mb}} \\ 0 & 0 & 0 & -\frac{1}{T_{Bd}} \end{bmatrix} \tag{3.34}$$

$$[Bt_{cm}] = \begin{bmatrix} 0 & 0 & 0 & 0 \\ \frac{K_{Ed}}{T_{Ed}} & -\frac{K_{Ed}}{T_{Ed}} & 0 & 0 \\ 0 & 0 & 0 & 0 \\ 0 & 0 & \frac{K_{Bd}}{T_{Bd}} & -\frac{K_{Bd}}{T_{Bd}} \end{bmatrix}$$

3.4.2 The VSC HVDC Back-to-Back Supplementary Controller

The VSC HVDC back-to-back system equipped with only an active power controller is not sufficient to damp all the torsional modes. Thus, a need exists for an additional control signal along with the VSC-HVDC back-to-back active power controller. The idea of applying such a supplementary stabilizing signal is to increase the damping in the power system.

Figure 3.9 shows the transfer function of a *PI* supplementary controller whose output controls the phase angle δ_{Esh} of the injected voltage V_{Esh} of the rectifier station. Various input signals can be used for the supplementary controller design: the speed deviation $\Delta\omega$, the generator accelerating power ΔP_a or the system frequency Δf. As it is known that the generator speed contains components of all the torsional modes [27], it is selected as the stabilizing signal in the supplementary controller design.

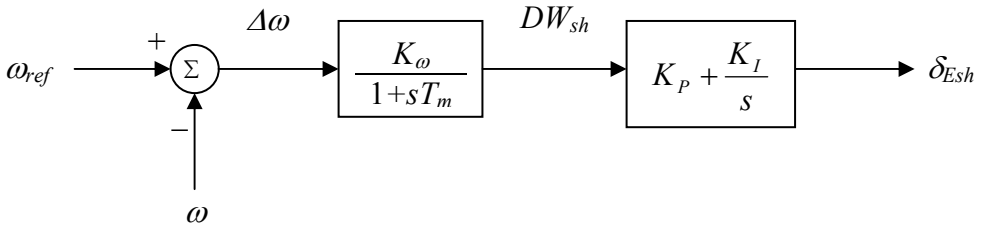

Figure 3.9 Structure of the VSC HVDC back-to-back supplementary controller.

The state-space equations of the supplementary controller are derived from the transfer functions of Figure 3.9 and are given by the following equations:

$$\left[\frac{dX_{dw}}{dt}\right] = \left[At_{dw}\right]\left[X_{dw}\right] + \left[Bt_{dw}\right]\begin{bmatrix}\omega_{ref}\\ \omega\end{bmatrix} \tag{3.35}$$

where

$$\left[X_{dw}\right] = \left[\delta_{Esh} \quad DW_{sh}\right]^T$$

$$\left[At_{dw}\right] = \begin{bmatrix} 0 & K_I - \dfrac{K_P}{T_m} \\ 0 & -\dfrac{1}{T_m} \end{bmatrix} \tag{3.36}$$

$$\left[Bt_{dw}\right] = \frac{1}{\omega_0}\begin{bmatrix} \dfrac{K_P K_\omega}{T_m} & -\dfrac{K_P K_\omega}{T_m} \\ \dfrac{K_\omega}{T_m} & \dfrac{K_\omega}{T_m} \end{bmatrix}$$

3.5 Dynamic Model of the Overall System

The overall equations of the system under study may be derived by performing some mathematical operations. In doing this, however, the transmission line equations have to undergo some minor changes.

With reference to Figure 3.1 and Equations (2.19) to (2.21), the equations for the series capacitor compensated transmission line of the system under study are given by

$$\left[\frac{dX_{TL}}{dt}\right] = \left[At_{TL}\right]\left[X_{TL}\right] + \left[Bt1_{TL}\right]\begin{bmatrix}V_{td}\\ V_{tq}\end{bmatrix} + \left[Bt2_{TL}\right]\left[V_b\right] \tag{3.37}$$

$$\begin{bmatrix} \dfrac{dV_{Cd}}{dt} \\ \dfrac{dV_{Cq}}{dt} \\ V_{td} \\ V_{tq} \end{bmatrix} = \left[Att_{TL}\right]\begin{bmatrix}V_{Cd}\\ V_{Cq}\end{bmatrix} + \left[Rt11_{TL}\right]\begin{bmatrix} \dfrac{di_d}{dt} \\ \dfrac{di_q}{dt} \end{bmatrix} + \left[Rt12_{TL}\right]\begin{bmatrix} \dfrac{di_{Ed}}{dt} \\ \dfrac{di_{Eq}}{dt} \end{bmatrix} \tag{3.38}$$

$$+ \left[Rt21_{TL}\right]\begin{bmatrix}i_d\\ i_q\end{bmatrix} + \left[Rt22_{TL}\right]\begin{bmatrix}i_{Ed}\\ i_{Eq}\end{bmatrix} + \left[Btt_{TL}\right]\left[V_b\right]$$

where

$$[X_{TL}] = \begin{bmatrix} i_{Ld} & i_{Lq} & V_{Cd} & V_{Cq} \end{bmatrix}^T$$

$$[At_{TL}] = \begin{bmatrix} -\omega_0 \frac{R_L}{X_L} & \omega & -\frac{\omega_0}{X_L} & 0 \\ -\omega & -\omega_0 \frac{R_L}{X_L} & 0 & -\frac{\omega_0}{X_L} \\ \omega_0 X_C & 0 & 0 & w \\ 0 & \omega_0 X_C & -\omega & 0 \end{bmatrix}$$

$$[Bt1_{TL}] = \begin{bmatrix} \frac{\omega_0}{X_L} & 0 \\ 0 & \frac{\omega_0}{X_L} \\ 0 & 0 \\ 0 & 0 \end{bmatrix} \qquad [Bt2_{TL}] = \begin{bmatrix} -\frac{\omega_0}{X_L}\sin\delta \\ -\frac{\omega_0}{X_L}\cos\delta \\ 0 \\ 0 \end{bmatrix}$$

$$[Att_{TL}] = \begin{bmatrix} 0 & \omega \\ -\omega & 0 \\ 1 & 0 \\ 0 & 1 \end{bmatrix} \tag{3.39}$$

$$[Rt11_{TL}] = \begin{bmatrix} 0 & 0 \\ 0 & 0 \\ \frac{X_L}{\omega_0} & 0 \\ 0 & \frac{X_L}{\omega_0} \end{bmatrix} \qquad [Rt12_{TL}] = \begin{bmatrix} 0 & 0 \\ 0 & 0 \\ -\frac{X_L}{\omega_0} & 0 \\ 0 & -\frac{X_L}{\omega_0} \end{bmatrix}$$

$$[Rt21_{TL}] = \begin{bmatrix} \omega_0 X_C & 0 \\ 0 & \omega_0 X_C \\ R_L & -\frac{\omega}{\omega_0} X_L \\ \frac{\omega}{\omega_0} X_L & R_L \end{bmatrix} \qquad [Rt22_{TL}] = \begin{bmatrix} -\omega_0 X_C & 0 \\ 0 & -\omega_0 X_C \\ -R_L & \frac{\omega}{\omega_0} X_L \\ -\frac{\omega}{\omega_0} X_L & -R_L \end{bmatrix}$$

$$[Btt_{TL}] = \begin{bmatrix} 0 \\ 0 \\ \sin\delta \\ \cos\delta \end{bmatrix}$$

Equation (2.15) for the synchronous machine is partitioned such that

$$\left[\frac{dX_{syn}}{dt}\right] = \left[At_{syn}\right]\left[X_{syn}\right] + \left[Bt1_{syn}\right]\begin{bmatrix} V_{td} \\ V_{tq} \end{bmatrix} + \left[Bt1_{syn}\right]\left[e_{fd}\right] \tag{3.40}$$

Without loss of generality, the sum of transmission line 2 reactance and the transformer leakage reactance on the rectifier station side of the VSC HVDC is designated as X_E. Similarly, the sum of transmission line 3 reactance and the transformer leakage reactance on inverter station side is designated as X_B. The equations for the VSC HVDC back-to-back system combining the transmission lines may be given by Equation (3.31). In these equations, V_t replaces V_E and V_B is considered to be the voltage of System II.

The electrical part of the system: By combining Equations (3.31), (3.37), (3.38), and (3.40), the following equations are obtained

$$\begin{bmatrix} \frac{dX_{Syn}}{dt} \\ \frac{dX_{DC}}{dt} \\ \frac{dX_{TL}}{dt} \end{bmatrix} = \left[At_{SL}\right]\begin{bmatrix} X_{Syn} \\ X_{DC} \\ X_{TL} \end{bmatrix} + \left[Bt_{SL}\right]\begin{bmatrix} V_{td} \\ V_{tq} \\ e_{fd} \\ |V_B| \\ V_b \end{bmatrix} \tag{3.41}$$

$$\begin{bmatrix} V_{td} \\ V_{tq} \end{bmatrix} = \left[Ci\right]\begin{bmatrix} X_{Syn} \\ X_{DC} \\ V_{Cd} \\ V_{Cq} \end{bmatrix} + \left[Di\right]\begin{bmatrix} e_{fd} \\ |V_B| \\ V_b \end{bmatrix} \tag{3.42}$$

The turbine-generator shaft and the excitation system: combining Equations (2.30), (2.34), and (2.38) forms the following equations

$$\begin{bmatrix} \frac{dX_{ms}}{dt} \\ \frac{dX_g}{dt} \\ \frac{dX_v}{dt} \end{bmatrix} = \left[Atp1\right]\begin{bmatrix} X_{ms} \\ X_g \\ X_v \end{bmatrix} + \left[Atp2\right]\left[Te\right] + \left[Btp\right]\begin{bmatrix} \omega_0 \\ P_{m0} \\ V_t \\ E_{ref} \end{bmatrix} \tag{3.43}$$

The air-gap torque Equation (2.14) is written as

$$T_e = [Tedq][X_{syn}] \tag{3.44}$$

where

$$[Tedq] = [-L_d i_q \quad L_q i_d \quad L_{ad} i_q \quad -L_{aq} i_d \quad L_{ad} i_q \quad -L_{aq} i_d] \tag{3.45}$$

The terminal voltage is given by

$$V_t = \sqrt{(V_{td}^{\ 2} + V_{tq}^{\ 2})} \tag{3.46}$$

Combining Equations (3.41) to (3.46), (3.33), and (3.35), the overall equations of the system are given by

$$\left[\frac{dX_t}{dt}\right] = [Attmd][X_t] + [Bttmd][U_t] \tag{3.47}$$

where

$$\begin{aligned}[X_t] = [&\delta_E \quad \delta \quad \delta_B \quad \delta_A \quad \delta_I \quad \delta_H \quad \omega_E \quad \omega \quad \omega_B \quad \omega_A \quad \omega_I \quad \omega_H \ldots \\ &C_v \quad P_H \quad P_I \quad P_H \quad e_{fd} \quad E_R \quad E_{SB} \quad i_d \quad i_q \quad i_{fd} \quad i_{1q} \quad i_{1d} \quad i_{2q} \ldots \\ &i_{Ed} \quad i_{Eq} \quad i_{Bd} \quad i_{Bq} \quad V_{dc} \quad i_{Ld} \quad i_{Ld} \quad V_{Cd} \quad V_{Cq} \quad m_E \quad m_{Er} \quad m_B \quad m_{Br} \quad \delta_{Esh} \quad DW_{sh}]^T\end{aligned}$$

$$[U_t] = [\omega_0 \quad P_{m0} \quad V_t \quad E_{ref} \quad V_{td} \quad V_{tq} \quad |V_B| \quad V_b \quad P_{Edcref} \quad P_{Edc} \quad P_{Bdcref} \quad P_{Bdc}]^T \tag{3.48}$$

The complete nonlinear model of the system and its controllers is a 40th order system.

The detailed mathematical operations for constructing the overall nonlinear differential equations are given in Appendix D.

3.6 Numerical Solution

The nonlinear differential equations of the system are solved using the fourth-order Runge-Kutta algorithm. MATLAB provides two powerful functions for the numerical solution of differential equations employing the Runge-Kutta-Fehlberg methods. They are **ode23** and **ode45** [42]. In the studies conducted in this thesis, the function **ode45** is used to solve the system nonlinear equations.

To start the computation, the initial values of all the system variables are to be calculated. The initial conditions of the system are shown in Figure 3.10, where all quantities are in per unit. The transmission line compensation level is assumed to be 50% corresponding to X_C = 0.35 per unit, and the real power generated from the synchronous machine, P_G, is assumed to be 0.90 per unit. The VSC HVDC back-to-back system is set to regulate the active power flowing from bus 2 to bus 3 and the reactive power flowing from bus 4 to bus 5 at 0.20 per unit and 0.05 per unit, respectively. The voltage magnitude at bus 3 is kept constant at 1.0 per unit.

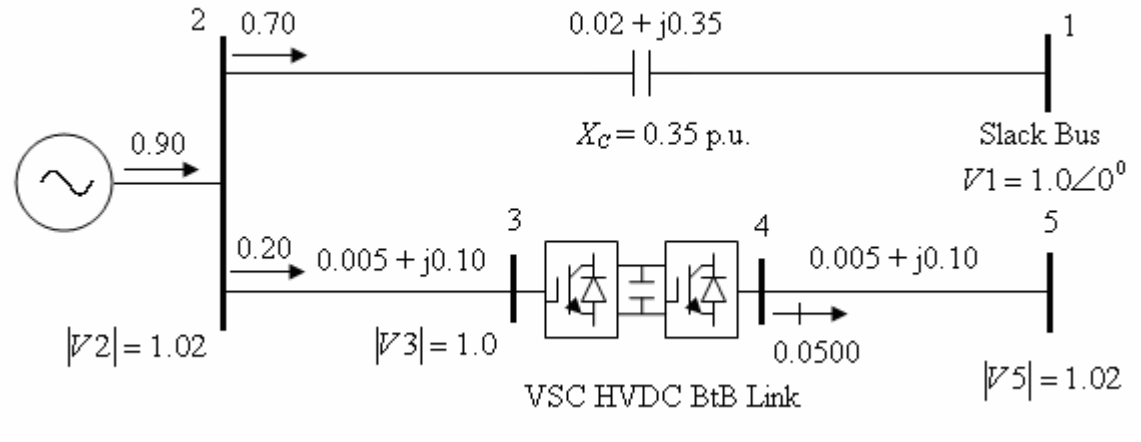

Figure 3.10 Initial conditions of the system for power flow analysis (P_{dc} = 0.20 p.u., X_C = 0.35 p.u.).

The bus voltages and the source voltages of the VSC HVDC back-to-back system are obtained using power flow analysis. Convergence is obtained in five iterations to a power mismatch tolerance of 1e-12 using Newton-Raphson algorithm, and in 55 iterations to a voltage mismatch tolerance of 1e-7 using Gauss-Seidel technique respectively. It is worth noting that, in these studies, the source voltages are assumed to have the following per unit limits $0.9 < |V_{sh}| < 1.1$ and initial values of $1.0\angle 0^0$ per unit. The power flow results are shown in Figure 3.11 where the real power direction is indicated by $\rightarrow$ and the reactive power direction is indicated by $\mapsto$. Bus and source voltages are given in Table 3.1.

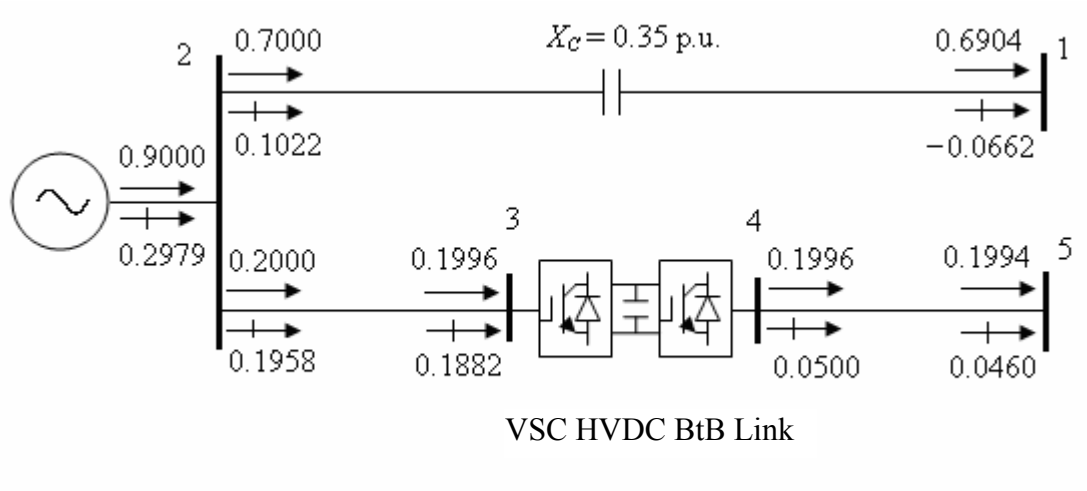

Figure 3.11 System power flow results (P_{dc} = 0.20 p.u., X_C = 0.35 p.u.).

Table 3.1 System bus and VSC voltages (P_{dc} = 0.20 p.u., X_C = 0.35 p.u.).

	System bus					VSC voltage	
	1	2	3	4	5	V_{sh1}	V_{sh2}
Magnitude (p.u.)	1.0000	1.0200	1.0000	1.0257	1.0200	0.9814	1.0307
Phase angle (deg)	0	13.7804	12.7120	1.7989	0.7194	11.5466	2.8807

The relative angular displacements of the various sections of the turbine-generator mechanical system with respect to the generator angle (rotor angle) are given by

$$\delta_{E0} = \delta_0$$

$$\delta_{B0} = \delta_0 + \frac{P_{m0}}{K_{gB}}$$

$$\delta_{A0} = \delta_{B0} + \frac{P_{m0} - F_B P_{m0}}{K_{BA}} \tag{3.49}$$

$$\delta_{I0} = \delta_{A0} + \frac{P_{m0} - F_A P_{m0} - F_B P_{m0}}{K_{AI}}$$

$$\delta_{H0} = \delta_{I0} + \frac{F_H P_{m0}}{K_{IH}}$$

The initial values of the other variables are readily obtained. For example, the synchronous machine and the transmission network variables are obtained through the voltage phasor diagrams of Figures 2.4 and 3.6. The initial conditions of the system controllers are computed by applying the steady-state input signals to the corresponding transfer functions.

3.7 Simulation of SSR under Large Disturbances: A Study Case

In order to demonstrate the dynamic performance of the study system under large disturbances, a three-cycle, three-phase fault at bus 2 is initiated at $t = 0.2$ seconds. The data of the VSC HVDC back-to-back controller parameters in this case study are given in Table 3.2. The system transient time responses during and after clearing this disturbance are given in Figures 3.12 to 3.21.

Table 3.2 Controller parameters (P_{dc} = 0.20 p.u., X_C = 0.35 p.u.).

Active power controller		
K_{Ed} = 6.0	T_{Ed} = 0.1 sec.	T_{me} = 0.2 sec.
K_{Bd} = 6.0	T_{Bd} = 0.1 sec.	T_{mb} = 0.2 sec.
Supplementary controller		
K_{ω} = 3.0		T_m = 0.01 sec.
K_P = 0.05		K_I = 0.10

Figures 3.12 to 3.17 show the time responses of the angle and angular speed of the individual masses of the turbine-generator as well as the shaft torsional torques. The generator stator currents in the d-q reference frame and the field current are shown in Figure 3.18. The generator terminal and field voltages and the voltage across the dc capacitor are also plotted in Figure 3.19. The active power flows through the transmission line and the two stations of the VSC HVDC back-to-back system are shown in Figure 3.20 as well. In addition to the above system variables, the control signals m_E, m_B and δ_{Esh} are also given in Figure 3.21. Examination of these results reveals that, under this operating condition and compensation level, the VSC HVDC back-to-back active power and supplementary controllers effectively damp SSR oscillations at this compensation level. For the critical compensation levels (i.e., 26.5%,

41.1%, 54.7%, and 68.4%), the dynamic performance of the system will be investigated in the next chapter.

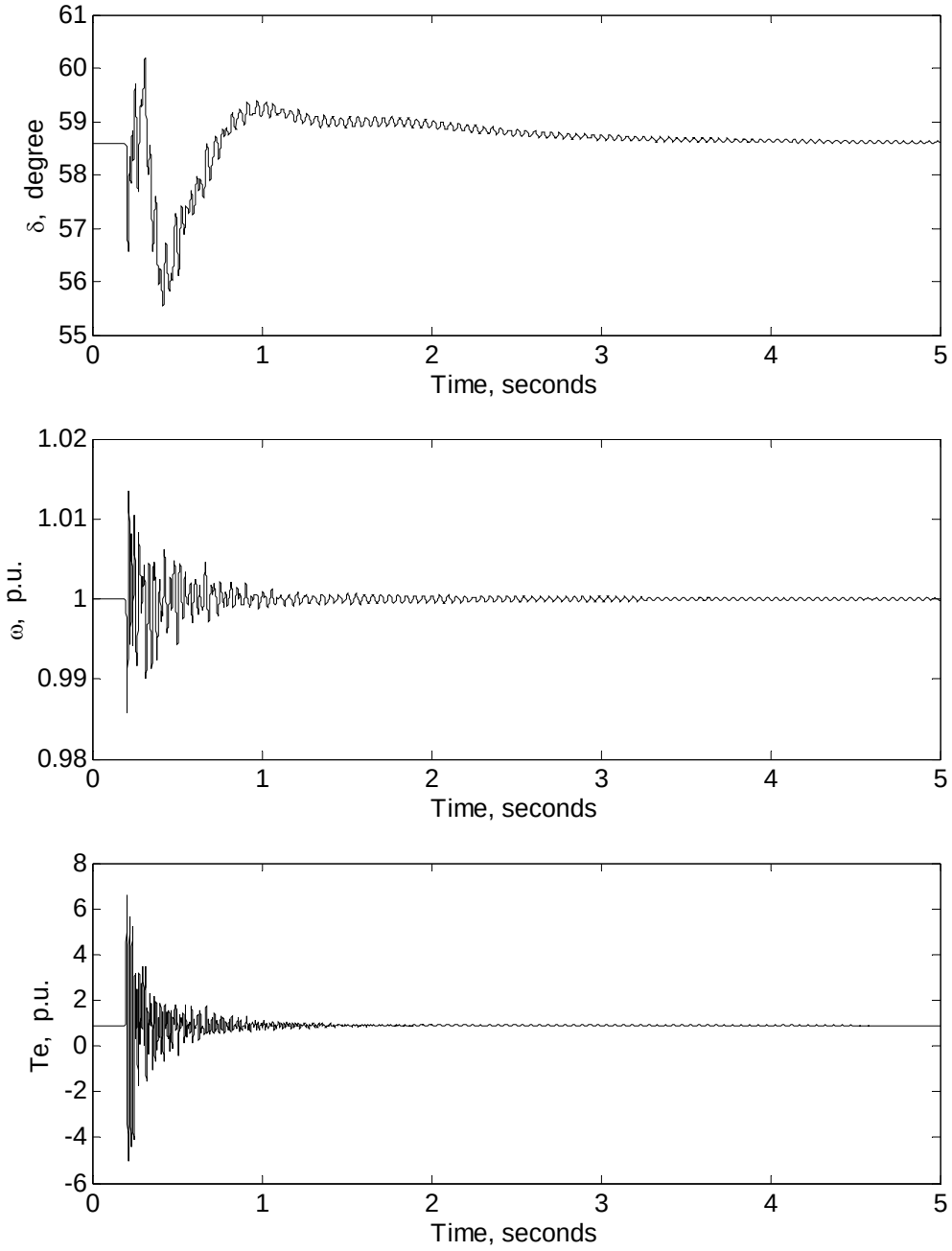

Figure 3.12 Time responses of the generator (GEN) rotor angle, angular speed and electromagnetic torque of the system due to a 3-cycle, three-phase fault: the VSC HVDC back-to-back active power and supplementary controllers are employed simultaneously (P_{dc} = 0.20 p.u., X_C = 0.35 p.u.).

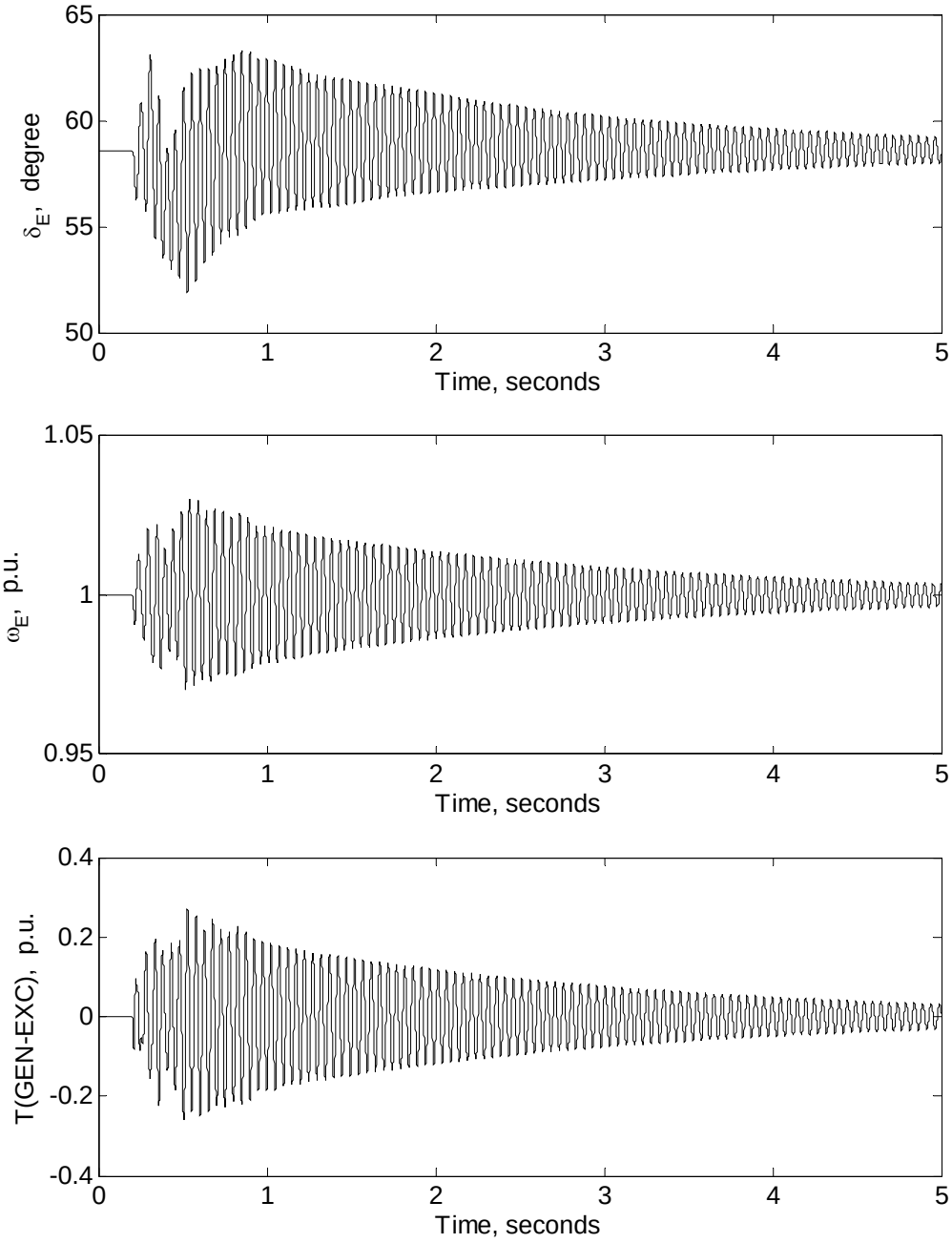

Figure 3.13 Time responses of the exciter (EXC) angle, angular speed and shaft torque between the generator (GEN) and the exciter (EXC) of the system due to a 3-cycle, three-phase fault: the VSC HVDC back-to-back active power and supplementary controllers are employed simultaneously (P_{dc} = 0.20 p.u., X_C = 0.35 p.u.).

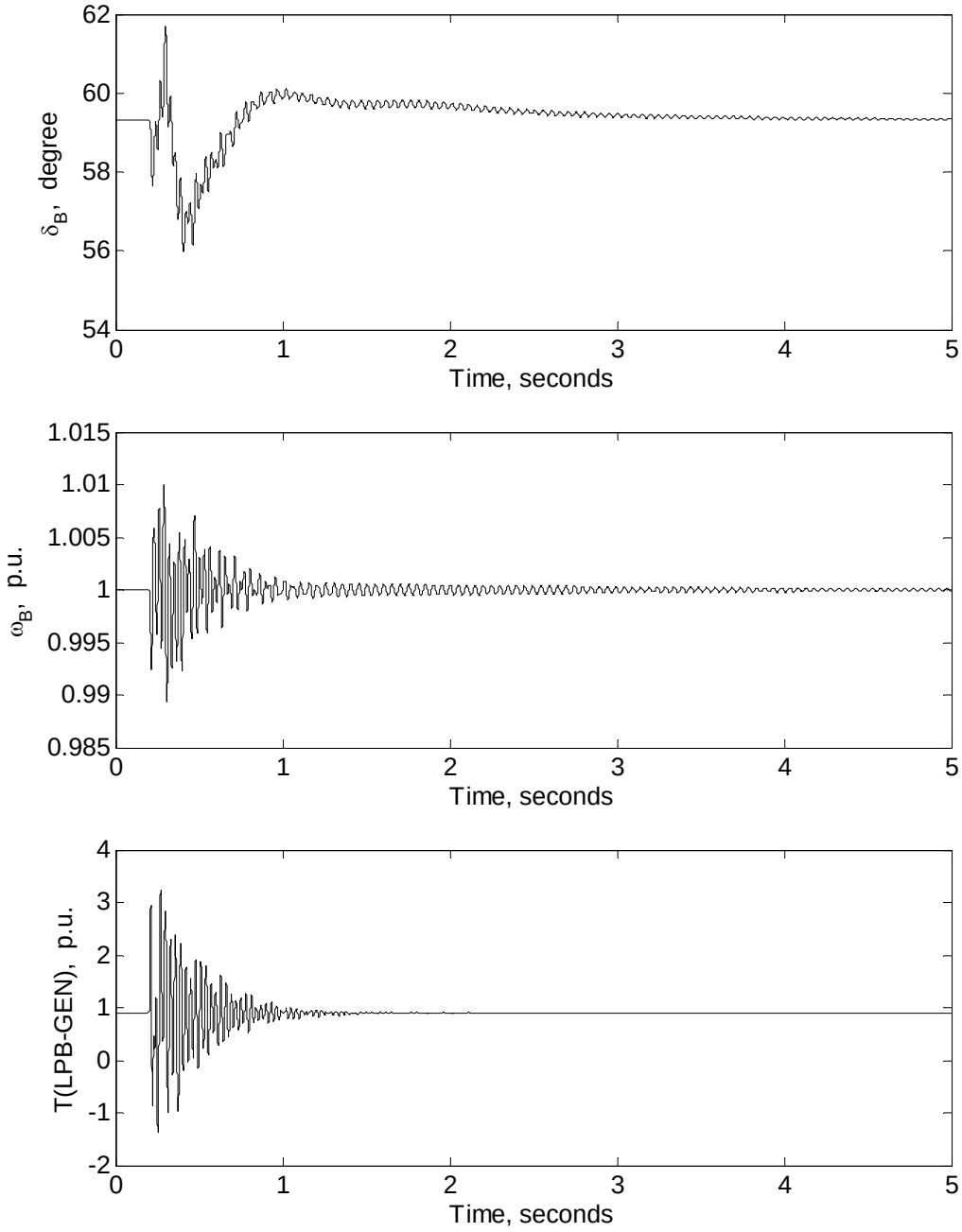

Figure 3.14 Time responses of the low pressure stage (LPB) angle, angular speed, and shaft torque between the low pressure stage (LPB) and the generator (GEN) of the system due to a 3-cycle, three-phase fault: the VSC HVDC back-to-back active power and supplementary controllers are employed simultaneously (P_{dc} = 0.20 p.u., X_C = 0.35 p.u.).

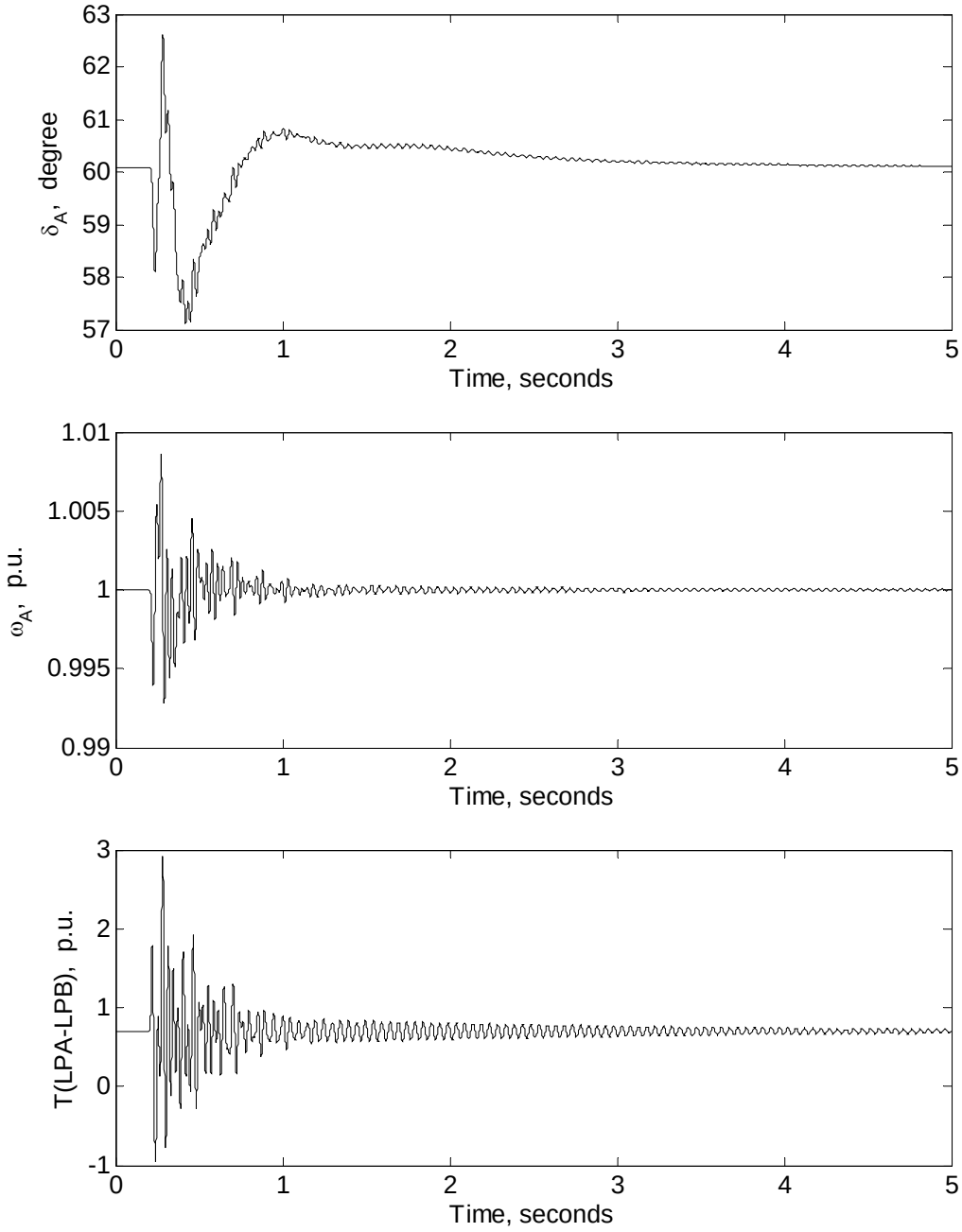

Figure 3.15 Time responses of the low pressure stage (LPA) angle, angular speed, and shaft torque between the two low pressure stages (LPA & LPB) of the system due to a 3-cycle, three-phase fault: the VSC HVDC back-to-back active power and supplementary controllers are employed simultaneously (P_{dc} = 0.20 p.u., X_C = 0.35 p.u.).

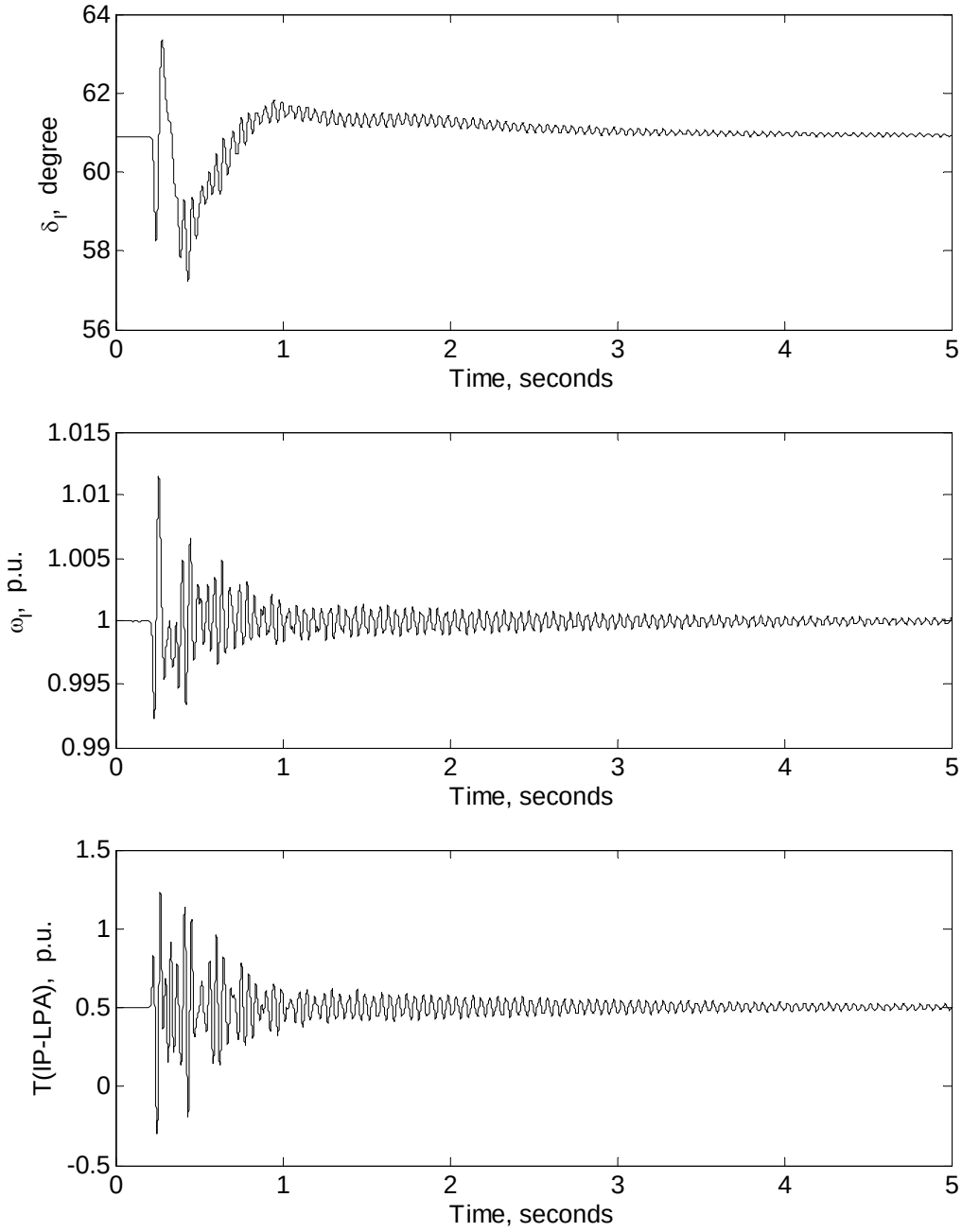

Figure 3.16 Time responses of the intermediate pressure stage (IP) angle, angular speed, and shaft torque between the intermediate pressure stage (IP) and the low pressure stage (LPA) of the system due to a 3-cycle, three-phase fault: the VSC HVDC back-to-back active power and supplementary controllers are employed simultaneously (P_{dc} = 0.20 p.u., X_C = 0.35 p.u.).

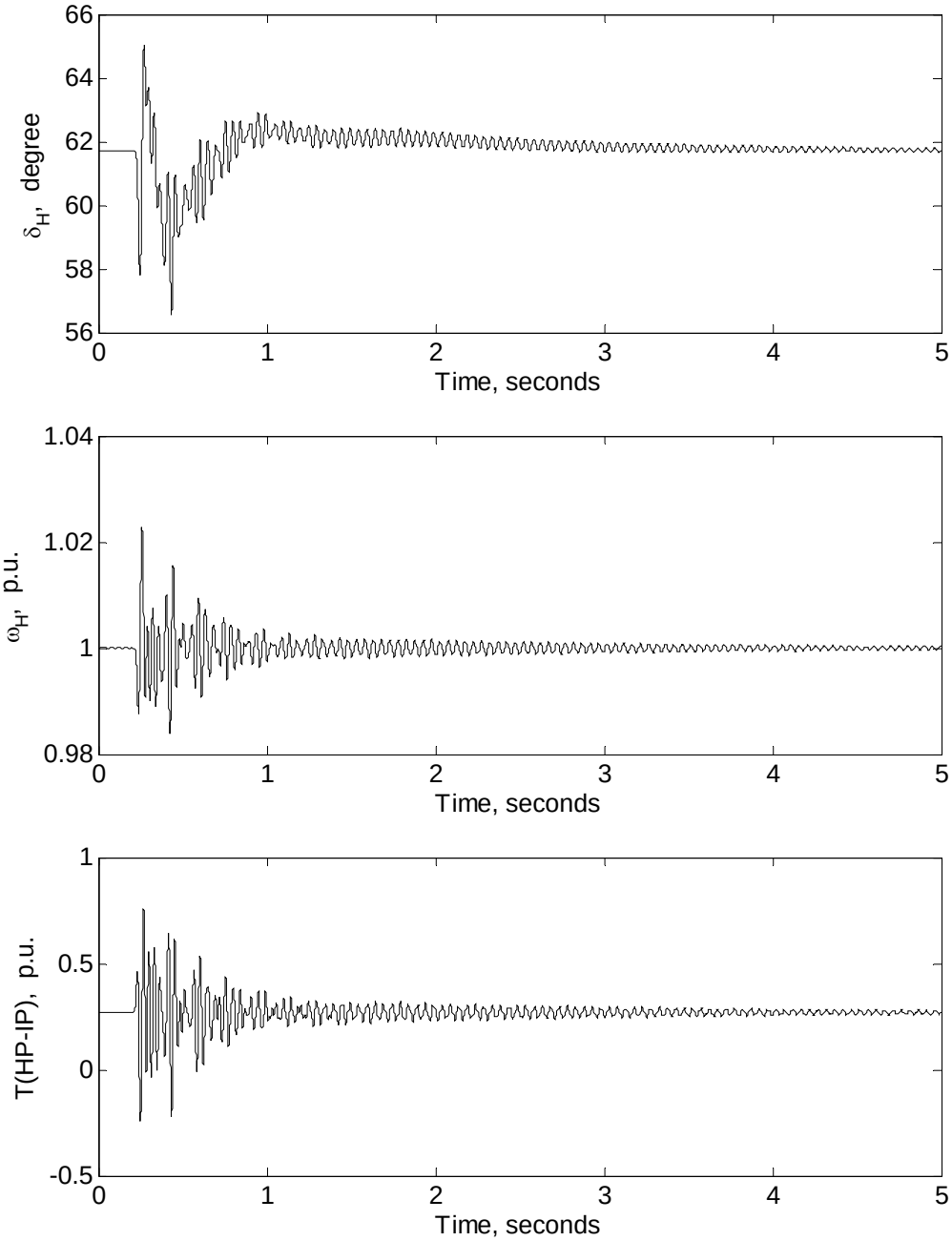

Figure 3.17 Time responses of the high pressure stage (HP) angle, angular speed, and shaft torque between the high pressure stage (HP) and the intermediate pressure stage (IP) of the system due to a 3-cycle, three-phase fault: the VSC HVDC back-to-back active power and supplementary controllers are employed simultaneously (P_{dc} = 0.20 p.u., X_C = 0.35 p.u.).

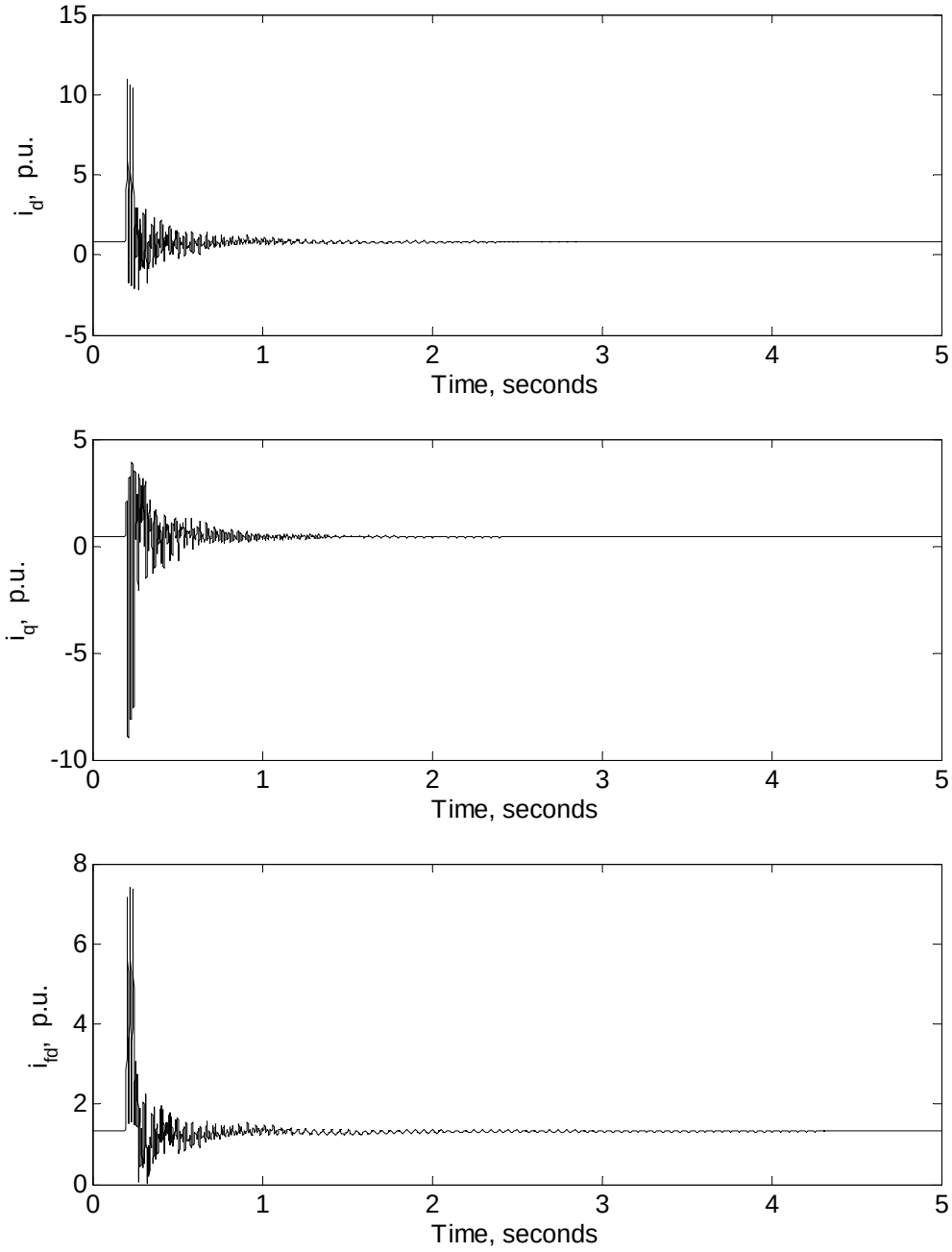

Figure 3.18 Time responses of the generator stator currents in the d-q reference frame and the field current of the system due to a 3-cycle, three-phase fault: the VSC HVDC back-to-back active power and supplementary controllers are employed simultaneously (P_{dc} = 0.20 p.u., X_C = 0.35 p.u.).

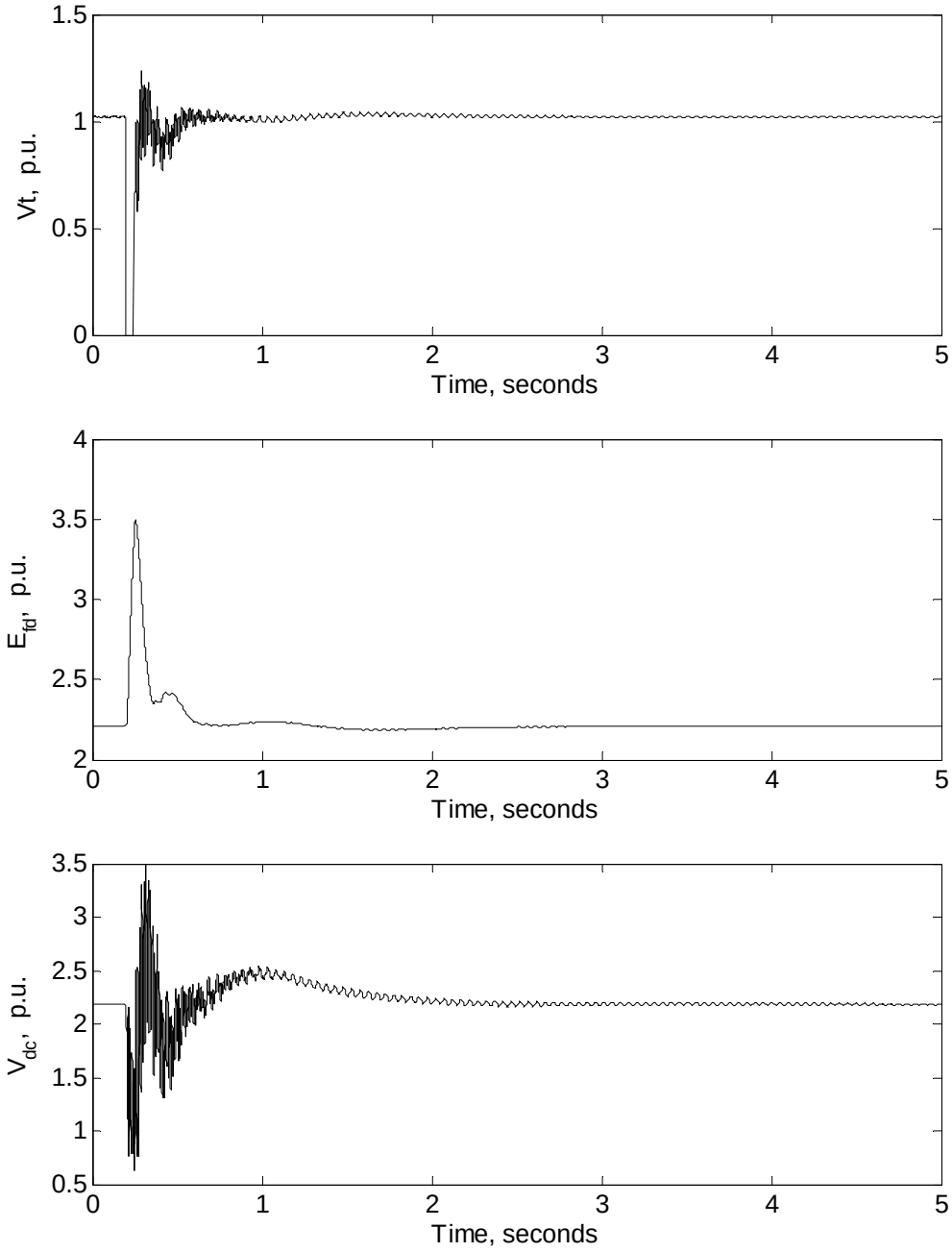

Figure 3.19 Time responses of the generator terminal and field voltages, and the voltage across the dc capacitor of the system due to a 3-cycle, three-phase fault: the VSC HVDC back-to-back active power and supplementary controllers are employed simultaneously (P_{dc} = 0.20 p.u., X_C = 0.35 p.u.).

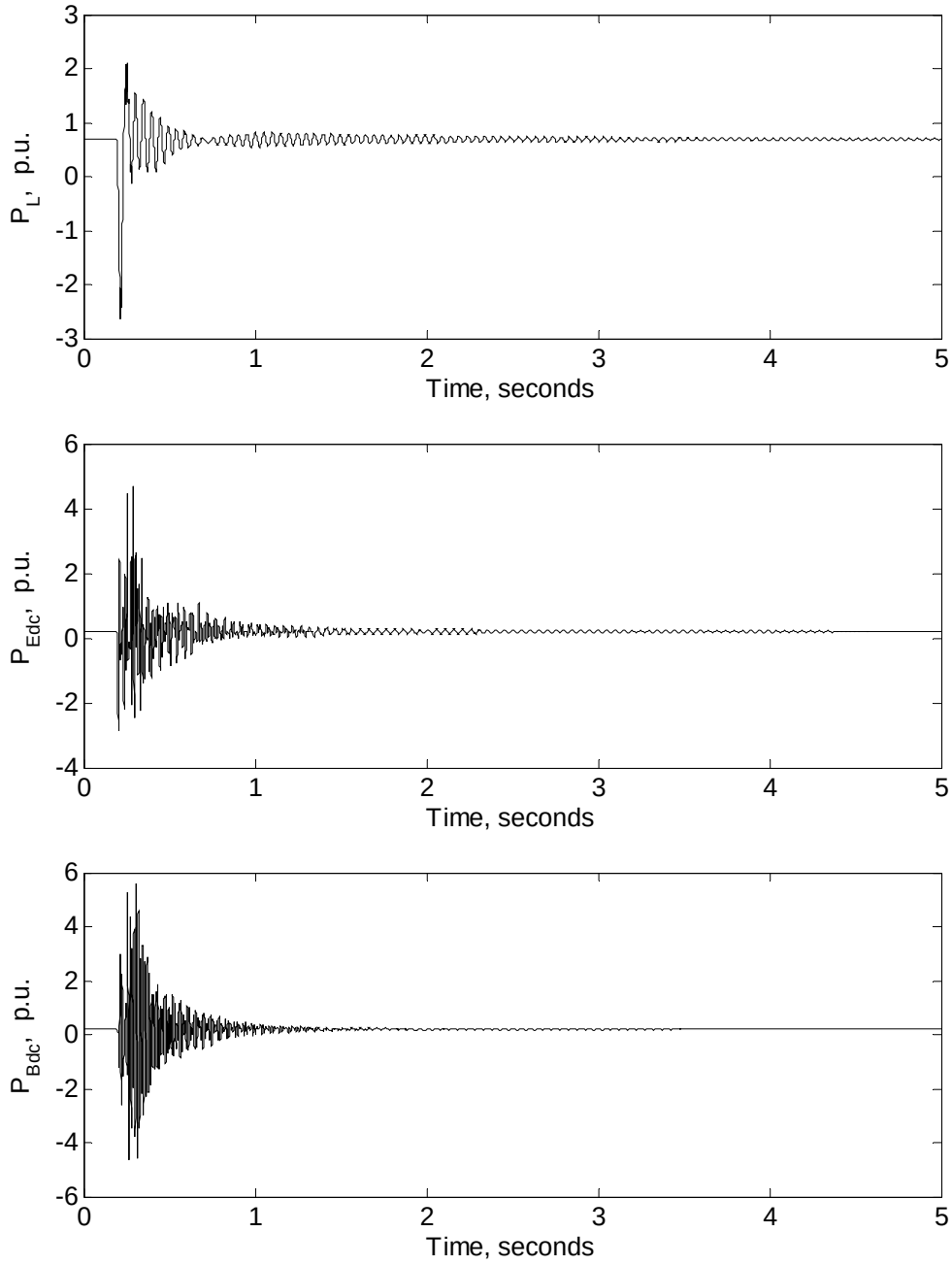

Figure 3.20 Time responses of the active power flows through the transmission line and the two stations of the VSCHVDC of the system due to a 3-cycle, three-phase fault: the VSC HVDC back-to-back active power and supplementary controllers are employed simultaneously (P_{dc} = 0.20 p.u., X_C = 0.35 p.u.).

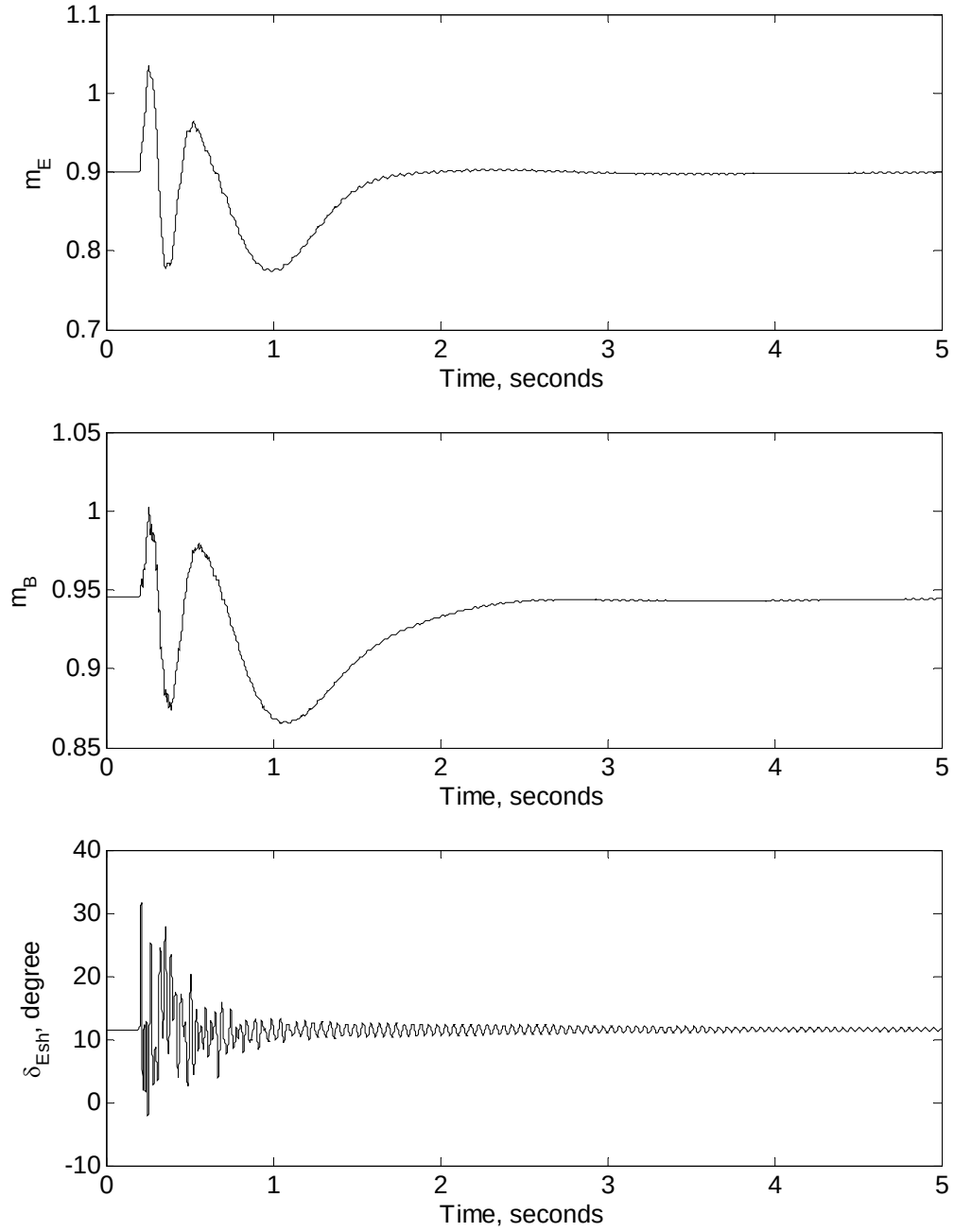

Figure 3.21 Time responses of the control signals of the system due to a 3-cycle, three-phase fault: the VSC HVDC back-to-back active power and supplementary controllers are employed simultaneously (P_{dc} = 0.20 p.u., X_C = 0.35 p.u.).

3.8 Summary

In this Chapter, a new concept for using the VSC HVDC back-to-back system with a designed supplementary controller for mitigation of SSR oscillations in a series capacitor compensated power system is proposed. A comprehensive approach for developing a time-domain analysis program is established. The dynamic performance of the system under a three-phase fault at the generator terminals is examined for a given compensation level. The results of such a case study have shown the effectiveness of the proposed controller in damping all SSR torsional modes.

4 EFFECTIVENESS OF THE VSC HVDC BACK-TO-BACK CONTROLLERS IN DAMPING SUBSYNCHRONOUS RESONANCE OSCILLATIONS

4.1 Introduction

Small-signal analysis using eigenvalue computation provides valuable information about the inherent dynamic characteristics of the power system. As it has been shown in Figure 2.10, torsional modes 1, 2, 3, and 4 become unstable at different compensation levels. In this chapter, the effectiveness of VSC HVDC back-to-back controllers in damping SSR oscillations at the critical compensation levels will be investigated. Moreover, the effect of the system loading on SSR oscillations is also explored.

4.2 Behaviour of the VSC HVDC Back-to-Back Controllers in Damping SSR Oscillations at the Critical Compensation Levels

To demonstrate the effectiveness of VSC HVDC back-to-back controllers in mitigation of SSR oscillations under large disturbances at the critical compensation levels, several studies of a three-cycle, three-phase faults at the generator terminals are carried out on the system under investigations for the following two cases:

Case I: The active power controller is in service and the supplementary controller is out of service.

Case II: Both the active power and the supplementary controllers are in service.

4.2.1 Damping Subsynchronous Torsional Oscillations at a Compensation Level of 26.5%

Figure 2.10 and Table 2.1 show that the real part of the eigenvalue corresponding to mode 4 reaches its maximum at a compensation level of 26.5% corresponding to X_C = 0.1855 per unit. The power flow and voltages of the system in this case are given in Figure 4.1 and Table 4.1 respectively. The corresponding data of the controllers are given in Table 4.2. The effect of VSC HVDC back-to-back controllers on the dynamic performance of the system due to a 3-cycle, three-phase fault at the generator terminals are shown in Figures 4.2 to 4.4.

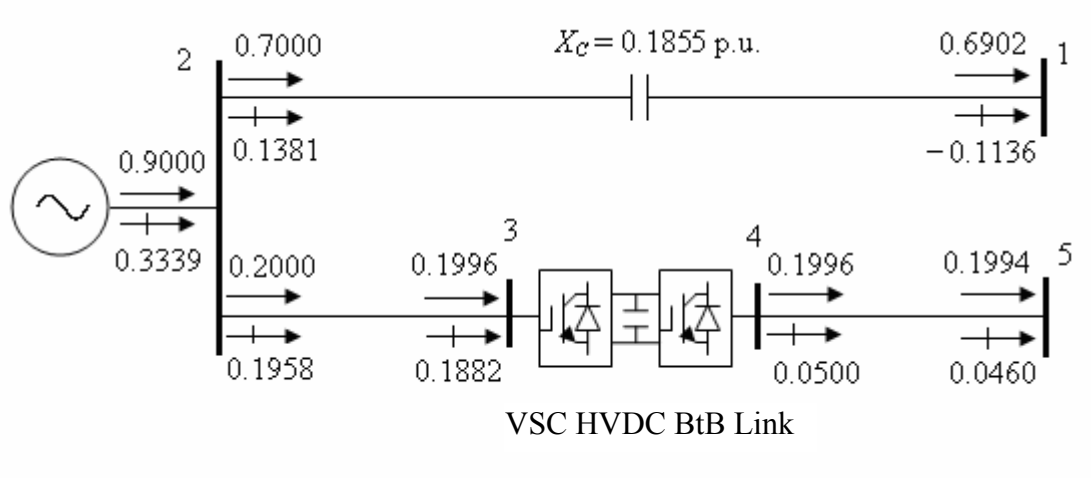

Figure 4.1 System power flow results (P_{dc} = 0.20 p.u., X_C = 0.1855 p.u.).

Table 4.1 System bus and VSC voltages (P_{dc} = 0.20 p.u., X_C = 0.1855 p.u.).

	System bus					VSC voltage	
	1	2	3	4	5	V_{sh1}	V_{sh2}
Magnitude (p.u.)	1.0000	1.0200	1.0000	1.0257	1.0200	0.9814	1.0307
Phase angle (deg)	0	20.5113	19.4429	1.7989	0.7194	18.2775	2.8807

Table 4.2 Controller parameters (P_{dc} = 0.20 p.u., X_C = 0.1855 p.u.).

Active power controller		
K_{Ed} = 6.0	T_{Ed} = 0.1 sec.	T_{me} = 0.2 sec.
K_{Bd} = 6.0	T_{Bd} = 0.1 sec.	T_{mb} = 0.2 sec.
Supplementary controller		
K_{ω} = 3.0		T_m = 0.01 sec.
K_P = 0.05		K_I = 0.10

The turbine-generator electromagnetic and shaft torsional torque responses due to a 3-cycle, three-phase fault at the generator terminals are shown in Figure 4.2 for Cases I and II. Figure 4.3 shows the generator rotor angle, angular speed and the terminal voltage of the system for the same two cases. Moreover, the time responses of the output control signals are shown in Figure 4.4.

As it can be seen from Figures 4.2, the turbine-generator torsional torques are, most often, not sinusoidal with a single frequency component, but contain contributions from all the torsional modes. Moreover, it can be noticed that the shaft section between the generator and the low pressure stage is subjected to the highest stresses. Figure 4.2 also shows that at this compensation level, the shaft torsional torques exhibit severe amplifications.

Comparing Figure 4.2 (a) with Figure 4.2 (b) reveals that the VSC HVDC back-to-back system equipped only with the active power controller is not capable in damping the shaft torsional torques. When the supplementary controller is employed in the system, Figure 4.2 (b) shows that both controllers effectively damp all the shaft torsional torques.

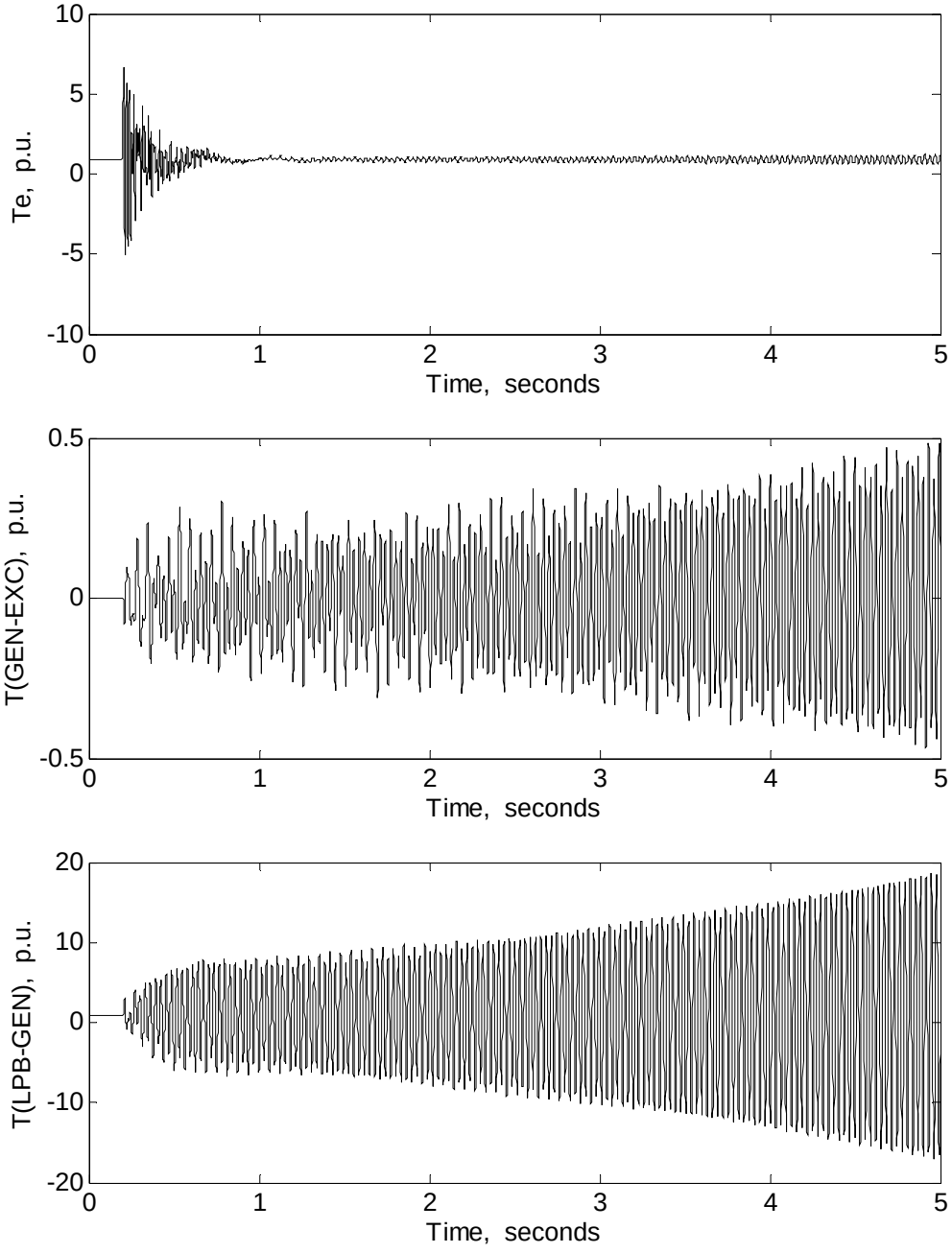

(a)

Figure 4.2 Turbine-generator electromagnetıc and shaft torsional torques during and after clearing a 3-cycle, three phase fault at the generator terminals: (a) Case I, (b) Case II (P_{dc} = 0.20 p.u., X_C = 0.1855 p.u.).

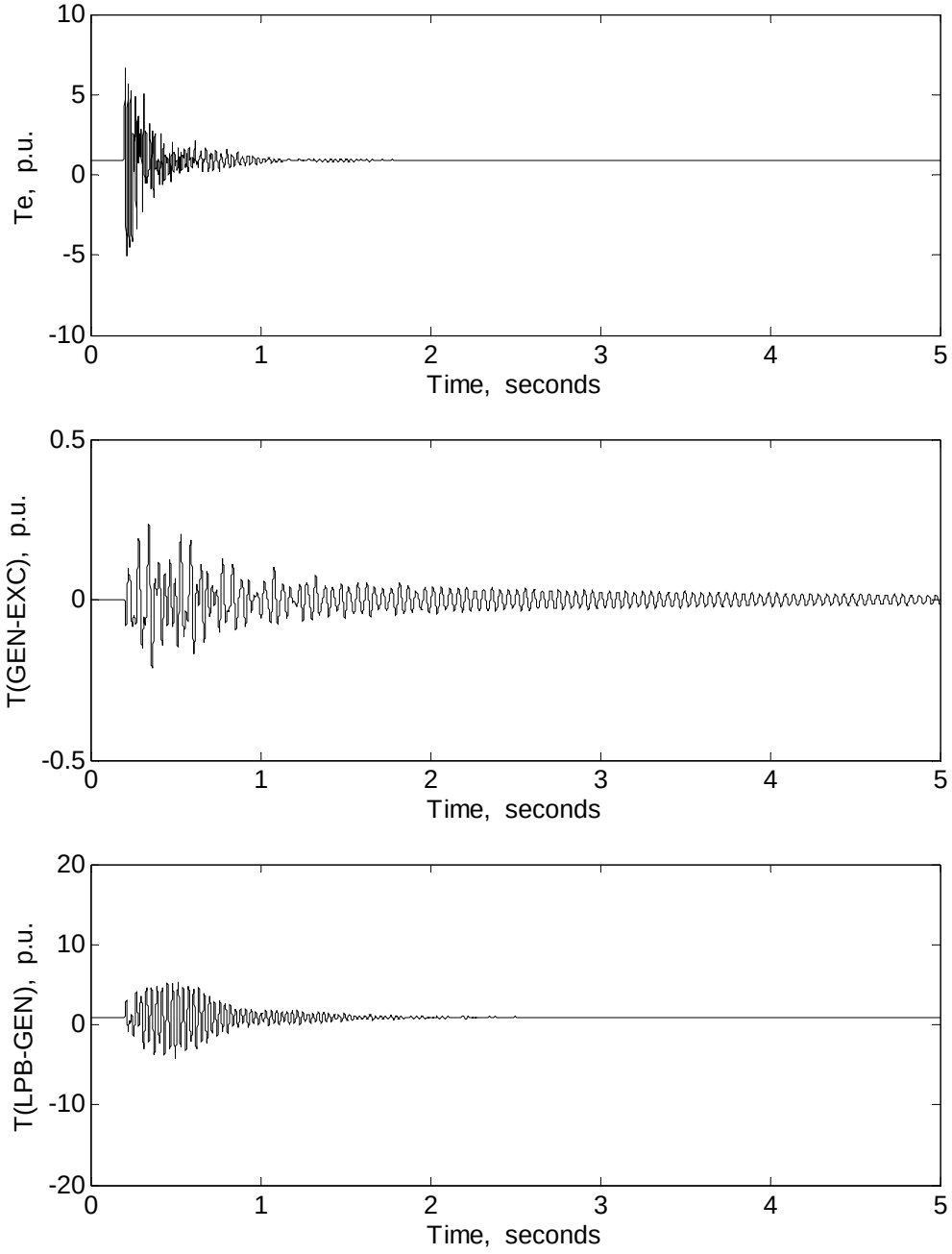

(b)

Figure 4.2 (continued)

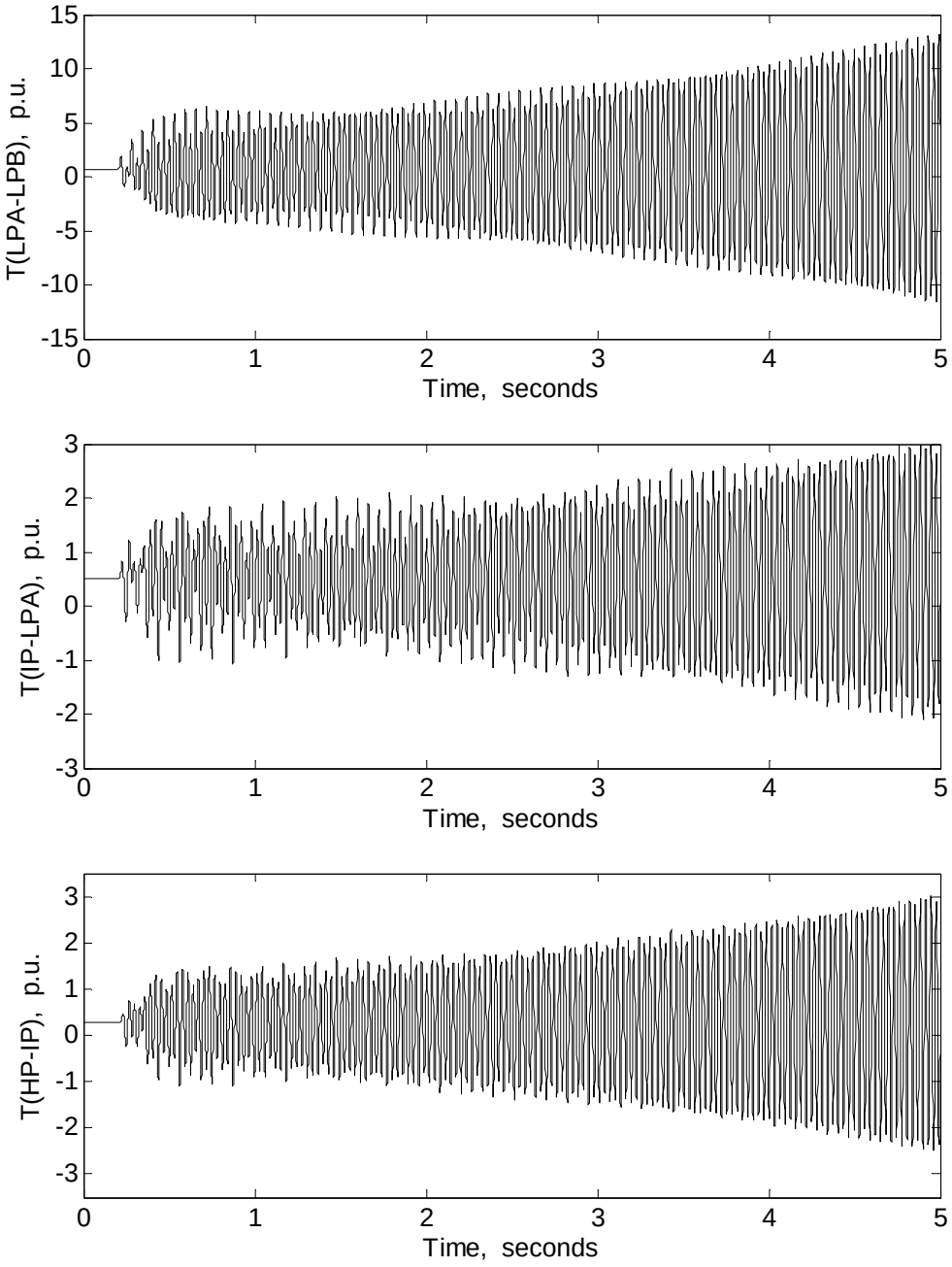

(a)

Figure 4.2 (continued)

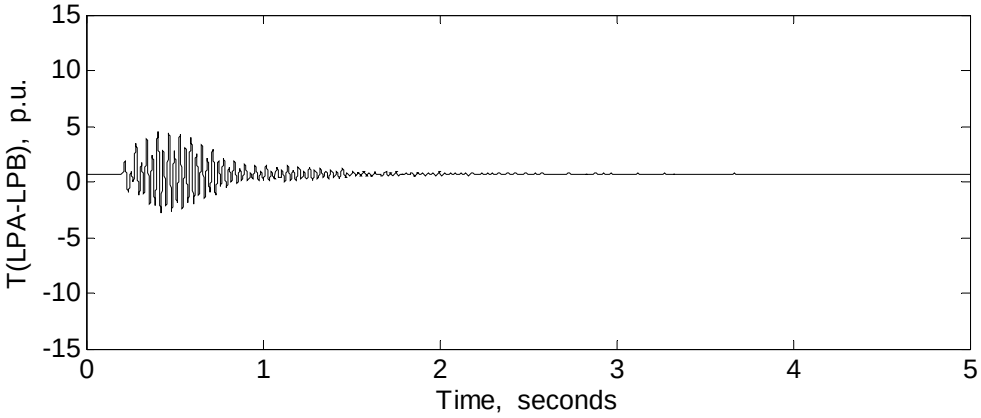

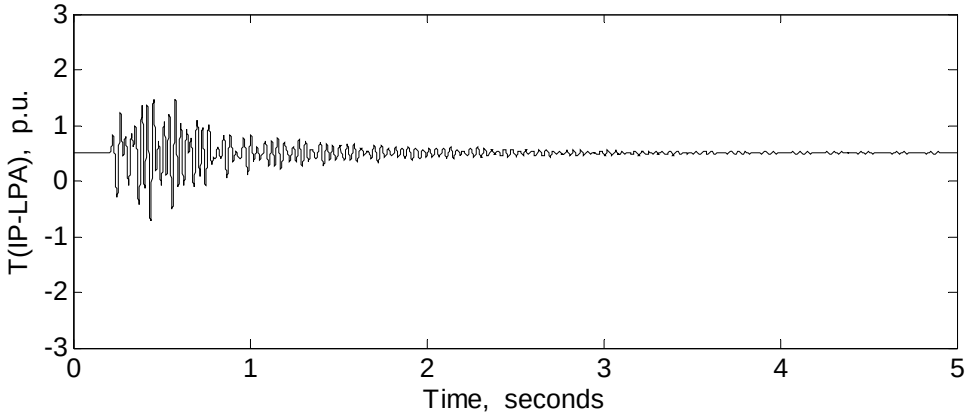

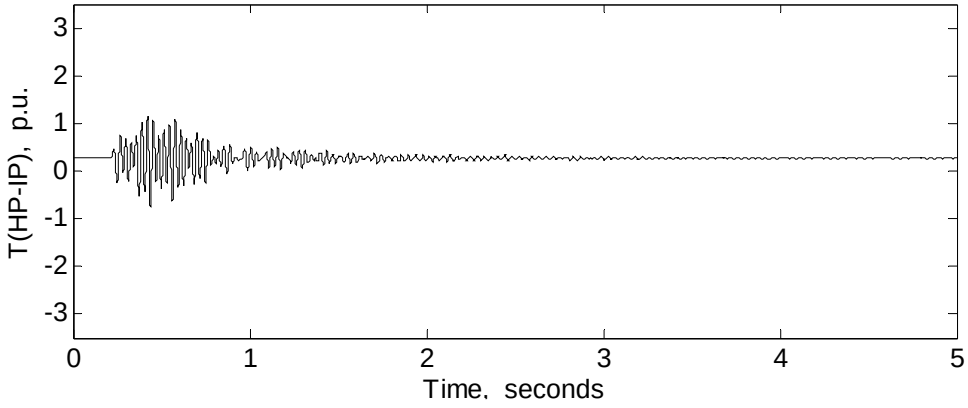

(b)

Figure 4.2 (continued)

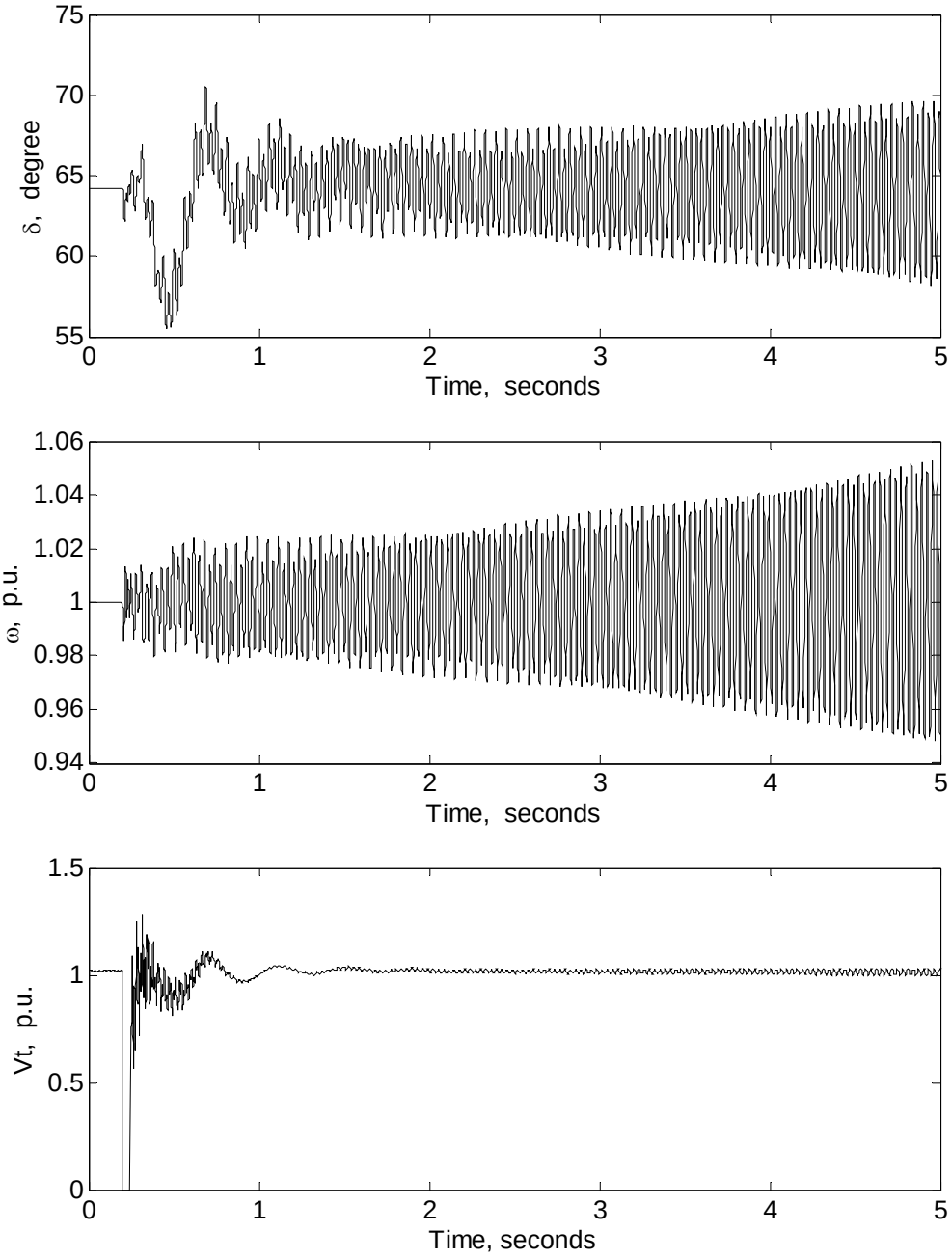

(a)

Figure 4.3 Generator rotor angle, angular speed, and terminal voltage responses to a 3-cycle, three-phase fault at the generator terminals: (a) Case I, (b) Case II (P_{dc} = 0.20 p.u., X_C = 0.1855 p.u.).

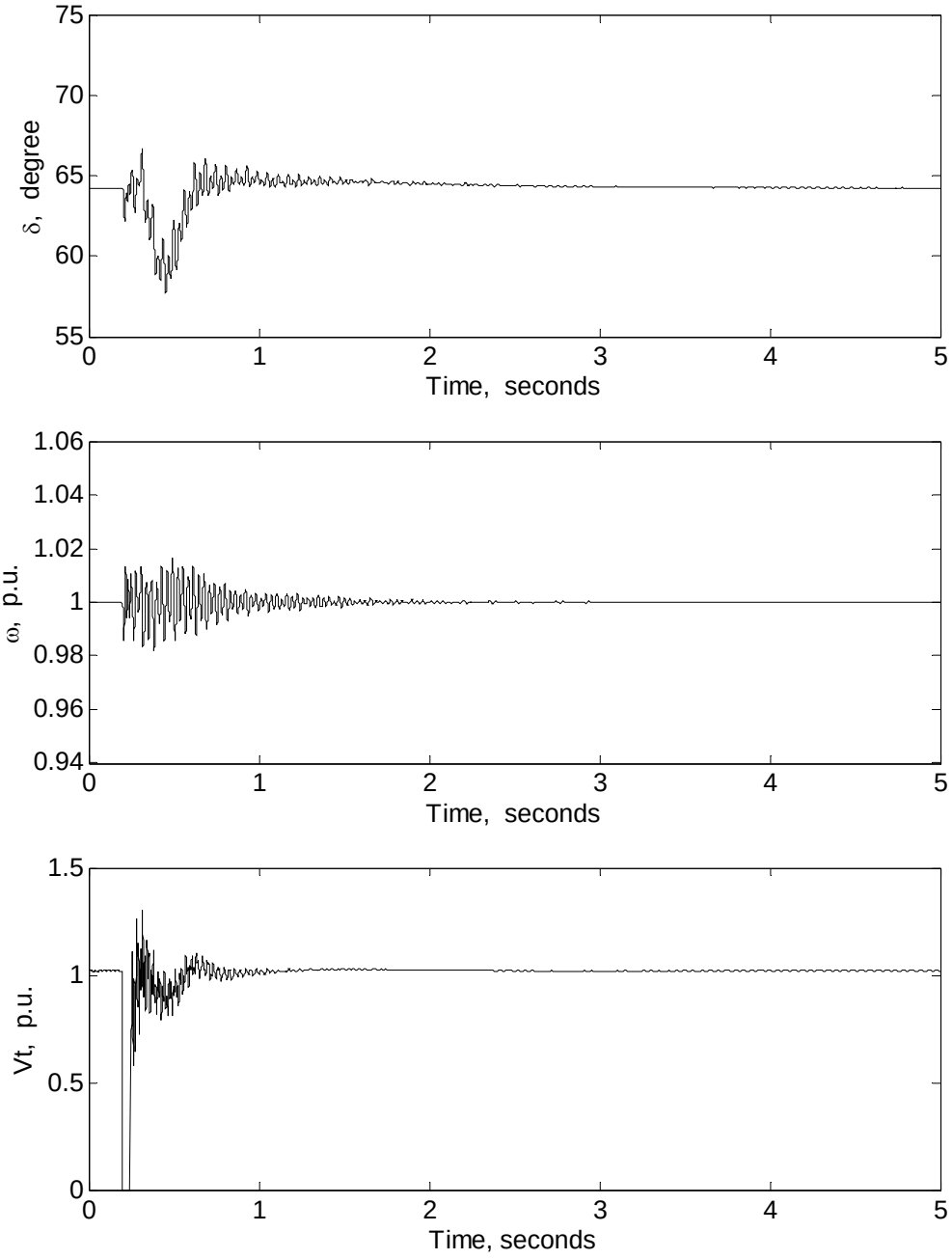

(b)

Figure 4.3 (continued)

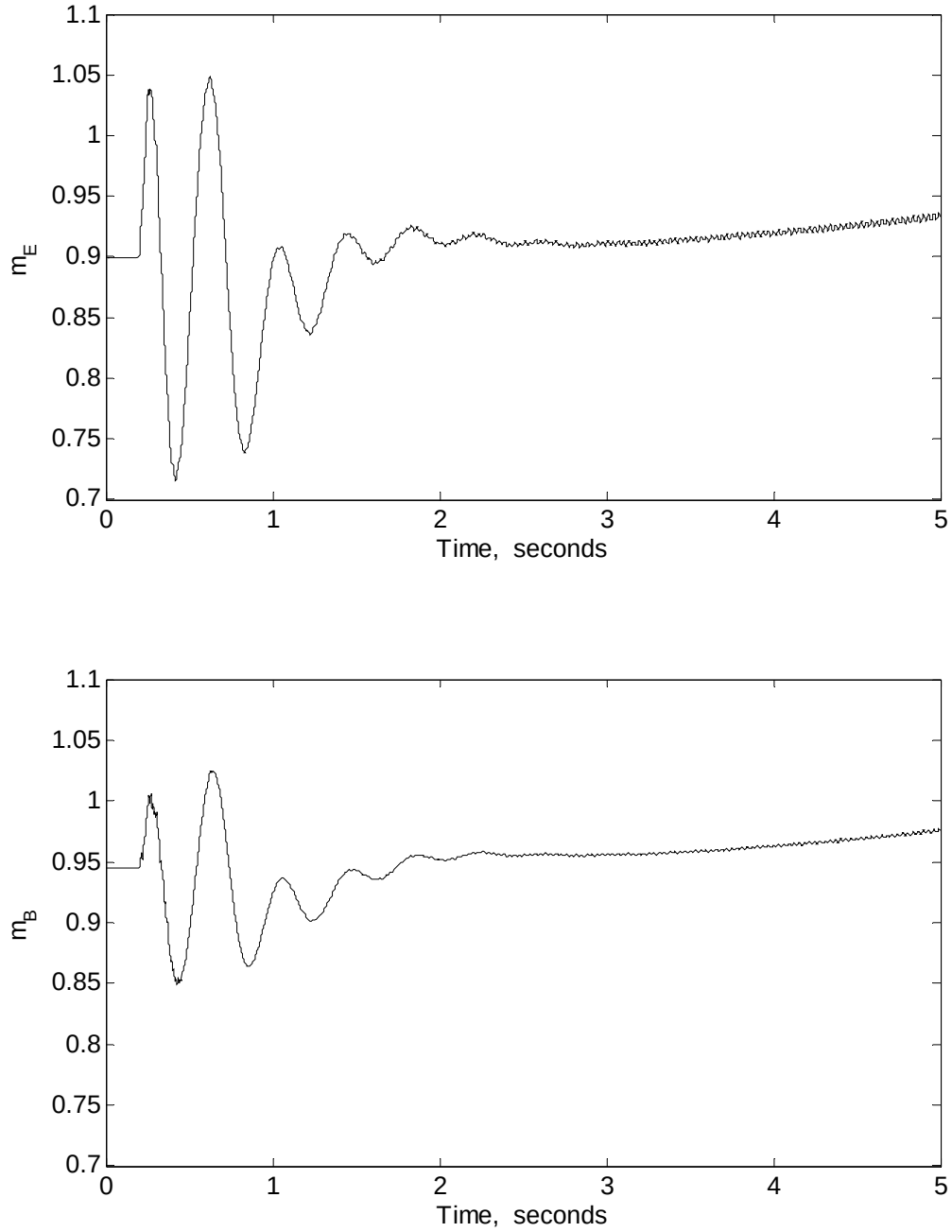

(a)

Figure 4.4 Time responses of the output control signals during and after clearing a 3-cycle, three-phase fault at the generator terminals: (a) Case I, (b) Case II (P_{dc} = 0.20 p.u., X_C = 0.1855 p.u.).

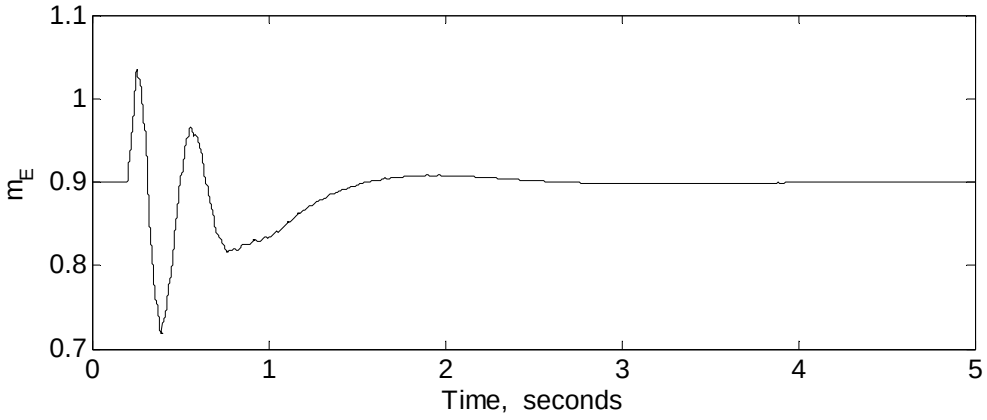

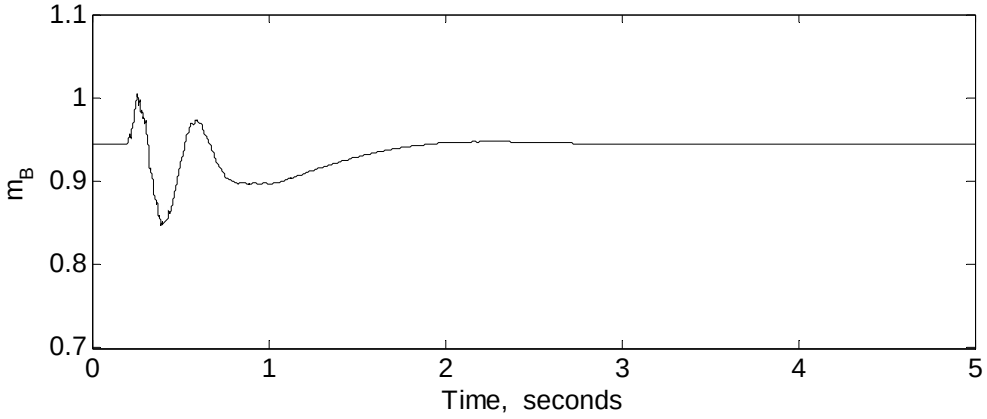

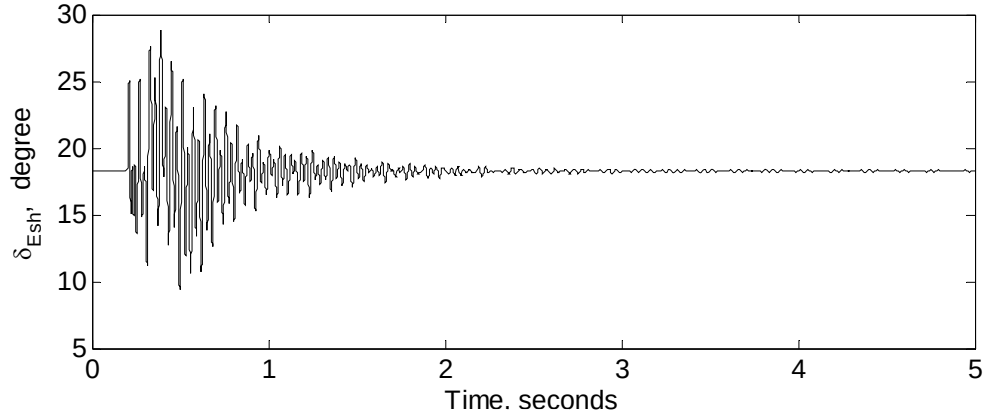

(b)

Figure 4.4 (continued)

4.2.2 Damping Subsynchronous Torsional Oscillations at a Compensation Level of 41.1%

As it can be seen from Figure 2.10, the real part of mode 3 eigenvalue reaches its maximum at a compensation level of 41.1% corresponding to $X_C = 0.2877$ per unit. The power flow and voltages of the system in this case study are given in Figure 4.5 and Table 4.3 respectively. The corresponding data of the controllers are given in Table 4.4. As it can be seen from Tables 4.1 and 4.2, the phase angle of bus 2 in the case of a compensation level of 41.1% (16.3023^0) is less than that corresponding to a compensation level of 26.5% (20.5113^0). This observation should be predicated since, increasing the compensation level results in an increase in the maximum power transferred from bus 2 to bus 1. Consequently, for the same amount of power transferred (0.7 per unit), the relative phase angle between buses 2 and 1 ($\theta_{21} = \theta_2 - \theta_1 = \theta_2 - 0^0 = \theta_2$) will be reduced. The effect of VSC HVDC back-to-back controllers on the dynamic performance of the system due to a 3-cycle, three-phase fault at the generator terminals are shown in Figures 4.6 to 4.8.

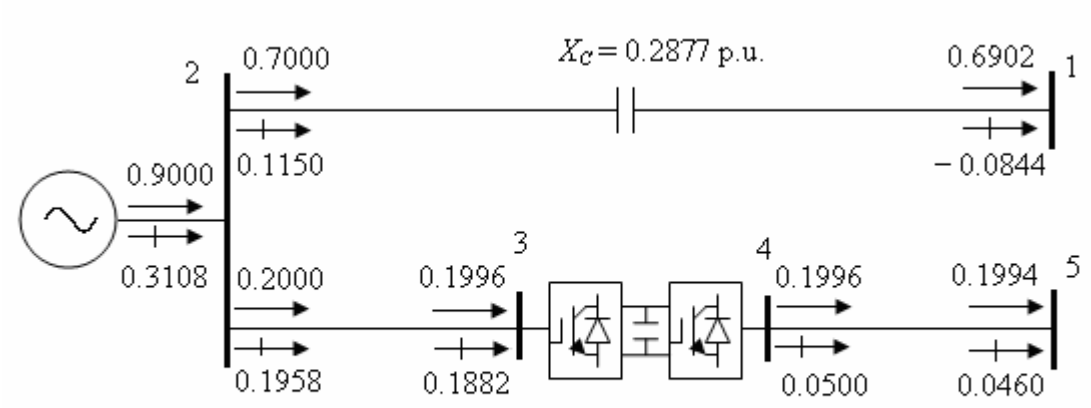

Figure 4.5 System power flow results ($P_{dc} = 0.20$ p.u., $X_C = 0.2877$ p.u.).

Table 4.3 System bus and VSC voltages (P_{dc} = 0.20 p.u., X_C = 0.2877 p.u.).

	System bus					VSC voltage	
	1	2	3	4	5	V_{sh1}	V_{sh2}
Magnitude (p.u.)	1.0000	1.0200	1.0000	1.0257	1.0200	0.9814	1.0307
Phase angle (deg)	0	16.3023	15.2339	1.7989	0.7194	14.0685	2.8807

Table 4.4 Controller parameters (P_{dc} = 0.20 p.u., X_C = 0.2877 p.u.).

Active power controller		
K_{Ed} = 6.0	T_{Ed} = 0.1 sec.	T_{me} = 0.2 sec.
K_{Bd} = 6.0	T_{Bd} = 0.1 sec.	T_{mb} = 0.2 sec.
Supplementary controller		
K_{ω} = 3.0		T_m = 0.01 sec.
K_P = 0.05		K_I = 0.10

Examination of the time responses of the shaft torsional torques shown in Figure 4.6 reveals that, although the VSC HVDC back-to-back active power controller only can damp all the shaft torsional torques, these oscillations are poorly damped. The supplementary controller, however, provides better damping in corporation with the active power controller.

4.2.3 Damping Subsynchronous Torsional Oscillations at a Compensation Level of 54.7%

The real part of mode 2 eigenvalue reaches its maximum at a compensation level of 54.7% corresponding to X_C = 0.3829 per unit. The power flow and voltages of the system in this case are given in Figure 4.9 and Table 4.5 respectively. The corresponding data of the controllers are given in Table 4.6. The effect of VSC HVDC back-to-back controllers on the dynamic performance of the system due to a 3-cycle, three-phase fault at the generator terminals are shown in Figures 4.10 to 4.12.

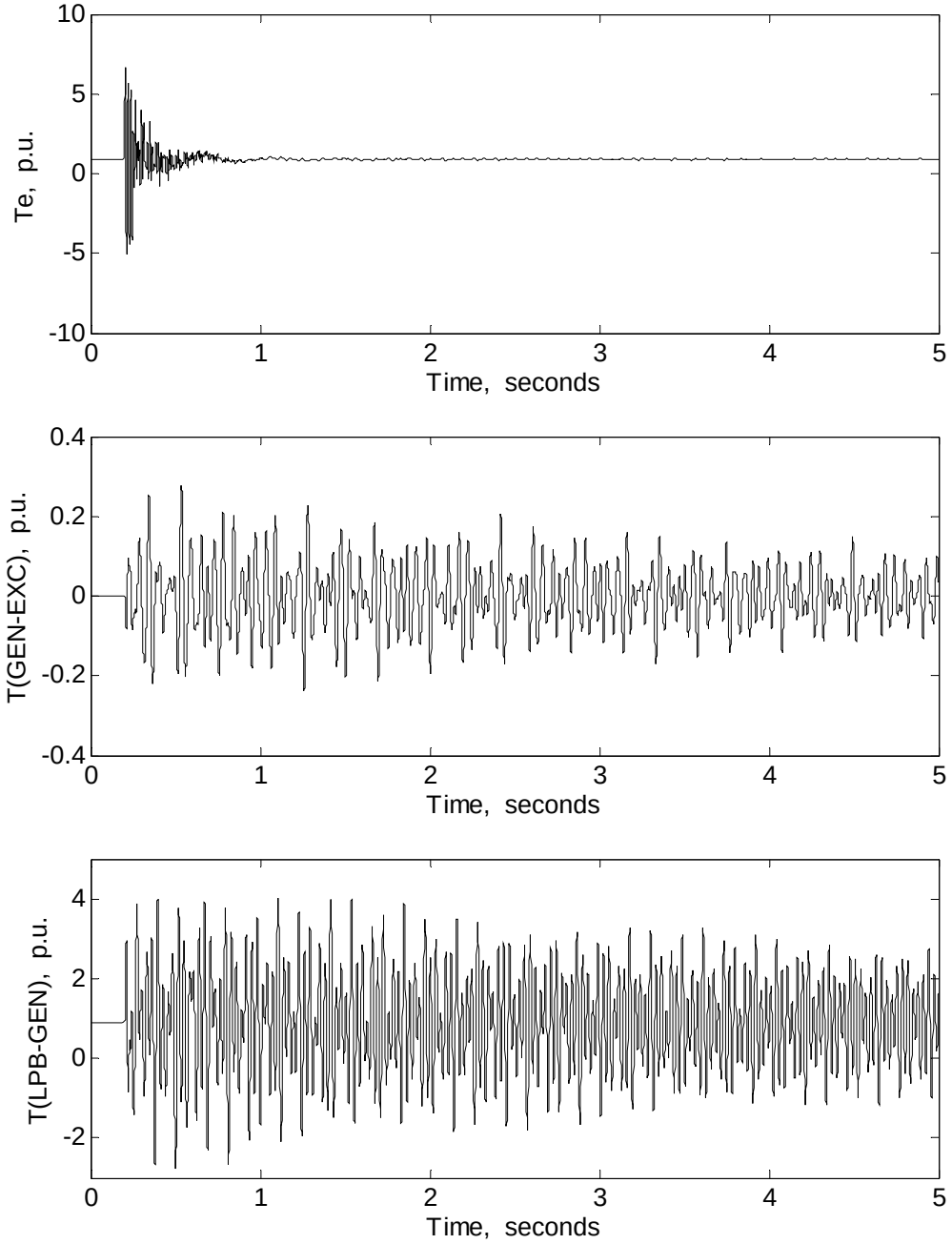

(a)

Figure 4.6 Turbine-generator electromagnetic and shaft torsional torques during and after clearing a 3-cycle, three phase fault at the generator terminals: (a) Case I, (b) Case II (P_{dc} = 0.20 p.u., X_C = 0.2877 p.u.).

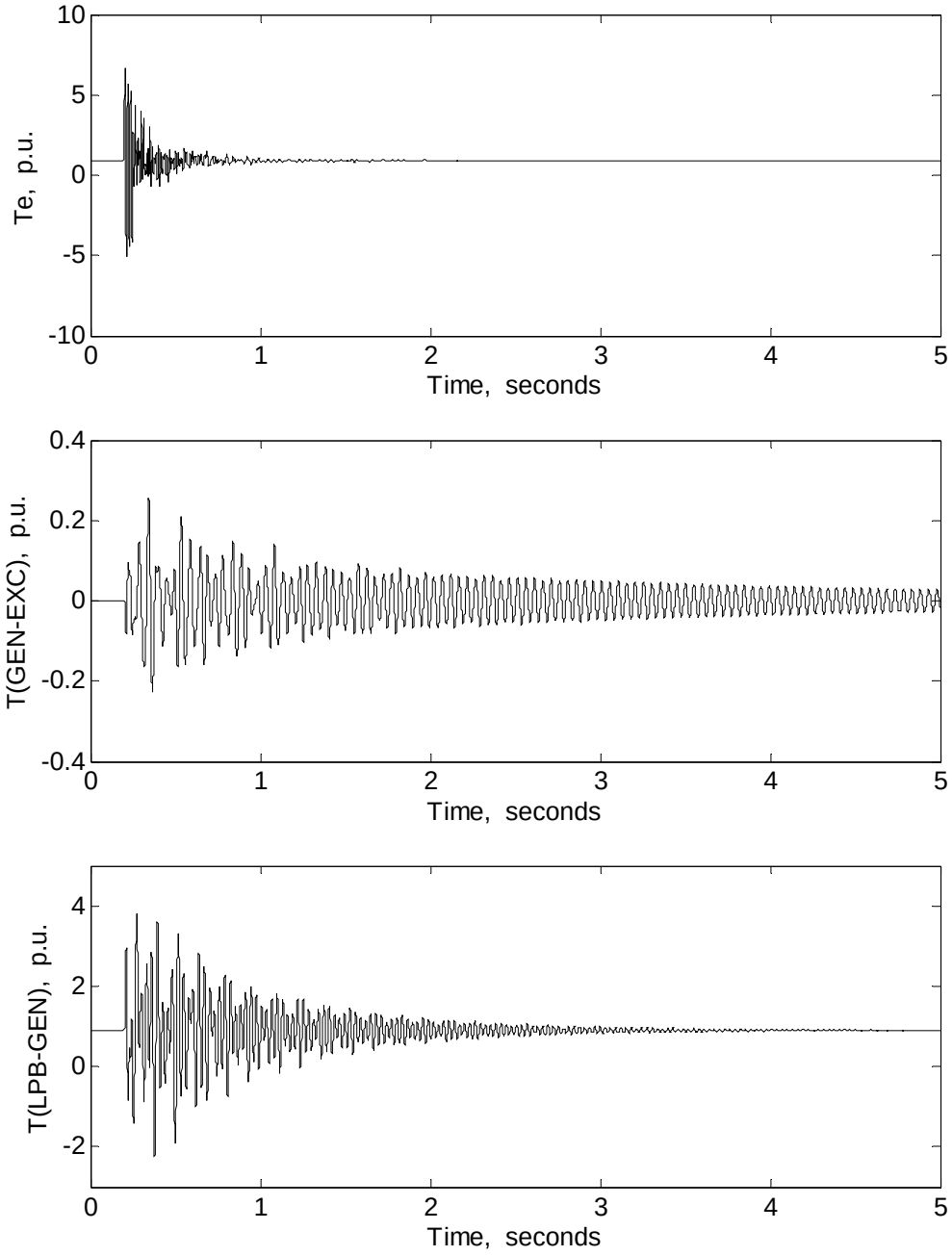

(b)

Figure 4.6 (continued)

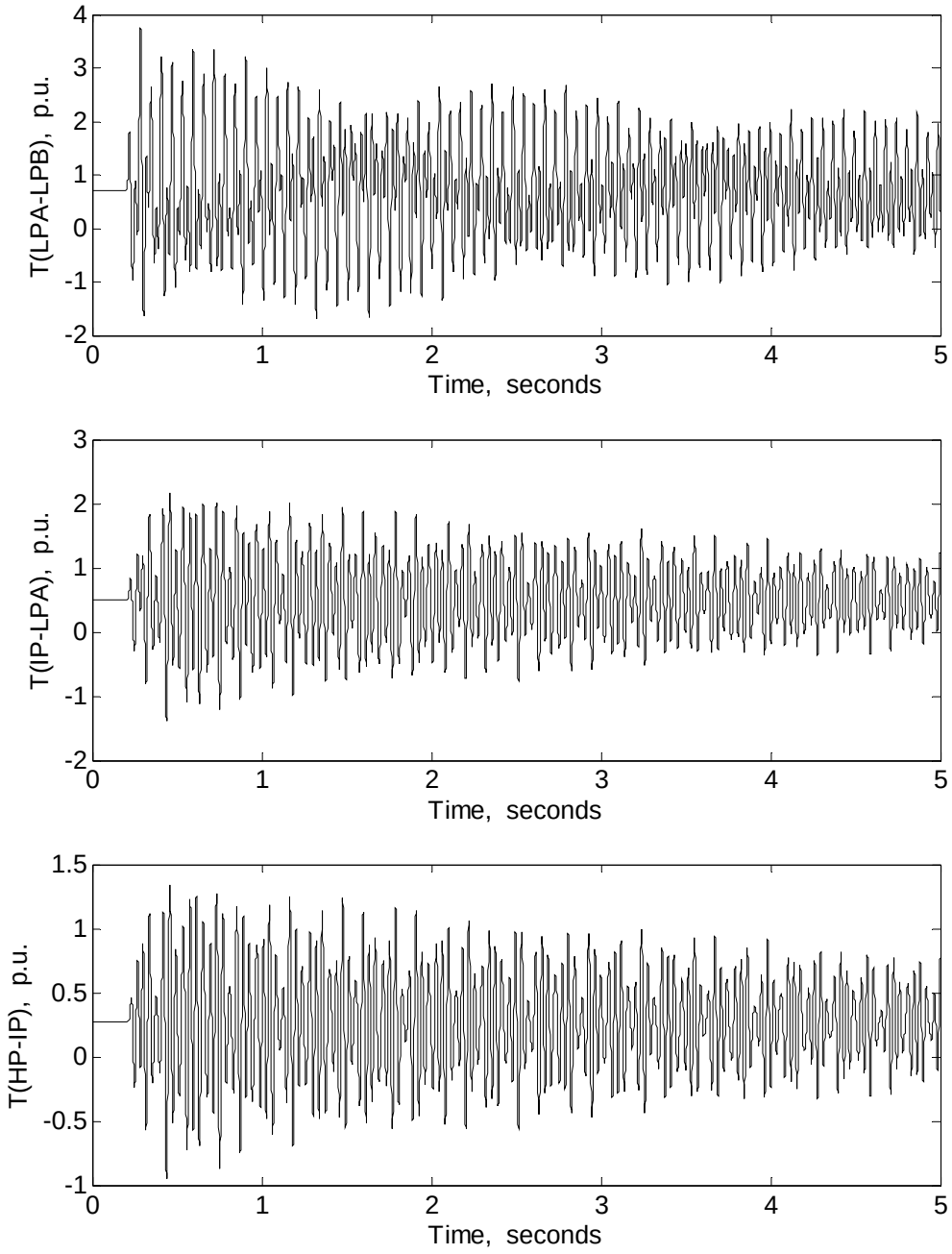

(a)

Figure 4.6 (continued)

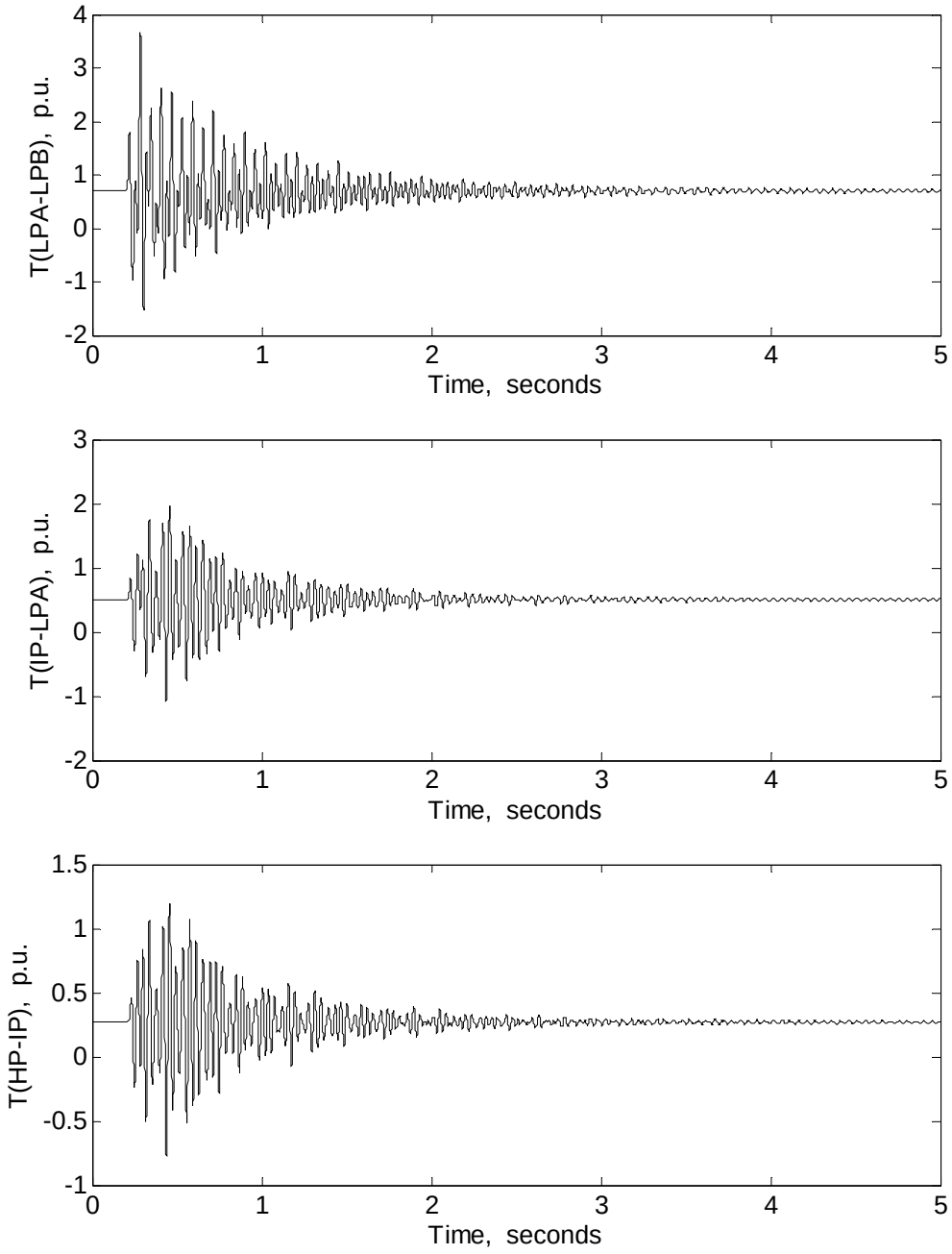

(b)

Figure 4.6 (continued)

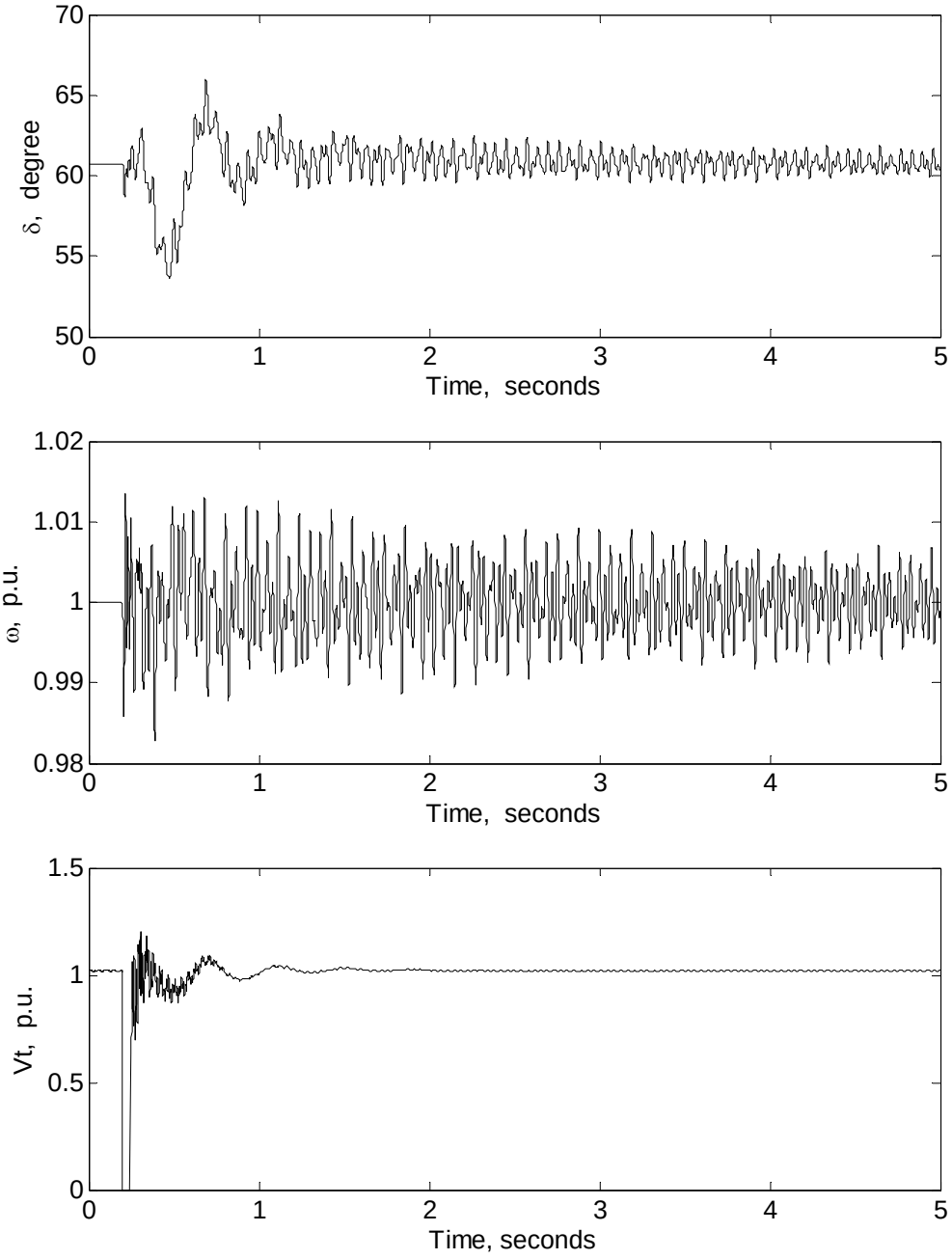

(a)

Figure 4.7 Generator rotor angle, angular speed, and terminal voltage responses to a 3-cycle, three-phase fault at the generator terminals: (a) Case I, (b) Case II (P_{dc} = 0.20 p.u., X_C = 0.1855 p.u.).

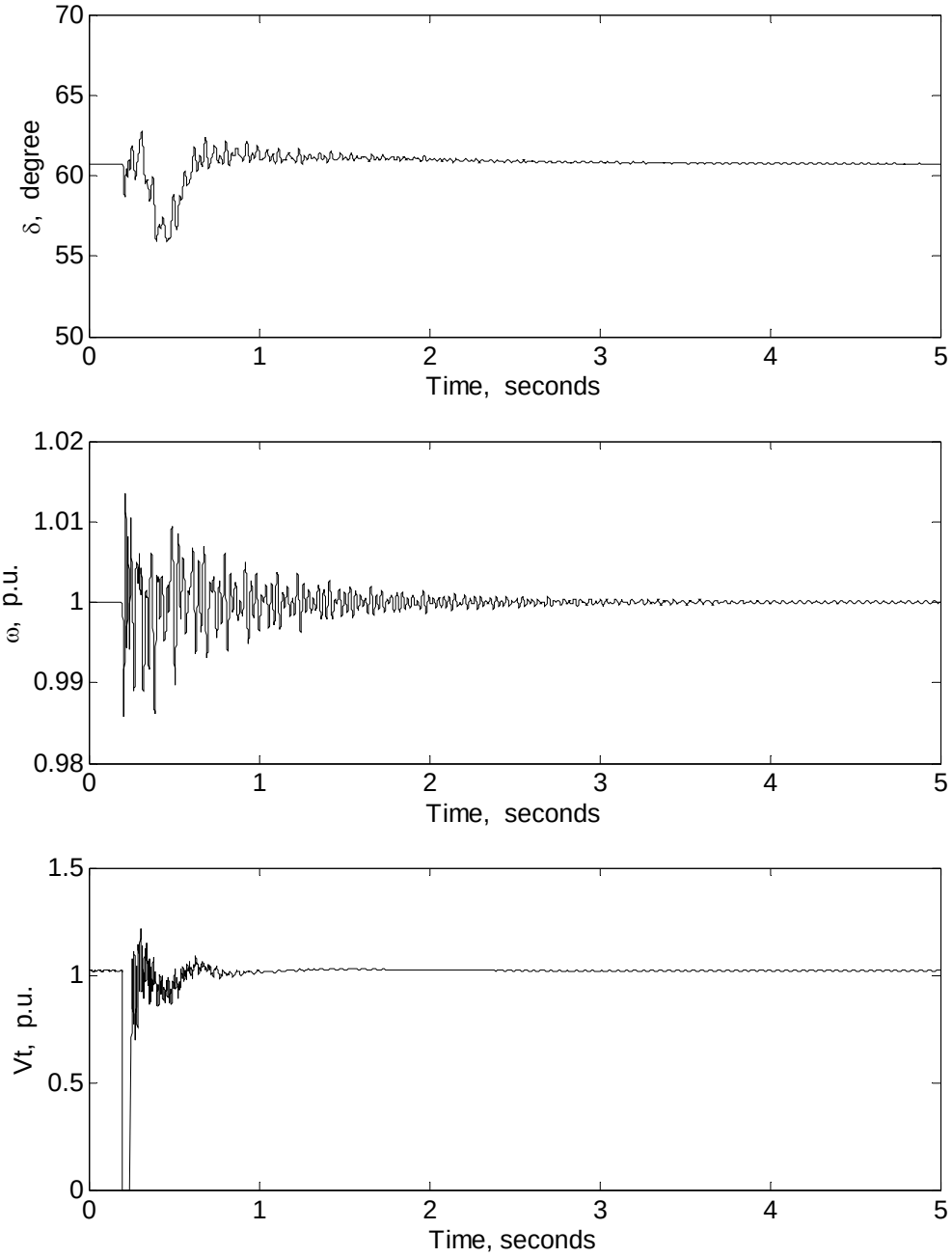

(b)

Figure 4.7 (continued)

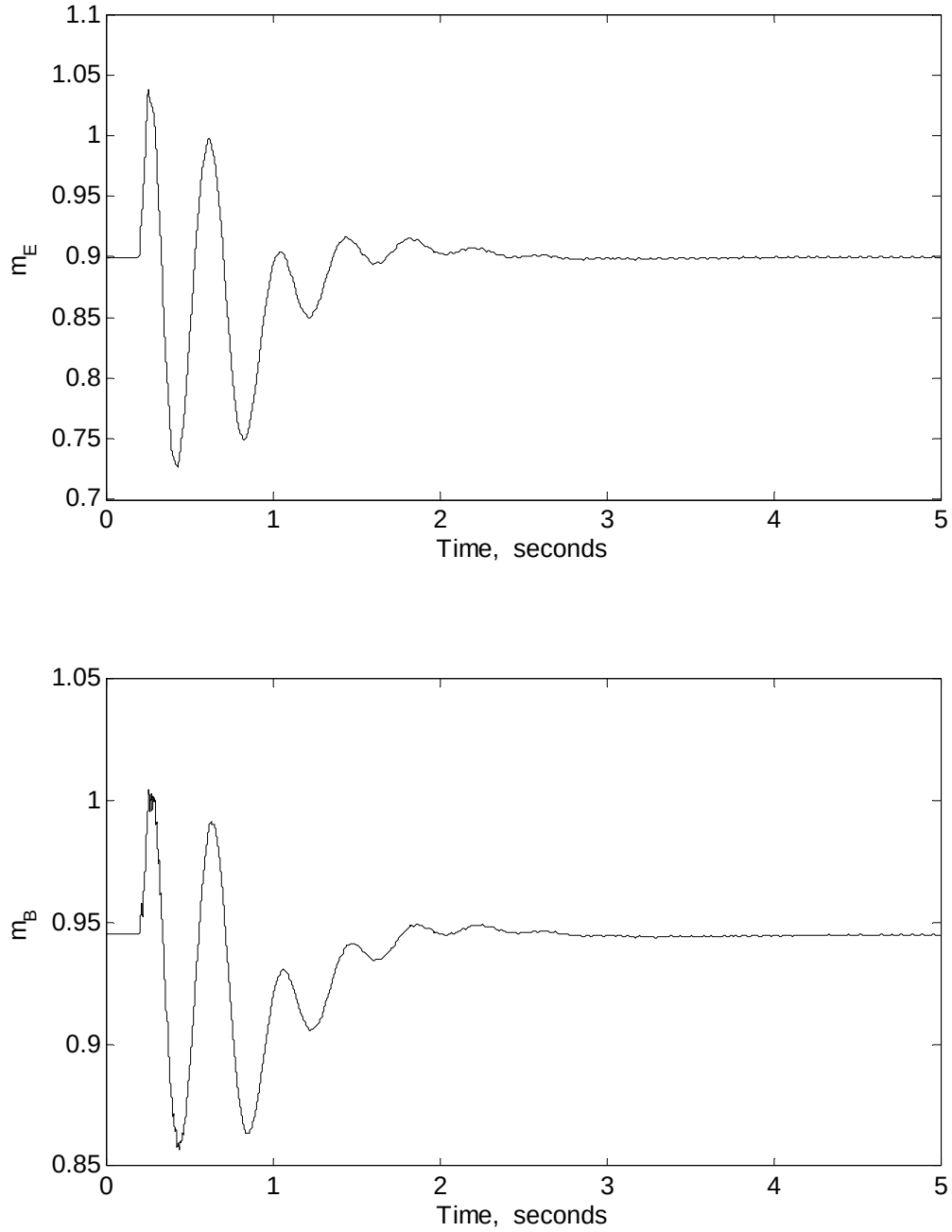

(a)

Figure 4.8 Time responses of the output control signals during and after clearing a 3-cycle, three-phase fault at the generator terminals: (a) Case I, (b) Case II (P_{dc} = 0.20 p.u., X_C = 0.2877 p.u.).

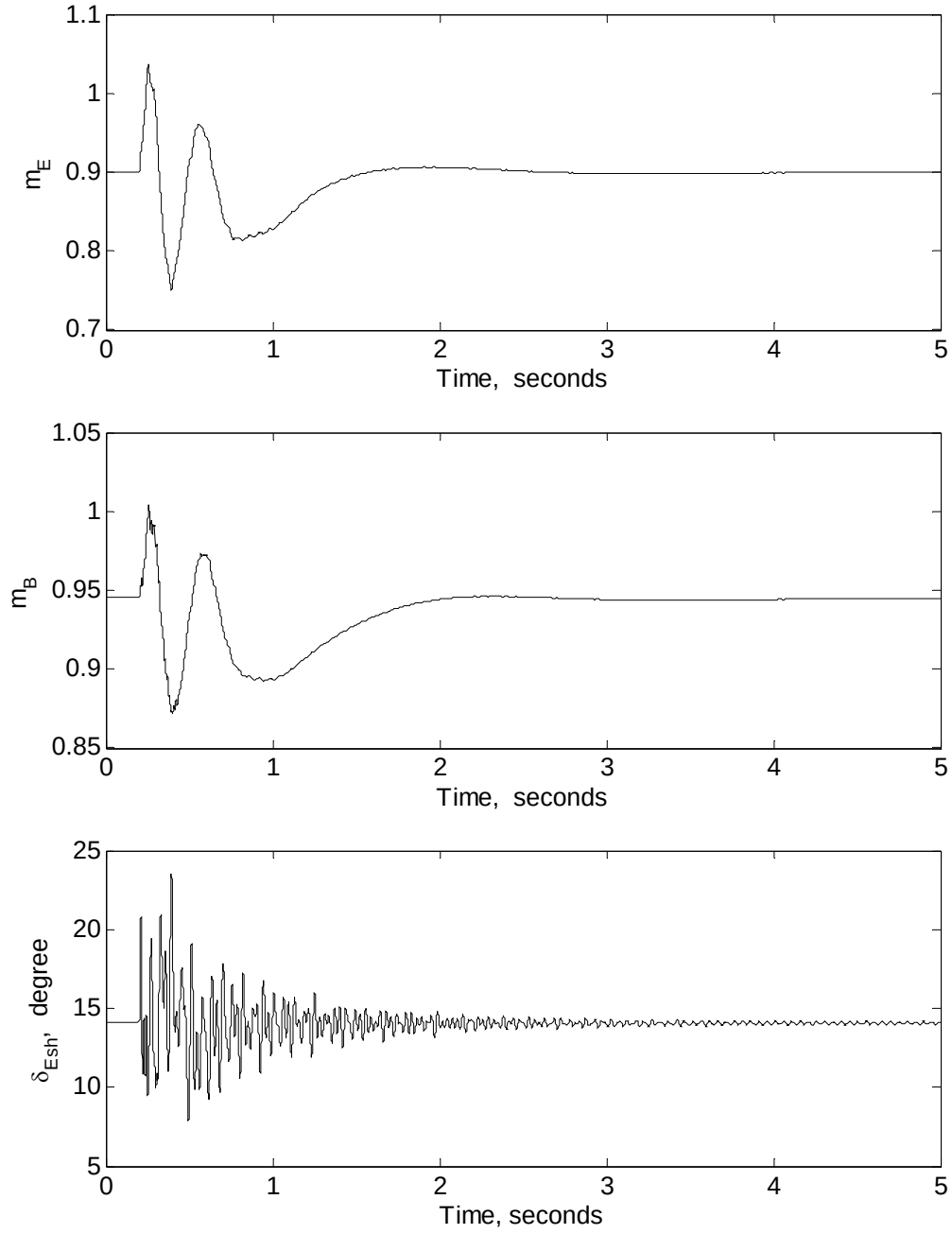

(b)

Figure 4.8 (continued)

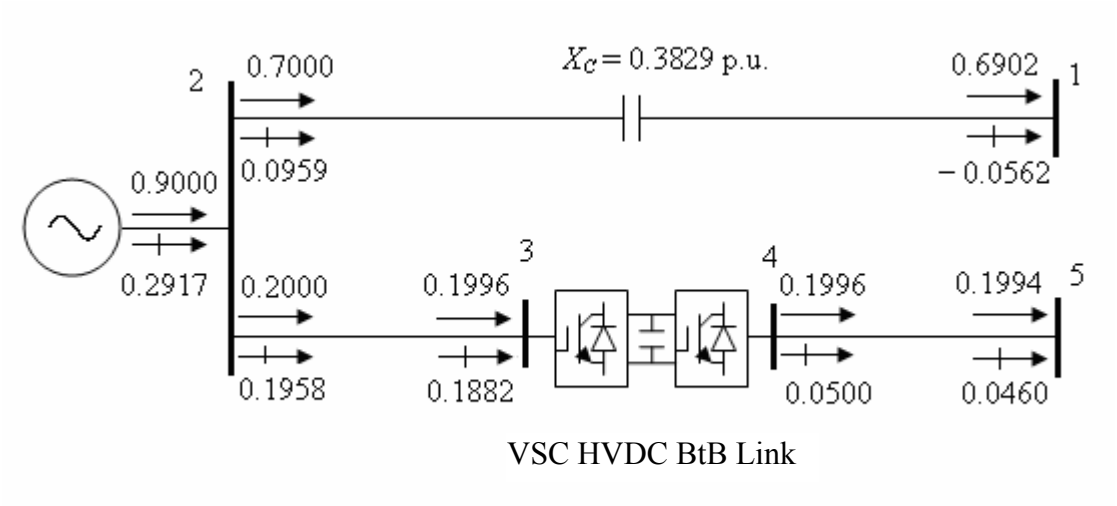

Figure 4.9 System power flow results (P_{dc} = 0.20 p.u., X_C = 0.3829 p.u.).

Table 4.5 System bus and VSC voltages (P_{dc} = 0.20 p.u., X_C = 0.3829 p.u.).

	System bus					VSC voltage	
	1	2	3	4	5	V_{sh1}	V_{sh2}
Magnitude (p.u.)	1.0000	1.0200	1.0000	1.0257	1.0200	0.9814	1.0307
Phase angle (deg)	0	12.4592	11.3908	1.7989	0.7194	10.2254	2.8807

Table 4.6 Controller parameters (P_{dc} = 0.20 p.u., X_C = 0.3829 p.u.).

Active power controller		
K_{Ed} = 6.0	T_{Ed} = 0.1 sec.	T_{me} = 0.2 sec.
K_{Bd} = 6.0	T_{Bd} = 0.1 sec.	T_{mb} = 0.2 sec.
Supplementary controller		
K_ω = 3.0		T_m = 0.01 sec.
K_P = 0.05		K_I = 0.10

Examination of the time responses of the shaft torsional torques shown in Figures 4.6 and 4.10 reveals that the system dynamic behaviour at compensation levels of 41.1% and 54.7% are almost similar. The VSC HVDC back-to-back active power controller only can damp all the shaft torsional torques. The supplementary controller, however, provides better damping in corporation with the active power controller.

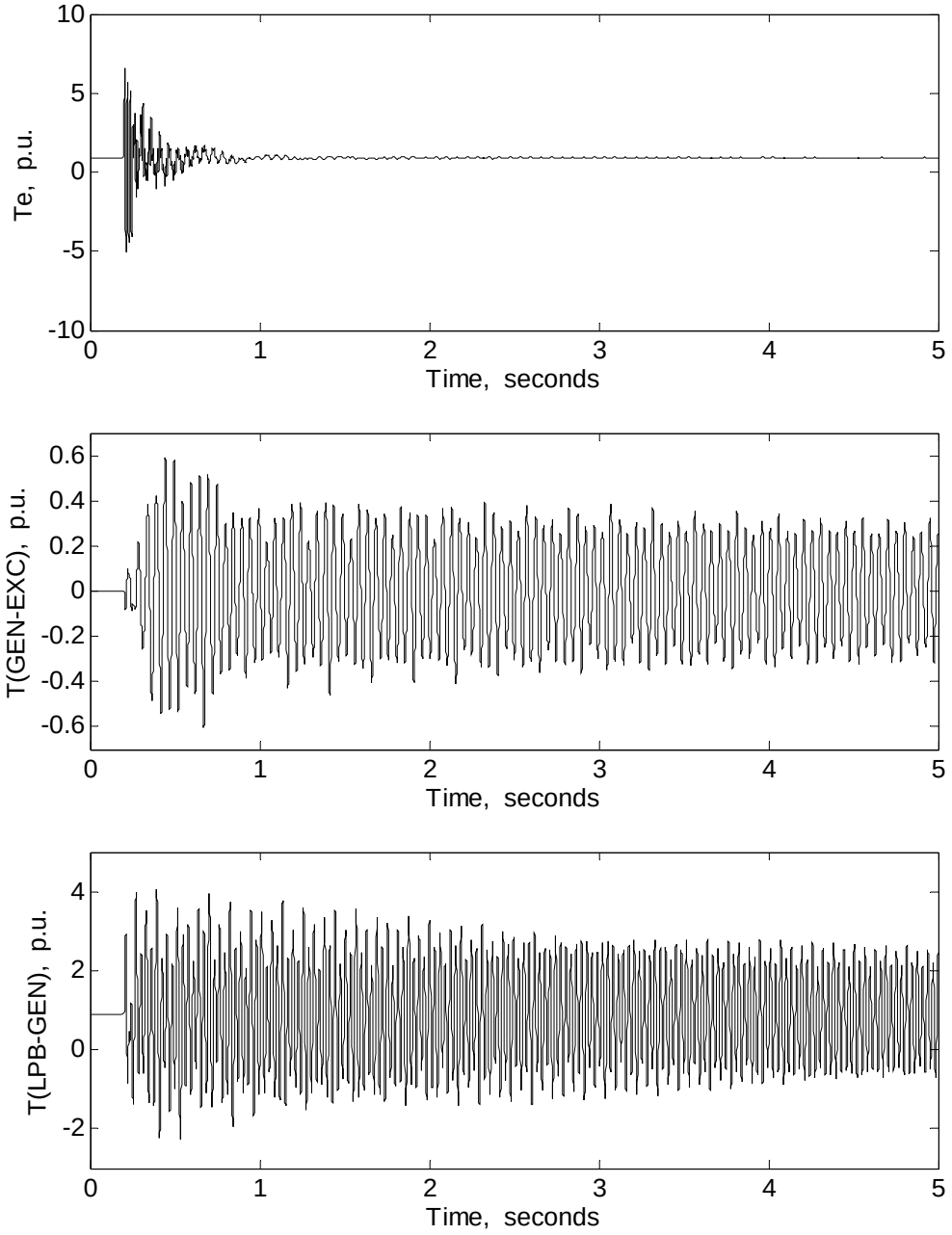

(a)

Figure 4.10 Turbine-generator electromagnetic and shaft torsional torques during and after clearing a 3-cycle, three phase fault at the generator terminals: (a) Case I, (b) Case II (P_{dc} = 0.20 p.u., X_C = 0.3829 p.u.).

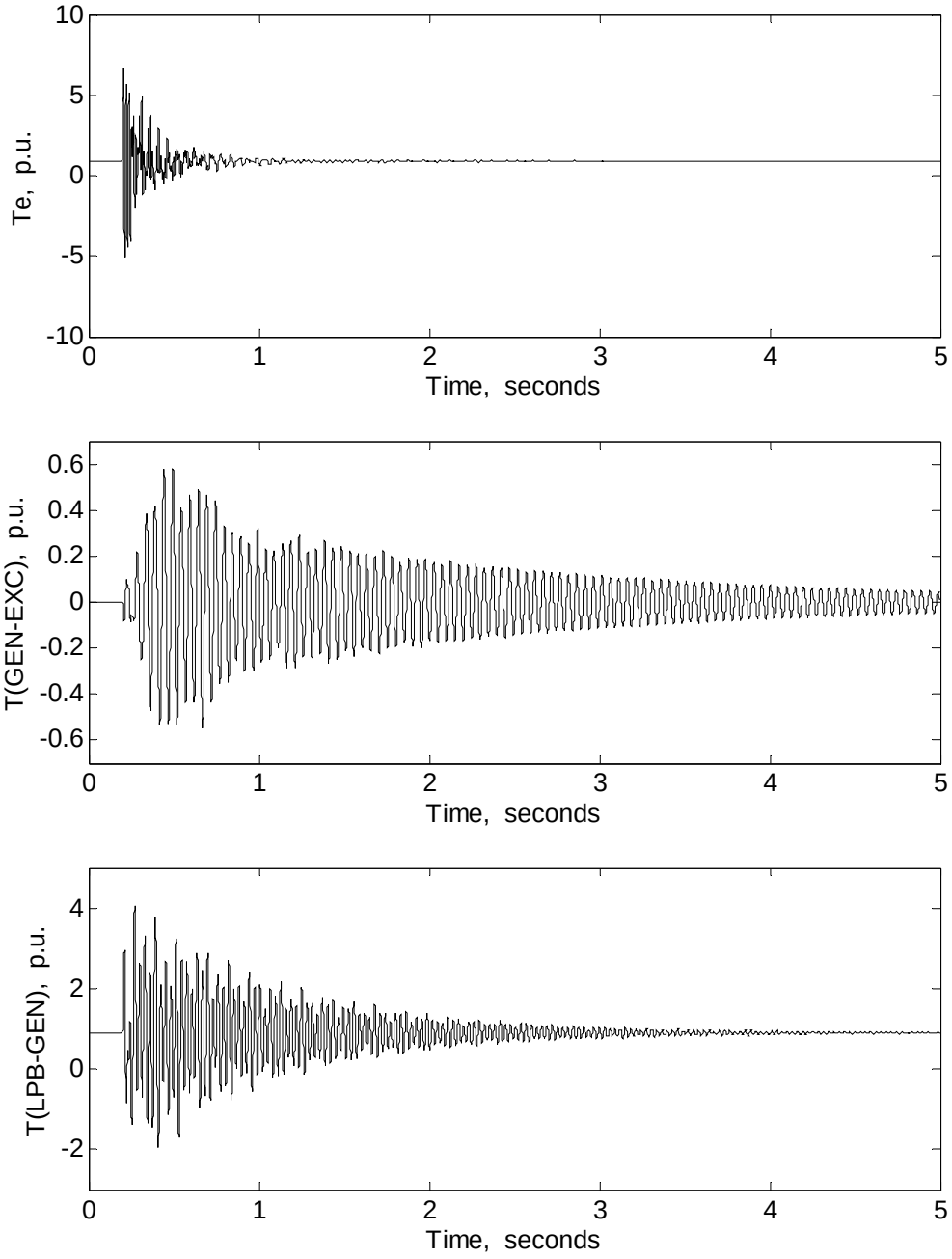

(b)

Figure 4.10 (continued)

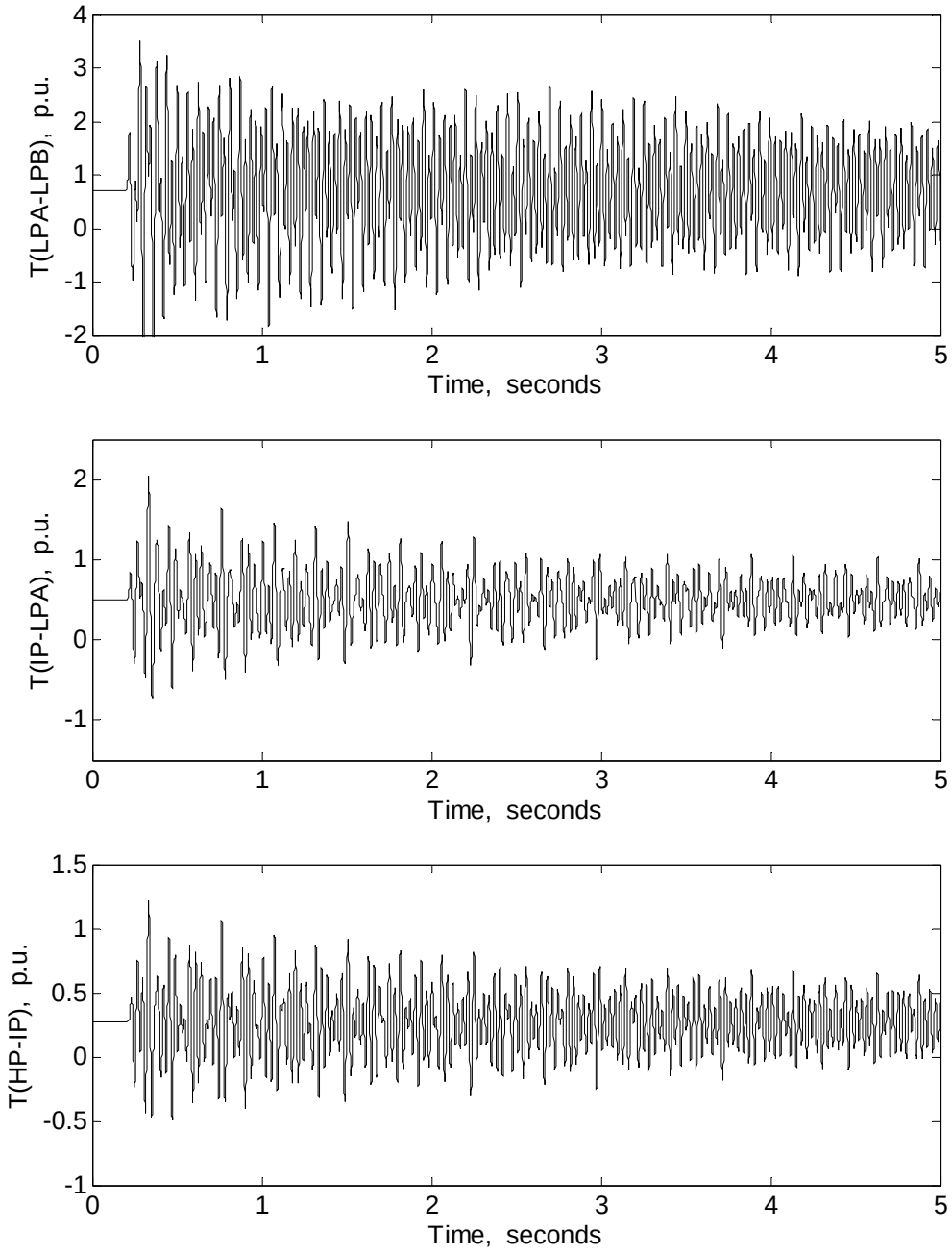

(a)

Figure 4.10 (continued)

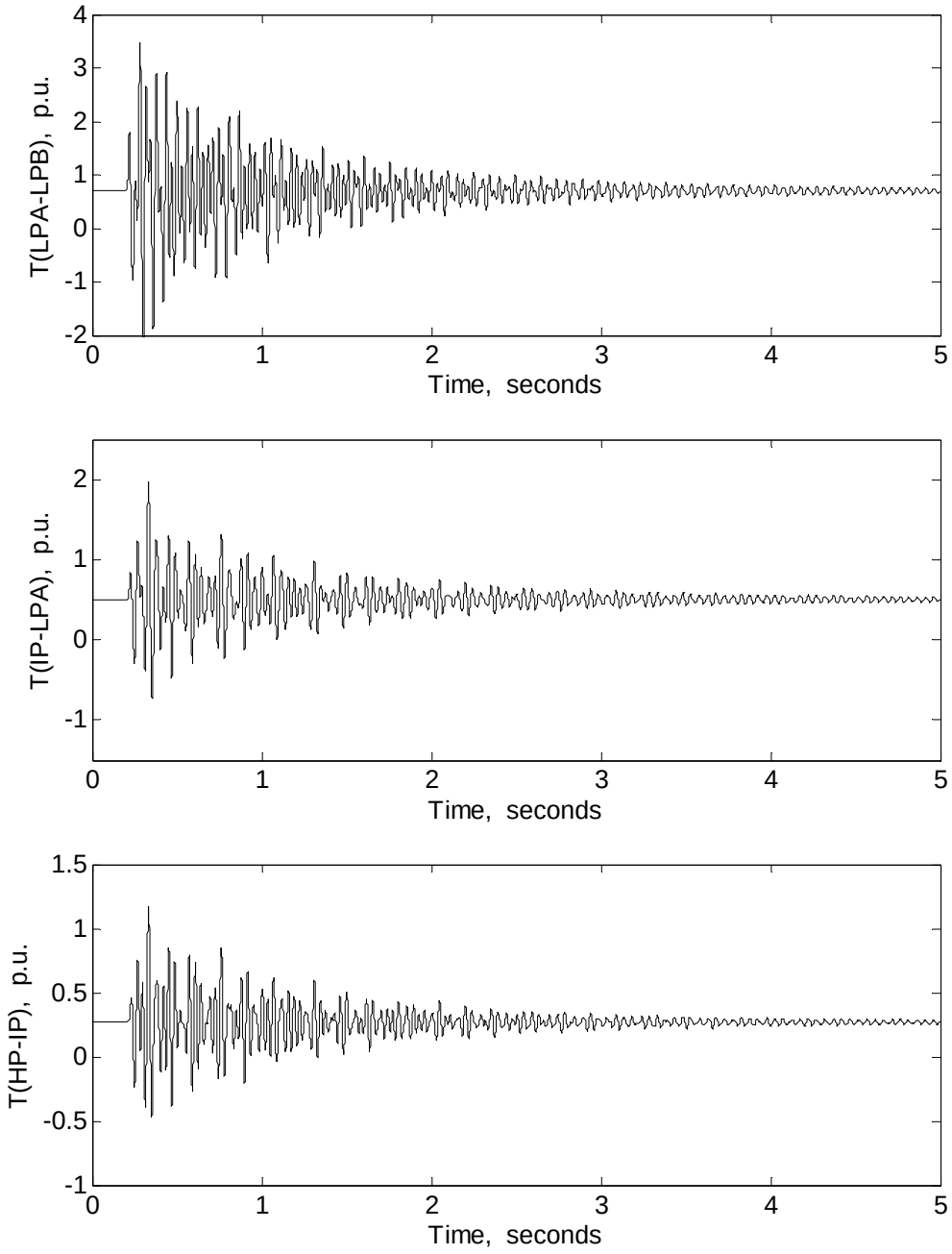

(b)

Figure 4.10 (continued)

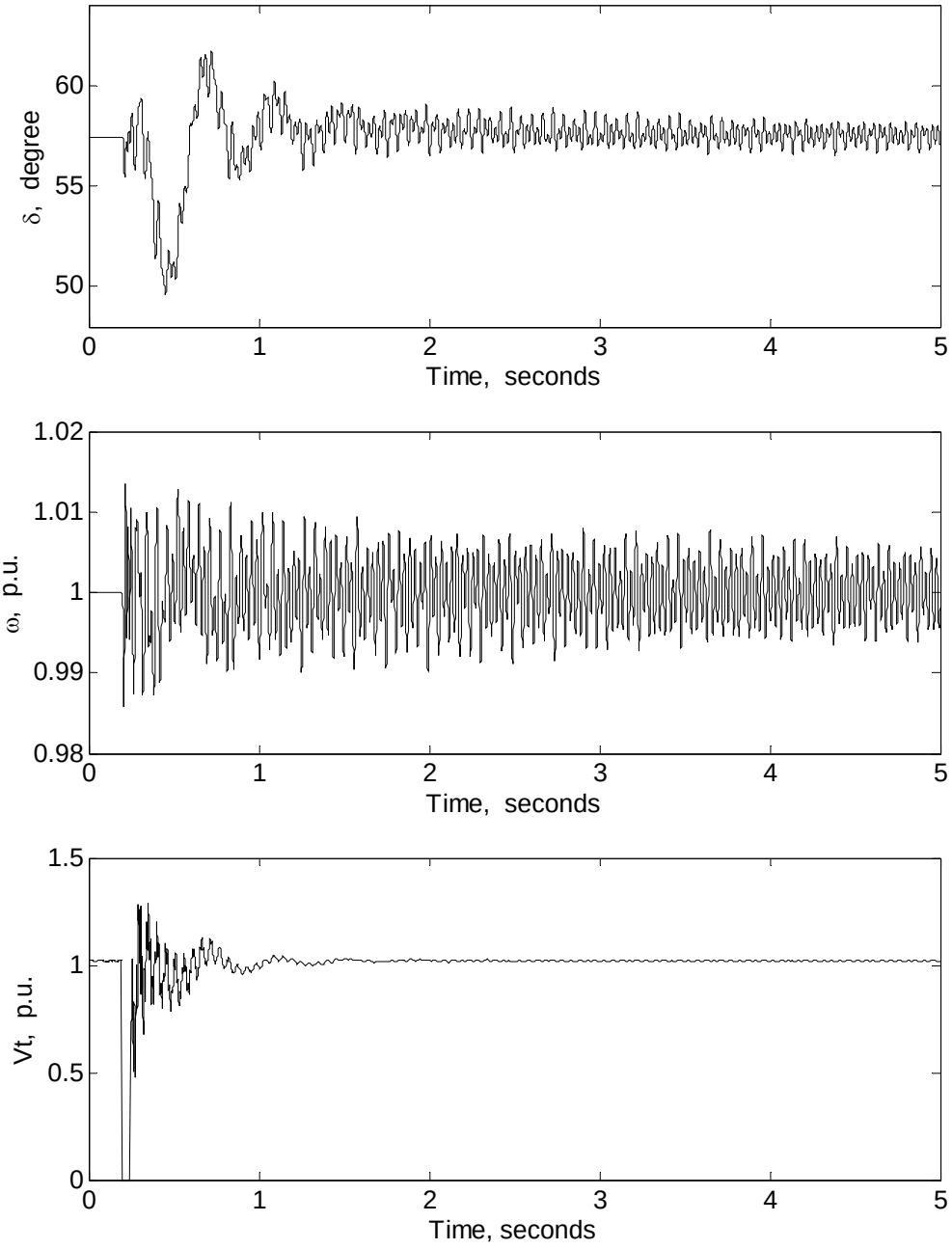

(a)

Figure 4.11 Generator rotor angle, angular speed, and terminal voltage responses to a 3-cycle, three-phase fault at the generator terminals: (a) Case I, (b) Case II (P_{dc} = 0.20 p.u., X_C = 0.3829 p.u.).

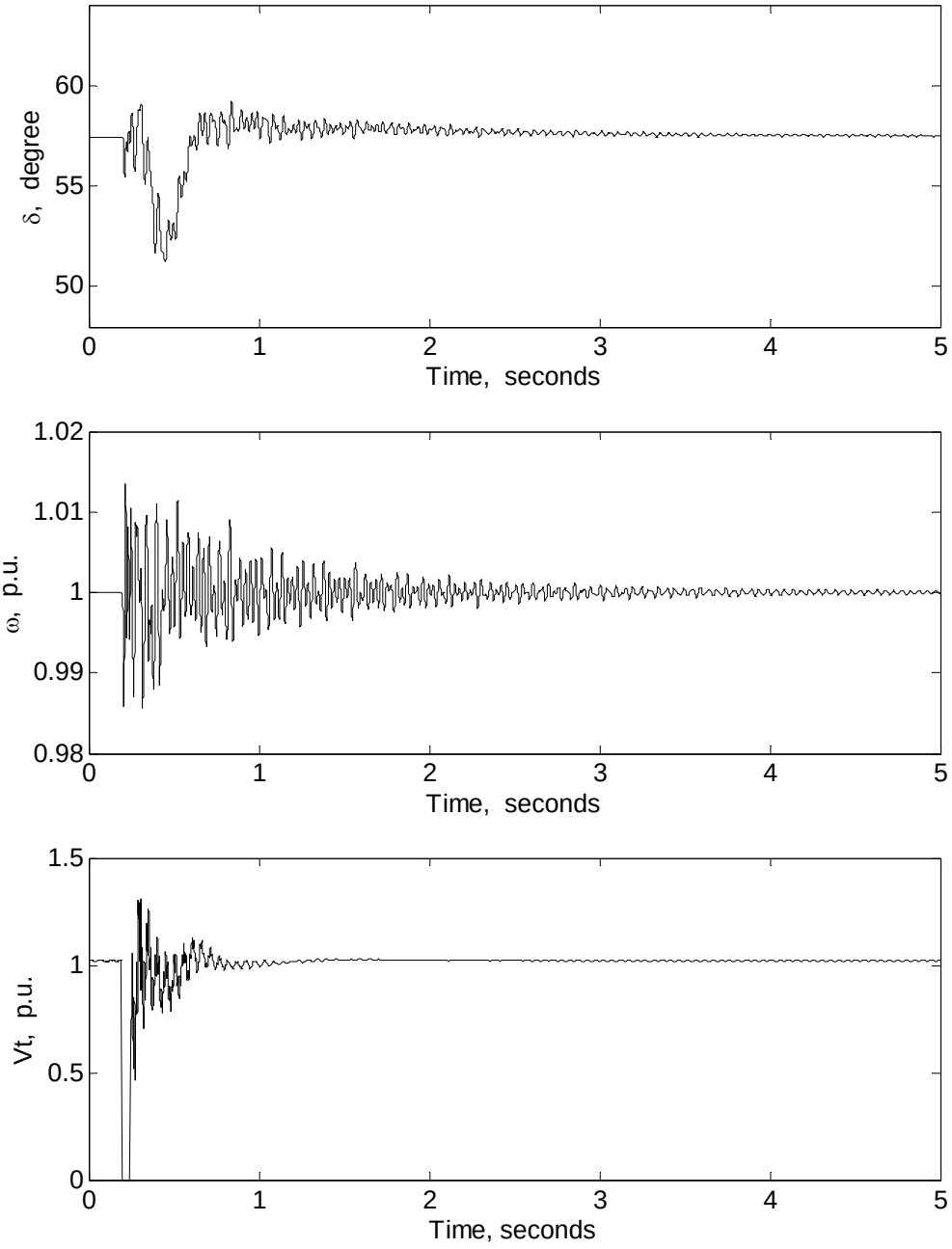

(b)

Figure 4.11 (continued)

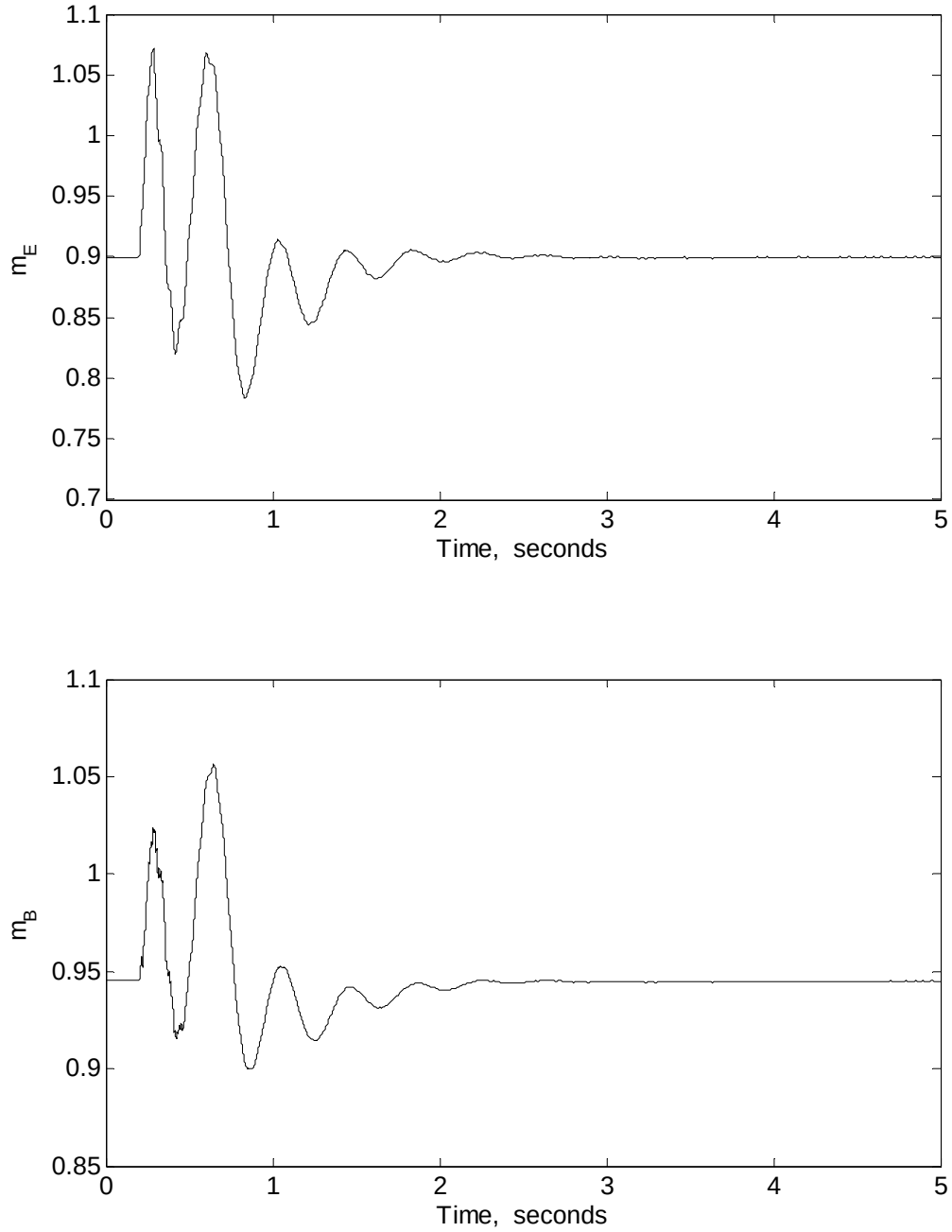

(a)

Figure 4.12 Time responses of the output control signals during and after clearing a 3-cycle, three-phase fault at the generator terminals: (a) Case I, (b) Case II (P_{dc} = 0.20 p.u., X_C = 0.3829 p.u.).

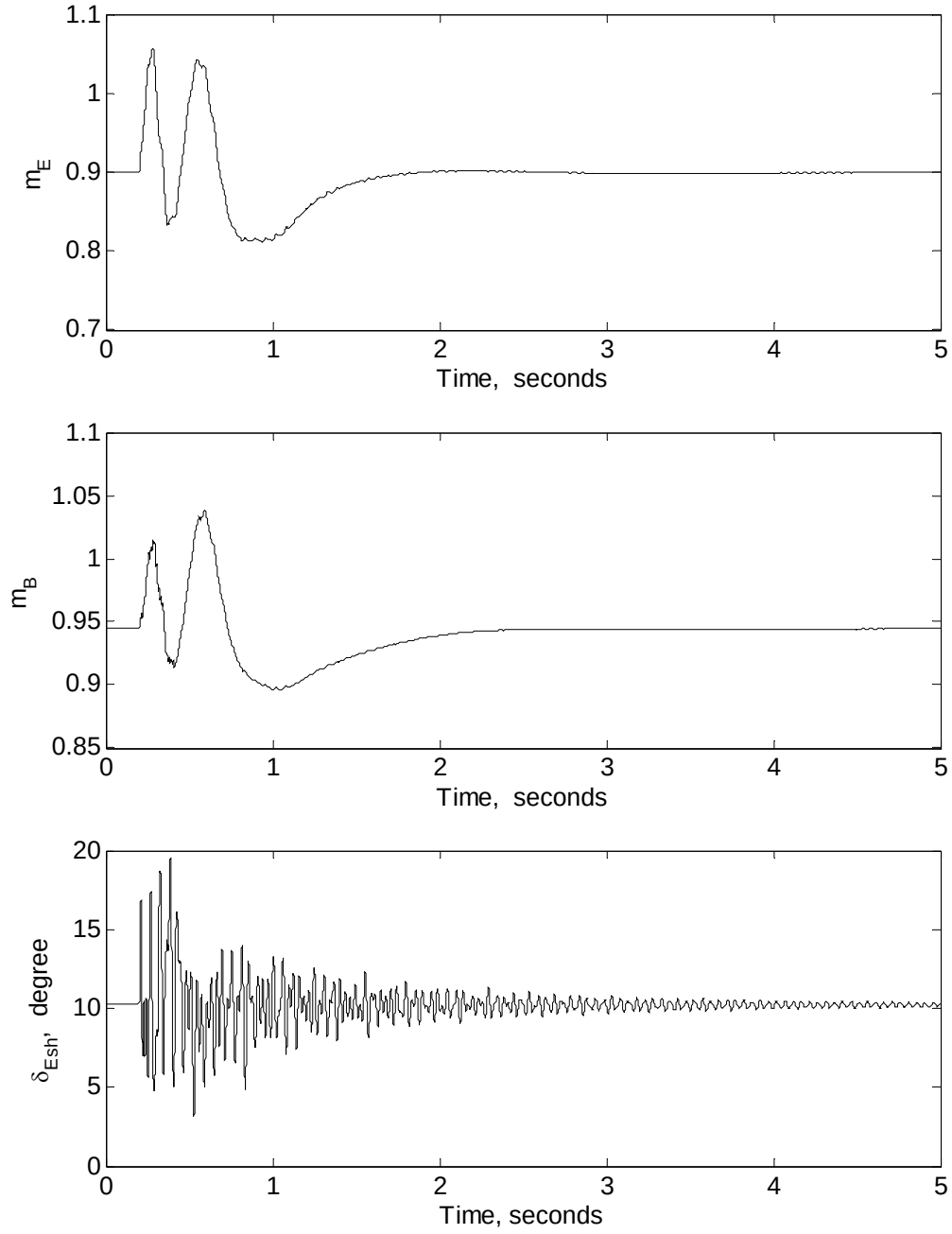

(b)

Figure 4.12 (continued)

4.2.4 Damping Subsynchronous Torsional Oscillations at a Compensation Level of 68.4%

It can be seen again from Figure 2.10 that the real part of mode 1 (15.7 Hz) eigenvalue reaches its the maximum at a compensation level of 68.4% corresponding to $X_C = 0.4788$ per unit. The power flow and voltages of the system are given in Figure 4.13 and Table 4.7 respectively. The corresponding data of the controllers are given in Table 4.8. The effect of VSC HVDC back-to-back controllers on the dynamic performance of the system due to a 3-cycle, three-phase fault at the generator terminals are shown in Figures 4.14 to 4.16.

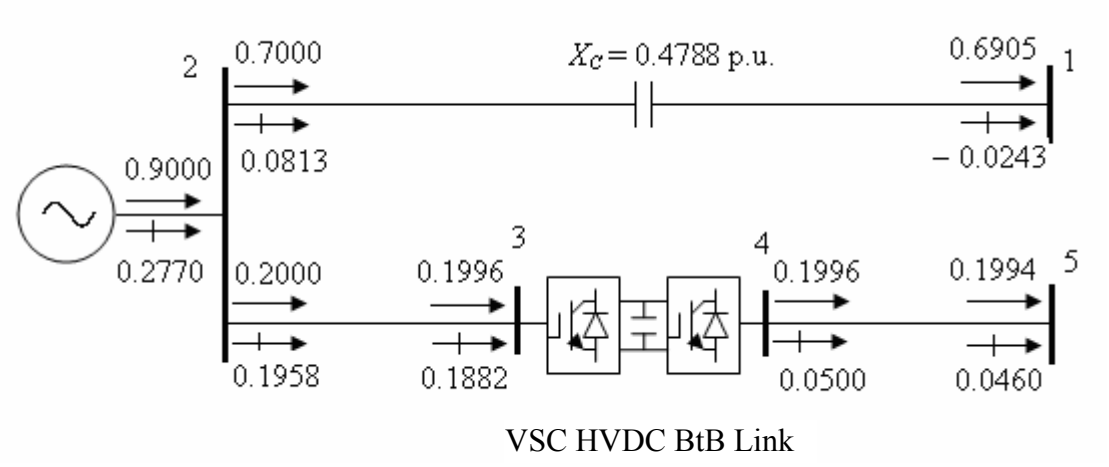

Figure 4.13 System power flow results ($P_{dc} = 0.20$ p.u., $X_C = 0.4788$ p.u.).

Table 4.7 System bus and VSC voltages ($P_{dc} = 0.20$ p.u., $X_C = 0.4788$ p.u.).

	System bus					VSC voltage	
	1	2	3	4	5	V_{sh1}	V_{sh2}
Magnitude (p.u.)	1.0000	1.0200	1.0000	1.0257	1.0200	0.9814	1.0307
Phase angle (deg)	0	8.6394	7.5710	1.7989	0.7194	6.4056	2.8807

Table 4.8 Controller parameters (P_{dc} = 0.20 p.u., X_C = 0.4788 p.u.).

Active power controller		
K_{Ed} = 1.0	T_{Ed} = 0.01 sec.	T_{me} = 0.04 sec.
K_{Bd} = 1.0	T_{Bd} = 0.01 sec.	T_{mb} = 0.04 sec.
Supplementary controller		
K_{ω} = 1.0		T_m = 0.01 sec.
K_P = 0.05		K_I = 0.10

As it can be seen from Figure 4.14, in the absence of the supplementary controller, the turbine-generator shaft system exhibits severe torsional torque amplifications. It can also be seen from Figure 4.15 that the generator terminal voltage is extremely unstable in this case. Figure 4.14 to 4.16 show, however, the effectiveness of the supplementary controllers in damping these severe torsional torques when it is employed along with the active power controller.

It is worth noting here that the limiters on the active power controllers shown in Figure 3.8 keep the amplitude modulation ratios m_E and m_B within the range of 0.5 and 1.2. The action of these limiters is clearly shown in Figure 4.16 (b) as the initial high values of m_E and m_B are clipped.

4.3 Behaviour of VSC HVDC Back-to-Back Controllers in Damping SSR Oscillations at Different Loading Conditions

In order to examine the robustness of the VSC HVDC back-to-back controllers, simulation studies with various power sharings between Line 1 and Line 2 were carried out without changing the generator output power or making any adjustment to the controller parameters. Moreover, the compensation level was assumed to be 26.5%. Two power sharing conditions designated as PS1 and PS2 are reported in the next subsection and Appendix E respectively.

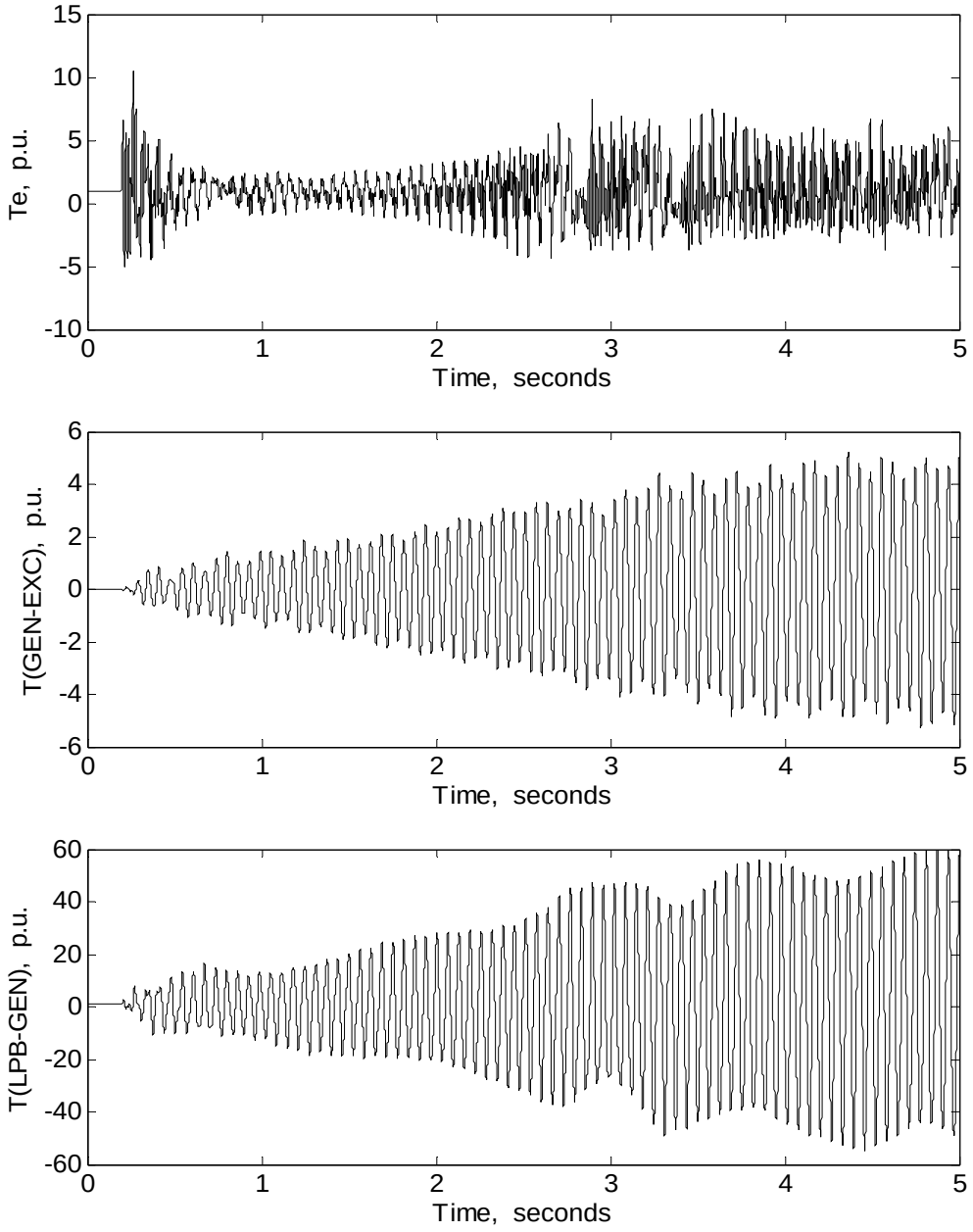

(a)

Figure 4.14 Turbine-generator electromagnetic and shaft torsional torques during and after clearing a 3-cycle, three phase fault at the generator terminals: (a) Case I, (b) Case II (P_{dc} = 0.20 p.u., X_C = 0.4788 p.u.).

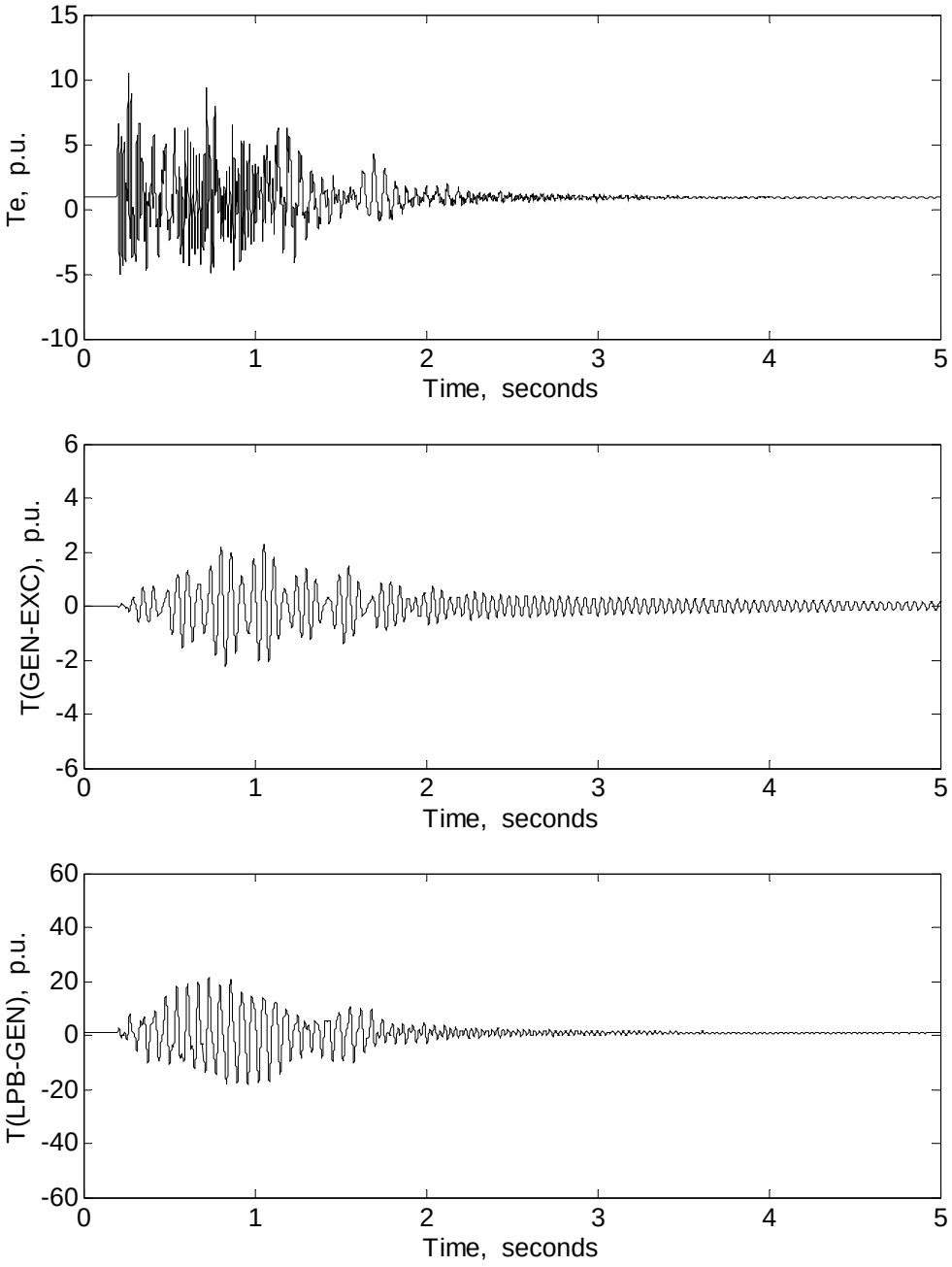

(b)

Figure 4.14 (continued)

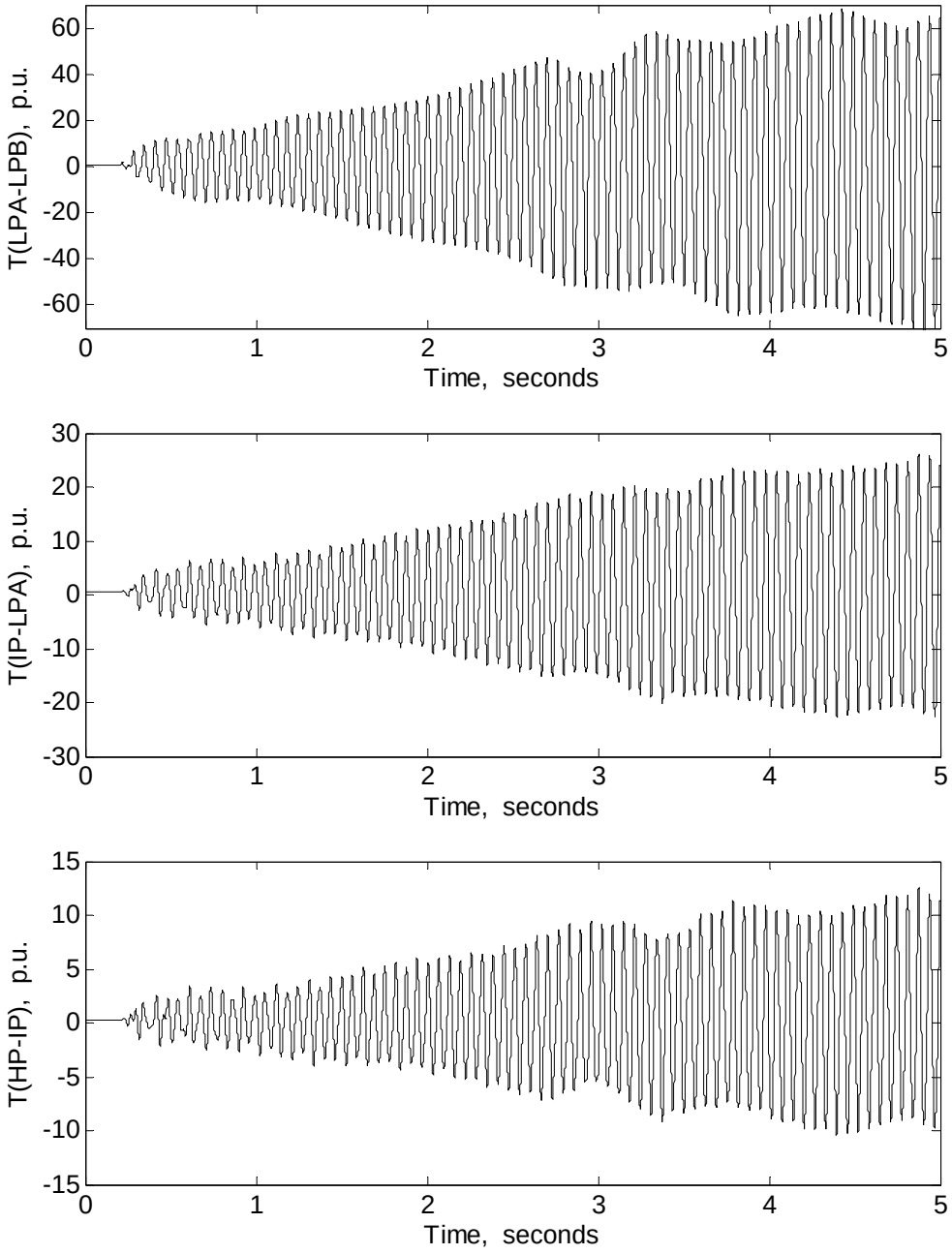

(a)

Figure 4.14 (continued)

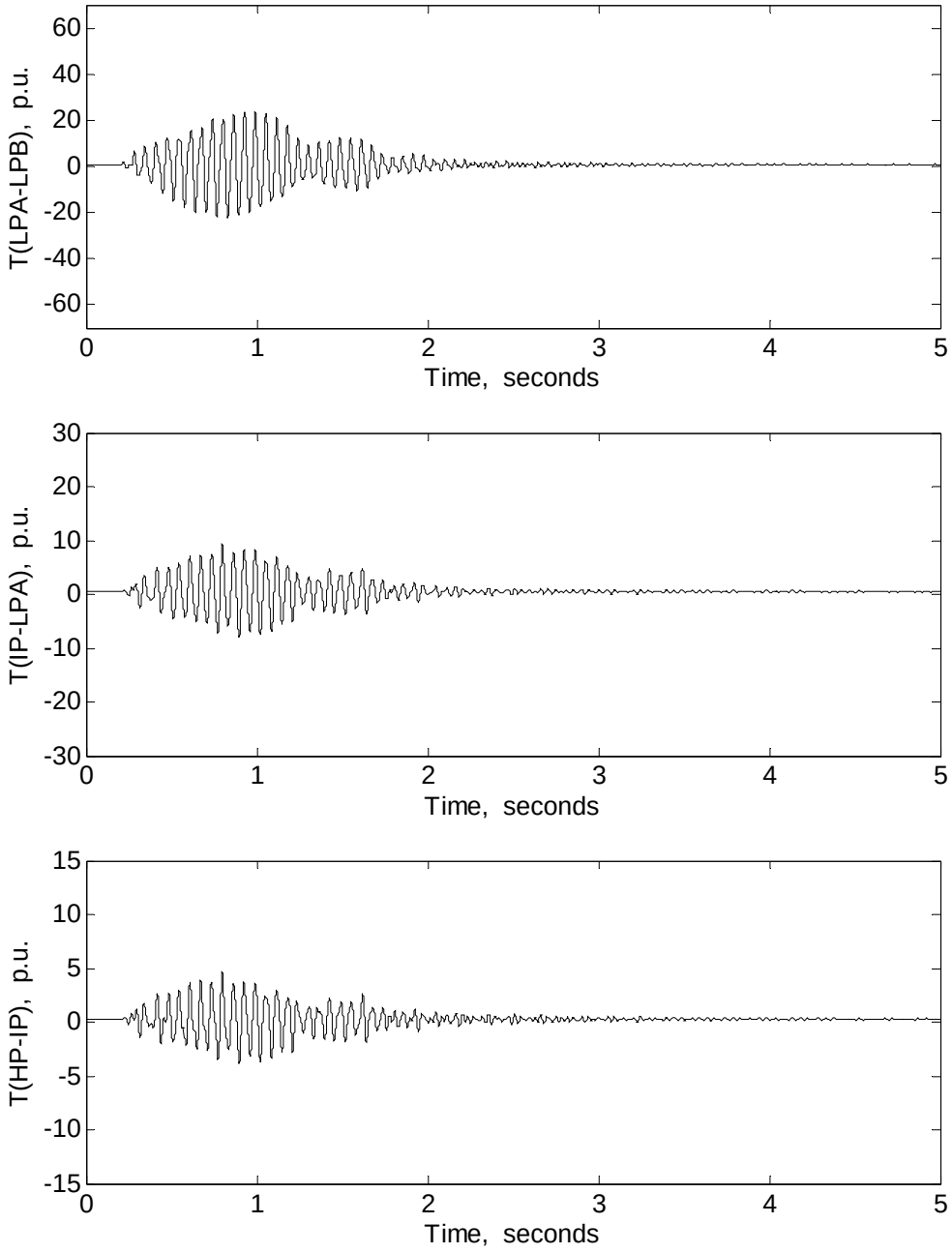

(b)

Figure 4.14 (continued)

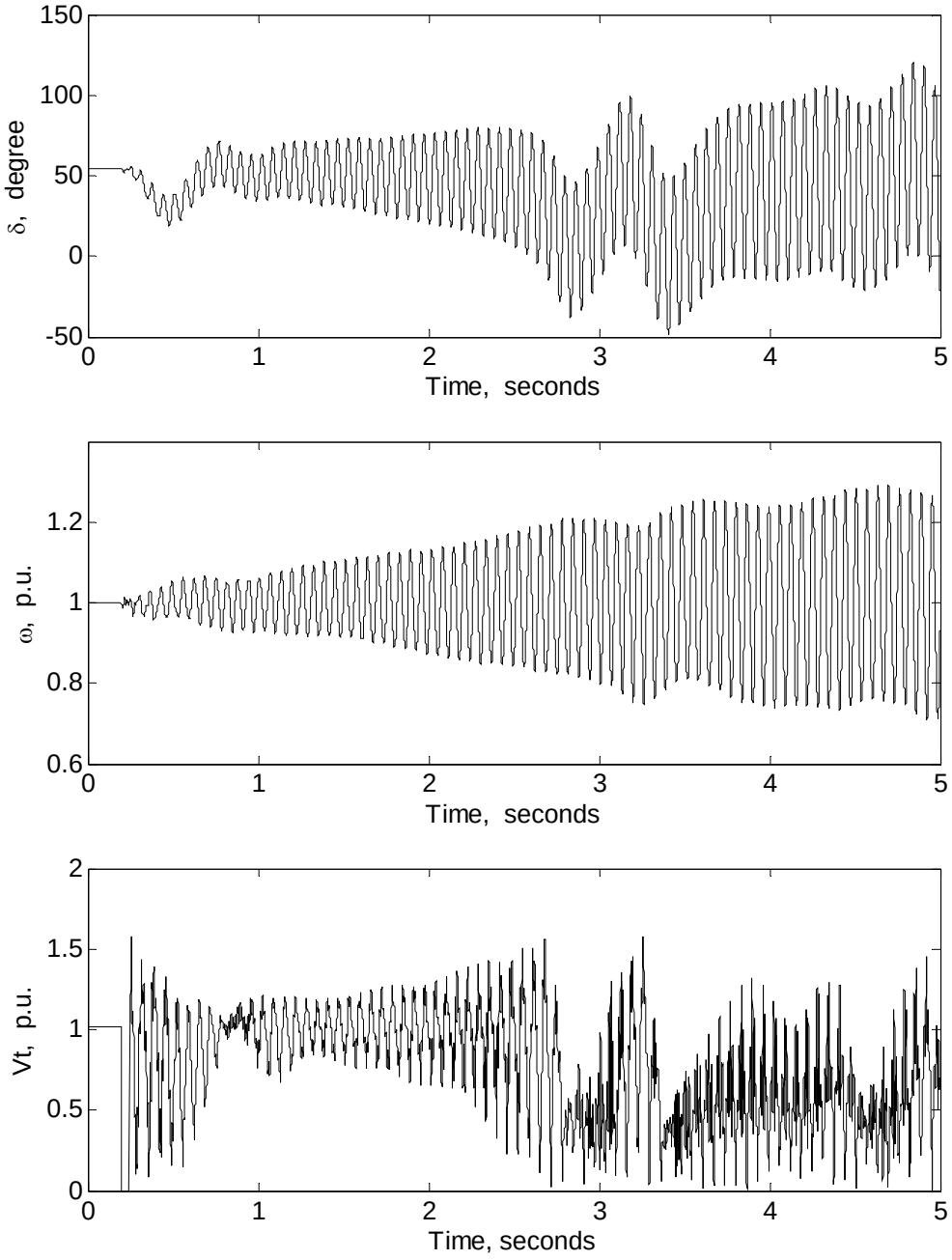

(a)

Figure 4.15 Generator rotor angle, angular speed, and terminal voltage responses to a 3-cycle, three-phase fault at the generator terminals: (a) Case I, (b) Case II (P_{dc} = 0.20 p.u., X_C = 0.4788 p.u.).

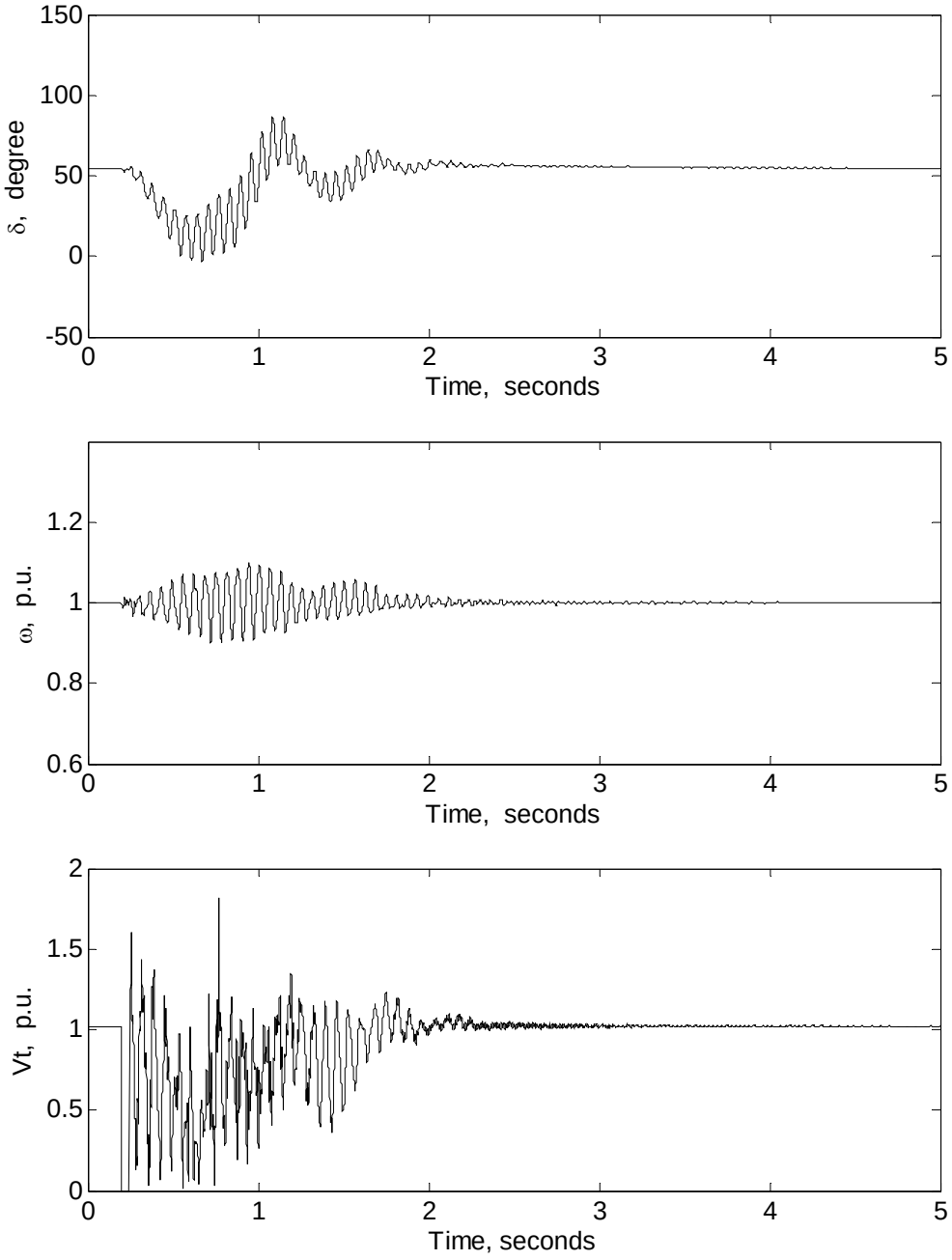

(b)

Figure 4.15 (continued)

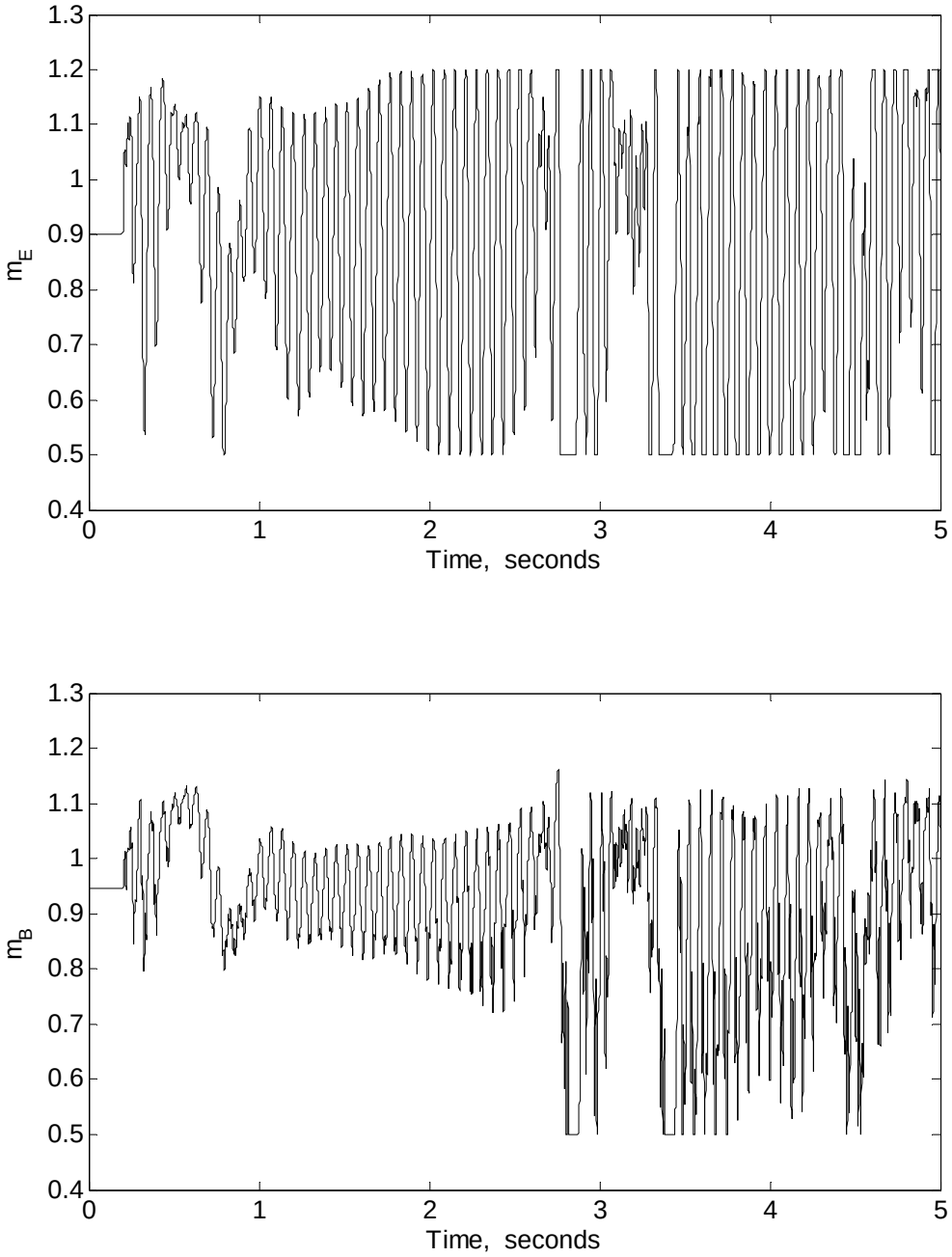

(a)

Figure 4.16 Time responses of the output control signals during and after clearing a 3-cycle, three-phase fault at the generator terminals: (a) Case I, (b) Case II (P_{dc} = 0.20 p.u., X_C = 0.4788 p.u.).

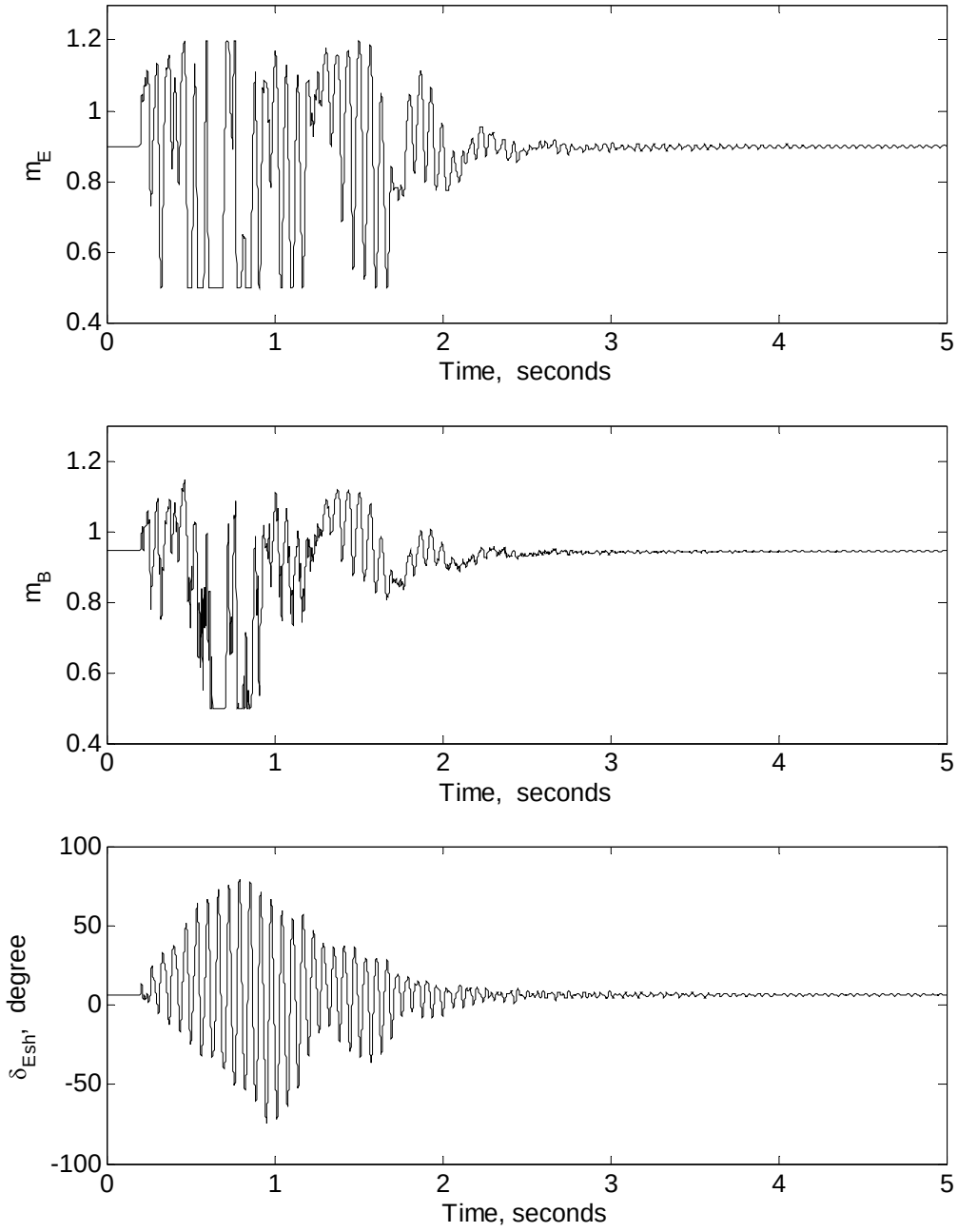

(b)

Figure 4.16 (continued)

4.3.1 PS1: System Dynamic Performance at P_{dc} = 0.40 p.u.

The system pre-disturbance operating condition in this case is such that Line 2 carries a real power of 0.4 per unit. The power flow and voltages of the system in this case are shown in Figure 4.17 and Table 4.9 respectively. The controller parameters are shown in Table 4.2.

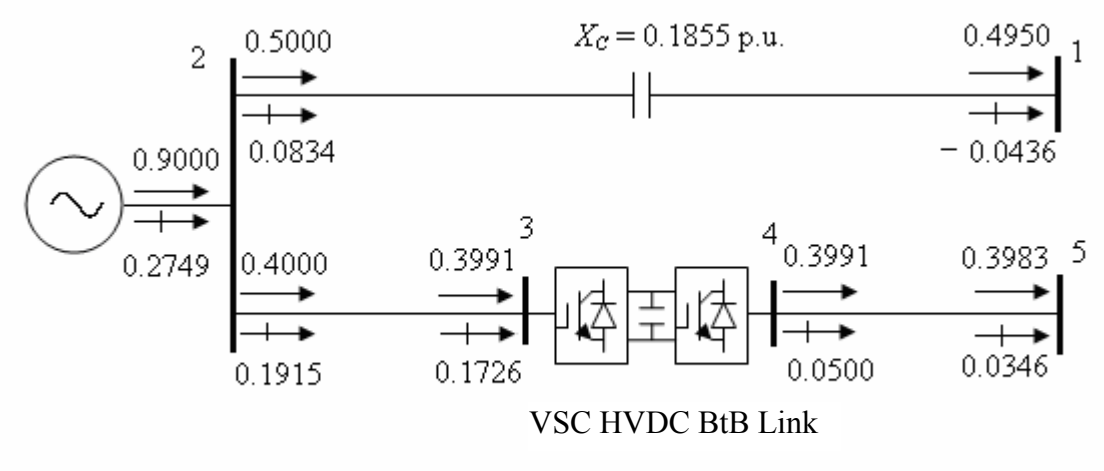

Figure 4.17 System power flow results (P_{dc} = 0.40 p.u., X_C = 0.1855 p.u.).

Table 4.9 System bus and VSC voltages (P_{dc} = 0.40 p.u., X_C = 0.1855 p.u.).

	System bus					VSC voltage	
	1	2	3	4	5	V_{sh1}	V_{sh2}
Magnitude (p.u.)	1.0000	1.0200	1.0000	1.0261	1.0200	0.9836	1.0317
Phase angle (deg)	0	14.5098	12.3159	3.5723	1.4006	9.9904	5.7329

The turbine-generator electromagnetic and shaft torsional torque responses due to a 3-cycle, three-phase fault at the generator terminals are shown in Figure 4.18 for Cases I and II. Figure 4.19 shows the generator rotor angle, angular speed and the terminal voltage of the system for the same two cases. Moreover, the time responses of the output control signals are shown in Figure 4.20.

As it can be seen from Figure 4.18, the proposed controller effectively damps all the shaft torsional torques at this loading condition. It is worth noting here that simulation results of PS2 (Figures E.2 to E.4, Appendix E) and other cases not reported in this thesis yield the same conclusion. Therefore, it can be concluded that the proposed supplementary controller is robust.

It is interesting to compare the output control signals of Figures 4.20(a) and 4.4(a). Theses figures show that increasing the power flow into the VSC HVDC system results in an increase in the amplitude of the active power controller output signals m_E and m_B. As it can be seen from Figure 4.20(a), the high values of m_E and m_B at P_{dc} = 0.4 per unit are clipped by the controller limiters. On the other hand, Figure 4.4(a) shows that at P_{dc} = 0.2 per unit, m_E and m_B are with the limits.

4.4 Summary

In this chapter, the effectiveness of VSC HVDC back-to-back controllers in damping SSR oscillations under large disturbances has been investigated through several cases of time-domain simulation studies. These investigations have revealed that the VSC HVDC back-to-back system equipped only with active power controller is not sufficient to damp all shaft torsional torques. The active power and supplementary controllers operating together, however, are effective in damping all the shaft torsional torques. Moreover, the proposed VSC HVDC back-to-back controllers effectively damp all the shaft torsional torques over a wide range of loading conditions.

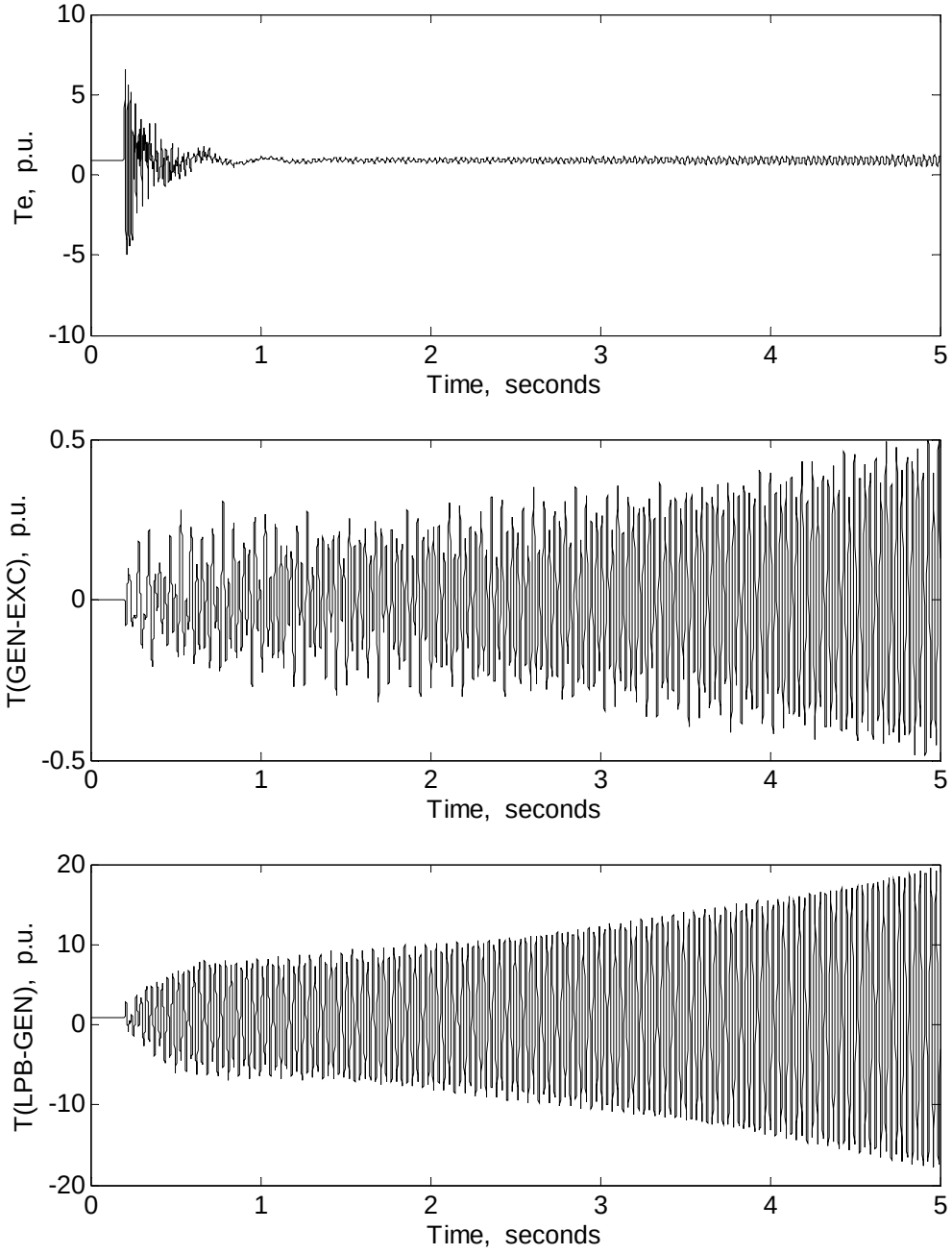

(a)

Figure 4.18 Turbine-generator electromagnetic and shaft torsional torques during and after clearing a 3-cycle, three phase fault at the generator terminals: (a) Case I, (b) Case II (P_{dc} = 0.40 p.u., X_C = 0.1855 p.u.).

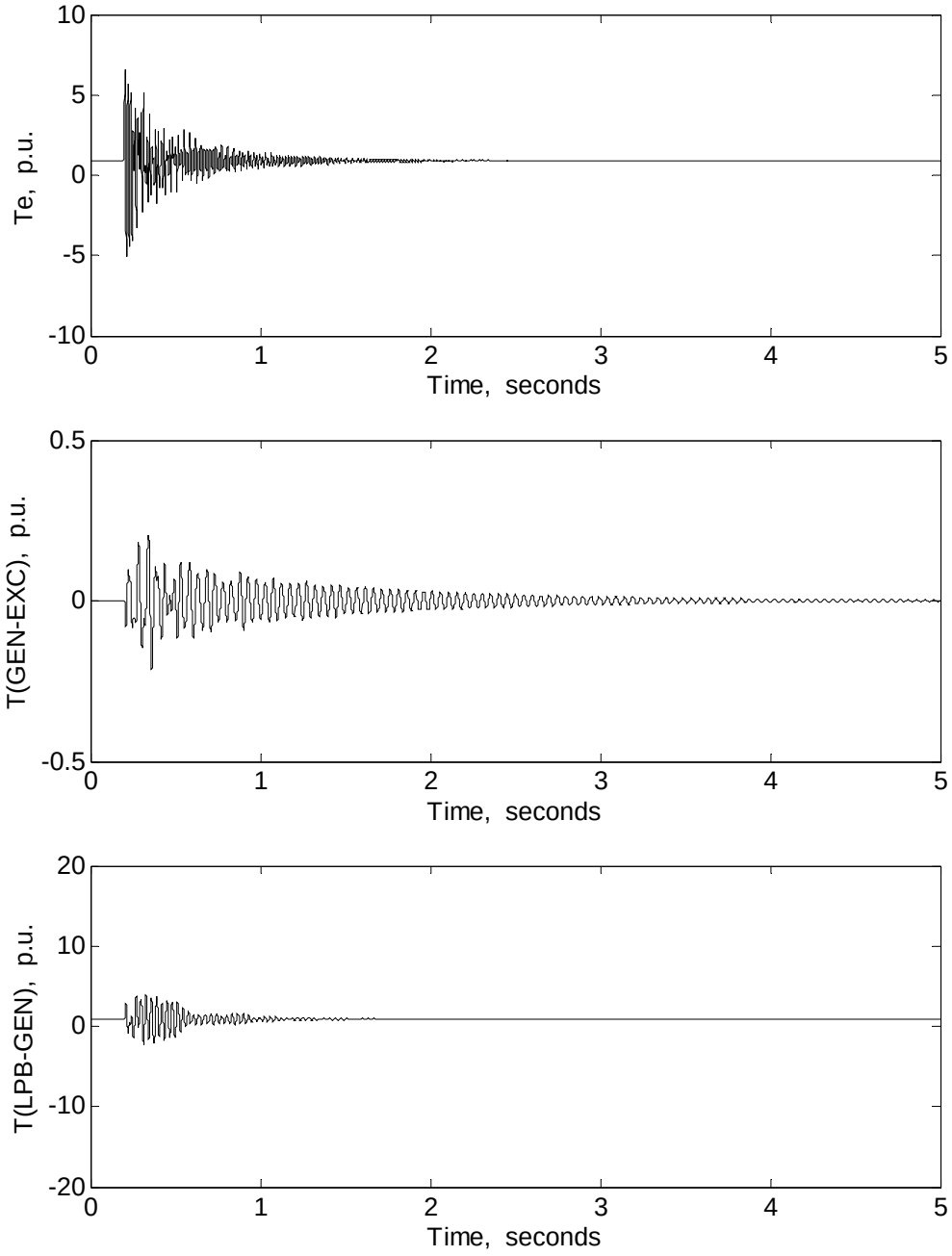

(b)

Figure 4.18 (continued)

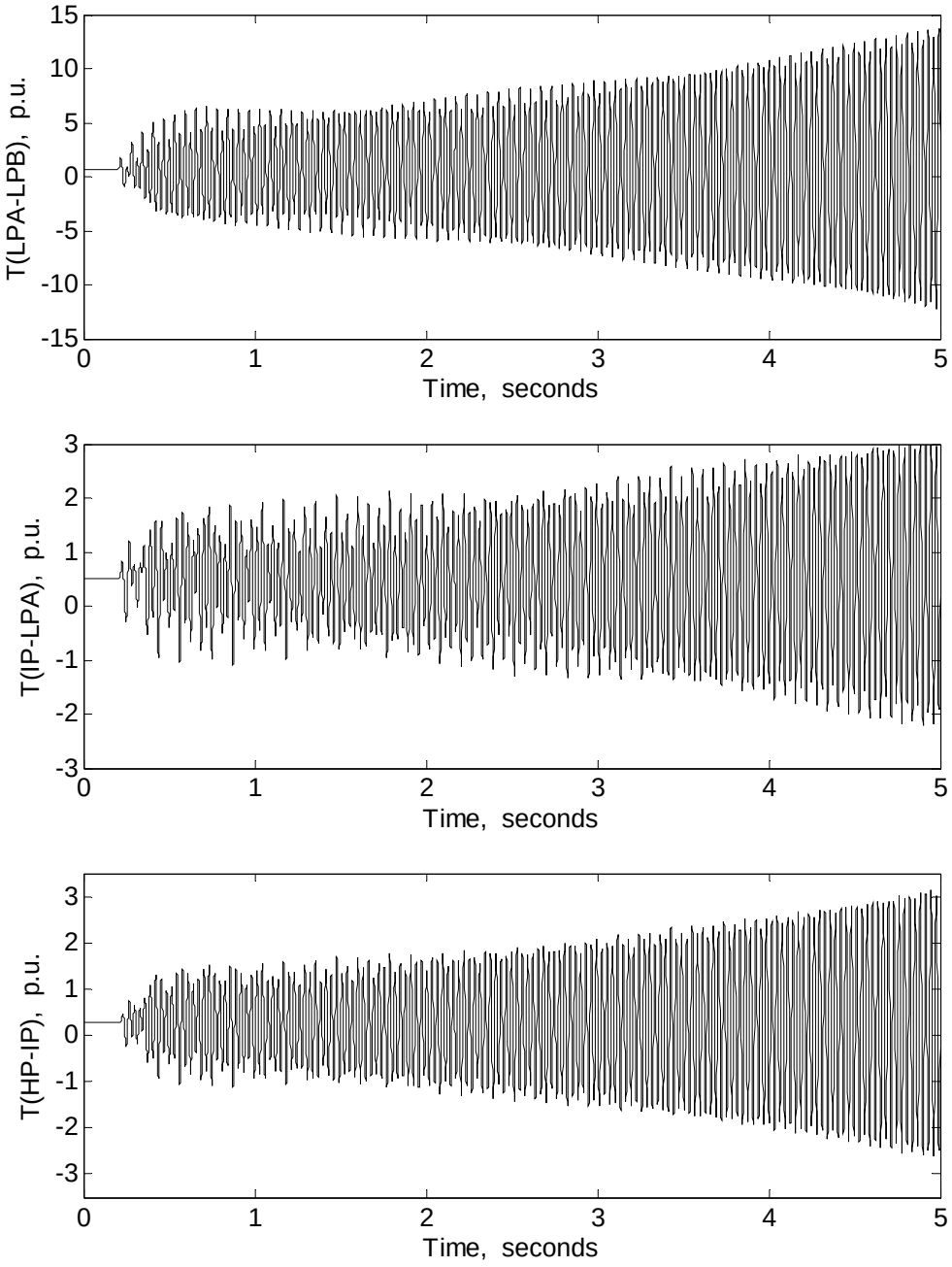

(a)

Figure 4.18 (continued)

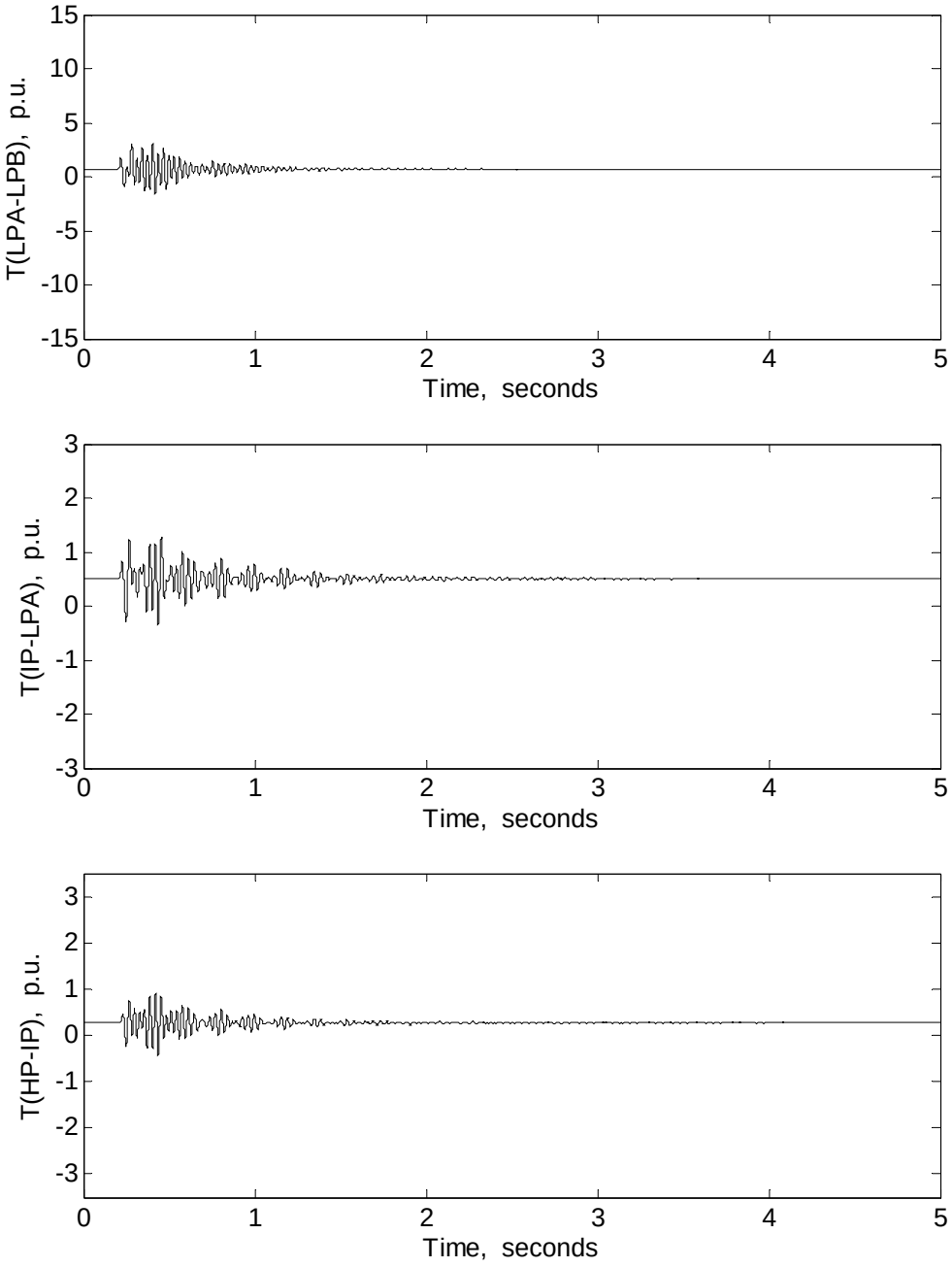

(b)

Figure 4.18 (continued)

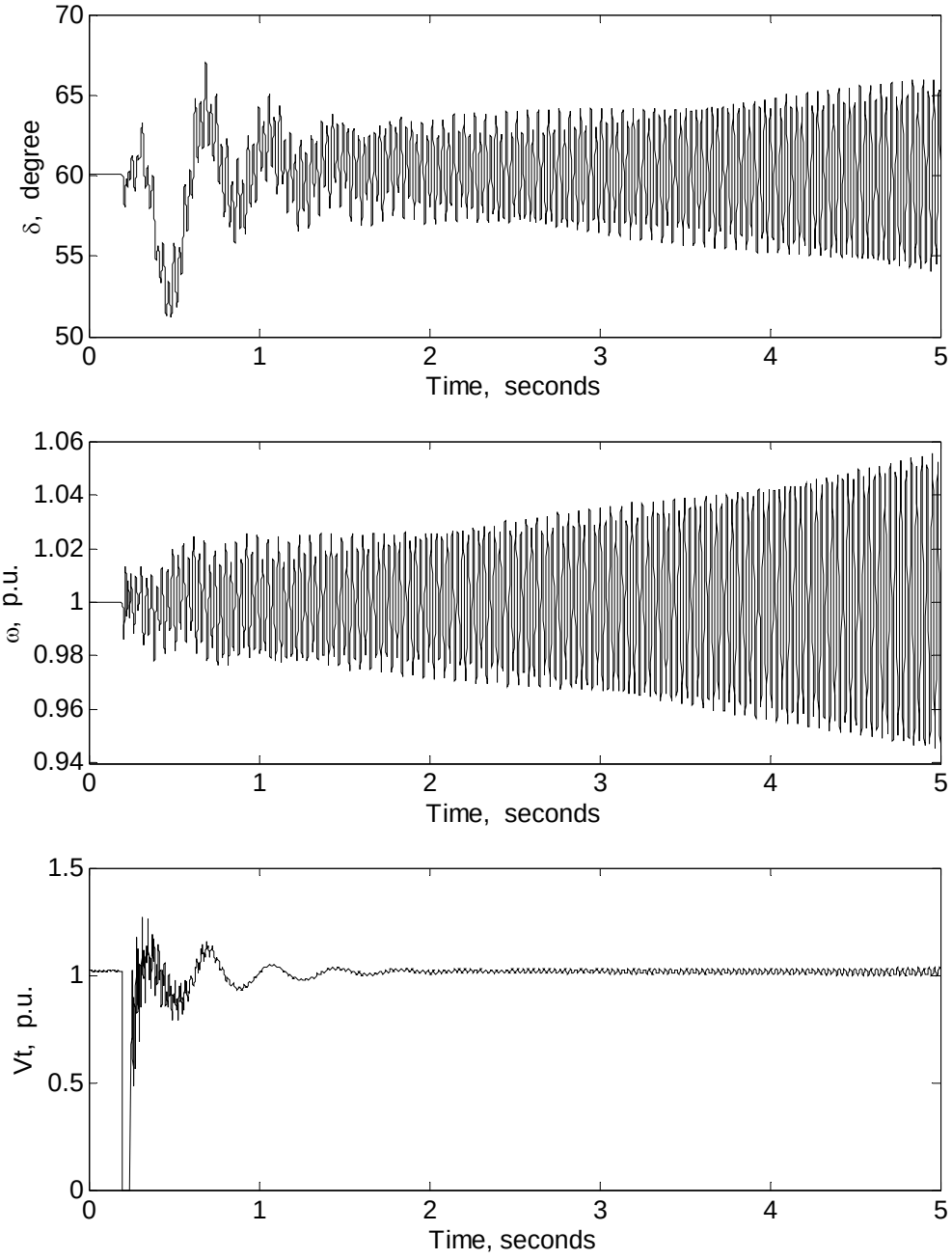

(a)

Figure 4.19 Generator rotor angle, angular speed, and terminal voltage responses to a 3-cycle, three-phase fault at the generator terminals: (a) Case I, (b) Case II (P_{dc} = 0.40 p.u., X_C = 0.1855 p.u.).

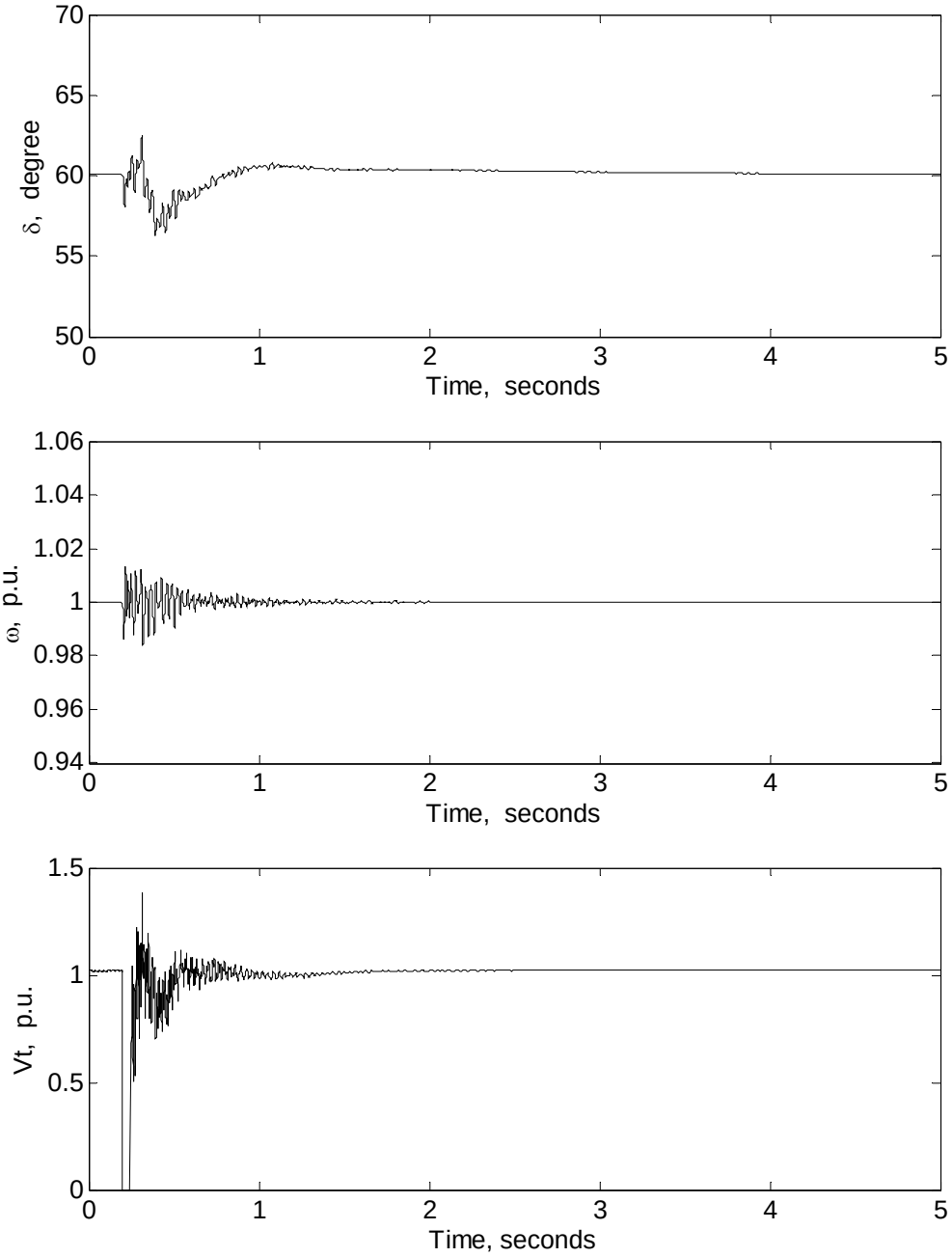

(b)

Figure 4.19 (continued)

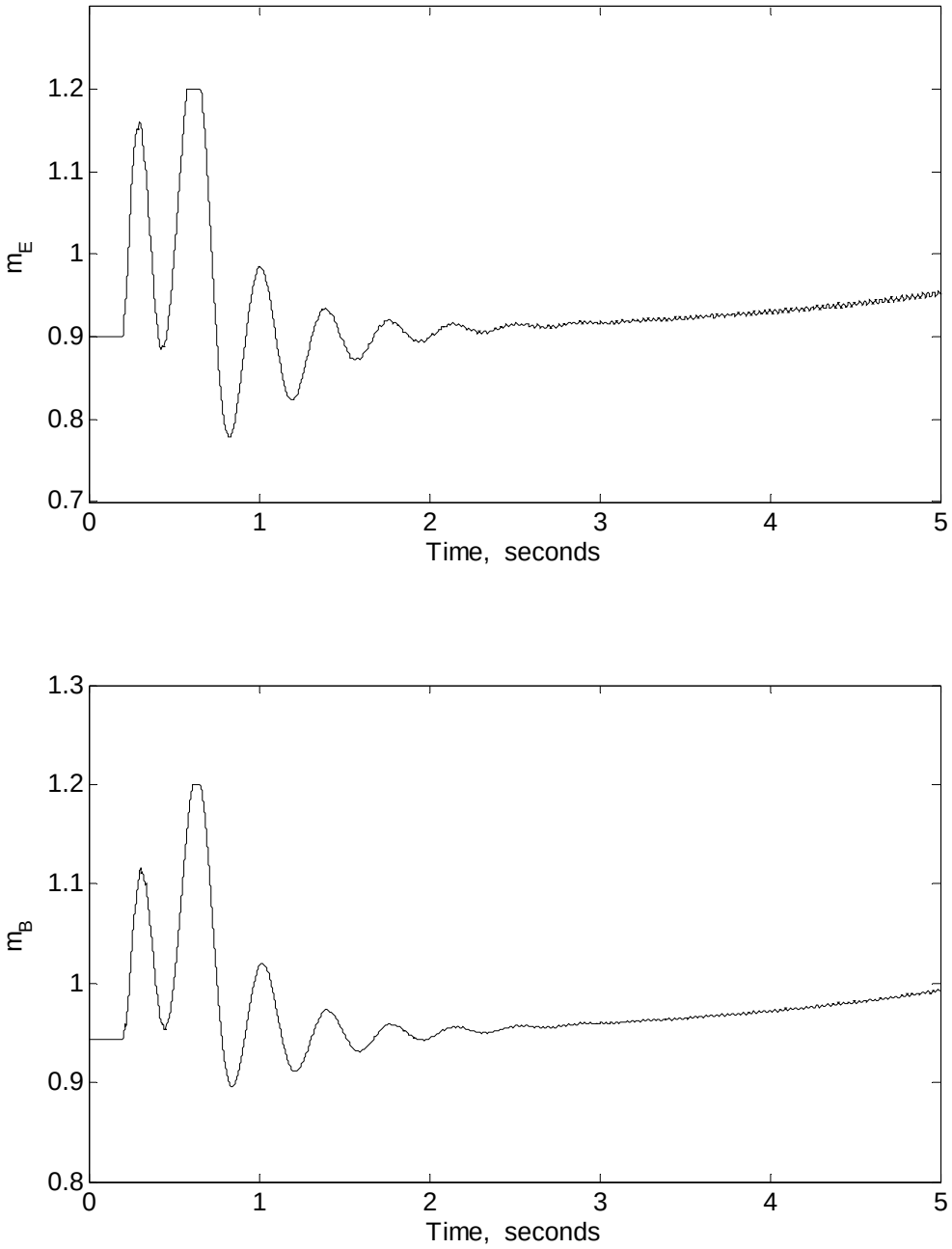

(a)

Figure 4.20 Time responses of the output control signals during and after clearing a 3-cycle, three-phase fault at the generator terminals: (a) Case I, (b) Case II (P_{dc} = 0.40 p.u., X_C = 0.1855 p.u.).

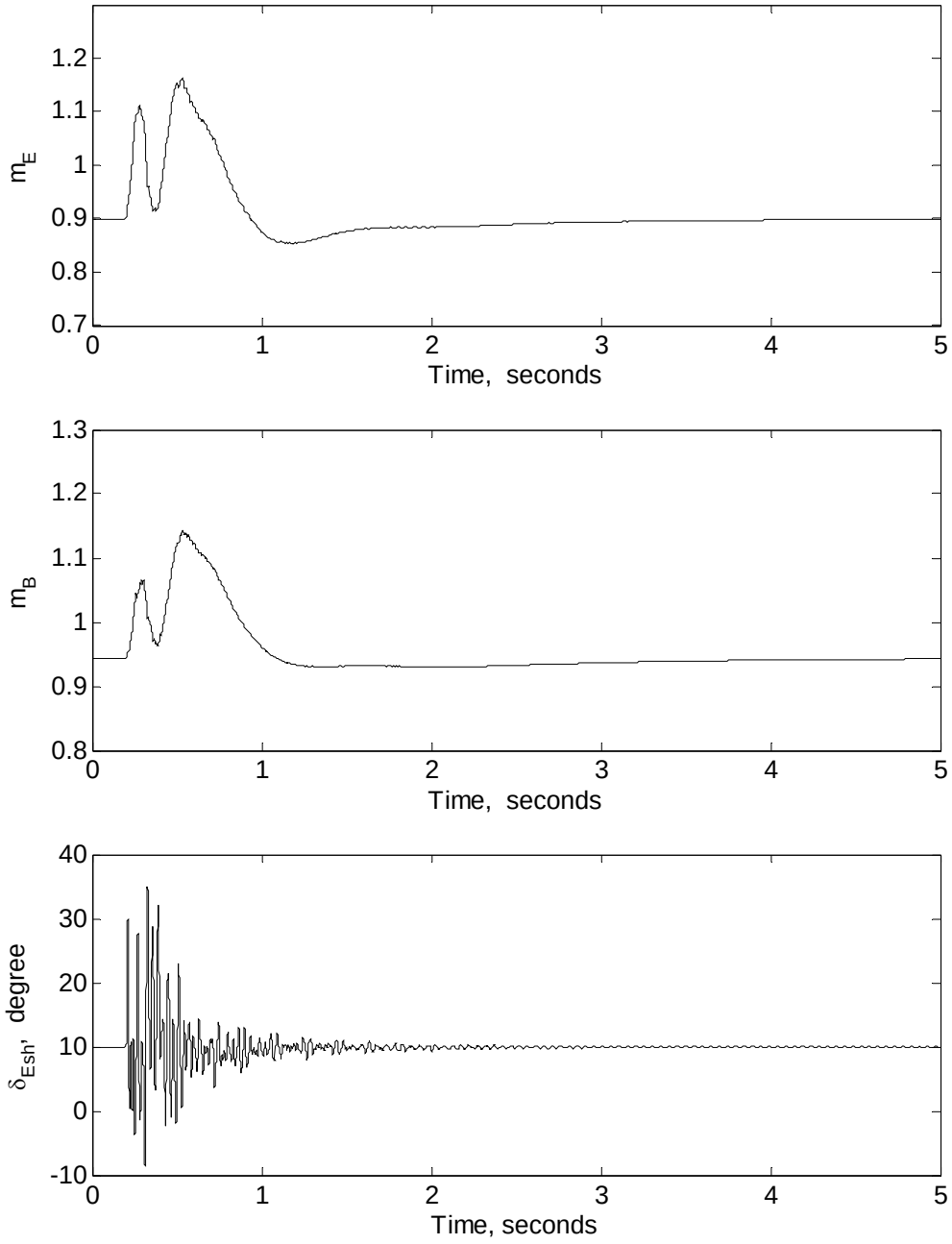

(b)

Figure 4.20 (continued)

5 SUMMARY AND CONCLUSIONS

5.1 Summary

Transmission capability limitations and the ways to overcome them are challenging problems facing power system engineers. The reasons for transmission limitations extend from steady state and thermal considerations to transient and dynamic stability of the power system. It can be due to unfavorable power flow pattern in the transmission system where some of the transmission lines may be very close to their thermal limits while other lines may have unnecessarily large thermal margins. Other reasons are transient and dynamic stability considerations, which impose limits on the power that can be transmitted while ensuring that the power system will be able to regain a new stable state following any expected disturbance. Due to these limitations, transmission lines are often loaded to levels below of their thermal capability and, in order to increase the loadability limit, some measures must be adopted. Series capacitive compensation is one of the most economical measures to increase transmission capability. It decreases the effective reactance of the compensated line and, hence, it can improve the power flow pattern among parallel transmission paths. At the same time, it increases the stability limit of the compensated line.

However, introducing a series capacitor in a transmission system implies the existence of natural oscillations in the electrical system having frequencies below the power frequency. Since the natural oscillations of the shaft system of most turbine-generators are also of frequencies below the power frequency, the possibility of the electromechanical Subsynchronous Resonance (SSR) exists if the frequencies of the electrical and mechanical oscillations are complements of the power frequency. SSR

results in violent torsional oscillations within the turbine-generator shafts which can destroy them (in the worst case) in only a few seconds.

As a result of the Flexible AC Transmission Systems (FACTS) initiative, considerable effort has been spent in the last fifteen years on the development of power electronic-based power flow controllers. These controllers usually employ self-commutated inverters as synchronous voltage sources to modify the prevailing transmission line voltage and thereby control the power flow. The potential benefits of these FACTS controllers are now widely recognized by the power system engineering and the transmission and distribution communities. Voltage sourced converter technology has been successfully applied in a number of installations world-wide for Static Synchronous Compensators (STATCOM), Unified Power Flow Controllers (UPFC), Static Synchronous Series Compensators (SSSC) and VSC HVDC back-to-back ties.

The VSC HVDC back-to-back tie employing PWM may well represent the ultimate FACTS device. Besides controlling the through power flow, it can supply reactive power and provide independent dynamic control at its two terminals.

A brief review of the new generation of the FACTS controllers based on Voltage Source Converters (VSCs), which can improve the security of a power system by enhancing its steady-state and transient stability is presented in Chapter 1. The nature of the SSR phenomenon and the various problems associated with it are also explained in this chapter. The primary focus in this research work is the utilization a VSC HVDC back-to-back link to damp all SSR torsional oscillations in a power system.

In Chapter 2, a linearized mathematical model is developed for investigating the SSR phenomenon under small disturbances. For this purpose, the IEEE first benchmark model which consists of a large turbine-generator connected to a large system through a series-capacitor compensated transmission line is used since it represents clearly the various features of the SSR phenomenon. The shaft system of the turbine-generator represents a linear six-mass-spring system. The detailed dynamic models of the individual system components are also presented in this chapter. The procedure used to derive the complete linearized model from the IEEE first benchmark model is explained

in this chapter. The studies conducted in the rest of the chapter are intended to investigate the effect of the compensation levels of the transmission line on SSR oscillations. The results of these investigations have provided the critical compensation levels in the system under studies.

In Chapter 3, a new concept for using the VSC HVDC back-to-back system with a designed supplementary controller for mitigation of SSR oscillations in a power system is proposed. The complete dynamic model of a typical HVAC/DC system incorporating a large turbine-generator and a VSC HVDC back-to-back system is developed to study SSR torsional oscillations under larger disturbances. The steady-state and dynamic models for the VSC-HVDC back-to-back system are also presented in this chapter. For power flow studies, the VSC HVDC is modeled by a series reactance together with a set of active and reactive nodal power injections at each end of the series reactance for each converter station. These powers are expressed as a function of the admittance, the nodal voltage and the source voltage at the bus. The VSC HVDC injection model is implemented into a full Newton-Raphson power flow program by adding the VSC HVDC power injections and their derivatives with respect to the AC network state variables, i.e. nodal voltage magnitude and angles, at the appropriate locations of the mismatch vector and Jacobian matrix. The original dimensions of the mismatch vector and Jacobian matrix are not altered. The attraction of this formulation is that it can be implemented easily in existing power flow programs. To formulate the overall dynamic system equations, the state equations of each dynamic device and the network developed in Chapter 2 are used in this chapter. The overall state matrices are then formed by augmenting the dynamic device models. To construct the state space model of each dynamic device, either its terminal voltage or its current injected into the network, whichever is more convenient, is assumed as the input, and the other as the output. Using this approach, the overall system model is developed to study SSR oscillations. The time-domain analysis technique is used for transient torque analysis. MATLAB computer programs have been developed to simulate the dynamic performance of the system due to a three-phase fault at the generator terminals.

The active power and the supplementary controllers are presented in this chapter to improve the damping of the power system oscillations. The main function of the active power controller is to regulate the active power flow on both sides of the VSC HVDC back-to-back system. This is done through the two proportional type controllers. The PI supplementary controller which uses the generator speed deviation as a stabilizing signal increases the damping in the power system. The robustness of the proposed controller in damping all SSR torsional modes is examined for a given compensation level.

In Chapter 4, detailed studies to investigate the effects of the compensation levels, the controller structure and its parameters, as well as the loading conditions on the damping of SSR oscillations are documented. These studies are intended to show the effectiveness of the proposed VSC HVDC controller in mitigation of SSR oscillations at the critical compensation levels as well as over a wide range of loading conditions.

5.2 General Conclusions

The studies conducted in this thesis yield the following conclusions:

1. The designed controllers for the VSC HVDC back-to-back system considered in this thesis are robust with respect to the critical compensation levels and a wide range of loading conditions.

2. The designed active power controller of the VSC HVDC back-to-back system is capable of damping SSR oscillations when the compensation levels are 41.1% and 54.7% corresponding to the unstable torsional Modes 3 and 2 respectively. These oscillations, however, are poorly damped by the active power controller. The supplementary controller provides better damping in corporation with the active power controller.

3. The other two unstable torsional modes, namely Modes 4 and 1, exhibit the most severe undamping at the compensation levels of 26.5% and 68.4% respectively. The active power controller is not capable of damping the shaft torsional torques in these two cases. When the supplementary controller is employed in the system, both controllers are effective in damping all the shaft torsional torques.

4. When the compensation level reaches around 68.4%, the value of the controller parameters significantly affects the system dynamic performance. Normally, the data of the controllers given in Table 4.8 results in a good system response. At the other compensation levels, the two controllers (the active power and the supplementary controllers), however, can provide robust dynamic performance over wide variations in controller parameters.

5. Increasing the active power flowing from the turbine-generator to the VSC HVDC back-to-back link does not significantly affect the effectiveness of the VSC HVDC back-to-back controllers on the dynamic performance of the system. It only results in an increase in the amplitude of the active power controller output signals m_E and m_B. The active power and the supplementary controllers can effectively damp all the shaft torsional torques over a wide rang of loading conditions.

REFERENCES

[1] Song, Y. H. and Johns, A. T., *Flexible AC transmission systems (FACTS)*, London, Institution of Electrical Engineers, 1999.

[2] Hingorani, N. G. and Gyugyi, L., *Understanding FACTS: concepts and technology of flexible AC transmission systems,* New York, IEEE Press, 2000.

[3] Acha, E., *FACTS: modelling and simulation in power networks,* Chichester, Wiley, 2004.

[4] Mathur, R. M. and Varma, R. K., *Thyristor-based FACTS controllers for electrical transmission systems,* Piscataway, NJ, IEEE, 2002.

[5] Edris, A. A., Adapa, R., Baker, M. H., Bohmann, L., Clark, K., Habashi, K., Gyugyi, L., Lemay, J., Mehraban, A. S., Myers, A. K., Reeve, J., Sener, F., Torgerson, D. R., and Wood, R. R., "Proposed terms and definitions for flexible AC transmission system (FACTS)," IEEE Transactions on Power Systems, vol. 12, no. 4, pp. 1848-1853, 1997.

[6] Mohan, N., Undeland, T. M., and Robbins, W. P., *Power electronics: converters, applications, and design,* New York, Wiley, 1995.

[7] Gyugyi, L., Hingorani, N. G., Nannery, P. R., and Tai, N. "Advanced static Var compensator using gate turn-off thyristors for utility applications." , 23-203. 1990. Paris, France, CIGRE.

[8] Gyugyi, L., "Dynamic compensation of AC transmission lines by solid-state synchronous voltage sources," IEEE Transactions on Power Delivery, vol. 9, no. 2, pp. 904-911, Apr.1994.

[9] Gyugyi, L., Schauder, C. D., and Sen, K. K., "Static synchronous series compensator: a solid-state approach to the series compensation of transmission lines," IEEE Transactions on Power Delivery, vol. 12, no. 1, pp. 406-417, Jan.1997.

[10] Sen, K. K., "SSSC-static synchronous series compensator: theory, modeling, and application," IEEE Transactions on Power Delivery, vol. 13, no. 1, pp. 241-246, Jan.1998.

[11] Gyugyi, L., Schauder, C. D., Williams, S. L., Rietman, T. R., Torgerson, D. R., and Edris, A., "The unified power flow controller: a new approach to power transmission control," IEEE Transactions on Power Delivery, vol. 10, no. 2, pp. 1085-1097, Apr.1995.

[12] Nabavi-Niaki, A. and Iravani, M. R., "Steady-state and dynamic models of unified power flow controller (UPFC) for power system studies," IEEE Transactions on Power Systems, vol. 11, no. 4, pp. 1937-1943, 1996.

[13] Schettler, F., Huang, H., and Christl, N. "HVDC transmission systems using voltage sourced converters – Design and applications." 2, 715-720. 2000. Seattle, WA, United States, Institute of Electrical and Electronics Engineers Inc. Proceedings of the IEEE Power Engineering Society Transmission and Distribution Conference.

[14] Asplund, G., Eriksson, K., and Svensson, K., "HVDC Light-DC transmission based on voltage sourced converters," ABB Review, no. 1, pp. 4-9, 1998.

[15] Raju, N. R., Venkata, S. S., and Sastry, V. V., "The use of decoupled converters to optimize the power electronics of shunt and series AC system controllers," IEEE Transactions on Power Delivery, vol. 12, no. 2, pp. 895-900, Apr.1997.

[16] Asplund, G., Eriksson, K., Jiang, H., Lindberg, J., Palsson, R., and Svensson, K. "DC transmission based on voltage source converters." Vol.4, 10. 1998. Paris, France, CIGRE.

[17] Arrillaga, J., *High voltage direct current transmission*, 2nd edition, London, UK, Institution of Electrical Engineers, 1998.

[18] IEEE Committee Report, "Proposed terms and definitions for subsynchronous oscillations," IEEE Transactions on Power Apparatus and Systems, vol. PAS-99, no. 2, pp. 506-511, Mar.1980.

[19] IEEE Subsynchronous Resonance Working Group, "Terms, definitions and symbols for subsynchronous oscillations [power systems]," IEEE Transactions on Power Apparatus and Systems, vol. PAS-104, no. 6, pp. 1325-1334, June1985.

[20] Anderson, P. M., *Subsynchronous resonance in power systems,* New York, IEEE Press, 1990.

[21] Yan, A. and Yao-nan, Y., "Multi-mode stabilization of torsional oscillations using output feedback excitation control," IEEE Transactions on Power Apparatus and Systems, vol. PAS-101, no. 5, pp. 1245-1253, May1982.

[22] Yu, Y., *Electric power system dynamics,* New York, Academic Press, 1983.

[23] Hamouda, R. M., Iravani, M. R., and Hackan, R., "Coordinated static VAR compensators and power system stabilizers for damping power system oscillations," IEEE Transactions on Power Systems, vol. PWRS-2, no. 4, pp. 1059-1067, Nov.1987.

[24] Larsen, E. V. and Swann, D. A. "Applying power system stabilizers. I. General concepts," 80-558 1980, Minneapolis, MN, USA, IEEE.

[25] Putman, T. H. and Ramey, D. G., "Theory of the modulated reactance solution for subsynchronous resonance," IEEE Transactions on Power Apparatus and Systems, vol. PAS-101, no. 6, pp. 1527-1535, June1982.

[26] Wasynczuk, O., "Damping subsynchronous resonance using reactive power control," IEEE Transactions on Power Apparatus and Systems, vol. PAS-100, no. 3, pp. 1096-1104, Mar.1981.

[27] Hammad, A. E. and El Sadek, M., "Application of a thyristor controlled var compensator for damping of subsynchronous oscillations in power systems," IEEE Transactions on Power Apparatus and Systems, vol. PAS-103, no. 1, pp. 198-212, 1984.

[28] Iravani, M. R. and Mathur, R. M., "Damping subsynchronous oscillations in power system using a static phase-shifter," IEEE Transactions on Power Systems, vol. PWRS-1, no. 2, pp. 76-83, 1986.

[29] Othman, H. A. and Angquist, L., "Analytical modeling of thyristor-controlled series capacitors for SSR studies," IEEE Transactions on Power Systems, vol. 11, no. 1, pp. 119-127, 1996.

[30] Patil, K. V., Senthil, J., Jiang, J., and Mathur, R. M., "Application of STATCOM for damping torsional oscillations in series compensated AC systems," IEEE Transactions on Energy Conversion, vol. 13, no. 3, pp. 237-243, Sept.1998.

[31] Perkins, B. K. and Iravani, M. R., "Dynamic modeling of a TCSC with application to SSR analysis," IEEE Transactions on Power Systems, vol. 12, no. 4, pp. 1619-1625, 1997.

[32] Pillai, G. N., Ghosh, A., and Joshi, A., "Torsional oscillation studies in an SSSC compensated power system," Electric Power Systems Research, vol. 55, no. 1, pp. 57-64, 2000.

[33] Agrawal, B. L. and Farmer, R. G., "Use of frequency scanning techniques for subsynchronous resonance analysis," IEEE Transactions on Power Apparatus and Systems, vol. PAS-98, no. 2, pp. 341-349, Mar.1979.

[34] Kundur, P., *Power system stability and control,* New York, McGraw-Hill, 1994.

[35] Anon, "First benchmark model for computer simulation of subsynchronous resonance," IEEE Transactions on Power Apparatus and Systems, vol. PAS-96, no. 5, pp. 1565-1572, 1977.

[36] Wasley, R. G. and Shlash, M. A., "Steady-state phase-variable model of the synchronous machine for use in 3-phase load flow studies," Proceedings of the IEEE, vol. 121, no. 10, pp. 1155-1164, 1974.

[37] Shaltout, A. A. M., "Subsynchronous resonance in large turbo-generators connected to series capacitor compensated power systems." Ph.D Thesis University of Saskatchewan, 1981.

[38] IEEE Committee Report, "Dynamic models for steam and hydo turbines in power system studies," IEEE Transactions on Power Apparatus and Systems, vol. PAS-92, no. 6, pp. 1904-1915, 1973.

[39] Sen, K. K. and Stacey, E. J., "UPFC-unified power flow controller: theory, modeling, and applications," IEEE Transactions on Power Delivery, vol. 13, no. 4, pp. 1453-1460, Oct.1998.

[40] Angeles-Camacho, C., Tortelli, O. L., Acha, E., and Fuerte-Esquivel, C. R., "Inclusion of a high voltage DC-voltage source converter model in a Newton-Raphson power flow algorithm," IEE Proceedings: Generation, Transmission and Distribution, vol. 150, no. 6, pp. 691-696, 2003.

[41] Thomas, J. L., Poullain, S., and Benchaib, A. "Analysis of a robust DC-bus voltage control system for a VSC transmission scheme." 119-124. 2001, London, UK, IEE.

[42] Saadat, H., *Power system analysis,* Boston, WCB/McGraw-Hill, 1999.

APPENDICES

A. COMPLEX POWER FLOW

The equivalent circuit one line diagram of the system illustrated in Figure 1.4 is shown in Figure A.1. The steady-state phasor diagram of the system is shown in Figure A.2.

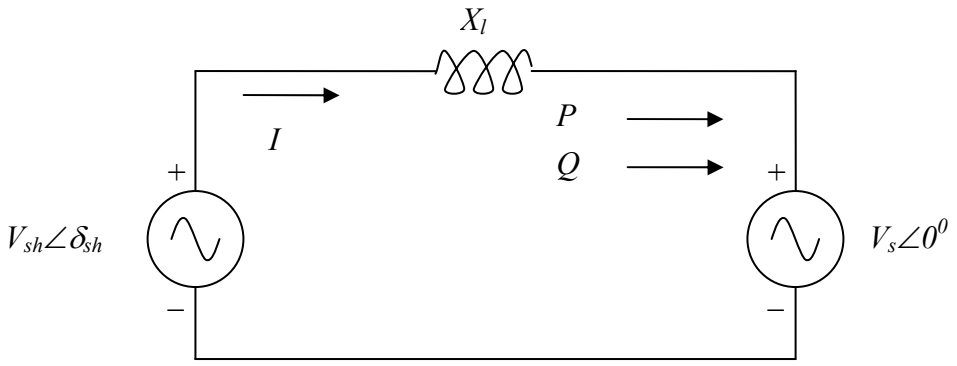

Figure A.1 The equivalent circuit of a VSC connected to an AC system through a lossless reactor.

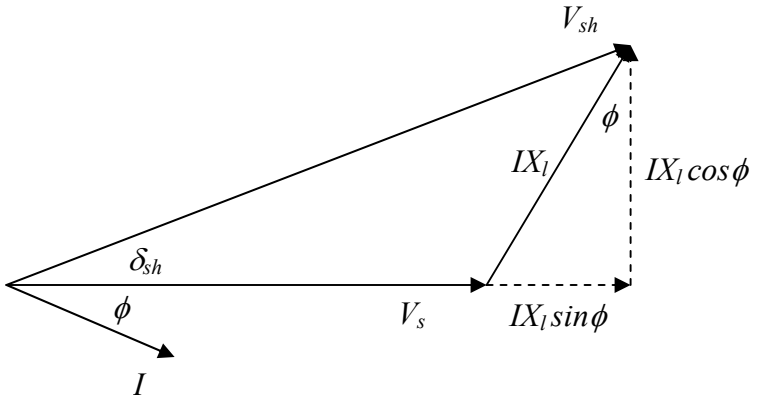

Figure A.2 Steady-state phasor diagram of a VSC connected to an AC system.

The active and reactive components of the complex power injected at the AC system can be expressed as:

$$P = VI\cos\phi \tag{A.1}$$

$$Q = VI\sin\phi \tag{A.2}$$

According to phasor diagram shown in Figure A.2, The following equations can be derived:

$$IX_l\cos\phi = V_{sh}\sin\delta_{sh} \tag{A.3}$$

$$IX_l\sin\phi = V_{sh}\cos\delta_{sh} - V_s \tag{A.4}$$

Therefore,

$$I\cos\phi = \frac{V_{sh}\sin\delta_{sh}}{X_l} \tag{A.5}$$

$$I\sin\phi = \frac{V_{sh}\cos\delta_{sh} - V_s}{X_l} \tag{A.6}$$

Substituting Equations (A.5) and (A.6) into Equations (A.1) and (A.2), gives

$$P = \frac{V_{sh}V_s\sin\delta_{sh}}{X_l} \tag{A.7}$$

$$Q = \frac{V_{sh}V_s\cos\delta_{sh}}{X_l} - \frac{V_s^{\,2}}{X_l} \tag{A.7}$$

B. SYSTEM DATA

Table B.1 Generator data (in per unit on 892.4 MVA and 26 kV base).

R_a = 1e-7	R_{fd} = 0.0013	R_{1d} = 0.0297
R_{1q} = 0.0124		R_{2q} = 0.0182
X_{ad} = 1.66		X_{aq} = 1.58
X_d = 1.79	X_q = 1.71	X_{ffd} = 1.7335
X_{11d} = 1.7177	X_{11q} = 1.6319	X_{22q} = 1.9029

Table B.2 Transmission line data (in per unit on 892.4 MVA and 500 kV base).

Series capacitor compensated transmission line (Line 1)	
R_L = 0.02	X_L = 0.7
Line 2	
R_{L2} = 0.005	X_{L2} = 0.1
Line 3	
R_{L3} = 0.005	X_{L3} = 0.1

Table B.3 VSC-HVDC back-to-back system data (in per unit on 892.4 MVA and 500 kV base).

VSC-HVDC rectifier station	
R_E = 0.0	X_E = 0.1
VSC-HVDC inverter station	
R_B = 0.0	X_B = 0.1
DC link	
X_{dc} = 0.5	
Active power controller	
Lim_max = 1.2	*Lim_min* = 0.5

Table B.4 Mechanical system data.

Mass	Shaft	Inertia M (seconds)	Damping D (p.u./p.u. speed)	Spring constant K (p.u./rad)
EXC		0.0684	0.017	
	GEN-EXC			2.822
GEN		1.736	0.099	
	LPB-GEN			70.858
LPB		1.768	0.100	
	LPA-LPB			52.038
LPA		1.716	0.100	
	IP-LPA			34.929
IP		0.311	0.025	
	HP-IP			19.303
HP		0.1856	0.008	

Table B.5 Governor and turbine system data.

$K_g = 25$	
$T_g = 0.1$sec.	$T_{ch} = 0.40$ sec.
$T_{rh} = 7.0$sec.	$T_{co} = 0.60$ sec.
$F_A = 0.22$	$F_B = 0.22$
$F_I = 0.26$	$F_H = 0.30$
Cvopen = 4.0 p.u./sec.	Cvclose = 4.0 p.u./sec.

Table B.6 Excitation system data.

$K_A = 2$	$K_E = 1.0$
$K_F = 0.03$	
$T_A = 0.04$ sec.	$T_E = 0.01$sec.
$T_F = 1.0$ sec.	
$V_{Rmax} = 4.75$ p.u.	$V_{Rmin} = -4.75$ p.u.

Table B.7 Initial operating conditions.

Generator real power	P_G = 0.90 p.u.
Generator terminal voltage magnitude	$\|V_t\|$ = 1.02 p.u.
System I	$V_{\mathrm{I}} = 1.0\angle 0^0$
System II magnitude	$\|V_{\mathrm{II}}\|$ = 1.02 p.u.
VSC-HVDC rectifier station bus(Bus 3) voltage magnitude	$\|V3\|$ = 1.0 p.u.
Reactive power flows into System II from VSC-HVDC inverter station	Q_4 = 0.05 p.u.

C. SMALL SIGNAL MODEL OF THE COMPLETE SYSTEM FOR THE IEEE FIRST BENCHMARK MODEL

In order to form the overall system equations, the equations derived in Chapter 2 for the individual system components are rewritten here again.

- 6th order state equation of synchronous machine (Equation 2.17).

$$\left[\frac{d\Delta X_{syn}}{dt}\right] = \left[A_{syn}\right]\left[\Delta X_{syn}\right] + \left[B_{syn}\right]\left[\Delta U_{syn}\right] \tag{C.1}$$

where

$$\left[\Delta X_{syn}\right] = \left[\Delta i_d \quad \Delta i_q \quad \Delta i_{fd} \quad \Delta i_{1q} \quad \Delta i_{1d} \quad \Delta i_{2q}\right]^T$$

$$\left[\Delta U_{syn}\right] = \left[\Delta V_{td} \quad \Delta V_{tq} \quad \Delta e_{fd} \quad \Delta\omega\right]^T$$

- State equation of transmission line (Equation 2.24)

$$\begin{bmatrix} \frac{d\Delta V_{Cd}}{dt} \\ \frac{d\Delta V_{Cq}}{dt} \\ \Delta V_{td} \\ \Delta V_{tq} \end{bmatrix} = [At]\begin{bmatrix} \Delta V_{Cd} \\ \Delta V_{Cq} \end{bmatrix} + [R1]\begin{bmatrix} \frac{d\Delta i_d}{dt} \\ \frac{d\Delta i_q}{dt} \end{bmatrix} + [R2]\begin{bmatrix} \Delta i_d \\ \Delta i_q \end{bmatrix} + [Bt]\begin{bmatrix} \Delta\omega \\ \Delta\delta \end{bmatrix} \tag{C.2}$$

- 12th order state equation of mechanical system (Equation 2.32)

$$\left[\frac{d\Delta X_{ms}}{dt}\right] = \left[A_{ms}\right]\left[\Delta X_{ms}\right] + \left[B_{ms}\right]\left[\Delta U_{ms}\right] \tag{C.3}$$

where

$$[\Delta X_{ms}] = [\Delta\delta_E \quad \Delta\delta \quad \Delta\delta_B \quad \Delta\delta_A \quad \Delta\delta_I \quad \Delta\delta_H \quad \Delta\omega_E \quad \Delta\omega \quad \Delta\omega_B \quad \Delta\omega_A \quad \Delta\omega_I \quad \Delta\omega_H]^T$$
$$[\Delta U_{ms}] = [\Delta T_e \quad \Delta P_H \quad \Delta P_I \quad \Delta P_A]^T$$

- 4th order state equation of governor and turbine system (Equation 2.36)

$$\left[\frac{d\Delta X_g}{dt}\right] = [A_g][\Delta X_g] + [B_g]\begin{bmatrix}\Delta P_{m0}\\ \Delta\omega_H\end{bmatrix} \tag{C.4))}$$

where

$$[\Delta X_g] = [\Delta C_V \quad \Delta P_H \quad \Delta P_I \quad \Delta P_A]^T$$

- 3rd order state equation of excitation system (Equation 2.40)

$$\left[\frac{d\Delta X_v}{dt}\right] = [A_v][\Delta X_v] + [B_v]\begin{bmatrix}\Delta V_t\\ \Delta E_{ref}\end{bmatrix} \tag{C.5}$$

where

$$[\Delta X_v] = [\Delta e_{fd} \quad \Delta E_R \quad \Delta E_{SB}]^T$$

- Equation of Air-gap (Equation2.45)

$$\Delta T_e = [Tedq0][\Delta X_{syn}] \tag{C.6}$$

- Equation of terminal voltage (Equation 2.47)

$$\Delta V_t = \begin{bmatrix}\frac{V_{td0}}{V_{t0}} & \frac{V_{tq0}}{V_{t0}}\end{bmatrix}\begin{bmatrix}\Delta V_{td}\\ \Delta V_{tq}\end{bmatrix} \tag{C.7}$$

Electrical part of the system: Combining Equations (C.1) and (C.2) to form the following equations

$$\begin{bmatrix} \frac{d\Delta X_{syn}}{dt} \\ \frac{d\Delta V_{Cd}}{dt} \\ \frac{d\Delta V_{Cq}}{dt} \end{bmatrix} = [Amt] \begin{bmatrix} \Delta X_{syn} \\ \Delta V_{Cd} \\ \Delta V_{Cq} \end{bmatrix} + [Bmt] \begin{bmatrix} \Delta e_{fd} \\ \Delta \omega \\ \Delta \delta \end{bmatrix} \tag{C.8}$$

$$\begin{bmatrix} \Delta V_{td} \\ \Delta V_{tq} \end{bmatrix} = [Ci] \begin{bmatrix} \Delta X_{syn} \\ \Delta V_{Cd} \\ \Delta V_{Cq} \end{bmatrix} + [Di] \begin{bmatrix} \Delta e_{fd} \\ \Delta \omega \\ \Delta \delta \end{bmatrix} \tag{C.9}$$

where

$$[Amt] = [AmtCi(1:8,:)]$$

$$[Bmt] = [BmtDi(1:8,:)]$$

$$[Ci] = [AmtCi(9:10,:)]$$

$$[Di] = [BmtDi(9:10,:)] \tag{C.10}$$

$$[AmtCi] = \begin{bmatrix} I_{6x6} & 0_{6x2} & -B_{syn}(:,1:2) \\ -R1 & 0_{4x4} & I_{4x4} \end{bmatrix}^{-1} \begin{bmatrix} A_{syn} & 0_{6x2} \\ R2 & 0_{4x4} & At \end{bmatrix}$$

$$[BmtDi] = \begin{bmatrix} I_{6x6} & 0_{6x2} & -B_{syn}(:,1:2) \\ -R1 & 0_{4x4} & I_{4x4} \end{bmatrix}^{-1} \begin{bmatrix} B_{syn}(:,3:4) & 0_{6x1} \\ 0_{4x1} & Bt \end{bmatrix}$$

Here, *AmtCi*(1:8, :) means all columns and 1 to 8 rows of *AmtC*i, *Bsyn*(:, 1:2) means all rows and 1 to 2 columns of *Bsyn*, I_{nxn} is an *n* by *n* identity matrix, and 0_{mxn} is an *m* by *n* matrix with all elements zero.

Combining Equations (C.6), (C.7), and (C.9) to form the following equation

$$\begin{bmatrix} \Delta T_e \\ \Delta V_t \end{bmatrix} = [Cmt] \begin{bmatrix} \Delta X_{syn} \\ \Delta V_{Cd} \\ \Delta V_{Cq} \end{bmatrix} + [Dmt] \begin{bmatrix} \Delta e_{fd} \\ \Delta \omega \\ \Delta \delta \end{bmatrix} \tag{C.11}$$

where

$$[Cmt] = \begin{bmatrix} Tedq0 & 0 & 0 \\ \begin{bmatrix} \frac{V_{td0}}{V_{t0}} & \frac{V_{tq0}}{V_{t0}} \end{bmatrix} [Ci] \end{bmatrix}$$

$$[Dmt] = \begin{bmatrix} 0 & 0 & 0 \\ \begin{bmatrix} \frac{V_{td0}}{V_{t0}} & \frac{V_{tq0}}{V_{t0}} \end{bmatrix} [Di] \end{bmatrix} \tag{C.12}$$

Shaft and excitation system: Combining Equations (C.3), (C.4), and (C.5) to form the following equations

$$\begin{bmatrix} \frac{d\Delta X_{ms}}{dt} \\ \frac{d\Delta X_{g}}{dt} \\ \frac{d\Delta X_{v}}{dt} \end{bmatrix} = [Ap1] \begin{bmatrix} \Delta X_{ms} \\ \Delta X_{g} \\ \Delta X_{v} \end{bmatrix} + [Ap2] \begin{bmatrix} \Delta T_{e} \\ \Delta V_{t} \end{bmatrix} + [Bp] \begin{bmatrix} \Delta P_{m0} \\ \Delta E_{ref} \end{bmatrix} \tag{C.13}$$

where

$$[Ap1] = \begin{bmatrix} A_{ms} & 0_{12x1} & B_{ms}(:, 2:4) & 0_{12x3} \\ 0_{4x11} & B_{g}(:, 2) & A_{g} & 0_{4x3} \\ & 0_{3x16} & Av & \end{bmatrix}$$

$$[Ap2] = \begin{bmatrix} B_{ms}(:, 1) & 0_{12x1} \\ 0_{4x2} & \\ 0_{3x1} & B_{v}(:, 1) \end{bmatrix} \tag{C.14}$$

$$[Bp] = \begin{bmatrix} 0_{12x2} & \\ B_{g}(:, 1) & 0_{4x1} \\ 0_{3x1} & B_{v}(:, 2) \end{bmatrix}$$

Combining Equations (C.11) and (C.13) to form the following equations

$$\begin{bmatrix} \frac{d\Delta X_{ms}}{dt} \\ \frac{d\Delta X_{g}}{dt} \\ \frac{d\Delta X_{v}}{dt} \end{bmatrix} = [Ap1] \begin{bmatrix} \Delta X_{ms} \\ \Delta X_{g} \\ \Delta X_{v} \end{bmatrix} + [Ap2Cmt] \begin{bmatrix} \Delta X_{syn} \\ \Delta V_{cd} \\ \Delta V_{cq} \end{bmatrix} + [Ap2Dmt] \begin{bmatrix} \Delta e_{fd} \\ \Delta \omega \\ \Delta \delta \end{bmatrix} + [Bp] \begin{bmatrix} \Delta P_{m0} \\ \Delta E_{ref} \end{bmatrix} \quad \text{(C.15)}$$

where

$$[Ap2Cmt] = [Ap2][Cmt]$$

$$[Ap2Dmt] = [Ap2][Dmt] \quad \text{(C.16)}$$

Entire system state equation: Combining Equations (C.8) and (C.15) to form the 27th order state equation of the complete system.

$$\left[\frac{d\Delta X}{dt}\right] = [A][\Delta X] + [B][\Delta U] \quad \text{(C.17)}$$

where

$$[\Delta X] = [\Delta\delta_E \quad \Delta\delta \quad \Delta\delta_B \quad \Delta\delta_A \quad \Delta\delta_I \quad \Delta\delta_H \quad \Delta\omega_E \quad \Delta\omega \quad \Delta\omega_B \ldots$$
$$\Delta\omega_A \quad \Delta\omega_I \quad \Delta\omega_H \quad \Delta C_v \quad \Delta P_H \quad \Delta P_I \quad \Delta P_A \quad \Delta e_{fd} \quad \Delta E_R \quad \Delta E_{SB} \ldots$$
$$\Delta i_d \quad \Delta i_q \quad \Delta i_{fd} \quad \Delta i_{1q} \quad \Delta i_{1d} \quad \Delta i_{2q} \quad \Delta V_{Cd} \quad \Delta V_{Cq}]^T$$

$$[\Delta U] = [\Delta P_{m0} \quad \Delta E_{ref}]^T$$

$$[A] = [App1(:,1) \quad App1(:,2) + App2(:,3) \quad App1(:,3:7) \quad App1(:,8) + App2(:,2) \ldots.$$
$$App1(:,9:16) \quad App1(:,17) + App2(:,1) \quad App1(:,18:27)]$$

$$[B] = \begin{bmatrix} Bp \\ 0_{8x2} \end{bmatrix} \quad \text{(C.18)}$$

$$[App1] = \begin{bmatrix} Ap1 & Ap2Cmt \\ 0_{8x19} & Amt \end{bmatrix}$$

$$[App2] = \begin{bmatrix} Ap2Dmt \\ Bmt \end{bmatrix}$$

D. DYNAMIC MODEL OF THE COMPLETE SYSTEM FOR THE HVAC/DC SYSTEM INCORPORATING A LARGE TURBINE-GENERATOR AND A VSC HVDC BACK-TO-BACK SYSTEM

In order to form the complete dynamic model of the system, the equations derived in Chapters 2 to 3 for the individual system components are rewritten here.

- Nonlinear equations of synchronous machine (Equation 3.40)

$$\left[\frac{dX_{syn}}{dt}\right] = \left[At_{syn}\right]\left[X_{syn}\right] + \left[Bt1_{syn}\right]\begin{bmatrix} V_{td} \\ V_{tq} \end{bmatrix} + \left[Bt1_{syn}\right]\left[e_{fd}\right] \tag{D.1}$$

where

$$\left[X_{syn}\right] = \begin{bmatrix} i_d & i_q & i_{fd} & i_{1q} & i_{1d} & i_{2q} \end{bmatrix}^T$$

- Nonlinear equations of transmission line (Equation 3.37 to 3.38)

$$\left[\frac{dX_{TL}}{dt}\right] = \left[At_{TL}\right]\left[X_{TL}\right] + \left[Bt1_{TL}\right]\begin{bmatrix} V_{td} \\ V_{tq} \end{bmatrix} + \left[Bt2_{TL}\right]\left[V_b\right] \tag{D.2}$$

$$\begin{bmatrix} \frac{dV_{Cd}}{dt} \\ \frac{dV_{Cq}}{dt} \\ V_{td} \\ V_{tq} \end{bmatrix} = \left[Att_{TL}\right]\begin{bmatrix} V_{Cd} \\ V_{Cq} \end{bmatrix} + \left[Rt11_{TL}\right]\begin{bmatrix} \frac{di_d}{dt} \\ \frac{di_q}{dt} \end{bmatrix} + \left[Rt12_{TL}\right]\begin{bmatrix} \frac{di_{Ed}}{dt} \\ \frac{di_{Eq}}{dt} \end{bmatrix} + \left[Rt21_{TL}\right]\begin{bmatrix} i_d \\ i_q \end{bmatrix} + \left[Rt22_{TL}\right]\begin{bmatrix} i_{Ed} \\ i_{Eq} \end{bmatrix} + \left[Btt_{TL}\right]\left[V_b\right] \tag{D.3}$$

where

$$[X_{TL}] = [i_{Ld} \quad i_{Lq} \quad V_{Cd} \quad V_{Cq}]^T$$

- Nonlinear equations of VSC-HVSC back-to-back system (Equation 3.31)

$$\left[\frac{dX_{DC}}{dt}\right] = [At_{DC}][X_{DC}] + [Bt1_{DC}]\begin{bmatrix} V_{Ed} \\ V_{Eq} \end{bmatrix} + [Bt2_{DC}]\begin{bmatrix} V_{Bd} \\ V_{Bq} \end{bmatrix} \tag{D.4}$$

where

$$[X_{DC}] = [i_{Ed} \quad i_{Eq} \quad i_{Bd} \quad i_{Bq} \quad V_{dc}]^T$$

- Nonlinear equations of mechanical system (Equation 2.30)

$$\left[\frac{dX_{ms}}{dt}\right] = [At_{ms}][X_{ms}] + [Bt_{ms}][U_{tms}] \tag{D.5}$$

where

$$[X_{ms}] = [\delta_E \quad \delta \quad \delta_B \quad \delta_A \quad \delta_I \quad \delta_H \quad \omega_E \quad \omega \quad \omega_B \quad \omega_A \quad \omega_I \quad \omega_H]^T$$

$$[U_{tms}] = [\omega_0 \quad P_H \quad P_I \quad P_A \quad T_e]^T$$

- Equations of governor and turbine system (Equation 2.34)

$$\left[\frac{dX_g}{dt}\right] = [At_g][X_g] + [Bt_g]\begin{bmatrix} \omega_0 \\ P_{m0} \\ \omega_H \end{bmatrix} \tag{D.6}$$

whree

$$[X_g] = [C_V \quad P_H \quad P_I \quad P_A]^T$$

- Equations of excitation system (Equation 2.38)

$$\left[\frac{dX_v}{dt}\right] = [At_v][X_v] + [Bt_v]\begin{bmatrix} V_t \\ E_{ref} \end{bmatrix} \tag{D.7}$$

where

$$[X_v] = \begin{bmatrix} e_{fd} & E_R & E_{SB} \end{bmatrix}^T$$

- Equation of air-gap (Equation 3.44)

$$T_e = [Tedq][X_{syn}] \tag{D.8}$$

- Equations of VSC HVDC back-to-back active power controller (Equation 3.33)

$$\left[\frac{dX_{cm}}{dt}\right] = [At_{cm}][X_{cm}] + [Bt_{cm}]\begin{bmatrix} P_{Edcref} \\ P_{Edc} \\ P_{Bdcref} \\ P_{Bdc} \end{bmatrix} \tag{D.9}$$

where

$$[X_{cm}] = \begin{bmatrix} m_E & m_{Er} & m_B & m_{Br} \end{bmatrix}^T$$

- Equations of VSC HVDC back-to-back supplementary controller (Equation 3.35)

$$\left[\frac{dX_{dw}}{dt}\right] = [At_{dw}][X_{dw}] + [Bt_{dw}]\begin{bmatrix} \omega_{ref} \\ \omega \end{bmatrix} \tag{D.10}$$

where

$$[X_{dw}] = \begin{bmatrix} \delta_{Esh} & DW_{sh} \end{bmatrix}^T$$

Electrical part of the system: Combining Equations (D.1), (D.2) and (D.4) to form the following equations:

$$\begin{bmatrix} \frac{dX_{Syn}}{dt} \\ \frac{dX_{DC}}{dt} \\ \frac{dX_{TL}}{dt} \end{bmatrix} = [At_{SL}] \begin{bmatrix} X_{Syn} \\ X_{DC} \\ X_{TL} \end{bmatrix} + [Bt_{SL}] \begin{bmatrix} V_{td} \\ V_{tq} \\ e_{fd} \\ |V_B| \\ V_b \end{bmatrix} \tag{D.11}$$

where

$$[At_{SL}] = \begin{bmatrix} At_{Syn} & 0_{6x5} & 0_{6x4} \\ 0_{5x6} & At_{DC} & 0_{5x4} \\ 0_{4x6} & 0_{4x5} & At_{TL} \end{bmatrix}$$

$$[Bt_{SL}] = \begin{bmatrix} Bt_{Syn} & 0_{6x1} & 0_{6x1} \\ Bt1_{DC} & 0_{5x1} & Bt2_{DC} & 0_{5x1} \\ Bt1_{TL} & 0_{4x2} & Bt2_{TL} \end{bmatrix} \tag{D.12}$$

Combining Equations (D.1), (D.3) and (D.4) to form the following equations

$$\begin{bmatrix} \frac{dX_{Syn}}{dt} \\ \frac{dX_{DC}}{dt} \\ \frac{dV_{Cd}}{dt} \\ \frac{dV_{Cq}}{dt} \\ V_{tq} \\ V_{tq} \end{bmatrix} = [AmtCi] \begin{bmatrix} X_{Syn} \\ X_{DC} \\ V_{Cd} \\ V_{Cq} \end{bmatrix} + [BmtDi] \begin{bmatrix} e_{fd} \\ |V_B| \\ V_b \end{bmatrix} \tag{D.13}$$

where

$$[AmtCi] =$$

$$\begin{bmatrix} I_{6x6} & 0_{6x7} & -Bt1_{syn} \\ 0_{5x6} & I_{5x5} & 0_{5x2} \; -Bt1_{DC} \\ -Rt11_{TL} \; 0_{4x4} & -Rt12_{TL} \; 0_{4x3} & I_{4x4} \end{bmatrix}^{-1} \begin{bmatrix} At_{Syn} & 0_{6x5} & 0_{6x2} \\ 0_{5x6} & At_{DC} & 0_{5x2} \\ Rt21_{TL} \; 0_{4x4} & Rt22_{TL} \; 0_{4x3} & Att_{TL} \end{bmatrix}$$

$$[BmtDi] =$$

$$\begin{bmatrix} I_{6x6} & 0_{6x7} & -Bt1_{syn} \\ 0_{5x6} & I_{5x5} & 0_{5x2} \quad -Bt1_{DC} \\ -Rt11_{TL} \quad 0_{4x4} & -Rt12_{TL} \quad 0_{4x3} & I_{4x4} \end{bmatrix}^{-1} \begin{bmatrix} Bt2_{Syn} & 0_{6x1} & 0_{6x1} \\ 0_{5x1} & Bt2_{DC} & 0_{5x1} \\ 0_{4x1} & 0_{4x1} & Btt_{TL} \end{bmatrix} \tag{D.14}$$

Decomposing Equation (D.13) to obtain terminal voltage equations in the d-q reference frame:

$$\begin{bmatrix} V_{td} \\ V_{tq} \end{bmatrix} = [Ci] \begin{bmatrix} X_{Syn} \\ X_{DC} \\ V_{Cd} \\ V_{Cq} \end{bmatrix} + [Di] \begin{bmatrix} e_{fd} \\ |V_B| \\ V_b \end{bmatrix} \tag{D.15}$$

where

$$[Ci] = [AmtCi(14:15,:)]$$

$$[Di] = [BmtDi(14:15,:)] \tag{D.16}$$

Shaft and excitation system: Combining Equation (D.5) to (D.8) to form the following equations

$$\begin{bmatrix} \frac{dX_{ms}}{dt} \\ \frac{dX_g}{dt} \\ \frac{dX_v}{dt} \end{bmatrix} = [Atp1] \begin{bmatrix} X_{ms} \\ X_g \\ X_v \end{bmatrix} + [Atp2Te][X_{syn}] + [Btp] \begin{bmatrix} \omega_0 \\ P_{m0} \\ V_t \\ E_{ref} \end{bmatrix} \tag{D.17}$$

where

$$[Atp1] = \begin{bmatrix} At_{ms} & 0_{12x1} & Bt_{ms}(:,2:4) & 0_{12x3} \\ 0_{4x11} & Bt_g(:,3) & At_g & 0_{4x3} \\ 0_{3x16} & & & At_v \end{bmatrix}$$

$$[Atp2Te] = \begin{bmatrix} Bt_{ms}(:,5) \\ 0_{7x1} \end{bmatrix} [Tedq] \tag{D.18}$$

$$[Btp]=\begin{bmatrix} Bt_{ms}(:,1) & 0_{12x3} \\ Bt_{g}(:,1:2) & 0_{4x12} \\ 0_{3x2} & Bt_{v} \end{bmatrix}$$

Combining Equations (D.11) to (D.17) to form 34th order nonlinear equations without VSC HVDC back-to-back controllers.

$$\begin{bmatrix} \frac{dX_{ms}}{dt} \\ \frac{dX_{g}}{dt} \\ \frac{dX_{v}}{dt} \\ \frac{dX_{syn}}{dt} \\ \frac{dX_{DC}}{dt} \\ \frac{dX_{TL}}{dt} \end{bmatrix} = [Att]\begin{bmatrix} X_{ms} \\ X_{g} \\ X_{v} \\ X_{syn} \\ X_{DC} \\ X_{TL} \end{bmatrix} + [Btt]\begin{bmatrix} \omega_0 \\ P_{m0} \\ V_{t} \\ E_{ref} \\ V_{td} \\ V_{tq} \\ |V_{B}| \\ V_{b} \end{bmatrix} \tag{D.19}$$

where

$$[Att]=\begin{bmatrix} Atp1 & Atp2Te & 0_{19x9} \\ 0_{15x16} & Bt_{SL}(:,3) & 0_{15x2} \quad At_{SL} \end{bmatrix}$$

$$[Btt]=\begin{bmatrix} Btp & 0_{19x4} \\ 0_{15x4} & Bt_{SL}(:,1:2) \quad Bt_{SL}(:,4:5) \end{bmatrix} \tag{D.20}$$

Entire system dynamic model: combining Equations (D.9) to (D.10) with (D.19) to form finally 40th order nonlinear equations of the system:

$$\left[\frac{dX_{t}}{dt}\right]=[Attmd][X_{t}]+[Bttmd][U_{t}] \tag{D.21}$$

where

$$[X_t] = [\delta_E \quad \delta \quad \delta_B \quad \delta_A \quad \delta_I \quad \delta_H \quad \omega_E \quad \omega \quad \omega_B \quad \omega_A \quad \omega_I \quad \omega_H \ldots$$
$$C_v \quad P_H \quad P_I \quad P_H \quad e_{fd} \quad E_R \quad E_{SB} \quad i_d \quad i_q \quad i_{fd} \quad i_{1q} \quad i_{1d} \quad i_{2q} \ldots$$
$$i_{Ed} \quad i_{Eq} \quad i_{Bd} \quad i_{Bq} \quad V_{dc} \quad i_{Ld} \quad i_{Ld} \quad V_{Cd} \quad V_{Cq} \quad m_E \quad m_{Er} \quad m_B \quad m_{Br} \quad \delta_{Esh} \quad DW_{sh}]^T$$

$$[U_t] = [\omega_0 \quad P_{m0} \quad V_t \quad E_{ref} \quad V_{td} \quad V_{tq} \quad |V_B| \quad V_b \quad P_{Edcref} \quad P_{Edc} \quad P_{Bdcref} \quad P_{Bdc}]^T$$

$$[Attmd] = \begin{bmatrix} Att & 0_{34x6} & \\ 0_{4x34} & At_{cm} & 0_{4x2} \\ 0_{2x7} & Bt_{dw}(:,2) & 0_{2x30} \quad At_{dw} \end{bmatrix} \tag{D.22}$$

$$[Bttmd] = \begin{bmatrix} Btt & 0_{34x4} \\ 0_{4x8} & Bt_{cm} \\ Bt_{dw}(:,1) & 0_{2x11} \end{bmatrix}$$

E. PS2: SYSTEM DYNAMIC PERFORMANCE AT P_{dc} = 0.6 p.u.

The power flow and voltages of the system in this case are shown in Figure E.1 and Table E.1 respectively. The corresponding data of the controllers are given in Table 4.2. The effect of VSC HVDC back-to-back controllers on the dynamic performance of the system due to a 3-cycle, three-phase fault at the generator terminals are shown in Figures E.2 to E.4.

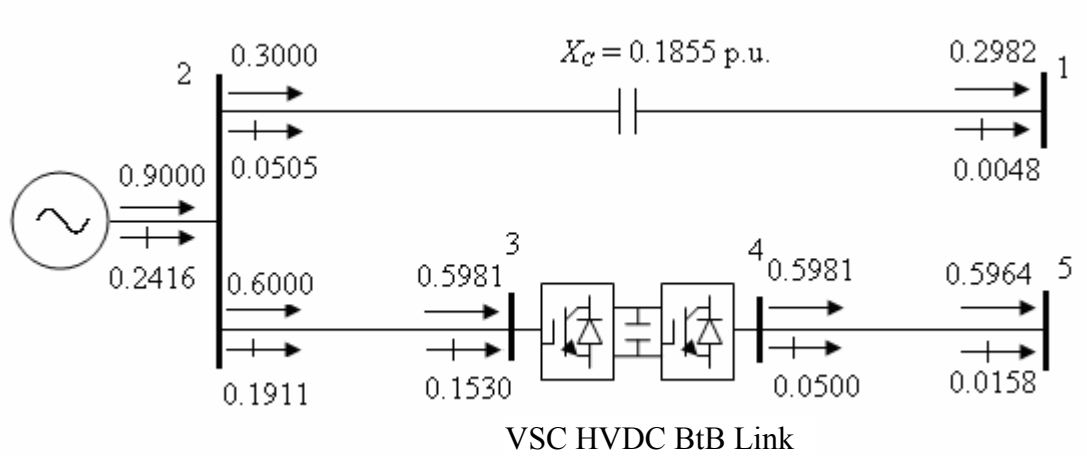

Figure E.1 System power flow results (P_{dc} = 0.60 p.u., X_C = 0.1855 p.u.).

Table E.1 System bus and VSC voltages (P_{dc} = 0.60 p.u., X_C = 0.1855 p.u.).

	System bus					VSC voltage	
	1	2	3	4	5	V_{sh1}	V_{sh2}
Magnitude (p.u.)	1.0000	1.0200	1.0000	1.0261	1.0200	0.9865	1.0327
Phase angle (deg)	0	8.6460	5.3275	5.3349	2.0727	1.8516	8.5706

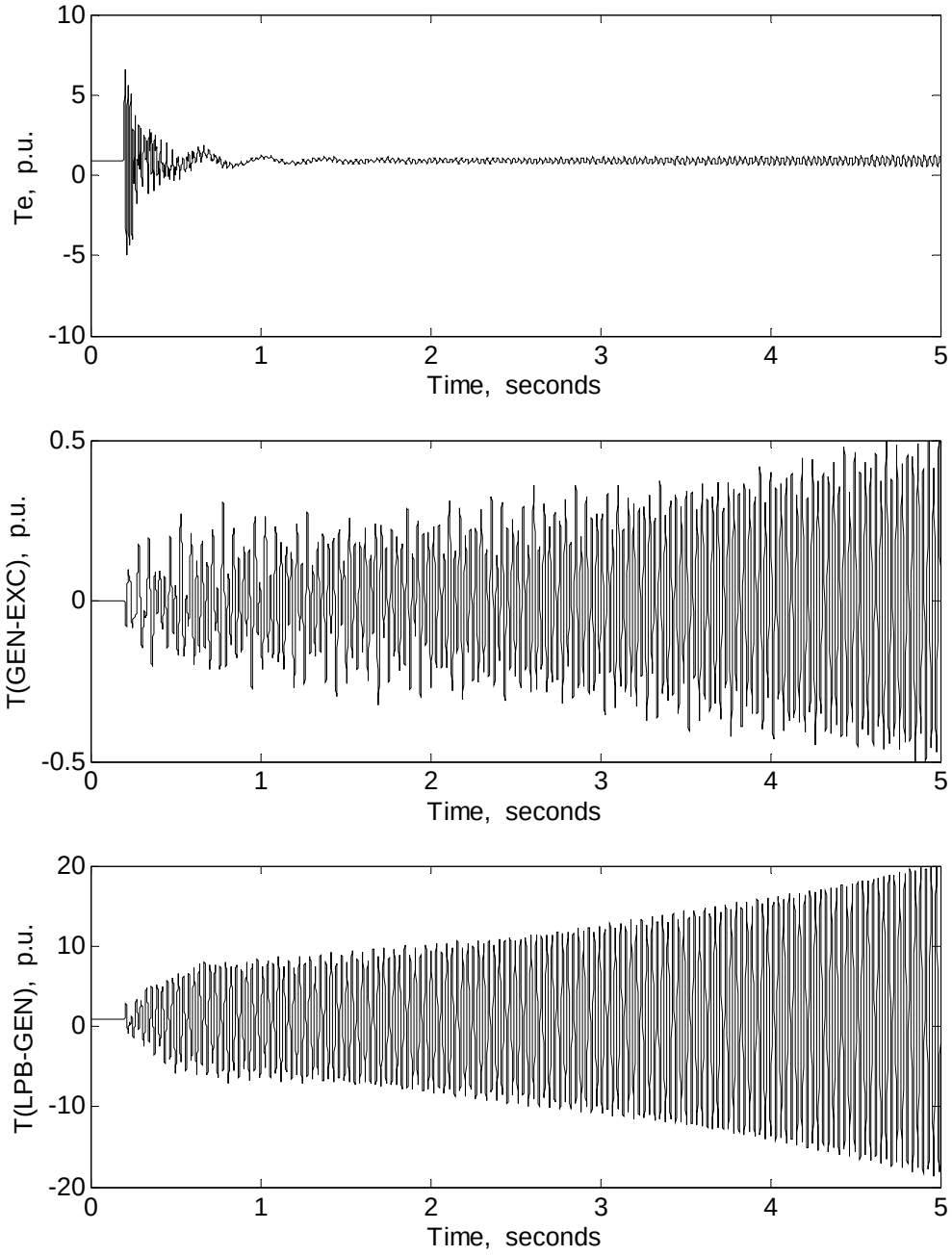

(a)

Figure E.2 Turbine-generator electromagnetic and shaft torsional torques during and after clearing a 3-cycle, three phase fault at the generator terminals: (a) Case I, (b) Case II (P_{dc} = 0.60 p.u., X_C = 0.1855 p.u.).

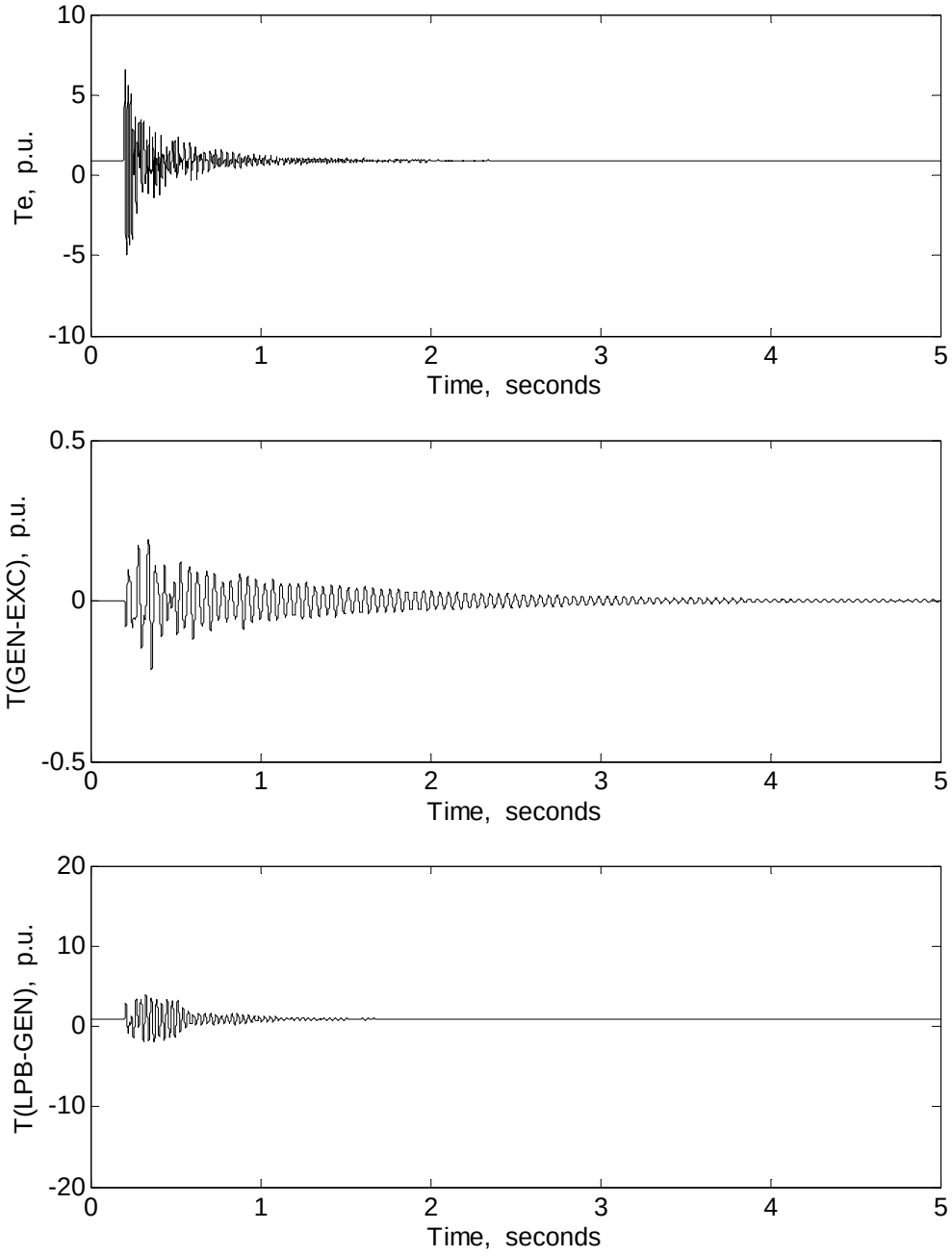

(b)

Figure E.2 (continued)

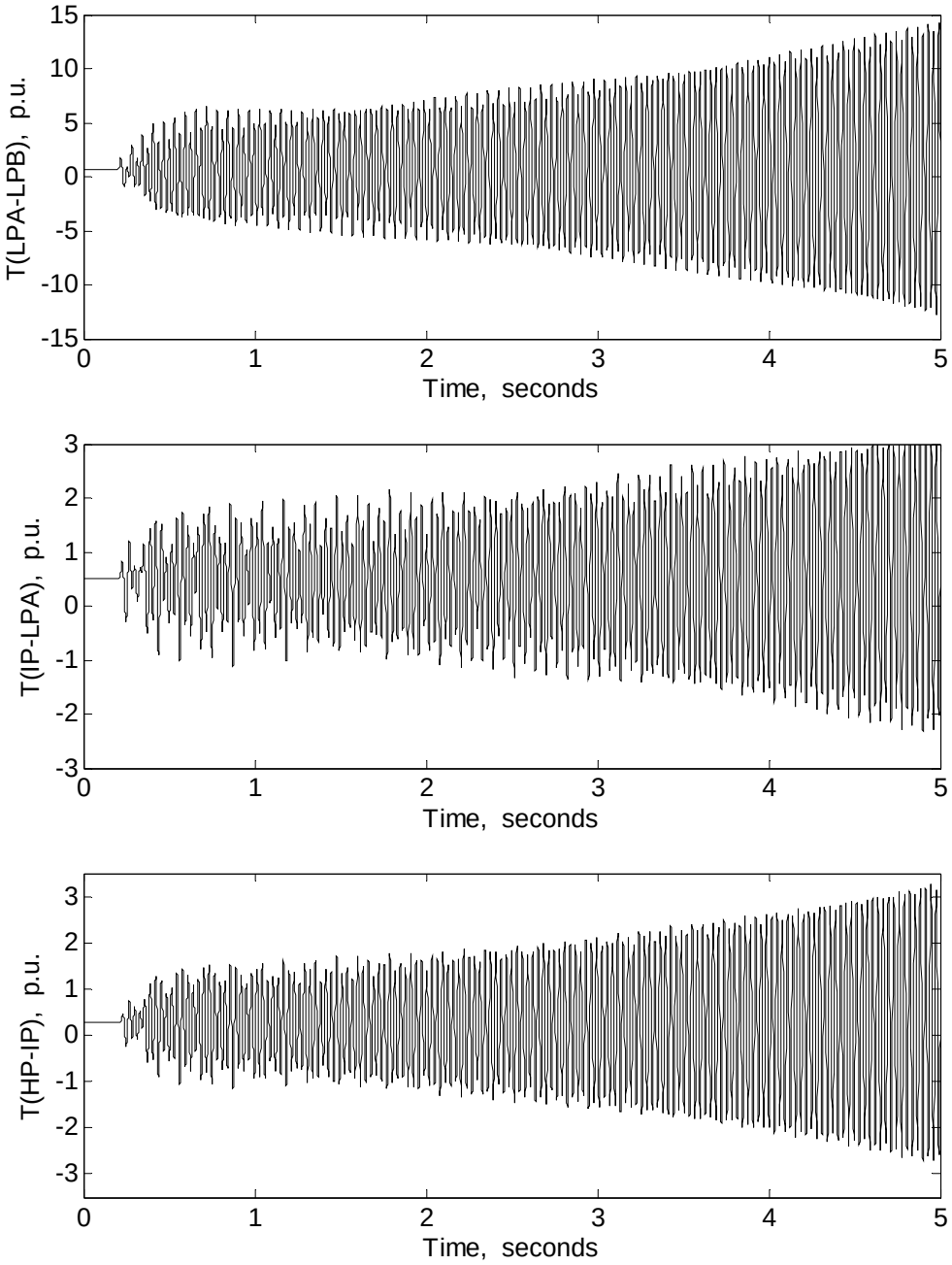

(a)

Figure E.2 (continued)

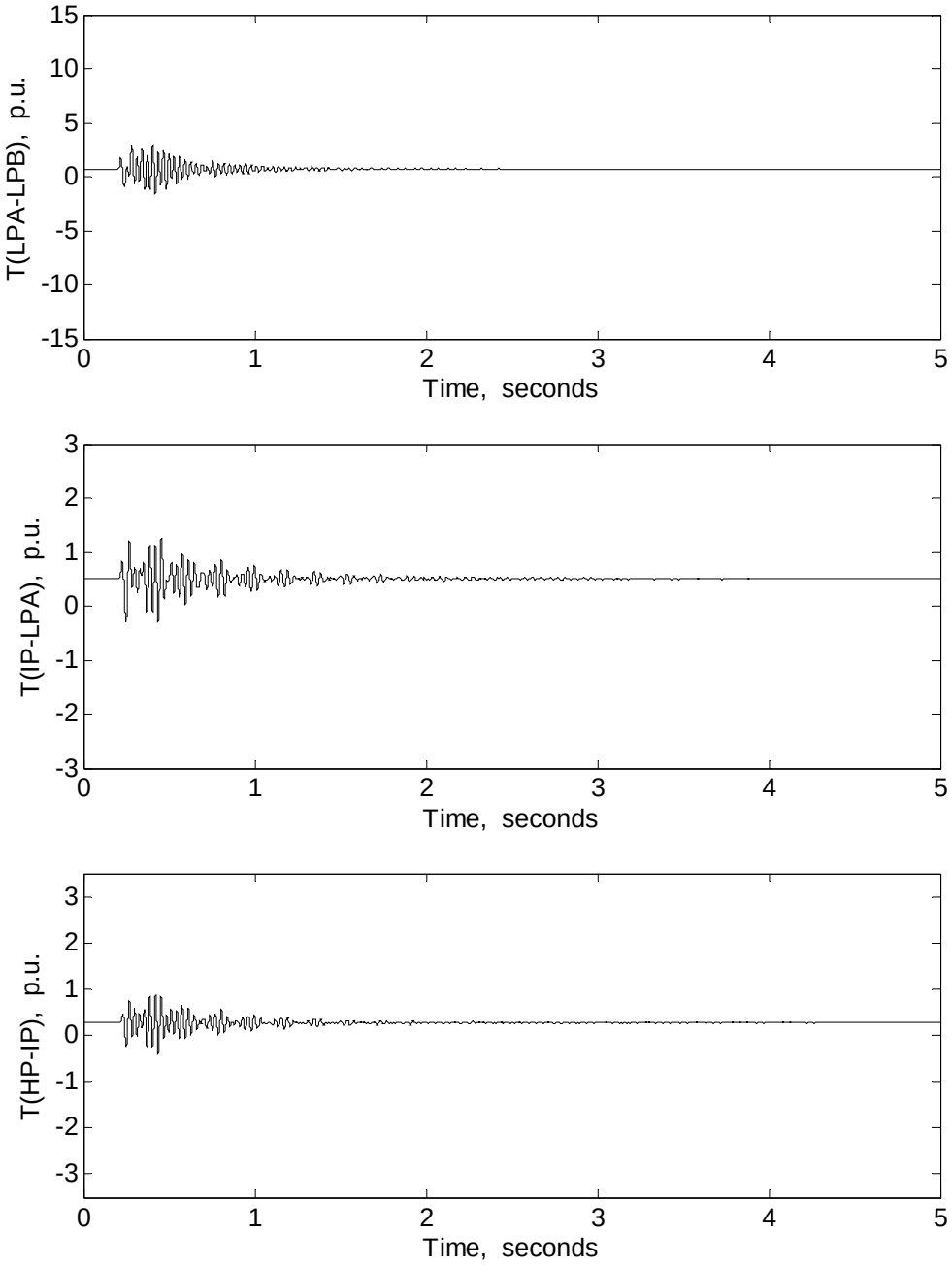

(b)

Figure E.2 (continued)

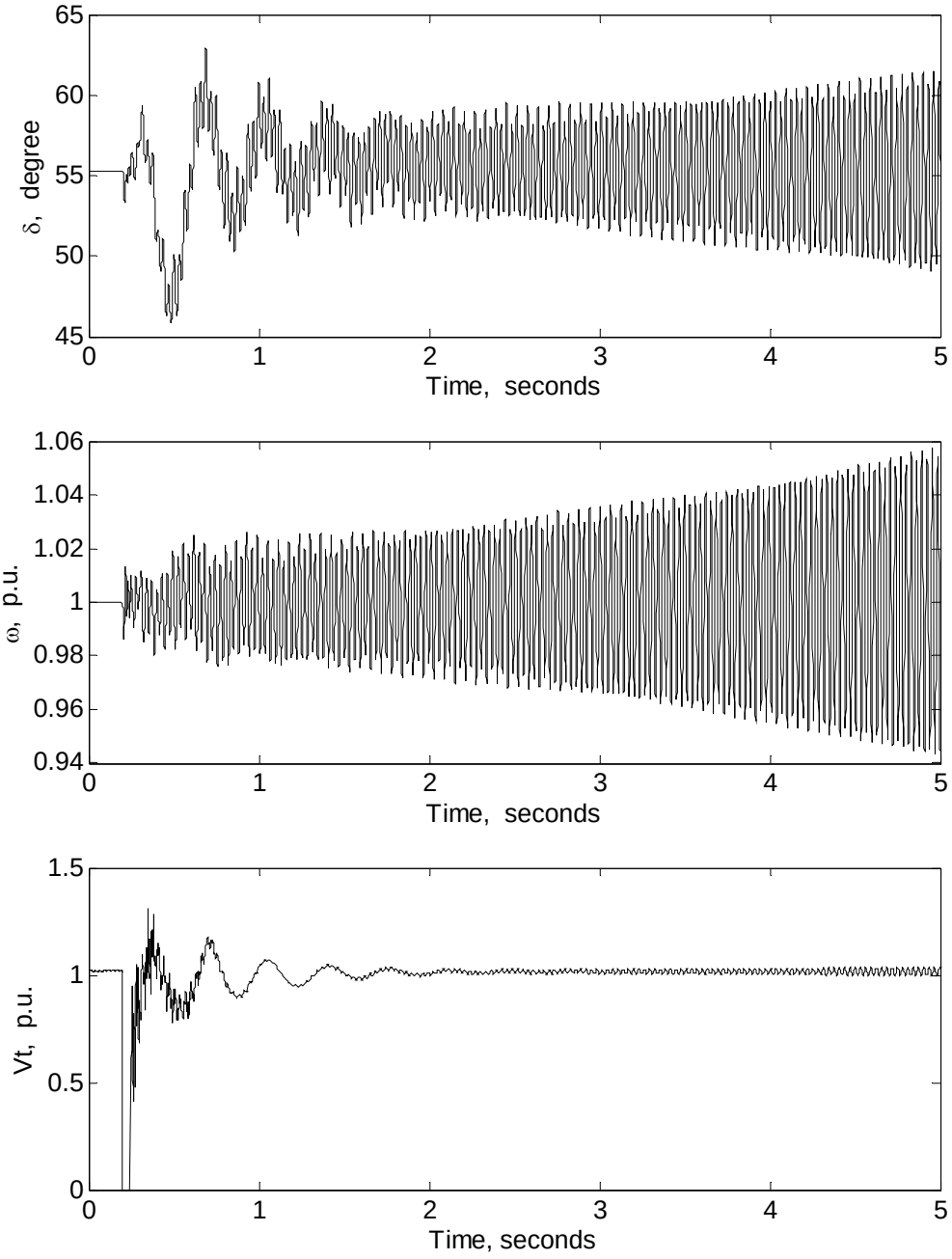

(a)

Figure E.3 Generator rotor angle, angular speed, and terminal voltage responses to a 3-cycle, three-phase fault at the generator terminals: (a) Case I, (b) Case II (P_{dc} = 0.60 p.u., X_C = 0.1855 p.u.).

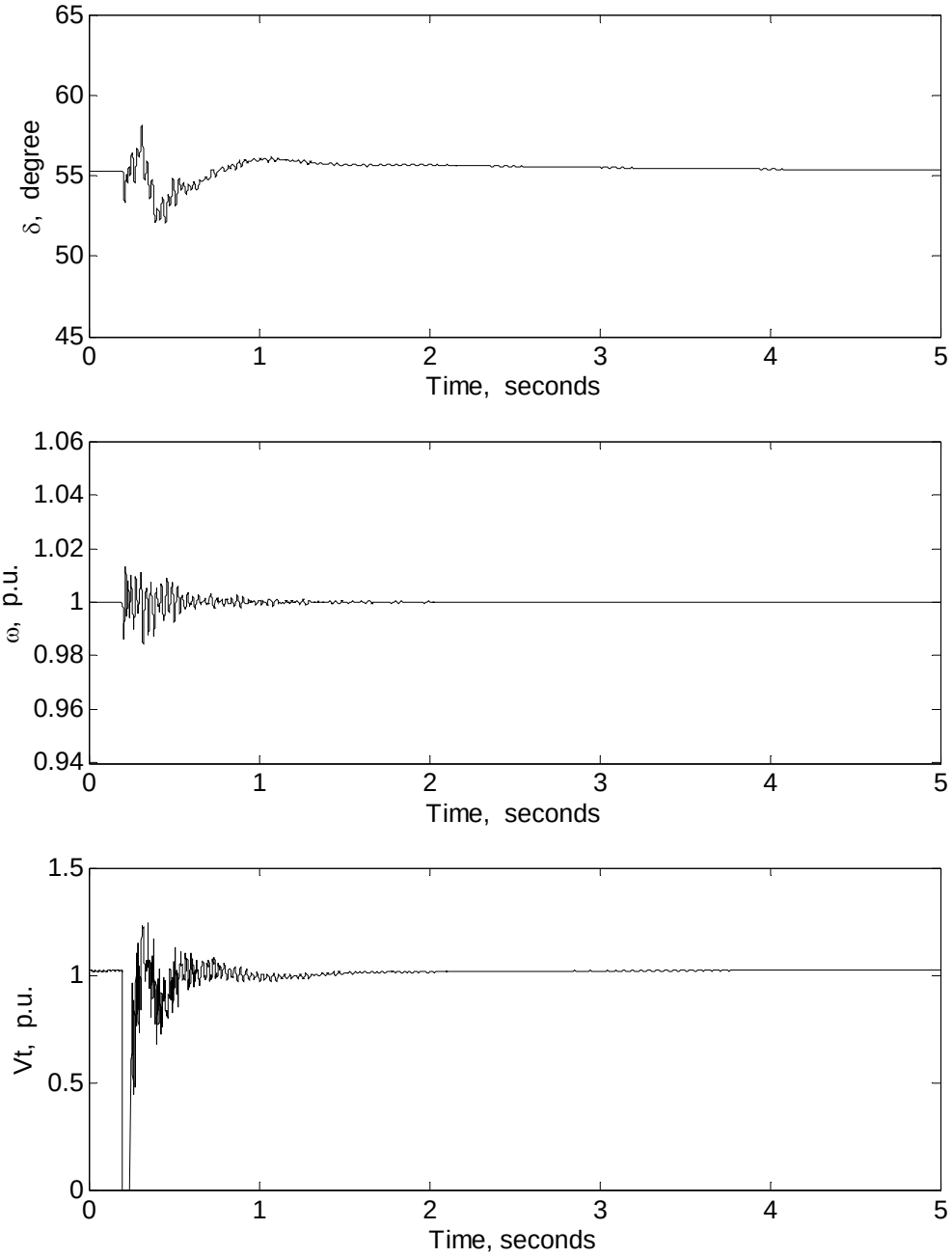

(b)

Figure E.3 (continued)

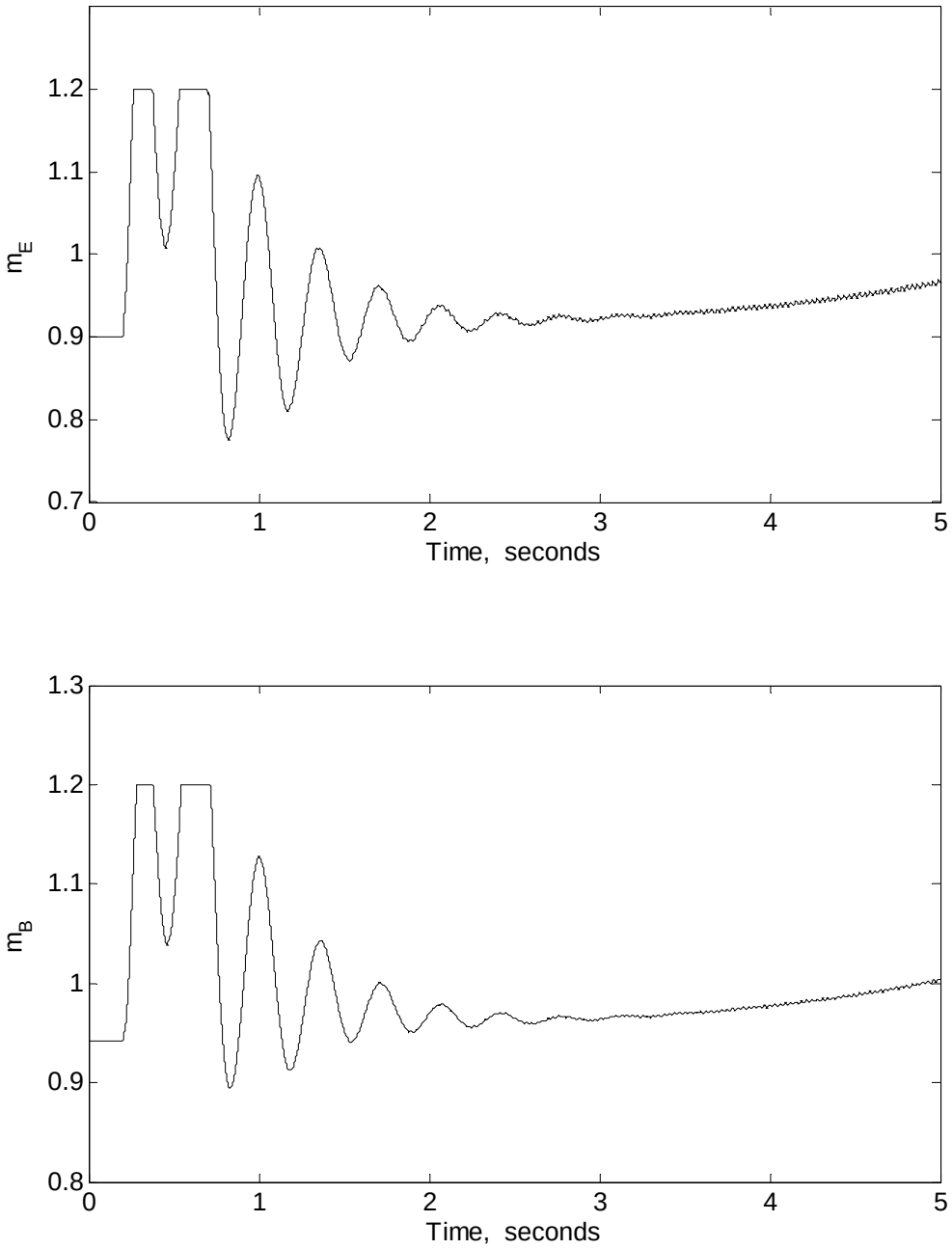

(a)

Figure E.4 Time responses of the output control signals during and after clearing a 3-cycle, three-phase fault at the generator terminals: (a) Case I, (b) Case II (P_{dc} = 0.60 p.u., X_C = 0.1855 p.u.).

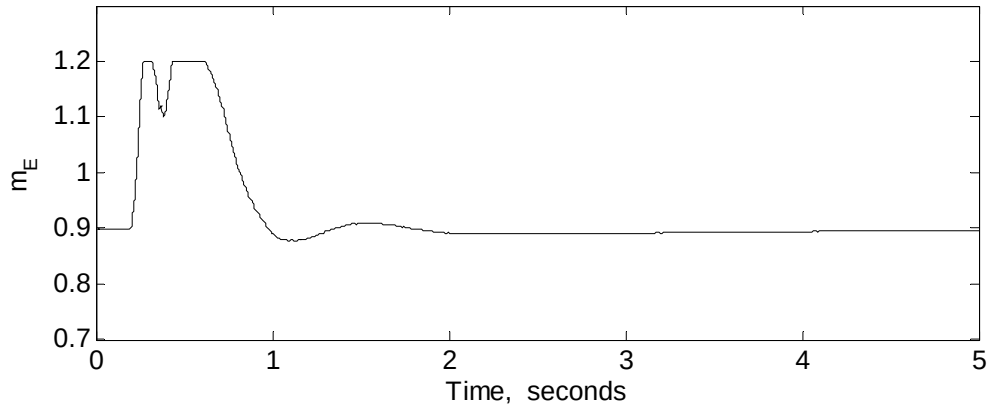

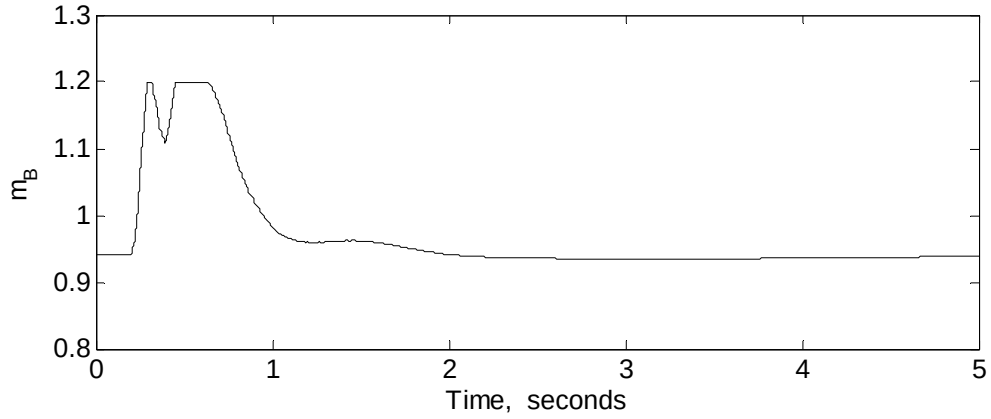

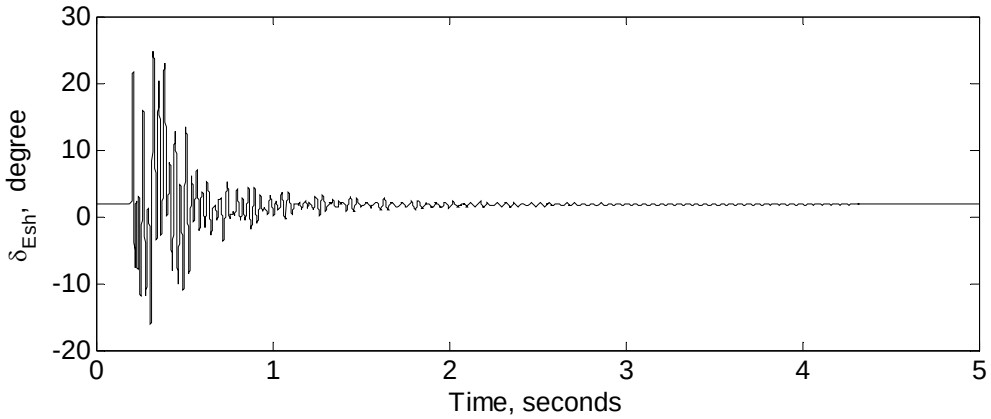

(b)

Figure E.4 (continued)